MOBILITY, PHYTOTOXICITY AND REMOVAL OF NANOMATERIALS IN A NATURAL WATER SAMPLE

SHANAZ JAHAN

FACULTY OF SCIENCE
UNIVERSITY OF MALAYA
KUALA LUMPUR

2018

MOBILITY, PHYTOTOXICITY AND REMOVAL OF NANOMATERIALS IN A NATURAL WATER SAMPLE

SHANAZ JAHAN

THESIS SUBMITTED IN FULFILMENT OF THE REQUIREMENTS FOR THE DEGREE OF DOCTOR OF PHILOSOPHY

DEPARTMENT OF GEOLOGY
FACULTY OF SCIENCE
UNIVERSITY OF MALAYA
KUALA LUMPUR

2018

UNIVERSITY OF MALAYA

ORIGINAL LITERARY WORK DECLARATION

Name of Candidate: Shanaz Jahan

Registration/Matric No: SHC140097

Name of Degree: Doctor of Philosophy

Title of Project Paper/Research Report/Dissertation/Thesis ("Mobility, Phytotoxicity and Removal of Nanomaterials in a Natural Water Sample")

Field of Study: Geology (Earth Sciences)

I do solemnly and sincerely declare that:

(1) I am the sole author/writer of this Work;
(2) This Work is original;
(3) Any use of any work in which copyright exists was done by way of fair dealing and for permitted purposes and any excerpt or extract from, or reference to or reproduction of any copyright work has been disclosed expressly and sufficiently and the title of the Work and its authorship have been acknowledged in this Work;
(4) I do not have any actual knowledge nor do I ought reasonably to know that the making of this work constitutes an infringement of any copyright work;
(5) I hereby assign all and every right in the copyright to this Work to the University of Malaya ("UM"), who henceforth shall be the owner of the copyright in this Work and that any reproduction or use in any form or by any means whatsoever is prohibited without the written consent of UM having been first had and obtained;
(6) I am fully aware that if in the course of making this Work, I have infringed any copyright whether intentionally or otherwise, I may be subject to legal action or any other action as may be determined by UM.

Candidate's Signature Date:

Subscribed and solemnly declared before,

Witness's Signature Date:

Name:

Designation:

MOBILITY, PHYTOTOXICITY AND REMOVAL OF NANOMATERIALS IN A NATURAL WATER SAMPLE

ABSTRACT

This research explored the mobility, phytotoxicity and removal of nanomaterials (NMs), in a natural water sample. In this research three metal based NMs, including one newly synthesized polyethylene imine coated silver nanoparticles, PEI@AgNPs (50 ± 10 nm) and two already reported polyethylene glycol coated zinc oxide nano-rods, PEG@ZnONRs (64 ± 10 nm) and uncoated titanium dioxide nanoparticles, TiO_2NPs (89 ± 20 nm) were synthesized. To investigate the effect of morphology, two more zinc oxide structures, i.e., zinc oxide nano-needles, ZnONNs (43 ± 10 nm) and zinc oxide micro-flowers, ZnOMFs (1.09 ± 0.2 μm) were also produced. Carbon based NMs comprising of carbon nanoparticles, CNPs (20± 10 nm) and graphene oxide quantum dots, GOQDs (50 ± 20 nm) were synthesized by following earlier work. Packed column experiments were systematically performed to explore the behavior of metal and carbon based NMs using natural river water as flowing medium. For NMs mobilization behavior, two metal based NMs i.e., PEG@ZnONRs and TiO_2NPs were selected and analyzed under hydroponic plant growth. The results obtained from the column transport experiments of metal based NMs revealed that, the surface coating play important role in the particle dissolution and ionic metal release. Typically, the ionic metals release i.e., Ag(I), Zn(II) and Ti(IV) were 3 %, 19 % and 12 % from PEI@AgNPs, PEG@ZnONRs and TiO_2NPs respectively. The findings obtained from the size and morphology effects depicted that, ZnONNs with small particle size (43 ± 10 nm nm) and simple needle shaped morphology was transported well compared to PEG@ZnONRs (64 ± 10 nm), and ZnOMFs (1.09 ± 0.2 μm) with large particle sizes and angular structures. The transport behavior of carbon based NMs was largely driven

by the particle surface charge. CNPs with high surface charge (-40 mV) transported more from the column compared to GOQDs (-24 mV). In addition, the presence of monovalent salt (NaCl) significantly affects the transport behavior of metal and carbon based NMs. Whereas, limited response was observed in the presence of divalent salt ($CaCl_2$). The findings achieved from the metal ion mobilization into the plant revealed that, Zn(II) ions due to the generation of oxidative stress significantly inhibit the physiological and biochemical activity of plant even at small concentration (40 µg/mL). In contrast, no adverse effects of Ti(IV) ions were observed at concentrations up to 200 µg/mL. This contrast finding was due to the distinct mobilization pattern indicating that, both metal ions exert different effects under similar environmental conditions. In remediation part, polymer modified mesoporous silica iron microcubes (P@MSIMC) adsorbent was successfully synthesized. The maximum removal efficiency of adsorbent for PEG@ZnONRs, TiO_2NP and PEI@AgNPs was 850 mg/g, 720 mg/g and 550 mg/g while, 600 mg/g and 504 mg/g for CNPs and GOQDs respectively. The kinetics of adsorption process fitted well with the pseudo-second-order kinetic model. Furthermore, the adsorption process was predominantly unaffected in presence of natural water coexisting ions suggesting that, the synthesized adsorbent is excellent for the remediation of metal and carbon based NMs from natural aqueous medium.

Keywords: Nanomaterials, Mobility, Ionic metal release, Phytotoxicity, Removal.

MOBILITI, KEFITOKSIKAN DAN PENYINGKIRAN BAHAN NANO DALAM SAMPLE AIR SEMULA JADI

ABSTRAK

Kajian ini meneroka pergerakan, kefitoksikan dan penyingkiran bahan nano dalam sampel air semulajadi. Dalam kajian ini, tiga NMs berasaskan logam termasuk zarah nano polietilena imina bersalut perak, PEI@AgNPs (50 ± 10 nm) dan dua yang telah dilaporkan polietilena glikol rod-nano zink oksida, PEG@ZnONRs (64 ± 10 nm) dan titanium dioksida yang tidak bersalut zarah-nano, TiO_2NPs (89 ± 20 nm) telah disintesis. Untuk mengkaji kesan saiz dan morfologi, dua struktur zink oksida lain iaitu zink oksida nano-jarum, ZnONNs (43 ± 10 nm) danzink oksida mikro-bunga, ZnOMFs (1.09 ± 0.2 μm) juga telah dihasilkan. NMs berasaskan karbon termasuk zarah-nano karbon, CNPs (20 ± 10 nm) dan titik kuantum grafin oksida, GOQDs (50 ± 20 nm) disintesis dengan mengikuti kerja-kerja awal yang telah dilaporkan. Eksperimen lajur yang dibungkus secara sistematik dilakukan untuk meneroka tingkah laku NMs berasaskan logam dan karbon menggunakan air sungai semula jadi sebagai medium yang mengalir. Bagi tingkah laku penggerak NMs, dua logam berasaskan NMs iaitu, PEG@ZnONRs dan TiO_2NPs dipilih dan pengambilan ion logam dan pengangkutan dianalisis di bawah pertumbuhan tumbuhan hidroponik. Hasil yang diperoleh dari eksperimen pengangkutan lajur dari NMs berasaskan logam mendedahkan bahawa salutan permukaan memainkan peranan penting dalam pembubaran zarah dan pembebasan logam ionik. Biasanya, pelepasan logam ionik, Ag(I), Zn(II) dan Ti(IV) masing-masing adalah 3%, 19% dan 12% daripada PEI@AgNPs, PEG@ZnONRs dan TiO_2NPs. Penemuan yang diperolehi dari kesan saiz dan morfologi yang digambarkan bahawa ZnONNs dengan saiz zarah kecil (43 ± 10 nm) dan morfologi berbentuk jarum mudah diangkut dengan baik berbanding dengan PEG@ZnONRs (64 ± 10 nm), dan

ZnOMFs (1.09 ± 0.2 μm) dengan saiz zarah besar dan struktur sudut. Tingkah laku pengangkutan NMs berasaskan karbon sebahagian besarnya didorong oleh caj permukaan zarah. CNPs dengan caj permukaan tinggi (-40 mV) dapat diangkut lebih banyak daripada lajur berbanding GOQD (-24 mV). Di samping itu, kehadiran garam monovalen (NaCl) memberi kesan ketara terhadap tingkah laku pengangkutan logam dan berasaskan NM berasaskan karbon. Sedangkan tindak balas terhad diperhatikan dengan adanya garam divalen ($CaCl_2$). Penemuan yang diperolehi daripada penggerak ion logam ke dalam tumbuhan mendedahkan bahawa, Zn(II) ion kerana penjanaan tekanan oksidatif dengan ketara menghalang aktiviti fisiologi dan biokimia tumbuhan walaupun pada kepekatan kecil (40 μg/mL). Sebaliknya, tiada kesan sampingan dari ion Ti(IV) diperhatikan pada kepekatan sehingga 200μg/mL. Penemuan kontras ini adalah disebabkan corak penggerak yang berbeza dari ion Zn(II) dan Ti(IV) yang menunjukkan bahawa kedua-dua ion logam menghasilkan kesan yang berbeza di bawah keadaan persekitaran yang serupa. Dalam bahagian pemulihan, agen penjerap berasaskan silika berliang meso berjaya disintesis. Penjerapan maksimum yang diperoleh untuk PEG@ZnOMRs, TiO_2NPs dan PEI@AgNPs ialah 850 mg/g, 720 mg/g dan 550 mg/g. Manakala, 600 mg/g dan 504 mg/g untuk CNPs dan GOQDs. Kinetik penjerap dipasang dengan baik dengan model kinetik tindak balas tertib kedua pseudo untuk kedua-dua bahan logam dan karbon. Proses penjerapan tidak terjejas dengan kewujudan anion dan kation bersama menunjukkan bahawa penjerap yang telah berjaya disintesis adalah sangat baik untuk pemulihan logam dan karbon NMs dari media berair semula jadi.

Kata kunci: Bahan nano, Mobiliti, Ionic logam pelepasan, Kefitokikar, Penyingkiran

ACKNOWLEDGEMENTS

I would like to express my sincere gratitude to Prof. Yatimah Binti Alias, and Dr Ahmad Farid Bin Abu Bakar for their advice, guidance, patience and motivation during this research project. As a supervisor, they provide constant academic and moral supports throughout the project and helped me in all the aspects of research and the writing of this thesis. I also would like to thanks to Prof. Dr Ismail Bin Yusoff for his support and guidance throughout the project.

My sincere gratitude goes to the University of Malaya, for granting me the opportunity to pursue my PhD program, allowing access to laboratories, equipments, library resources and all other supports during the period of study.

I am also grateful to the University of Malaya High Impact Research Grant HIR grant-UM C/625/1/HIR/MOHE/SC/04 from the Ministry of Higher Education Malaysia which financially supported this work.

I also would like to acknowledge all my former academic supervisors, teachers and instructors, they all are academic mentor and serve as a role model throughout my academic career.

My heartfelt appreciation goes to my dear father *Hafiz-ur-Rahman* my beloved mother *Qaiser Jahan* (Late), and my brothers and sisters for their unconditional emotional and spiritual support during the program.

TABLE OF CONTENTS

LIST OF FIGURES

LIST OF TABLES

LIST OF SYMBOLS AND ABBREVIATIONS

μ	:	Micro
ξ	:	Zeta
AgNPs	:	Silver nanoparticles
BET	:	Brunauer-Emmett-Teller
C_o	:	Concentrations (mg/L) measured initially at the time (0)
CNP	:	Carbon nanoparticles
DW	:	Deionized water
EDS	:	Energy-dispersive X-ray spectroscopy
FESEM	:	Field emission scanning electron microscopy
FTIR	:	Fourier transform infrared spectroscopy
GOQDs	:	Graphene quantum dots
ICP-MS	:	Inductively coupled plasma mass spectrometry
IC	:	Ion chromatography
K_1	:	Pseudo-first-order rate constant
K_2	:	Pseudo-second-order rate constant
LPOX	:	Lipid peroxidation
Min	:	Time in minutes
NMs	:	Nanomaterials
NPs	:	Nano particles
NOM	:	Natural organic matter
P@MSIMC	:	Polymer-modified mesoporous silica iron micro cubes
PEG	:	Polyethylene glycol
PEG@ZnONRs	:	PEG-coated zinc oxide nano-rods

PEI	:	Polyethylene imine
PEI@AgNPs	:	PEI-coated silver nanoparticles
Qe	:	Equilibrium adsorption capacity
Qm	:	Maximum adsorption capacity
Qt	:	Adsorption at time t
R_d	:	Deposition rate
Rpm	:	Rotation per minute
RW	:	River water
SPR	:	Surface plasmon resonance
TCC	:	Total chlorophyll content
TiO_2NPs	:	Titanium dioxide nanoparticles
UV-Vis	:	Ultraviolet-visible spectroscopy
XRD	:	X-ray powder diffraction
ZnONNs	:	Zinc oxide nano-needles
ZnOMFs	:	Zinc oxide micro-flowers

CHAPTER 1: INTRODUCTION

1.1 General Introduction

Nanomaterials (NMs) based industries are growing exponentially due to the rapid rise of information technology and advanced materials. With this rapid production, NMs will be ubiquitous in both the natural and engineered environments and has created notable concern with environmental regulations (Hegde et al., 2016; Syberg et al., 2016) and industrial associations (Som et al., 2012).

According to the new definition (European commission., 2011), the term nanomaterials (NMs) may be described as any synthesized material containing particles, in an unbound state or as an aggregate or as an agglomerate and where, 50 % or more of the particles are in the number size distribution, one or more external dimensions is in the size range 1 nm to 100 nm. (Pereira et al., 2017). Nanomaterials may exhibit properties different from their non-nano forms, and these different properties have raised questions about potential human health and environmental risks (Boverhof et al., 2015).

Most commonly used NMs are metal and carbon based materials. Metal oxide NMs including titanium dioxide (TiO_2) and zinc oxide (ZnO) have made their way into personal care products and catalytic applications (Bhuyan et al., 2016; Lewicka et al., 2011; Weir et al., 2012; Xu et al., 2015). Nanosilver, primarily known for antibacterial properties (Duran et al., 2016) and is used in approximately 20% of the NMs containing products. Graphene and carbon based NMs are also widely used nanostructures which are particularly desirable for their mechanical, electrical, optical and thermal properties (Angiola et al., 2016; Nandi et al., 2016). These materials are synthesized in a variety of shapes, sizes and surface properties, including C60 “buky

balls", carbon nanotubes and graphene quantum dots (Lv et al., 2016; Zhang et al., 2016a) to boost their practical applications. With these advancements in nanotechnology, the widespread utilization of nano products usher serious concern about their release into the aquatic, terrestrial and atmospheric environment. For example, recent studies found the occurrence of NMs in wastewater effluent, sludges and biosolids (Gottschalk et al., 2013) which pinpoint the introduction into the terrestrial environment through their application for agriculture purposes (Oleszczuk et al., 2011). In addition, nanosilver and carbon nanotubes have also been reported to be present in estimated amount from production to disposal or release, considering high production and release estimates as of 2010 (Keller et al., 2013).

Additionally, nanotechnology has a great potential to improve environmental and water quality. Usage of NMs in membranes, adsorption and catalysis can revolutionize the water treatment technologies. While most of the industries embracing nanotechnology in the manufacturing process for the novel properties of NMs. Natural waters and ecosystems will likely face unknown consequences from the introduction of these advanced materials in the environment. Moreover, unique size, shape and properties of NMs may challenge the engineered systems as the current treatment facilities did not consider these anthropogenic contaminants in design.

Due to all these growing concerns about potential risks from exposure to NMs, the U.S. Environmental Protection Agency, proposed a budget of $2.1 billion (which is $201 million increase from the 2010 endorsed budget) to understand the potential risks of NMs (Duvall et al., 2011). Environmental monitoring and regulations is also a big challenging task for the rapid growth of numerous NMs. Furthermore, environmental degradation is quite possible from the manufacturing, usage and disposal steps, making the condition more critical to regulate the outbreak of NMs.

Therefore, studies should be conducted to investigate the behavior of NMs in the real natural environment and the factors responsible for nano ecotoxicology. Moreover, the potential removal steps or advanced methodologies are needed to explore and to minimize the impact of NMs in the natural water environment.

1.2 Problem Statement

Although the potential for nanotechnology in environmental engineering is immense, the challenge is to ensure the sustainable development of nanotechnology instead of a future environmental liability. Understanding the behavior, mobility and removal processes are essential for regulating and monitoring the potential concerns generated from nanotechnology. Most of the previous research reports focused on the behavior of NMs under synthetic solution in deionized water. However, the behavior of NMs in the natural aqueous environment studies rarely taken into account. In addition, the investigation of NMs mobilization through the contaminated water into the living objects such as plant is of key importance and need to be considered.

Another important feature which is mainly unexplored is the comparative analysis of the mobilization behavior of a single and the mixture of different NMs, which may affect their mobilization and the consequences produced in return. Therefore, systematic research approach is required to fill this current knowledge gap. Furthermore, there should be an amplified technique for the removal of metal and carbon based NMs from the natural aqueous medium. Hence, this doctoral research addresses the fundamental effects of natural complex environment on the NMs behavior, mobility and the development of efficient remediation technique for NMs removal.

1.3 Research Objectives

This work aims at the development of a better understanding of the behavior transport or mobilization of NMs and its efficient remediation from the natural aqueous medium.

The main objectives of this research are,

1- To synthesize and characterize metal and carbon based nanomaterials of different shape, size and surface charge.

2- To investigate the mobility of metal and carbon based nanomaterials through porous column transport and mobilization of metals ions into the plant.

3- To develop a potential remediation process to remove metal and carbon based nanomaterials from natural water sample.

1.4 Research Scope

Understanding the behavior of NMs in the natural aqueous environment will assist risk assessments by guiding the toxicity testing of nanomaterial formulations under real environmental conditions. This should be coupled with the development of appropriate measurement techniques that can quantify both concentrations and particle sizes with appropriate quality assurance and quality control. From the literature it is evident that surface properties of NMs is fundamental in determining their behavior and these properties will need to be considered in any hazard ranking.

The proposed research is expected to greatly improve fundamental knowledge of NMs transport, ionic release, and mobilization and aggregation behavior in natural aqueous media. The results obtain from the natural aqueous medium will be compared with the synthetic solutions. As the coupling of detailed experimental research in natural and synthetic solution in deionized water will provide rigorous testing of

conceptual models of NMs behavior in subsurface systems. This will improve to culminate knowledge in the development of numerical simulator capable of predicting NMs behavior over a range of conditions that might be encountered in natural systems. It is further anticipated that the experimental methods can be adapted or directly used to predict the behavior of NMs in subsurface systems.

Measurements of the NMs dissolution, aggregation and ionic release behavior, not only predicts its short-term and long-term stability, but will also assist in the development of techniques to distinguish the properties of NMs under natural and synthetic environment. These measurements will mainly focus on particle concentration, size and surface characteristics. Transport and toxicity testing of NMs, and its distribution using the plant model will assist in determining the critical in-vivo knowledge about the dose and time dependent toxicity.

Determination of the significant behavior of NMs will facilitate in designing the hazard ranking of nanomaterial toxicity, as a precursor of toxicity testing. More specifically, the comparison of NMs behavior in natural verses synthetic water, will demonstrate the effects of natural co-existing colloids. The results obtained through this project on the transport behavior and mobilization of NMs may lead to change in the existing policy on the synthesis, surface modification and stabilization of NMs from synthesis to utilization and disposal steps. Furthermore, the development of sustainable remediation process for the removal of NMs will be helpful economically and can be utilized in NMs remediation technologies.

1.5 Outline of the Thesis

This thesis is written in the conventional style format using the guidelines of Institute of Post Graduate Studies (IPS), University Malaya. The thesis consists of five chapters, with different aspects relevant to the topic of the study.

Chapter 1: This chapter includes a brief introduction to the research background, aims and objectives and the overall conceptual framework designed for this study.

Chapter 2: This chapter reviews the literature of metal and carbon based materials and the factors affecting the behavior, mobilization and removal of NMs and highlight the existing gaps in the knowledge base.

Chapter 3: This chapter describes the general methodology adopted for the overall research carried out in this project.

Chapter 4: This chapter describes the results and discussions of the NMs synthesis, characterization, ionic dissolution, transport and retention behavior of metal and carbon based NMs in natural river water (a). The influence of NMs physicochemical properties and the effect of solution chemistry were also discussed in detail (b). The results obtained from mobilization of selected metal based NMs, the uptake and translocation and the physiological and biochemical impacts on growth of red bean model plant system were demonstrated (c). The results acquired from single and co-exposure of two metal ions on uptake kinetics was also elaborated (d). In addition, the removal of all metal and carbon based NMs was described by synthesizing a polymer-modified mesoporous silica iron microcubes as adsorbent (e). The details of the adsorption kinetics with isotherm models and removal efficiency were also discussed in details (f).

Chapter 5: In the last chapter, results and the key findings of the whole research were summarized. In addition, the recommendations and future directions were also discussed.

CHAPTER 2: LITERATURE REVIEW

2.1 Introduction

Human advancement profoundly becomes a major source of environmental pollution via fast development and extensive use of materials in everyday life. In recent years, nanotechnology has become a major state of the art for scientific and economic development. However, their epidemic usage and high dose introduction effectively produce a deleterious effect on the aquatic and terrestrial ecosystem. The examples of some extensively used NMs are metal and carbon based materials. Metal based NMs such as silver nanoparticles (Li et al., 2016; Liu et al., 2017; Ocsoy et al., 2017) zinc oxide nanoparticles (Atchudan et al., 2016; Barhoum et al., 2017) titanium dioxide nanoparticles (Petala et al., 2016; Ranjan et al., 2016) are widely utilized for many domestic and industrial applications. The examples of carbon based NMs includes graphene oxide nanoparticles (Hu et al., 2016; Ji et al., 2017; Wang et al., 2017) carbon nanotubes and carbon nanoparticles (Alatalo et al., 2016; Huang et al., 2013; Sun et al., 2016b) which find their way in various industrial and environmental applications.

Along with the expending use of these NMs in daily life, there is a growing concern over their ecological toxicity. These NMs with distinct surface properties entered the ecosystem either intentionally or unintentionally and affect the ecosystem. Recently a research group (He et al., 2015) summarizes that, NMs when released into the environment interacted with the biota of ecosystem through three-way pathways i.e., nano-bio-eco interaction and produce nanotoxicity. As displayed in the graphical representation (Figure 2.1), NMs after manufacture, enters the aqueous system through application or disposal route where their behavior are influenced by the dynamic interaction among different environmental compartments. To understand these

interactions it is necessary to elaborate the impact of NMs physicochemical properties and the factors affecting the behavior of NMs in natural aqueous system.

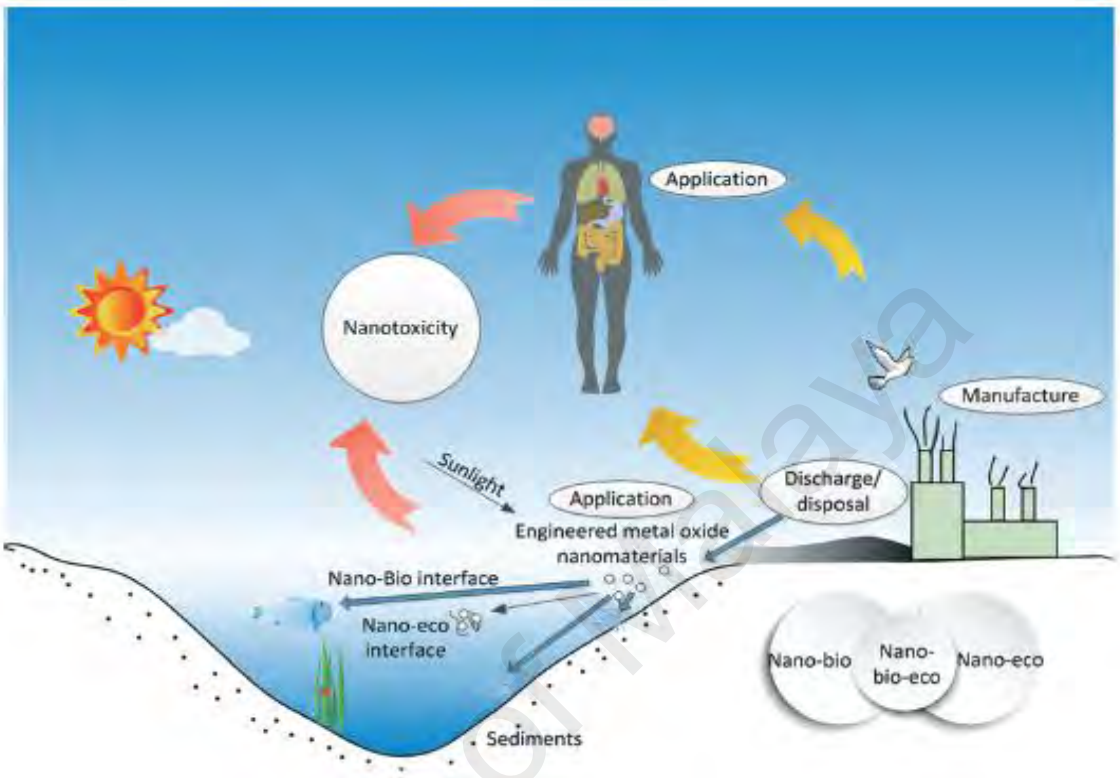

Figure 2.1: Illustration of the three-way interactions during NMs manufacture, use and disposal (He et al., 2015).

Marvelous innovations in the nanotechnology are the result of NMs physicochemical properties, which make them promising candidates for their increased utilization in products. However, at the same time these unique properties ultimately provoke concern over ecological toxicity (Maurer-Jones et al., 2013). Estimating the behavior of NMs in natural aqueous environment and predicting their transport and transformation properties are necessary steps in the assessment and management of the risks of this technology. For this purpose, NMs must be characterized well to fully understand the impact of physicochemical properties of NMs to better understand and predict what happens to NMs when they exposed absorbed, transport and distributed to the objects of environment and ecosystem. To predict the

behavior of NMs when exposed to aqueous system requires experimental data in 3 general areas. 1) To characterize the NMs at the point of exposure to natural aqueous system. 2) To investigate how the properties of the NMs change between their starting point and every possible point of exposure to natural aqueous system. 3) The ability of NMs to absorbed, transport into the living systems. Furthermore, the mechanistic details and factors related to characteristics of NMs and natural aqueous medium are of critical importance.

Because of all these diverse range of needed information, the range of NMs transports behavior techniques are required to attain these informations. For point 1, the characterization techniques are needed that can monitor the structural composition, surface coatings, surface charge and morphological properties of NMs. For point 2, analytical methods are required that can closely monitor and quantify the transformation of NMs and the impact of various environmental factors such as medium pH, ionic strength and naturally occurring dissolved organic matters. For point 3, living model systems are needed to investigate the interactions, transport and mobilization of NMs in complex living tissues, enabling to predict the effect of NMs properties, and types of effects they have at the tissue levels.

NMs such as silver nanoparticles (AgNPs) owing to its unique optical, electrical, and thermal properties are being incorporated into products range from photovoltaics to biological and chemical sensors. The most common application of AgNPs is because of its antimicrobial activity that continuously releases a low level of silver ions to provide protection against bacteria. AgNPs are also being used in numerous technologies and incorporated into applications such as, biosensors, in conductive inks, and for enhanced optical applications such as surface-enhanced Raman scattering (SERS). Worldwide, the present production of AgNPs is estimated at about 500 t/a (Mueller and Nowack,

2008), and a steady increase on the volume manufactured is predicted for the next few years (Boxall et al., 2007a).

Titanium dioxide nanoparticles (TiO_2NPs) due to its high diffraction index and strong light scattering and incident-light reflection capability, is widely used as white pigment. Due to its high UV resistance ability they are mainly found in high-factor sun protection creams, textile fibers or wood preservatives. Other applications of TiO_2NPs includes they are actively used in solar cells (Ahn et al., 2014; Sabba et al., 2014; Sigdel et al., 2014) photocatalysis (Brauer et al., 2014; Mou et al., 2014) anatase activity (Chen et al., 2014) oxidation of CO (Zhou et al., 2014) reduction of CO_2 to CH_4 (Fang et al., 2014) and also as food additives.

Similarly, zinc oxide nanoparticles (ZnONPs) are widely utilized in several environmental applications and are the third highest used metal-containing nanomaterials. It is reported that the worldwide annual production of ZnONPs is 31,500–34,000 t per year, and ranking after to TiO_2 among various metal based NMs. These nanoparticles are widely utilized in personal care products like sunscreens as well as applications in catalysis, chemical manufacturing, optical devices, and in biosensing applications (Boonyanitipong et al., 2011). In addition, owing to its high antibacterial activity and stability, ZnONPs are becoming the extremely attractive materials in fields of food additives, packing and agriculture, and biomedicine (Zhao et al., 2014; Sirelkhatim et al., 2015). From the literature it was estimated that, around 8–20% ZnONPs enter the water environment, with the mean reported concentration of 6.97 mg/kg in EU area in sediments. (Feng et al., 2016; Piccinno et al., 2012; Sun et al., 2016a).

Carbon based NMs such as carbon nanoparticles (CNPs) because of its distinct surface properties have gain interest in neumerous environmental remediation

techniques (Chen et al., 2007; Xiao et al., 2010). These particles also gain tremendous application in field of biology and nanomedicine (Marchesan et al., 2015) as sensor (Saetia et al., 2014) in printed electronics (Wang et al., 2015b) and in several catalytic techniques (Xiao et al., 2014).

Graphene oxide nanoparticles (GONPs), a single aromatic sheet of bonded sp^2 carbon atoms due to its unique optical, electronic and catalytic properties have been widely used in diverse environmental (Kumar et al., 2014; Shih et al., 2014; Zhang et al., 2014) industrial (Bag et al., 2014; Kumar et al., 2014) nano-biosensing (Tabrizi et al., 2014) nanomedicine (Feng et al., 2013; Weaver et al., 2014) and in photocatalytic (Ong et al., 2014) applications. Applications of NMs still in progress a lot of research groups actively utilizes these nanomaterials either by grafting, surface functionalizing or by making hybrid nanocomposite which renders NMs to more reactive in industrial and environmental remediation processes.

In the present era of science and technology, all these mentioned NMs are profoundly produced in various forms, shapes, sizes and surface coatings. These enumerable forms of NMs not only enhance their industrial applications but also raise potential concern towards ecosystem and human health (Boxall et al., 2007b). Furthermore, in addition to other NMs, the production and use of metal based NMs dramatically increases (Ping et al., 2007) due to huge commercialization and substantial utilization in numerous market products (Lem et al., 2012).

This widespread production and utilization of metal based NMs; raise its concern towards ecotoxicology. Once released into the environment the zero valent metal (M^o) readily oxidized to ionic metal (M^+) (Dobias et al., 2013) which is reported as the main source of toxicity related to metal based NMs (Kittler et al., 2010). These ionic species profoundly accumulate into the natural water systems (Philippe et al., 2014)

and create toxicity (Kalbassi et al., 2011). Amid the synthesis and application, one of the unavoidable problems associated with metal based NMs is its instability due to high surface energy (Lu et al., 2007). To overcome this problem researchers fabricate stabilizing polymers at the surface of NMs to minimize the electrostatic repulsion and prevent aggregation (Bayram et al., 2015).

Though, in this way making them good candidates for practical application (Perni et al., 2014). However, surface stabilization also increases the concern of unknown reactions when these particles subjected to introduce into the natural environmental matrices. The behavior of polymer coated metal based NMs comparing to uncoated NMs, is not very well understood. Though, several previous reports described that the presence of dissolved ions, and natural organic matter (NOM) profoundly affects the metal based NMs behavior (Aiken et al., 2011; Fabrega et al., 2011). However, limited data exist to understand the behavior of coated and uncoated metal based NMs exposed to the natural aqueous environment (Duncan, 2014; Piccapietra et al., 2011).

As reported earlier (Furman et al., 2013) that naturally dissolved ionic salts and NOM can have significant effect on behavior of NMs. NOM is a by-product of decaying plant material typically present in dissolved form in natural water. The NOM level found in most of natural water ranges from 0.1 to 20 mg/L (Rodrigues et al., 2009). It was reported earlier the presence of NOM profoundly affects the transport and toxicity of NMs (Aschberger et al., 2011). Hence, concern regarding effect of surface coating, size dependent dissolution (Liu et al., 2010b), dissolution kinetics, and aggregation behavior of metal based NMs is of great interest and need to be explored to understand its toxicity to the aquatic environment.

Carbon based NMs owing to their profound potential in various advanced applications rapidly expand the interest of the scientific community. Despite its

exciting application outlook, the knowledge about the environmental behavior of these NMs is in their infancy and has to be addressed. Understanding the factors, affecting the behavior is essential for practical application of these materials in various sectors such as land application of sewage sludge and groundwater recharge and other environmental applications. Graphene oxide (GO) is a new kind of carbon based nanomaterial and is widely used in various industries such as agriculture, biomedical application, sensor technologies and in several environmental applications. The reactivity of GOQDs is predominantly due to the surface properties containing a large number of hydrophilic groups, such as carboxylic, phenolic and hydroxyl groups which enabled it to be easily dispersed in water and can flocculate in the presence of ionic salts (Konkena et al., 2012; Wu et al., 2013).

Similarly, carbon nanoparticles (CNPs) have recently attracted tremendous attentions due to their low toxicity, good water solubility, robust photostability, high chemical inertness and excellent biocompatibility and largely utilized in several industrial and environmental applications. However, the environmental impact and the factors affecting the CNPs behavior are not studied in detail so far. Moreover, the effect of physicochemical properties of both CNPs and GOQDs and the factors of natural complex water is yet to be disclosed. As several studies revealed that regardless of the route of NMs release and exposure (Khin et al., 2012) sediments and porous subsurface have been identified as likely environmental sink for NMs (Gottschalk et al., 2011) in which NMs undergo subsequent transport and transformation (Lowry et al., 2012).

In order to investigate the toxicity of NMs, recent efforts pinpoint the environmental behavior and risk factors associated with the NMs. In addition, several recent research effort appreciating the need of environmental assessment together with

the NMs behavior, transport, and toxicity, to promote sustainable use of these novel materials. Carbon based NMs including carbon nanotubes (Eckelman et al., 2012; Verdugo et al., 2014), carbon nano dots (Xiao et al., 2016) and graphene oxide (Combarros et al., 2016; Xie et al., 2016) similar to metal nanoparticles (Elsaesser et al., 2012; Hedberg et al., 2016) have found to be toxic towards the aqueous environment. Increased application and uncontrolled production of these NMs to a large extent will likely lead to the release in the environment and ecosystem causing damage to the cellular level.

Moreover, long-term stability studies showed that graphene oxide is highly unstable in natural surface water and readily interact with other environmental surfaces. This may play a key role in the transformation of these emerging NMs in aquatic environments. Despite significant research on graphene NMs applications, research on their environmental risk is in its initial stage, and there are only a few published reports available on the aqueous behavior of GOQDs. Hence, behavior of this emerging material in the natural aqueous environment is crucial and need to be investigated for sustainable implementation (Chowdhury et al., 2014).

Although certain literature is emerging from the past few years reporting ecotoxicology of synthesized NMs, but the mechanistic basis of exposure and related NMs behavior under different environmental conditions are poorly understood, especially in the natural aqueous environment. Moreover, there are many challenges and controversies exist, but knowledge transfer from NMs intrinsic properties, colloidal chemistry, as well as detailed material and geological sciences will enable ecotoxicological studies to facilitates and to move forward in this new multidisciplinary field (Farre et al., 2009).

To gain better understanding of NMs transport behavior, investigation using porous media is widely reported in literature. Because of simple methodology and experimental diversity to investigate NMs transport at different operational parameters and aqueous chemical conditions, the technique is of practicle importance. Transport of NMs through porous media under environmentally relevant conditions, such as the variations in water flow rate and ionic strength making it possible to investigate and modeled the transport of NMs under natural aqueous conditions.

There are several previous reports dealing with the transport of NMs through saturated porous media (Kasel et al., 2013; Sasidharan et al., 2014; Wang et al., 2012). For instance, Zhang and others described the transport of cerium oxide nanoparticles under saturated silica media (Zhang et al., 2016c). They studied the influence of operational parameters and effect of aqueous chemical variation on transport of cerium oxide nanoparticles. In another study (Xia et al., 2017) researchers studied the cation inhibited transport of graphene oxide nanomaterials in saturated porous media. They found that the transport of negatively charged nanoparticles in porous media is largely affected by medium cations. The observed inhibition was mainly because of the interaction of cations with packing material (quartz sand) and graphene oxide due to cation bridging effect. Using quartz sand as packing material, the transport and deposition of graphene oxide was also extensively studied by Peng and others in saturated porous media (Peng et al., 2017) and so many others.

2.2 Factors Affecting Behavior of NMs

The gap between NMs synthesis, and its predicted environmental behavior urge the scientific community to introduce the robust, stable, ecofriendly methods for a save synthetic processes (Happo et al., 2013) and save disposal. The in-bound characteristics of NMs greatly affect their transport into the environment. For example,

the toxicological effects belong to the metal doped NMs primarily due to its high stability toward aggregation and their ability to react with complex natural organic matter (Liu et al., 2012b). In addition, some report (Nathalie Adam 2014) claims that the transport and toxicological impact of NMs is solely attributed to its dissolved ion concentration rather than nanomaterial itself or its aggregated form.

As aggregation is directly related to the transport of nanomaterials, the stability towards aggregation play a crucial role in the long-term toxicity production. Certain environmental factors such as pH of solution, concentration of salt, type of electrolyte and organic acids such as humic acid produces huge impact in the dissolution and aggregation of ZnONPs in aquatic ecosystem (Cupi et al., 2015; Han et al., 2014; Majedi et al., 2014). Transformations of these NMs, such as agglomeration, dissolution, sedimentation or surface modification, by interacting with naturally occurring moieties, could greatly alter the degree of environmental release (Maurer-Jones et al., 2013; Peijnenburg et al., 2015).

2.2.1 Physicochemical Properties of NMs

The physicochemical properties of NMs, such as surface coatings, elemental composition, size and shape or morphology greatly influence the aggregation and transport behavior of NMs under complex natural environment.

NMs functionalized with anionic surfactant or polymers are believed to be more mobile because of stability coating which imparts stronger electrostatic repulsion between NMs themselves. For example, great retention ability was observed in sodium dodecyl sulfate coated single walled carbon nanotubes (SWCNT) due to decreased critical aggregation in porous medium (Bouchard et al., 2012).

Similarly, sodium dodecyl benzene sulfonate (SDBS) incorporate negative charge on the surface of graphene oxide nanoparticles and increases the transport potential in aqueous solution (Liu et al., 2015a). However, increased concentration of surfactant up to the certain limit decreases the transport behavior of NMs by forming electric double layer. Furthermore, the properties of the surface head group of the surfactant or polymer also play role in the mobility and degree of aggregation (Mehta et al., 2009). Similarly, in case of cationic surfactant and polymer, the nature of surface coating dictates its dissolution, sorption and release into the aqueous system (Ellis et al., 2016).

Recently, there is a much interest in grafting polymers such as polyethylene imine (PEI) and polyethylene glycol (PEG) and other hydrophilic, neutral polymers at the surfaces of NMs. The surface coating with polymers minimizes the extent of NMs aggregation by providing stability. Basically, surface-bound polymers are effective in masking surface charge and reducing electrokinetic effects such as particle electrophoretic mobility (Lee et al., 2016). In addition to surface functionalities, size and surface morphology has reported as a controlling factor in the dissolution, ionic release and behavior of NMs. For example, the toxicity behavior of NMs increases as the size of nanoparticles decreases (Azam et al., 2012; Lei et al., 2016).

TiO_2 due to their unique characteristics like unusual shape, size and other morphological and structural properties, have gained substantial impact on their transport in the ecosystem (Nam et al., 2014). TiO_2 show huge toxicity to the environment (Ge et al., 2013; Strobel et al., 2014) by bio persistence and non-degradable properties which make them a potent candidate for possible long term chronic effects (Fadeel et al., 2012). However, TiO_2 are often reported as less toxic than many other NMs during species sensitivity distributions (Hendren et al., 2011).

A group of researchers (Peretyazhko et al., 2014) investigated the size dependent oxidative dissolution and the effect of pH on the thiol functionalized methoxyl polyethylene glycol silver nanoparticles (PEGSH-AgNPs). They found that the extant of PEGSH-AgNPs dissolution in acetic acid was higher compared to water due to the protonation of the surface Ag_2O layers. Protonation led to weakening and breaking of the surface Ag_2O bonds, thus resulting in more Ag^+ release into the acidic solution. They also experienced that like the previous report (Liu et al., 2010b; Silva et al., 2014), solubility of AgNPs increased as their sizes decreased, both in the neutral and acidic medium.

According to this study, after dissolution, the particle morphology did not change when observed under TEM analysis. Nevertheless, other factors like dissolved organic species, type of ligand and suspended particulate materials may alter the morphology and aggregation properties in the aquatic ecosystem. These observations showed that irrespective of the particle sizes, medium pH, and change in solution chemistry, AgNPs could be considered as non-reactive towards oxidative dissolution. In addition to size, surface charge and concentration also play a major role in the toxicity of AgNPs. Previously, a group of researchers (Silva et al., 2014) examined that surface coating or organo-coating imparts stability to the NMs and causes of the inhibition of aquatic vertebrate models growth by suppressing certain biologically important enzymes. Moreover, certain aquatic plants were also susceptible to the dissolved AgNPs through uptake and bioaccumulation into the different plant parts. Therefore, surface chemistry of NMs has a strong influence on their mobility, transport and aggregation behavior.

2.2.2 Physicochemical Properties of Aqueous Medium

Solution chemistry, such as pH and ionic strength, and presence of certain dissolved natural organic matters are important controlling factors for mobility and aggregation

of NMs (Surette et al., 2016). The solution pH through determining the zeta potential values at the surface of NMs, influencing the stability and electrophoretic mobility in the solution. Basically, pH can alter the electrophoretic mobility of particles by decreasing the stability when the pH reaches the point of zero charge (pzc) or isoelectric point. A lower zeta potential tends to aggregate NMs in solution, whereas a high zeta potential values (negative or positive) imparts the NMs stability in suspensions.

Ionic properties are another factor controlling the extent of NMs behavior. Many studies have investigated the impact of ionic strength on NMs behavior. The aggregation and deposition between NMs and porous media are strongly dependent on ionic strength. For example, the mobility of graphene oxide nanoparticles increases in low ionic strength solution and retention increases as the ionic strength increases (Liu et al., 2013). The presence of certain electrolytes in solution such as Na-Ca electrolyte system, determine the mobility or retention of NMs and cause aggregation due to bridging effect between electrolyte and NMs (Qi et al., 2014a).

Similarly, the retention of AgNPs was much more pronounced in the presence of Ca^{2+} than K^{+} due to cation bridging but decreasing the solution ionic strength enhanced the mobility of surfactant-stabilized AgNPs (Liang et al., 2013). Furthermore, the increase in ionic strength of divalent salts such as $CaCl_2$, highest deposition or retention of NMs was observed in porous media (Jaisi et al., 2008). In addition to electrolytes, the presence of natural humic substances also affects the behavior of NMs. For example, the ionic release behavior of Zn(II) was greatly influenced by humic acid and maximum ionic dissolution was observed in the presence of humic substances as shown in Figure 2.2. This behavior also results in the decrease of zeta potential values (Han et al., 2014). Several other factors such as NMs

concentration (Hoffmann et al., 1995) and UV- radiation also impose greater effect on oxidative dissolution and aggregation (Yu et al., 2013) behavior of NMs.

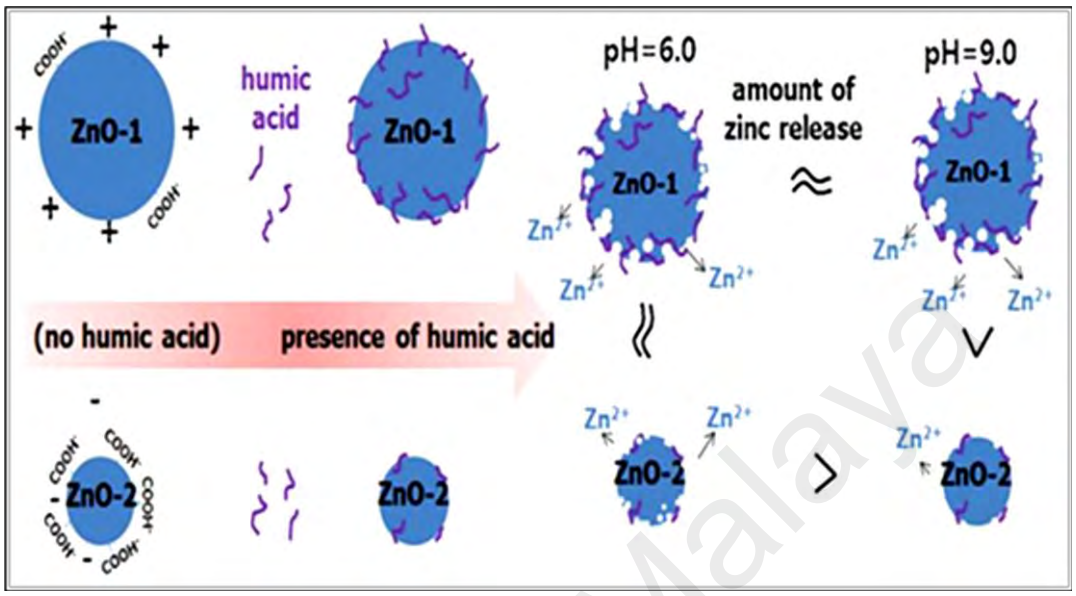

Figure 2.2: Effect of Humic acid on the aggregation, dissolution, and release of ionic Zn(II) from ZnONPs (Han et al., 2014).

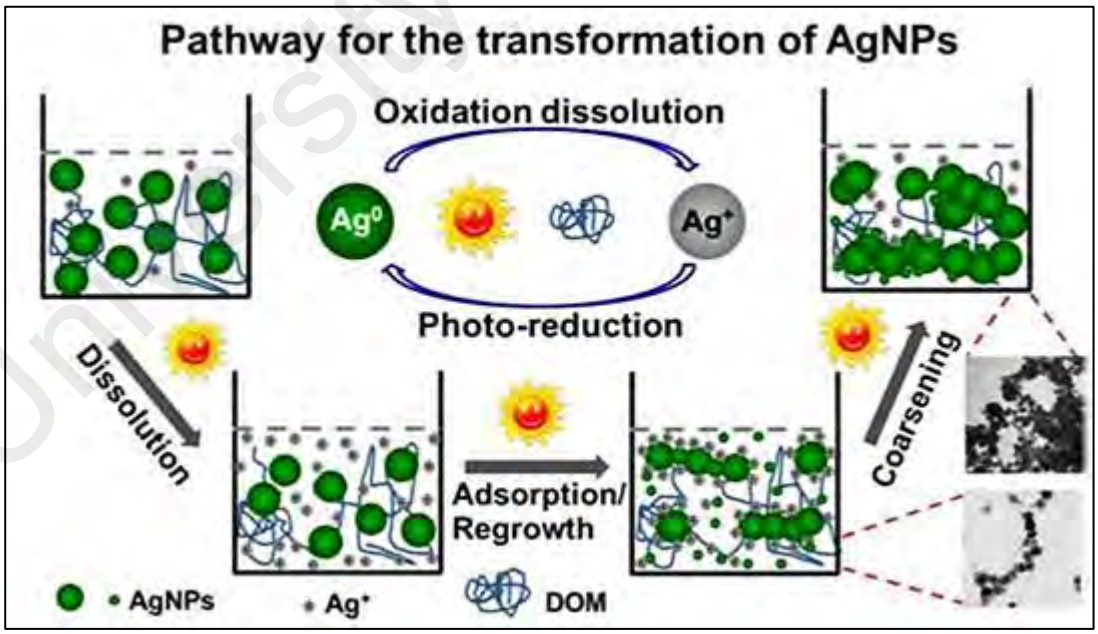

Figure 2.3: Transformation pathways of AgNPs in aquatic ecosystem under the influence of sunlight and dissolved natural organic matter (Yu et al., 2013).

Another research group (Yu et al., 2013) proposed the three stage pathway for the transformation of AgNPs. According to this study, the UV-light from sun induces the aggregation of AgNPs resulting in the larger particle symmetry, self-assembly, and particle fusion processes. In addition, sunlight through oxidative reductive mechanisms stimulated the dissolution of AgNPs into the aquatic stream which is considered to be the major toxicity related to any metal based NMs. These dissolved ions then may adsorb on the surface of dissolved organic species resulting in the reconstitution of smaller particles which cross-linked together to form coarse aggregates as shown from Figure 2.3.

Several studies revealed that, dissolution is one of the main causes that control the behavior of NMs in an aqueous system. Dissolution mainly occurs through oxidation of metal based NMs and release of ionic metal into the solution. Various studies showed that size of NMs have a dominant effect on the dissolution behavior in natural water (Liu et al., 2010b). Previously, it was reported that the dissolution is effected by NMs surface coating as well as pH, dissolved oxygen content and ionic composition of water (Levard et al., 2012; Li et al., 2011c). Previous report suggested that the higher dissolution of both PVP and SiO_2 coated AgNPs in acid pond water and sea water as 0.7-4% and 7-12% respectively. However, after 15 days the dissolved Ag fraction was lowered from the start of the experiment. Suggesting that, the stabilized Ag species such as AgCl is not dissolved in ionic species but most likely precipitated as AgCl(s) (Quik et al., 2014).

Aggregation is another phenomenon which control the dissolution rate in natural water systems. A previous study revealed that, citrate-coated AgNPs formed diversified large aggregates when mixed with natural water shortly due to precipitation and complexation. Whereas, tween-coated AgNPs were stabilized for longer time period in natural water without aggregation, suggesting these particles

will persist longer than unstabilized particles and thus will release more Ag (Li et al., 2011c). However, there are several other factors such as, surface modification, biotransformation and presence of natural ligands which assist the dissolution, aggregation or precipitation and bioavailability of NMs in natural water system (Gondikas et al., 2012).

In previous report (Fu et al., 2014), determined the transformation and destabilization of graphene oxide (GO) nanoparticles in a natural reducing environment containing sulfides. They found that in the concentration of sulfide as low as 0.5 mM, the GO were significantly destabilized by the reduction of oxygen-containing groups at the surface. Whereas, in the presence of humic acid, GO became stabilized due to steric hindrance. GO is adsorbed at the surface of humic acid through electrostatic interaction and through π-π stacking interactions. These interactions significantly blocked the GO oxygen-containing groups at the surface and inhibited the oxidation-reduction process.

To assess the aqueous mobility of GO more precisely, a researcher (Ren et al., 2014), studied the effect of Al_2O_3 on the aggregation and deposition of GO. According to the results obtained from this study, the aggregation of GO by dissolved Al_2O_3 depends on the ionic strength as well as the pH of the solution. The study showed that the GO became destabilized in the high concentration of metal chlorides due to effective charge screening, whereas the presence of poly (acrylic acid) or NaH_2PO_4 increased the pH of the solution and stabilized the GO, either by electrostatic interaction or by steric repulsion. Therefore, the presence of abundant electrolytes and dissolved organic species in the natural aquatic environment could effectively alter the behavior of GO and these exacerbates must be taken into account while determining the crucial insights of toxicity.

Furthermore, several studies have reported to support GO as a degradable material through photo-Fenton degradation; however, the toxicity of their degradable products such as polycyclic aromatic hydrocarbons may have toxicological implications to human and to the environment (Bai et al., 2014). GO in the form of nanocomposites are widely used in sensor technology (Li et al., 2014; Xue et al., 2014). Generally, metals nanoparticles combine on the surface of graphene materials to achieve higher reactivity. However, these composites are much more lethal than the individual metal nanoparticles and can cause greater cytotoxicity when introduced internally into the cells.

Dissolved natural organic matter (NOM) is another important factor that control the behavior of NMs. A research group (Wang et al., 2016b) summarized the effect of interactions between NMs and NOM (Figure 2.4).

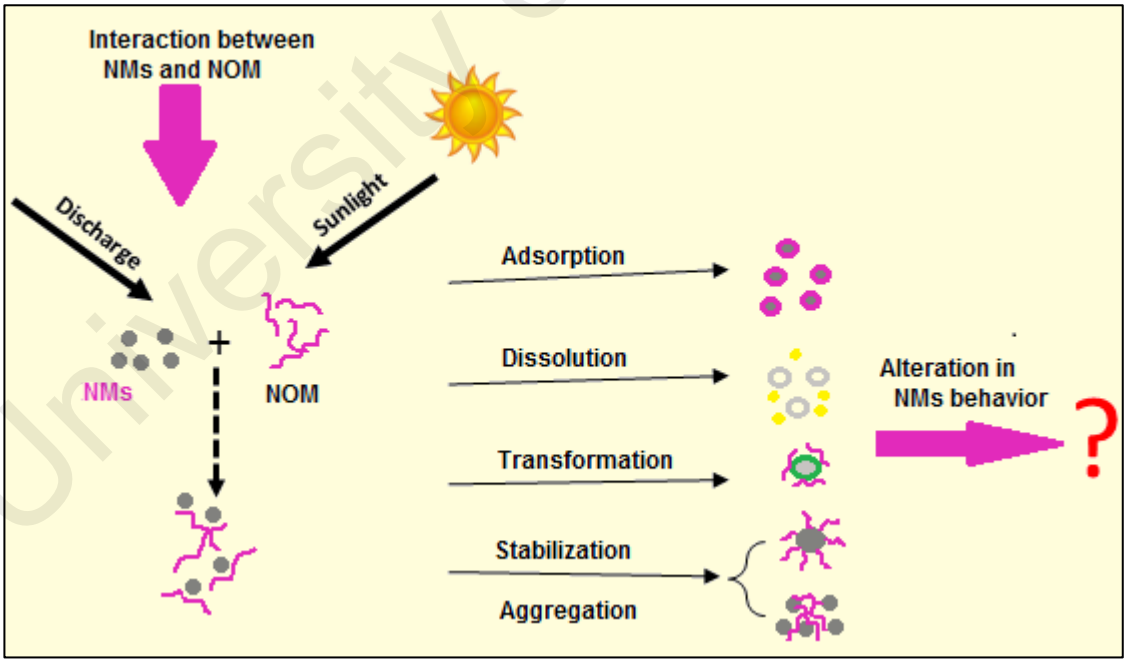

Figure 2.4: Effects of NOM on the surface properties of NMs (Wang et al., 2016b).

They found that, the main environmental processes influenced by NOM are adsorption, stabilization/aggregation, dissolution and surface transformation of NMs.

The adsorption or desorption properties of NMs are depend upon the nature of NOM. NMs interacted with NOM resulted in surface adsorption, dissolution and surface modification of NMs. For soluble NMs, their dissolution was generally promoted by interactinn with NOM although dissolution suppression was also reported. Besides dissolution, surface stabilization by NOM coating at the surface and aggregation of NMs are other two main surface transformation can occur on the NMs surface in the presence of NOM. Therefore, it was concluded that NOM can alter the behavior of NMs through changing surface properties and leads to the unknown electrostatic interactions and steric repulsion between NMs and environmental objects.

Despite number of studies on the NMs-NOM interaction, research gape still exist in most of the important areas (Wang et al., 2016b). The results obtained from the number of pionering studies on the NMs-NOM interaction are unable to directly explain the environmental process on large-scale aquatic system. Althouth methamatical models are powerful tools for explaining these interactions however, to date these methamatical models are less accurate due to lack of available data. These data includes attachment efficiency, dissolution rate which can well predict the behavior of NMs under complex conditions.

Most of the interaction studies are conducted under laboratory conditions which are far away from reflecting the actual scenario in natural environment. Transformation of NMs is another factor which influence the nature of NMs-NOM interactions and thereby making it harder to understand these interactions and their long-term environmental impact. Up to now, number of studies are seeking to clearify the specific mechanism altering the behavior of NMs nonetheless, the relationship between NOM mediated NMs toxicity has not been clearly understood.

The overall factors highlighted in this literature review are summarized in Scheme 2.1, which control the transport behavior of NMs in natural aqueous system. Altogether, up to the point of view of NMs behavior, the summarized data represent that the physicochemical properties, shape, size, surface charge and stability coating immensely control the dissolution, ionic release and aggregation behavior of NMs. Additionally, the environmental properties and solution chemistry such as pH, temperature, ionic strength, UV light, and dissolved total suspended materials drives mobility and control the behavior of NMs. Overall, these materials through dissolution released ionic species, which showed a spontaneous major source of damage to aqueous ecosystem.

The concentration of NMs also dictates and controls its behavior in a natural environment; therefore studies should be conducted using realistic environmental concentration. Kinetics is also an important parameter, and should be taken into account in NMs behavior studies in order to ascertain aggregation and dissolution behavior up to a longer exposure period.

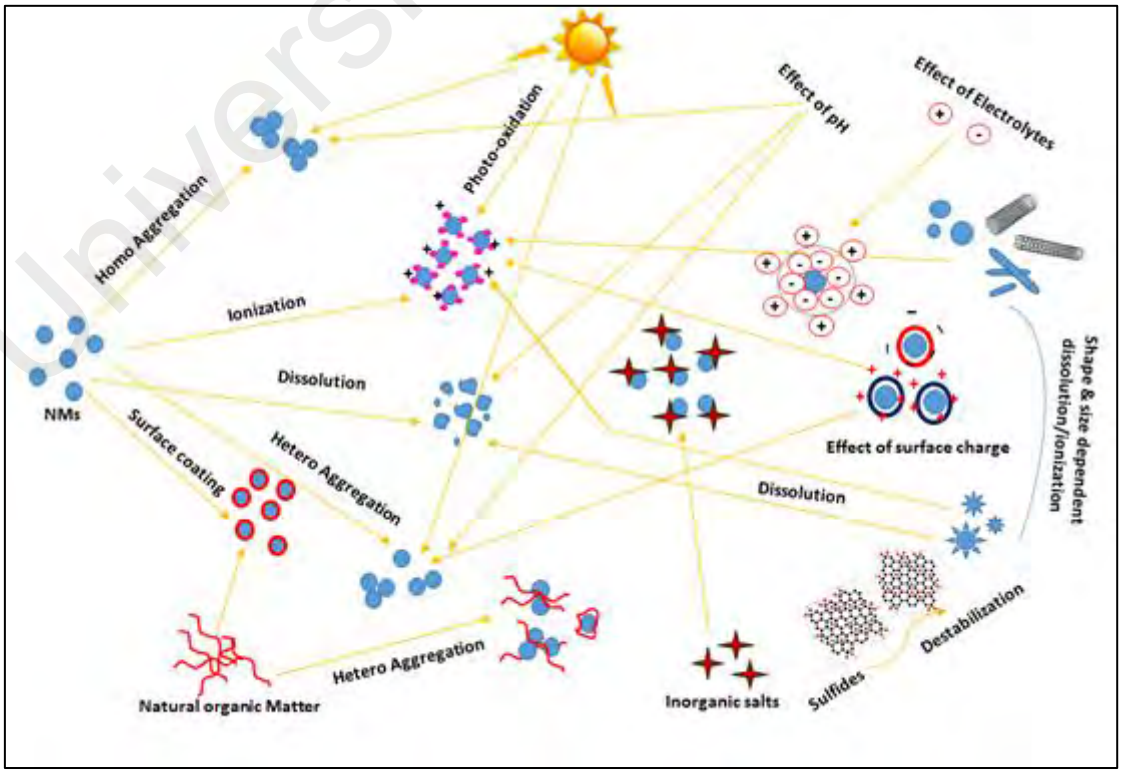

Scheme 2.1: Factors effecting the transport of NMs in the natural aqueous environemnt

2.2.3 Saturated Porous Media

The transport behavior of NMs in saturated porous media depends on the attachment or retention abilities of NMs. Though there are several other factors which influence the transport of NMs. Recently, Goldberg and co-workers (Goldberg et al., 2017) investigated the factors that control the verticle transport in saturated porous media. Catagorically, these factors are divided into two classes i.e., non-exponential (particle interaction, surface charge and mass influent) and exponential factors (aspect ratios, particle attraction condition and influent mass) that control the retention and transport (Figure 2.5).

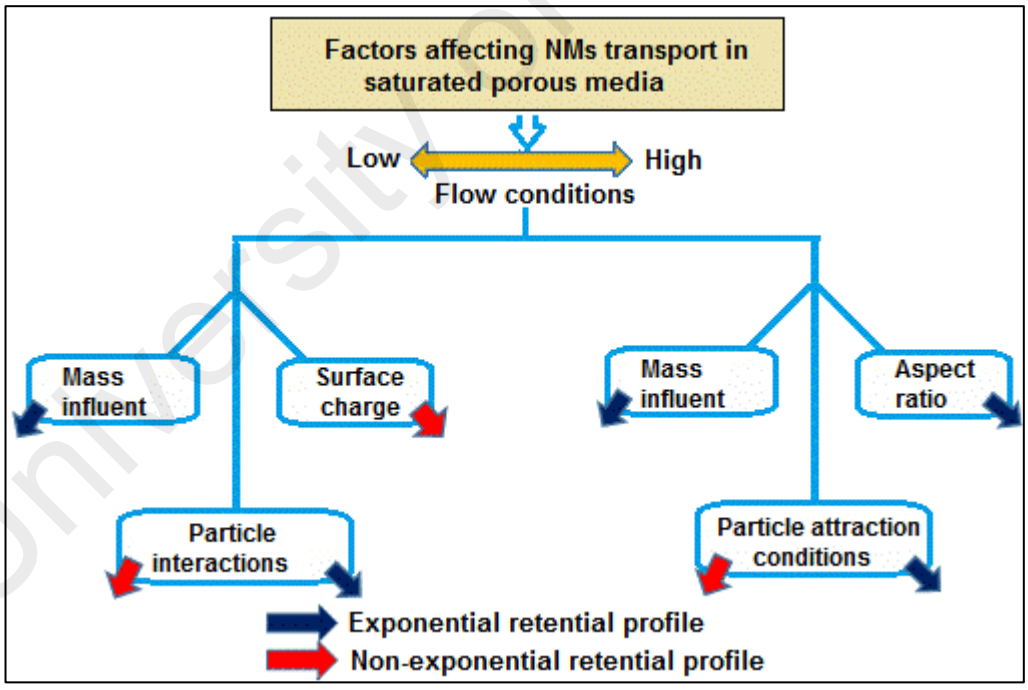

Figure 2.5: Factors influence the NMs transport in saturated porous media

The aspect ratio is the height of the transport column divided by the column diameter whereas, mass influent is the effect of mass or concentration of NMs passing through

the column. In another latest report (Wang et al., 2016a) the authors summarized the key findings from previous investigation and concluded that NMs transport in porous media is controlled by the combination of various factors related to the physical and chemical properties of the nanoparticle, nature of flow medium and flow rate.

The properties of NMs such as particles size, shape, surface charge, particles concentration have strong influences on the transport of NMs in porous media (Raychoudhury et al., 2012). None the less, the amount of studies on how particle shape affects NMs transport in porous media is far from adequate (Knappenberger et al., 2015). Previous reports suggested higher retention of rod-shaped particles than spherical particles in column experiments (Salerno et al., 2006). On the contrary, different result was observed by another research group (Liu et al., 2010c) who compared transport of spherical and rod-shaped microspheres. They observed less retention of rod-shaped colloids compared to spherical particles which was explained by preferential alignment of the rod-shaped colloids along the flow field.

These contradictory investigations revealed that the knowledge of the role of particle shape also plays on the transport of NMs in porous media is very limited and therefore needs further investigations (Wang et al., 2016a). Furthermore, the nature of porous media (i.e., solid-water, air-water, and air-water-solid interfaces) medium type such as glass beads, sand, grabbed soils and quartz sands) also affects NMs transport. In addition to this, the grain size of porous media (Garner et al., 2014), surface roughness, grain surface charge and moisture content due to ‘saturated’ (means all soil pores are fully filled with water) or ‘unsaturated’ soil means that the air phase exits in the soil pores (Figure 2.6) may introduce additional mechanisms of NMs retention and transport in porous media (Chen et al., 2010).

Some other factors include medium flow direction, flow velocity, medium pH, and medium ionic composition (Sharma et al., 2014).

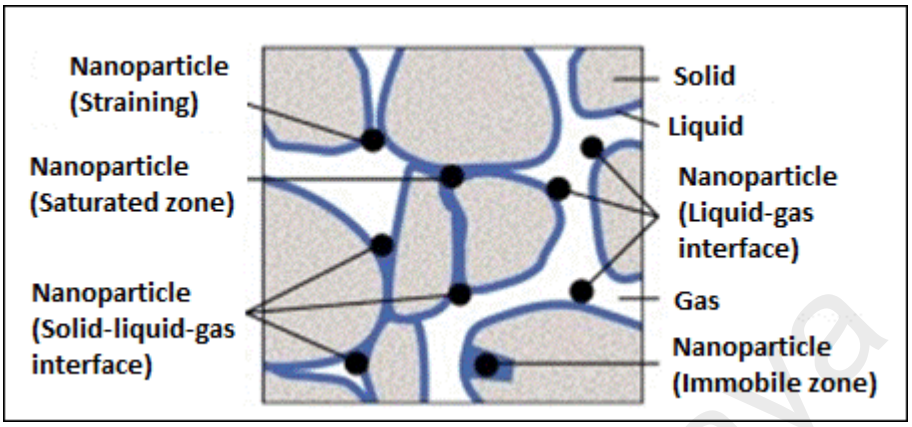

Figure 2.6: NMs transport in unsaturated porous media (Torkzaban et al., 2008).

2.3 Techniques Monitoring NMs Transport Behavior

There are several different techniques in monitoring the transport of NMs (Table 2.1) but many suffers with the inaccurate identification, quantification and matrix effect limitations.

In addition to other monitoring techniques; one of the most widespread detection technique for the identification, quantification and elemental characterization of NMs is ICP-MS. Taking advantages of the sensitivity robustness and low detection limit (up to pg g^{-1} with a wide dynamic range up to 9 orders of magnitude) this technique is widely utilized in monitoring the transport of NMs in to the different medium. Additionally, ICP-MS is independent of the virtual matrix effect (Costa-Fernandez et al., 2016).

A very important aspect of increasing utilization of this technique is that, it is not only enables a reliable elemental characterization of NMs, but it also provides a valuable information to quantify the release of ions from NMs. This parameter is of great importance in determining the transformation of NMs, such as dissolution, ionic

release and to investigate the cytotoxicity produced due to uptake of NMs up to the cellular level (Caballero-Diaz et al., 2013).

Table 2.1: Techniques monitoring the transport of NMs.

S. no	Nanomaterials	Techniques Employed	Medium	Limitations	References
1.	Gold and magnetite NMs	Nanoparticle tracking system (NTA)	Sediment-water	Tracking particles should be spherical in shape. Smaller particles appears dimmed or neglected due to light scattering by large particles	(Luo et al., 2017)
2.	Silica nanoparticles	ICP-OES	Porous media	High negative charge density limits the transport of Si-NPs due to electrostatic repulsion.	(Zeng et al., 2017)
3.	Graphene oxide	UV–Vis Spectrophotometer	water-saturated porous media	Use of UV–vis Spectrophotometer is limited to monitor the variation in the absorbance of colloidal or suspended species	(Wang et al., 2017)
4.	TiO_2NPs	SP-ICP-MS	Environmental waters.	Detection limit for NP diameter is 37 nm	(Vidmar et al., 2017)
5.	Fe_3O_4	flame atomic absorbance spectrometry	Plant	Absorbance misleading by refractory elements	(Iannone et al., 2016)
6.	Au/Ag-NPs, ZnO-NPs	ICP-MS	Partially saturated sand columns	-	(Yecheskel et al., 2016)
7.	AuNPs, AgNPs	Particle tracking method	water-saturated medium	surface-charge-dependent transport	(Naftaly et al., 2016)
8.	Gold nano-spheres, single-walled carbon nanotubes	UV–Vis spectrophotometer	saturated porous media	Limited to monitor the concentration of colloidal NPs	(Afrooz et al., 2016)

2.4 NMs Mobilization into the Plants

Another important feature in determining the behavior of NMs is the transport or mobilization of NMs into the living object such as plants. Recent investigations revealed that, NMs due to extensive utilization and components of numerous consumer goods and industrial products have the potential for high environmental build up and

finally disposed of in the natural aqueous system. After disposal, NMs may transport to plant life cycle and affect the plants differently at the physiological, biochemical, nutritional, and genetic levels. The toxicity threshold of NMs varies from one plant species to another. These toxicity responses to NMs are driven by a series of factors, including the NMs characteristics, plants species (Figure 2.7), and environmental conditions. However, a complete understanding of the dynamics of interactions between plants and NMs is not clear enough yet.

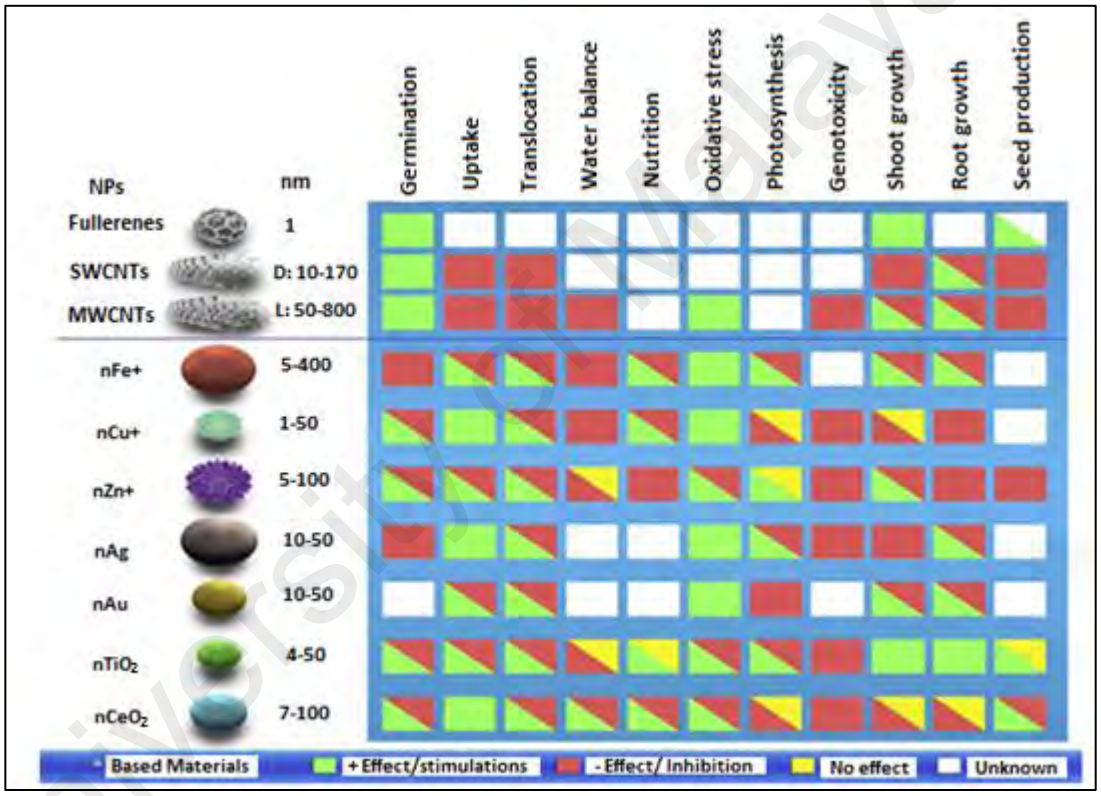

Figure 2.7: General trends of effects for NMs in plant growth. The contradictory responses have been detected (two colors in the same box), denoting that their effects depend on the specific kind of ENM, their concentration, and the plant species (Zuverza-Mena et al., 2017).

A good understanding of the interactions between NMs and plant systems is of paramount importance for assessing the toxicity and their possible tropic transport (Gardea-Torresdey et al., 2014). The properties that make NMs unique could adversely affect plants or favorably transform into good agriculture production. However, the

literature provides diverse, and often contradictory, results on the plant responses to NMs exposure. For example, (Mukherjee et al., 2014) and (Wang et al., 2013b) studied the transport of ZnONPs into the green peas and cowpea plants respectively. They found that ZnO was largely accumulated into the root tissues in a concentration-dependent manner. This accumulation was resulted in the generation of oxidative stress, and reduction in the physiological activities of plants.

Metal based NMs particularly metal oxides, due to their unique characteristics anticipated increased NMs utilization that prone to produce detrimental effects upon intentional or accidental release into the environment (Nel et al., 2006). In phytotoxicological investigations, several studies revealed that the interactions potentially depend upon the composition, shape, surface area and charge of NMs and plant anatomy (George et al., 2009; Ma et al., 2010; Moussa et al., 2016; Nordmann et al., 2015; Soni et al., 2015; Wang et al., 2014) .In comparison with other metal oxides, zinc oxide (ZnO) and titanium dioxide (TiO_2) nanoparticles are widely used due to their superior electrical, catalytic and light absorption capacity. Though, uptake, translocation and toxicity of ZnO and TiO_2 into the plants were studied previously. Nonetheless, the knowledge gaps in physiological and biochemical effects still exist in investigation of the effect of different metal oxides on same plant species under identical conditions. Furthermore, very little research is documented to encounter the impact of negatively charged metal oxides on plant growth stimulation or inhibition.

The behaviors and combined toxicity of metal oxides mixtures are rarely studied. However, results from a limited number of pioneering studies suggest that the toxic potential of metal oxides mixture are distinct from those of individual counterparts (Tong et al., 2015). In addition, there are no reports exist so far which deals with the comparative physiological and biochemical study using two negatively charged metal

oxides both in single versus mixture approach. In determining the physiological and biochemical impacts of NMs, another important aspect which is poorly understood in general is the kinetic evaluation of the NMs uptake into the plant tissues. As kinetics data observed how NMs are taken up into the plants and describe well about the short-term and mid-term uptake and distribution of NMs in plants.

The physiological impact of AgNPs to plant germination and growth extensively studies by several research groups (Nair et al., 2014; Thuesombat et al., 2014; Vannini et al., 2014) investigated the effect of different concentration of AgNPs on the germination of *Triticum aestivum L.* seedlings. They observed that AgNPs adversely effect on the seedling growth and causes modification of root tip cells due to alteration in several protein expressions. TEM analysis shows that this alteration is mainly due to the dissolved Ag^{+} from AgNPs. A research group (Frazier et al., 2014), investigated the effect of TiO_2NPs uptake on the growth, development and RNA expression of the tobacco plant (*Nicotiana tabacum*). The study found that synchronous increase in the exposure concentration of TiO_2NPs significantly inhibits germination rates, retard root length and biomasses of tobacco seedlings on 3-weeks exposure. Moreover prolonged TiO_2NPs exposure also influences the gene expression profile of micro RNAs that play an important role in plant development and tolerance to environmental stresses. TiO_2 NMs create interferences in root cell wall water uptake, generate oxidative stress and cause lipid peroxidation of tobacco cell membrane.

The previous study (Castiglione et al., 2014) determines the toxicity of TiO_2NPs on *Vicia Narbonensis L* seed germination. In this study seeds were exposed to different concentration of nanoparticles for 72 hours under environmental conditions. After 3 days treatment, the roots were collected for toxicological studies. They found that

phytotoxic activity of TiO_2NPs was due to the ROS production which resulted in DNA fragmentation through induced oxidative stress in the root apex.

Another group (Anjum et al., 2014) investigated the potential impact of graphene oxide nanoparticles (GONPs) in germination of faba bean (*Vicia faba L*). In this study they investigated effect of different concentrations of GONPs on the germination potential of faba been seedlings. Results revealed that GONPs, significantly inhibits the growth rate and activity of stress controlling enzymes through electrolyte leakage. In contrast, another study (Wang et al., 2014) determine the toxicity and translocation of GONPs both under normal and stress condition in *Arabidopsis* plants. They found that exposure of GONPs for 4 weeks did not produce any adverse effect in plant growth. However, GONPs under drought stress or salt concentration in the presence of PEG 6000 (20%) and NaCl (200mM) resulted in reduced root length.

A group (Larue et al., 2014) investigated the frightening internalization of AgNPs after exposure into the crop *Lactuca sativa* which retained into the leaves even after thorough washing with acidified water. During this study, they found that AgNPs effectively entrapped into the lettuce leaves through stomatal and cuticular penetration, diffused into the leaf tissues and form a complex with thiol-containing molecules after oxidation of AgNPs at the surface.

Therefore, knowing these facts the toxicity of these altered crops is questionable when exposed to human, although little is documented about the human toxicity by consumption of NMs particularly metal based NMs exposed crops. However, dissolution bioaccumulation and complexation via binding affinity may cause DNA damage or alteration in gene expression through inhibitory effect on DNA replication (Li et al., 2013). The literature from the physiological impacts and

mobilization of NMs into the plant species revealed that, the impact of NMs internalization is largely depending on the NMs characteristics and varied from one plant species to another. Though there is a lack of knowledge base in determining the effect of different NMs on a similar plant species under similar experimental conditions. Furthermore, there is still need in determining the kinetic uptake and physiological impacts of NMs up to the longer time period in order to investigate the reversal of NMs toxicological effects due to certain plant biological activities.

2.4.1 Factors Affecting the NMs Mobilization in Plants

Several studies revealed that the toxicity of NMs in plants is based on the plant-NMs physicochemical interaction resulting in the development of phytotoxicological effects on plant growth. There are several principle factors which influenced the interaction of NMs to plants. The main factors are concentration, size, shape, surface charge, surface area and stability of NMs. As Figure 2.7 represents, several factors such as NMs shape, size and surface properties dictates the toxicity response to plant growth. However, the effect of these properties varied from one plant species to another. Some other factors include the plant species, plant life cycle, NMs concentration and exposure period and growth media.

The corresponding size of the seeds also play fundamental role in describing the interaction with NMs. For example, single-walled carbon nanotubes display higher toxic effects in small-seeded than large-seeded species because of surface to volume ratio (Canas et al., 2008). Likewise, the smaller size of NMs is believed to cause higher plant toxicity than larger sized NMs. Another study manifested that small sized (0.6-2 nm) silver colloid showed more toxicity in flax, barley and ryegrass than 5 nm and 20 nm silver nanocolloids (El-Temsah et al., 2012). Another major factor that affects the toxicity is the concentration of NMs. For example, ZnONPs at concentration of 1000

mg/L, caused the death of almost all the tissues of ryegrass root tip (Lin et al., 2008b). Similarly, in another study Nair & Chung suggested that silver nanoparticles at as minimum concentration as 1mg/L, caused significant physiological and molecular level stress resulting in reduced root growth and root apex death. For instance, most the previous phytotoxicity in plants species reported with higher a concentration, (Lopez-Moreno et al., 2010) that may not be realistic than real environment. Therefore, studies with more realistic NMs concentration are needed at this time. Further, these studies should be conducted for longer exposure period to investigate if plants after sometimes recovered from the initial toxicity exhibited by NMs. The effects of NMs thus vary from one plant species to another, the types of NMs, concentration, size, and exposure period also effect in determining the toxicity of NMs.

2.4.2 Techniques Monitoring NMs Mobilization to Plant

There are several different techniques monitoring the mobilization of NMs into the plants like ICP-MS, ICP/OES, flame atomic absorbance spectrometry and X-ray absorption, and X-ray fluorescence (XRF) techniques. Recently a research groups (Ma et al., 2017; Vinkovic et al., 2017) described the transport and distribution of cerium oxide (CeO_2) and silver nanoparticles (AgNPs) in cucumber and pepper plant tissues, respectively and metal uptake were quantified by ICP-MS, transmission electron microscope (TEM), X-ray absorption, and X-ray fluorescence (XRF) techniques. Similarly, in another study (Dan et al., 2016) investigated the plant uptake and accumulation of CeO_2 nanoparticles into four crop species by single particle ICP-MS method. Several other techniques like flame atomic absorbance spectrometry are also utilized for the determination of NMs transportation into the plants. For example, a group (Lannone et al., 2016) quantifies the transport and mobilization of iron

nanoparticles in wheat (*Triticum aestivum L.*) development by flame atomic absorbance spectrometry. ICP/OES is another reported technique (Lopez-Moreno et al., 2017) for the evaluation of ZnO nanoparticles on corn seedlings. However, in obove all mentioned techniques, the ICP-MS is the most utilized technique for the determination and quantification of metal uptake into the plants tissues because of its sensitivity robustness and low detection limit as discussed in section 2.3.

2.5 Remediation of NMs

With the continuously growing number of products containing NMs, the environmental release of NMs during production, use, and end-of-life becomes inevitable. Owing to its vast industrial utilization and disposal, NMs has been recognized as a source of pollution in the natural aquatic system. Despite of the well documented toxicity of metal based NMs such as zinc, titanium and silver NMs; they are actively used in various industries and discharged into water bodies (Nam et al., 2014). In present time, NMs pollutants are highly observable even at low concentrations. In which most of them are very stable towards biodegradation, sunlight exposure and naturally occurring oxidizing agents; thus creating a potential danger for (ecological and health problems) irrigation, drinking and agricultural purposes. Therefore, removal of NMs contaminants from natural water prior to their utilization is necessary through the development of eco-friendly, cost effective removal techniques.

In the present era of scarcity of water resources, effective treatment or NMs pollutant remediation is proved to be a major prerequisite for a growing economy (Adeleye et al., 2016). It is critical to develop and implement advanced treatment technologies with high efficiency and low capital requirements and time consumption. Among the various treatments (Sarkka et al., 2015; Zimoch et al., 2014), recent advanced processes in nano-material sciences have been attracting the attention of

scientists. Figure 2.8, represents the present methodologies used for the pollutant removal from the aqueous environment. However, most of these methodologies suffered from high operation and maintenance cost, high energy requirement, toxic degradation products and also sometimes offers incomplete removal. Therefore, in the above context, there is a real requirement for more efficient and powerful technologies for natural water treatment.

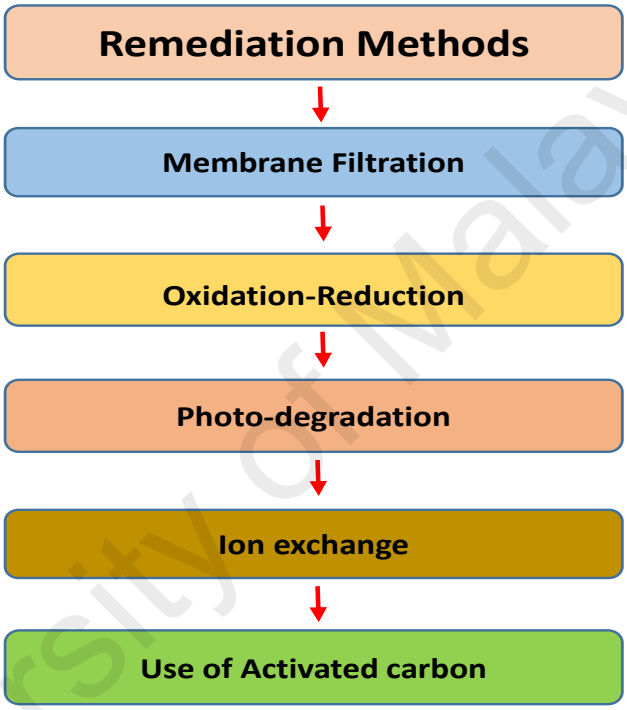

Figure 2.8: The presented methodologies used for the remediation of pollutants from the aqueous environment.

Nanotechnology has been cited in different literatures, as one of the most advanced processes for water treatment. Based on the nature of NMs, these materials are categorized into three main classes. Nano-membranes (1), nano-catalysts (2) and nano-adsorbents (3). Nano- membranes are extensively used in wastewater treatment process in which the pressure driven treatment has been proved ideal for improving water quality (Rao, 2014). In the second class, mostly metal oxides or semiconductors have gained considerable attention. Different types of nano-catalysts are employed for the

pollutant removal through electrocatalysts, Fenton reaction based catalyst and oxidative-reductive catalysts (Dutta et al., 2014; Kurian et al., 2015; Ma et al., 2015a).

In a nano-adsorption technology, numerous and effective works have been published recently with the aim to investigate the removal of pollutants using nano-adsorbent. Nano-adsorbents are broadly classified into various groups based on their role in the adsorption process. It includes metal based nanoparticles, nano-structured mixed oxides, magnetic nanoparticles and metal oxide nanoparticles. Moreover, various types of silicon nano-material are also used as nano-adsorbents such as silicon nanotubes, silicon nanoparticles and silicon nano-sheets.

Various technologies such as ion exchange, membrane filtration, electrolytic removal and reduction have been reported for the removal of NMs. But these technologies suffer several disadvantages of high operation and maintenance cost, high energy requirement or incomplete removal. Thus, to prevent deteriorating surface water quality there is a need for exploring alternative remediation techniques for efficient NMs removal even at low aqueous concentrations (Ruparelia et al., 2008). Many kinds of adsorbent materials such as carbon based materials (Pattanayak et al., 2000) zeolite, cyclodextin (Badruddoza et al., 2013), and chitosan (Vunain et al., 2016) have been employed for the NMs removal purposes. However, none or very few studies focus on the removal of NMs from the natural water system. Since the natural water contains various kinds of interfering materials which may collectively pose inhibitory effects on the effectiveness of removal processes.

In present time silica based materials has been actively incorporated into various fields of applied and health sciences because of its nontoxic (Xia et al., 2009), thermally stable (De Matteis et al., 2015), optically transparent (Shi et al., 1997), biocompatible (Catauro et al., 2015), chemically inert (Ide et al., 2015) and well-

known surface properties (Mhamane et al., 2016). These properties of silica-based materials made them a good candidate for various biological, catalytical and environmental applications. The use of silica confers great stability to the nanoparticles dispersion against changing of pH and concentration of electrolytes (Mulvaney et al., 2000). Additionally, the incorporation of iron oxides increases the removal efficiency by increasing the surface area (Ponder et al., 2001). A research group (Zhang et al., 2016b) synthesized monodispersed hollow aluminosilica microspheres for the removal of methylene blue and Congo red from aqueous solution with maximum adsorption capacities of 87.80 mg/g and 252.53 mg/g respectively.

In addition, a research group (Bao et al., 2017), synthesized mercaptoamine-functionalised silica-coated magnetic nanoparticles for the removal of mercury and lead ions from wastewater. The basic mechanism for metal ions removal was based on sorption phenomenon which likely occurred by chelation of the amine group and ion exchange between heavy metal ions and thiol functional groups of the nanoadsorbent. The underlying method displayed maximum adsorption capacities for mercury and lead ions were 355 and 292 mg/g, respectively. Similarly, in another study (Bao et al., 2016), they demonstrated that, the selective removal of zinc(II) ions with amino-functionalized magnetic silica nano-adsorbent. The adsorbent was synthesized by solvothermal method which showed maximum removal efficiency for zinc(II) ions as 69.5 mg/g.

However, the proposed method suffers from complex and time consuming methodology for the synthesis of nano adsorbent. Furthermore, the synthesized adsorbent can be utilized within the pH values of 1-5 which limits its utilization for zinc(II) removal from natural water with a pH range from 5-7.

In other research reports Nithya and Yao et al, described the removal of Cr(VI) ions from aqueous solution using silica nanocomposites (Nithya et al., 2016; Yao et al.,

2016). All these studies suggested that the excellent adsorbent properties of silica micro/nano composites in combination with the unique porous structures, making them an ideal candidate for natural and wastewater treatment. Table 2.2, represented the summarized data of some adsorbents previously synthesized for the remediation of metals and organic pollutants.

Table 2.2: Reported adsorbents used for the remediation of metals and organic pollutants.

S. No	Adsorbent Type	Synthetic Method	Size of Adsorbent (nm)	Adsorbate	Removal Efficiency (mg/g, mg/L)	References
1	Silica Microparticles	Silanization method	1.2 µm	Hg(II)	185 mg/g	(Yu et al., 2012)
2	Aluminosilica Microsphere	Forcing hydrolysis method	1 µm	Methyleneblue and Congo red	87 and 252 mg/g respectively	(Zhang et al., 2016b)
3	DNA-Chitosen complex	Electrostatic complexation	-	Fullerene,nanot-ubes, and AUNPs	1.9, 26, and 20 mg/L respectively	(Zinchenko et al., 2013)
4	β-Cyclodextrin Nanofiber	Electrospinning technique	-	Methyleneblue	826 mg/g	(Zhao et al., 2015)
5	Ni/Mg/Al hierarchical materials	Hydrothermal method	2-3 µm	Congo red and Cr(IV)	1250, and 103.4 respectively	(Lei et al., 2017)
6	Fe/SiO_2-NH_2 hollow sphere	Stober method	950 nm	Cr(IV)	8 mg/L	(Yao et al., 2016)
7	Bioinspired 2D-carbon/Fe_3O_4 nanocomposite	Pyrolysis	11-20 nm	AS(III)	57 mg/g	(Venkateswarlu et al., 2016)
8	EDTA-Graphene oxide composite	Oxidation and silylation process	-	Pb(II)	479 mg/g	(Madadrang et al., 2012)
9	Mercaptoamine-functionalised silica-coated magnetic nano-adsorbents	Co-precipitation methods	13.6 nm	Hg(II) and Pb (II)	355 and 292 mg/g respectively	(Bao et al., 2017)
10	Multiwalled carbon nanotubes	Refluxing and Co-precipitation methods	14 nm	Cd(II)	87.81 mg/g	(Gatabi et al., 2016)

11	Quercetin modified α-Fe_2O_3 nanoparticles	Chemical impregnation method	-	Congo red	427.35 mg/g	(Satheesh et al., 2016)
12	Amino-functionalized Fe_3O_4@SiO_2 magnetic nano-adsorbent	solvothermal method	80 nm	Zn(II)	169.5 mg/g	(Bao et al., 2016)
13	Iron-oxide Nanoparticles	Precipitation method	19.9 nm	Cu(II) and Pb(II)	19.61 and 47.62 mg/g	(Tamez et al., 2016)
14	Superparamagnetic maghemite (γ-Fe_2O_3) nanoparticles	Flame Spray Pyrolysis	15.7 nm	Pb(II) and Cu(II)	69 and 34 mg/g respectively	(Rajput et al., 2017)
15	Thiol-functionalized MCM-41 mesoporous silica	Evaporation induced self-assembly	-	Cu(II), Pb(II), Ag(I) and Cr(III)	38.12, 66.04, 92.08 and 13.84 mg/g respectively	(Wu et al., 2010)
16	Magnetic Iron nanoparticles	Teflon-sealed autoclave method	250 nm	Methylene blue and Congo red	44.38 and 11.22 mg/g respectively	(Zhang et al., 2011)
17	Magnetite nanorods	Thermo decomposition method	22 nm	Cr(III)	1 mg/g	(Zhu et al., 2011)
18	Magnetite nanorods	Pulsed current electrochemical method	900-1000 nm	Fe(II), Pb(II), Zn(II), Ni(II), Cd(II) and Cu(II)	127, 113, 107, 95, 88 and 76 mg g^{-1} respectively	(Karami, 2013)
19	Ionically modified magnetic nanomaterials	Condensation reaction	15 nm	As(V) and Cr(VI)	50.5 and 35.2 mg/g respectively	(Badruddoza et al., 2013)
20	Sulphurised activated carbon	Carbonization and sulphurization	-	Zn(II)	147 mg/g	(Krishnan et al., 2016)
21	Silica gel modified with 2,4,6-trimorpholino-1,3,5-triazin	Reflux	-	Ag(II)	0.38 mg/g	(Madrakian et al., 2006)
22	Silica nanocomposites	Hydrothermal method	200 nm	Cr(III)	37.44 mg/g	(Egodawatte et al., 2015)
23	Multi-carboxyl-functionalized silica gel	Surface grafting method	-	Cu(II), Cd(II), Ni (II) and Zn(II)	47.07, 41.48, 30.80 and 39.96 mg/g	(Li et al., 2014)
24	PEI-grafted magnetic nano powder	Co-precipitation method	500-800 nm	Cu(II), Zn(II) and Cd(II)	157.8, 138.8 and 105.2 mg/g respectively	(Pang et al., 2011)

For the remediation purposes several technologies has already been developed for the removal of organic and metal pollutants in which nano-based materials was found to be efficient, cost effective and with low capital requirement and time consumption. However, new eco-friendly remediation techniques are required for fast and efficient NMs removal process in the natural aqueous medium.

2.5.1 Factors Affecting Remediation Process

Factors controlling the properties of nano-adsorbents are size, surface chemistry, agglomeration state, shape and fractional dimension, chemical composition, and solubility (Bao et al., 2017; Zhang et al., 2016d). The concentration of adsorbate is another factor which describes the effectiveness of the remediation process. For instance, a study revealed that the adsorption of Cr(VI) decreases as the initial concentration increases. Whereas, at lowest concentration maximum adsorption was observed (Fu et al., 2017).

Contact time is also an important factor in adsorption process. Earlier adsorption report for the removal of Cu(II) and Zn(II) revealed that the adsorption of metal ions was fast during the initial contact time of 30 min with 97.5% to 90% removal respectively (Salam et al., 2011). In Addition, another study demonstrated that particle size of the adsorbent and reaction temperature also affects the remediation process. For example a group (Ali et al., 2016) studied the effect peanut hulls size on the removal efficiency, they found that smallest peanut hulls has the highest Cu% removal then the larger particle size.

This effect was apparent due to increased surface area of peanut hulls which facilitates higher adsorptive active sites for Cu adsorption. They also studied the effect of reaction temperature on adsorption process and found that, for this particular type

of adsorbent the removal efficiency increases from 83% to 87% as the temperature of the reaction mixture increases from 25-65 ºC. In conclusion, all these factors are significant and need to be demonstrated in designing any effective remediation technique for the removal of metal and non-metal pollutant.

2.5.2 Techniques Used to Monitor Remediation Process

There are various techniques used to monitoring the remediation process. For instance; a groups of researchers (Bagbi et al., 2017; Sleiman et al., 2017) established a removal of lead and phosphate using zero valent iron (ZVI). The removal process was monitored by Atomic absorption spectrometer and flame atomic absorption spectroscopy (AAS) respectively. Similerly, in another study a research group (Razzaz et al., 2016) described the removal of Pb(II) and Cu(II) ions by Chitosan nanofibers functionalized by TiO_2 as adsorbent. The adsorbtion of metal ions was monitored by the Inductively coupled plasma atomic emission spectrophotometer (ICP-AES).

In addition to above spectroscopic techniques, inductively coupled plasma-optical emission spectroscopy (ICP-OES) was also used for determination of metal ion concentration in water samples (Lingamdinne et al., 2017). Inductively coupled plasma mass spectrometery (ICP-MS) is another very useful technique to determine the dissolved concentration of metal ions with detection limits in a parts-per-billion or subparts-per-billion (Rodriguez et al., 2016) after the completion of adsorption experiments. The supernatent solution were collected, acidified and analyzed by ICP-MS using reference material as standard.

2.6 Study Area and Geographical Input

The vast industrialization, uncontrolled urbanization and rapid economic development increase the pollution load around many cities into river system and

changes the water quality. In Malaysia one of the most important rivers is Klang River. The approximate length of this river is 120 km and the total catchment area is about 1288 km^2. The river have 11 main tributaries such as Sungai Batu, Sungai Gombak, Sungai Ampang, Sungai Penchala which received high percentile of sewage discharge from food, chemicals, semi-conductor and electrical industries, rubber processing and palm oil processing discharges (Naji et al., 2010). Furthermore, agricultural activities well as atmospheric fallout also increase the degree of river water pollution. The river mainly flows through the whole city of Kuala Lumpur and eventually flows into the straits of Malacca. In this research the river water samples from seven different locations was selected based on the urbanization and population of the area. Approximately more than 4.4 million people (16% of the national population) living around this area (Naji et al., 2010). Therefore, it may act as better source of most polluted natural water and act as a better candidate to study the mobilization and removal of NMs.

CHAPTER 3: METHODOLOGY

3.1 Introduction

In this chapter, specific details of methodology for the synthesis of NMs, details of characterization techniques, natural water sampling and processing, evaluation of NMs transport behavior, metals uptake and mobilization into the plant and the remediation of NMs were discussed. For remediation study, the synthesis of polymer modified mesoporous silica iron microcubes, NMs adsorption, adsorption kinetics and adsorption isotherm were elaborated. Figure 3.1, represented the framework for overall methodology adopted in this research.

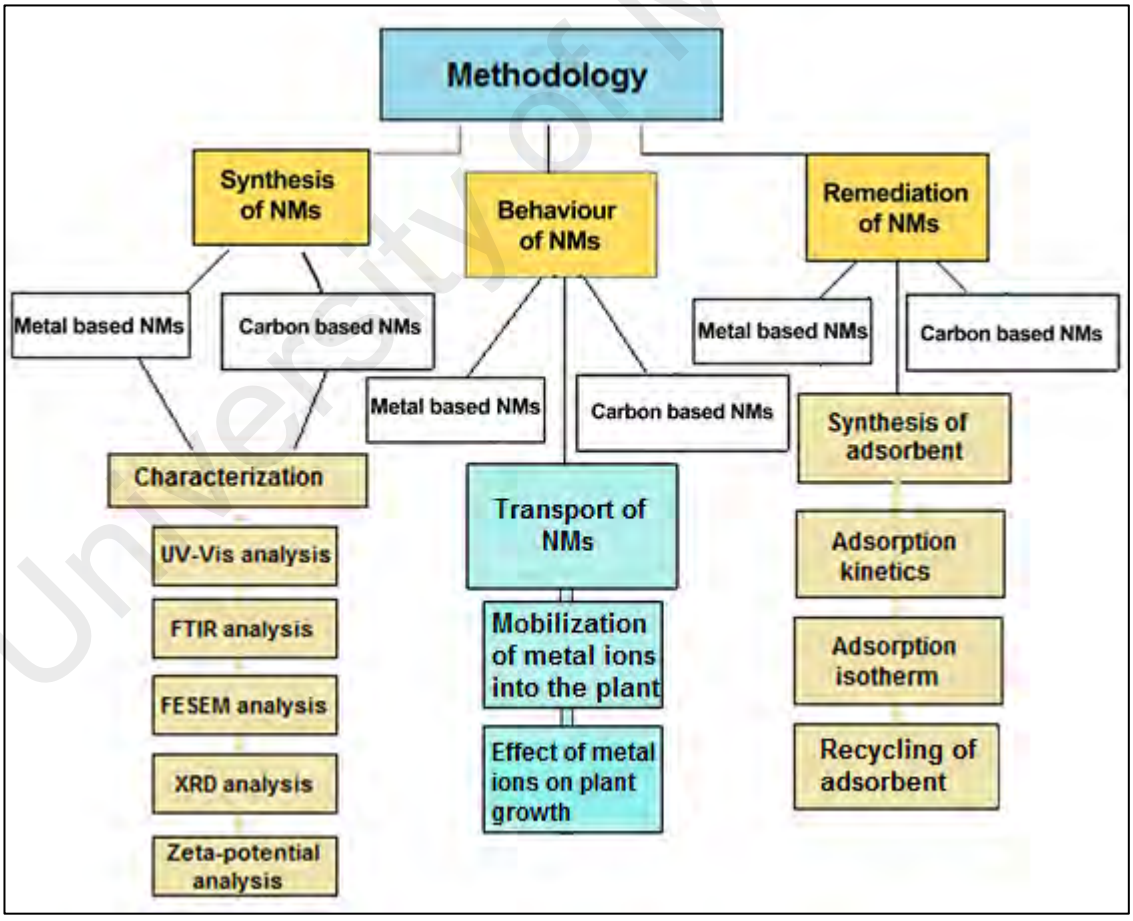

Figure 3.1: Frame work for methodology.

3.2 Synthesis of NMs

In this research metal and carbon based NMs comprising of three metal and two carbon based NMs were synthesized. In metal based NMs, polyethylene imine coated silver nanoparticles (PEI@AgNPs) were newly synthesized in this research. Whereas, polyethylene glycol coated zinc oxide nano-rods (PEG@ZnONRs) and titanium dioxide nanoparticles (TiO_2NPs) were synthesized by following previous published reports with slight modifications (Pimentel et al., 2014; Brauer et al., 2014). For morphological comparison of NMs, two zinc oxide structures i.e., zinc oxide nano-needles and zinc oxide micro-flowers were also synthesized. Since the comparison of the effect of morphology of metal based NMs has to stick to the similar metal and the mobility behavior should be compared under similar experimental conditions. Therefore, to investigate the role of morphology, zinc oxide nanoneedles (ZnONNs) and zinc oxide microflowers (ZnOMFs) were also synthesized by following modified published reports (Pimentel et al., 2014; Wahab et al., 2007a) and the mobility pattern of all synthesized zinc oxide structures was compared.

Carbon based NMs including carbon nanoparticles and graphene oxide quantum dots were synthesized by following earlier reports (Jahan et al., 2013; Tang et al., 2012). The details of the synthesis of all metal and carbon based NMs are described below in details. Recently, a growing research interest was developed in attachment of polymers such as cationic polymer polyethylene imine (PEI) and anionic polymer polyethylene glycol (PEG) and other hydrophilic polymers at the surface of NMs. The polymer attachment at the surface not only minimizes the extent of particle aggregation by providing stability, but also modified the aqueous mobility of NMs. Therefore, to determine the impact of polymer surface coating in particle dissolution, aggregation and mobilization, the synthesized silver and zinc NMs were surface functionalized with cationic PEI and anionic PEG polymers. This imparts positive and negative surface

potential to NMs, respectively in order to investigate the effect of surface charge on mobility. While titanium dioxide NMs were kept polymer uncoated for comparison study.

3.2.1 Synthesis of Metal based NMs

3.2.1.1 Synthesis of PEI Coated Silver Nanoparticles (PEI@AgNPs)

In a typical synthesis of PEI@AgNPs, $AgNO_3$ (5mM): L-cysteine (0.112mg/ml): PEI (500 µL into 5 ml of DW) was mixed in a molar ratio of [1: 0.008: 0.006]. Then freshly prepared solution of $NaBH_4$ (1x 10^{-6} M) was added to the reaction mixture. The mixture was then heated and stirred at 75 ºC and ~1100 rpm respectively. After 10 min, the color of the solution becomes brown which correspond to the synthesis of polymer coated silver nanoparticles PEI@AgNPs. The mixture was heated and stirred for further 2 hours for the maximum synthesis of monodispersed PEI@AgNPs. After synthesis, the PEI@AgNPs solution was centrifuged (Thermo/Multifuge X3 FR ultracentrifugation) at 10,000 rpm for 15 minutes to remove unreacted precursors, washed twice with ethanol and conductivity (Thermo Scientific Orion Star A112 conductivity meter) was measured to ensure the removal of residual ions (Li et al., 2010).

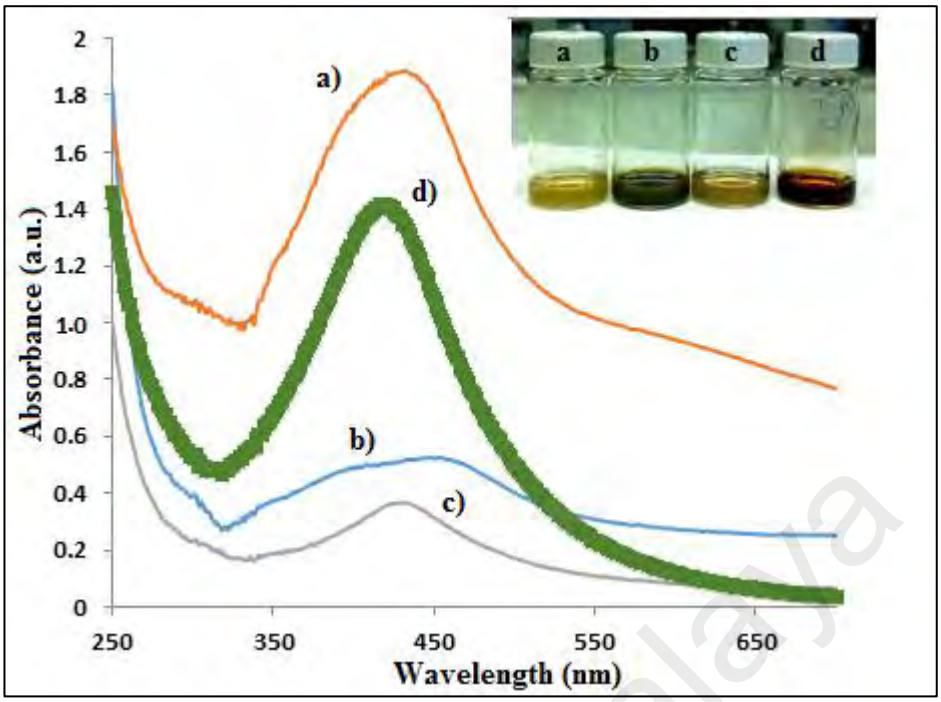

Figure 3.2: Optimization of PEI@AgNPs in presence of HCl at pH 3 (a), in absence of PEI (b), in absence of L-cystine (c) and in presence of all reactants i.e., $AgNO_3$+ L-cystine+ PEI+ $NaBH_4$(d).

The optimization of synthesized PEI@AgNPs was carried out in presence of HCl at pH-3 (a), in absence of PEI (b), in absence of L-cystine (c) and in the presence all reactants i.e., $AgNO_3$+L-cystine+PEI+$NaBH_4$ (d) as represented in Figure 3.2. The best particles were formed in presence of all reactants (d). The complete synthetic reaction scheme of PEI@AgNPs is presented in Scheme 3.1.

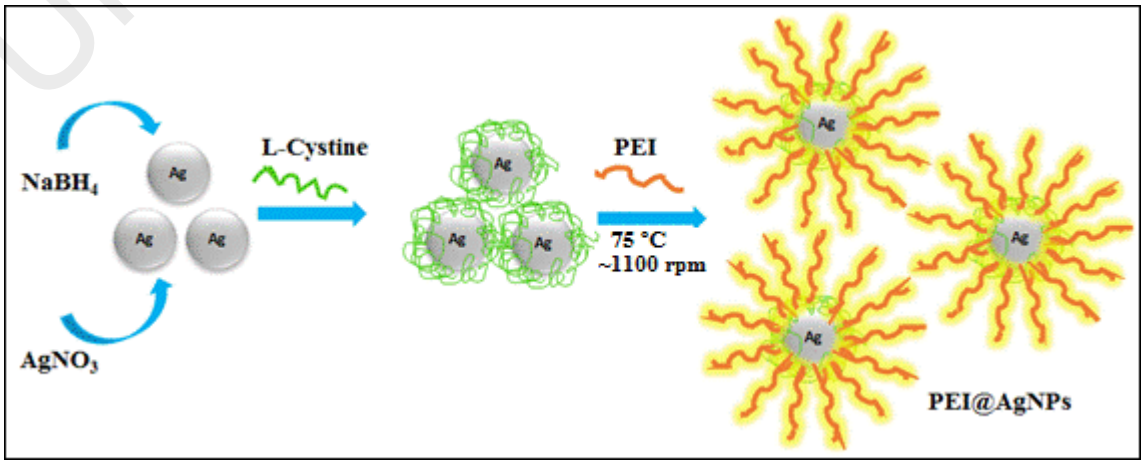

Scheme 3.1: Schematic representation for the synthesis of PEI@AgNPs.

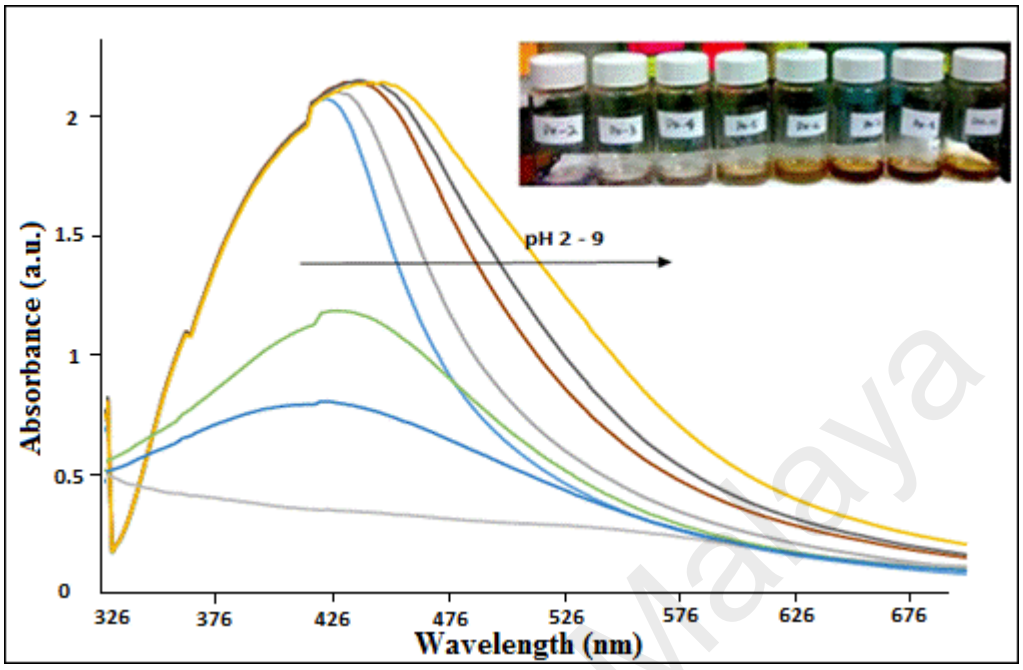

Figure 3.3: Effect of solution pH on synthesized PEI@AgNPs.

After synthesis of PEI@AgNPs, the stability was determined under a wide range of solution pH. As shown by Figure 3.3, the synthesized particles were quite stable at pH range from 5-8. However, as the pH increases, the color of the solution of PEI@AgNPs intensified due to cross-linking phenomenon among the silver nanoparticles (discussed in detail in chapter 4).

3.2.1.2 Synthesis of Zinc Oxide Structures

Synthesis of PEG Coated Zinc Oxide Nano-rods (PEG@ZnONRs)

PEG@ZnONRs was synthesized by following published protocol by Pimentel et al., 2014 with slight modifications. Briefly, 3.9 g of Zinc acetate dihydrate solution (0.45M) in deionized water was mixed with NaOH solution (8 M). The continues stirring of the solution yield a transparent Zn $(OH)_4^{-2}$ solution. The mixture was

allowed to cool down at room temperature then 5g of PEG in 90 ml of deionized water (6.9 mM) was mixed with 12 ml of Zn (OH) $_4^{-2}$. The resulting mixture was heated hydrothermally at 100 ºC for 5 h.

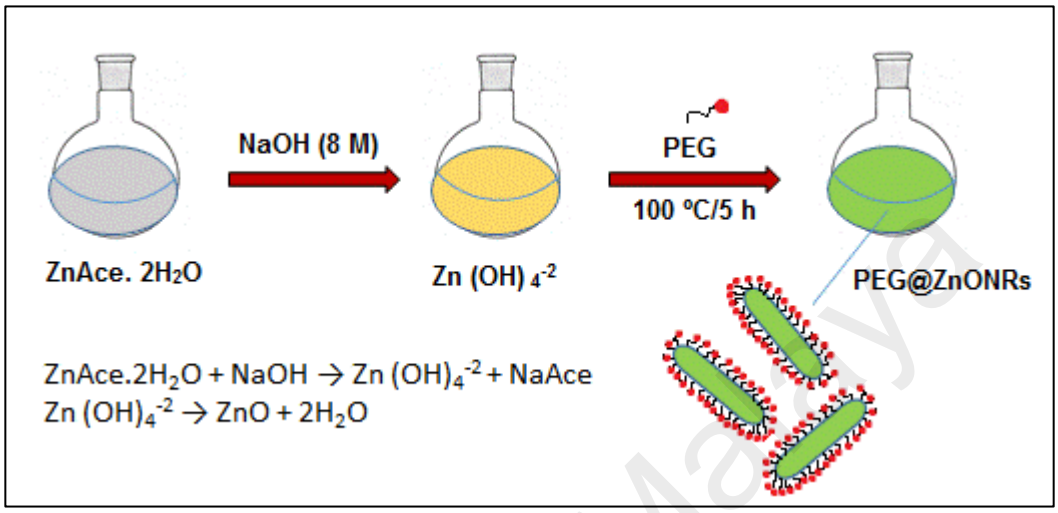

Scheme 3.2: Schematic representation for the synthesis of PEG@ZnONRs

The white precipitates of PEG@ZnONRs were then washed several times with 2-propanol and DW water and centrifuged at 4500 rpm for 10 min to remove unreacted precursors. The complete schematic representation for the synthesis of PEG@ZnONRs is presented in Scheme 3.2.

Synthesis of Zinc Oxide Micro-flowers (ZnOMFs)

ZnOMFs were synthesized following the same methodology as described in synthesis of PEG@ZnONRs except variation in the heating temperature and time i.e., 150 ºC for 24 h. After synthesis the precipitates were washed as described in the synthesis of PEG@ZnONRs.

Synthesis of Zinc Oxide Nano-needles (ZnONNs)

In the synthesis of ZnONNs 0.1 M zinc acetate dihydrate dissolved in 25 ml of deionized water was mixed drop wise with 8 M aqueous solution of sodium hydroxide

(10 ml) while stirring it continuously. The stirring was continued for 15 min. Subsequently, the resultant solution was transferred to sonication bath where it was sonicated for 1 h. The white precipitate formed was filtered, washed with the methanol and dried at room temperature.

3.2.1.3 Synthesis of Titanium dioxide Nanoparticles (TiO_2NPs)

For the synthesis of TiO_2NPs, reported methodology by Brauer et al., 2014 was followed with slight modifications. Typically, 15ml of the titanium isopropoxide solution was mixed with 10 ml of 2-propanol (solution A). In a beaker 100 ml chilled deionized water was added and the pH was adjusted to ~3 with HCl (solution B). Dropwise addition of solution A to solution B, with vigorous stirring at 1100 rpm, produced white precipitates of TiO_2NPs. The precipitates were washed several times with deionized water and centrifuged at 4500 rpm for 15 min to remove unreacted precursors. The overall process of TiO_2NPs synthesis is presented in Scheme 3.3.

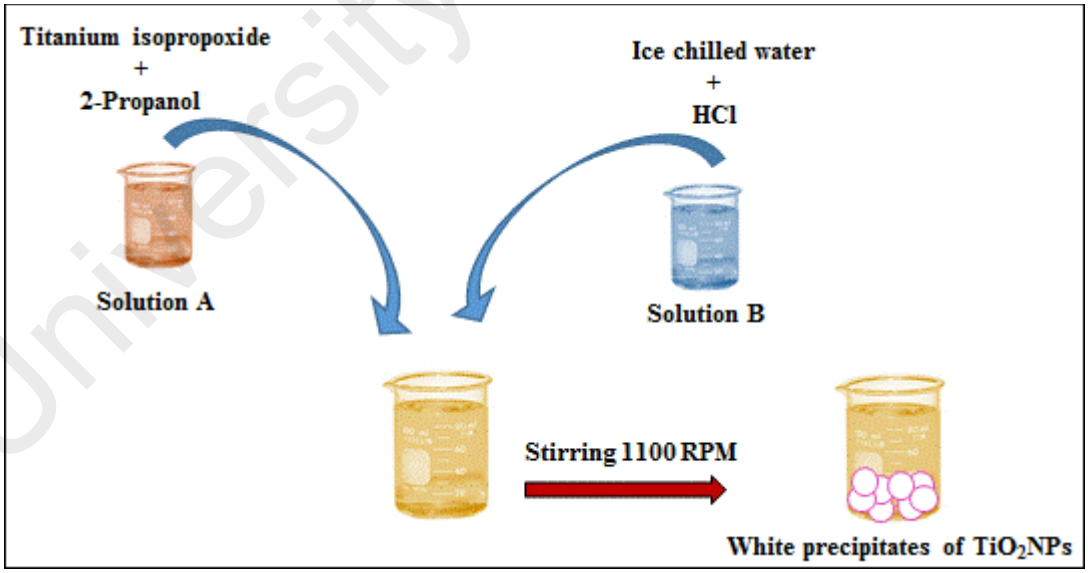

Scheme 3.3: Schematic representation for the synthesis of TiO_2NPs.

3.2.2 Synthesis of Carbon Based NMs

3.2.2.1 Synthesis of Carbon Nanoparticles (CNPs)

CNP was synthesized by following previous report by Jahan et al., 2013. Firstly, 0.0927 g of boric acid was dissolved in 15 mL of deionized water and then mixed with 0.025 g of N-(4-hydroxyphenyl) glycine at pH 9 (Scheme 3.4).

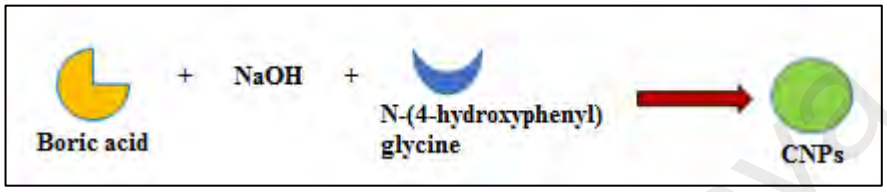

Scheme 3.4: Schematic representation for the synthesis of CNPs.

The mixture was then allowed to react hydrothermally with vigorous stirring at 6000 rpm at 300 ºC for 2.5 h. The resulting dark brown solution of CNPs was dissolved in deionized water, rinsed thoroughly with anhydrous ethanol and centrifuged at 5000 rpm for 15 min. The precipitate was then washed with deionized water several times to remove adsorbed ethanol.

3.2.2.2 Synthesis of Graphene Oxide Quantum Dots (GOQDs)

GOQDs were synthesized by hydrothermal pyrolysis of sucrose molecules (Tang et al., 2012) at 400 ºC for four hours. Typically, 6 g of sucrose molecules were dissolved in 10 ml of deionized water and the pH of the solution was adjusted to 9 by adding sodium hydroxide (1M). The resulting mixture was heated hydrothermally producing a pale yellow solution of GOQDs from colorless (Scheme 3.5). Subsequently, the solution is allowed to dry in an oven at 100 ºC to remove the water molecule and the resulting product of GOQDs in powder form is stored at room temperature for further characterization.

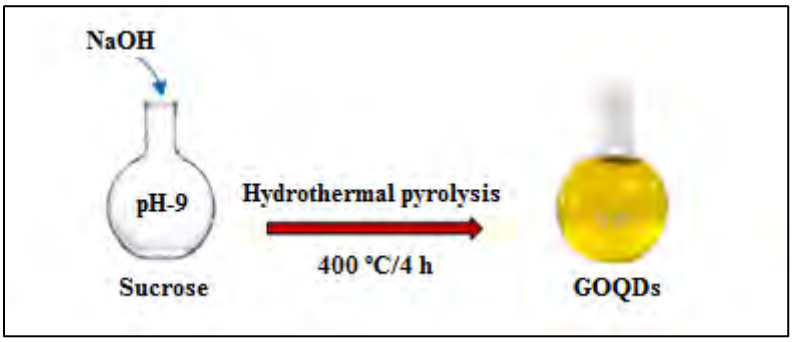

Scheme 3.5: Graphical representation of the synthesis of GOQDs.

3.3 Characterization of NMs

3.3.1 Ultraviolet Visible Spectroscopy (UV-Vis)

All the synthesized metal and carbon based NMs were characterized by UV-visible spectroscopy. The NMs samples were prepared in deionized water (2 ml total volume) and deionized water was used as reference solution in reference cell. The spectra was taken at fast scan rate; slit width =1, with spectral range between 200-700 nm. For all the UV-visible investigations, SHIMADZU-3600 UV-VIS-NIR was used Figure 3.4a.

3.3.2 Fourier Transform Infrared Spectroscopy (FTIR)

The synthesized NMs were also characterized by FTIR spectroscopy. The synthesized NMs were dried properly into the powder form and FTIR spectra were taken by placing 2 mg of sample into the sample holder. All the spectra were taken at attenuated total reflectance (ATR) mode using Perkin Elmer Spectrum-400 instrument (Figure 3.4b). Each spectrum was taken within the spectral range of 400-4000 cm^{-1}.

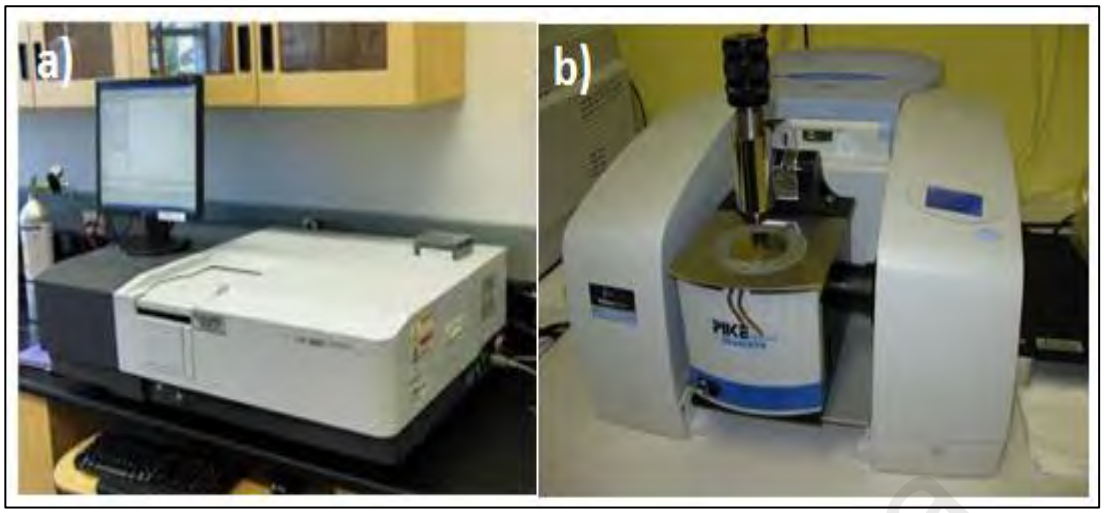

Figure 3.4: The UV-Vis (a), and FTIR spectrophotometer (b).

3.3.3 Field Emission Scanning Electron Microscopy (FESEM)

For the surface structure characterizations, size and morphological investigations of all synthesized NMs; FESEM technique was utilized by using FESEM, Hitachi-SU8220 (Figure 3.5a). The sample was prepared by drying a drop of NMs solution into the clean ITO thin film at conductive side and images were taken at bright field detection mode.

For the FESEM analysis of plant tissues, the plant parts were cut into thin slice using clean blade, dried on ITO thin film and images were taken using bright field detection mode.

3.3.4 X-Ray Diffraction (XRD)

The phase identification of synthesized NMs was determined by X-ray powder diffraction (XRD) technique. For XRD characterizations of synthesized NMs, 5 mg of samples was used and powder XRD technique was employed at 20 ˚C with scan range

between 5-80˚. All spectra were taken by utilizing XRD, PANalytical-EMPYREAN (Figure 3.5b).

Figure 3.5: Instruments used for FESEM (a), and XRD analysis (b).

3.3.5 Brunauer-Emmett-Teller (BET)

BET analysis is an important analytical technique which explains the physical adsorption and desorption of gas molecules on a solid surface for the measurement of the specific surface area of materials.

In this research the important informations about the synthesized mesoporous silica adsorbent material was characterized by BET analyzer (Micromeritics ASAP2020) Figure 3.6a to determine the surface area, pore size and pore diameter. For this purpose 10 mg of powder sample were placed into the sample holder and BET analysis were performed. Nitrogen gas was used for adsorption and desorption property investigation of synthesized mesoporous silica material.

3.3.6 Particle Size and Zeta-Potential Analyzer

For the determination of particle size and zeta-potential, particle size analyzer in low volume disposable cuvettes Malvern Nanosizer zn3600 was used (Figure 3.6b).

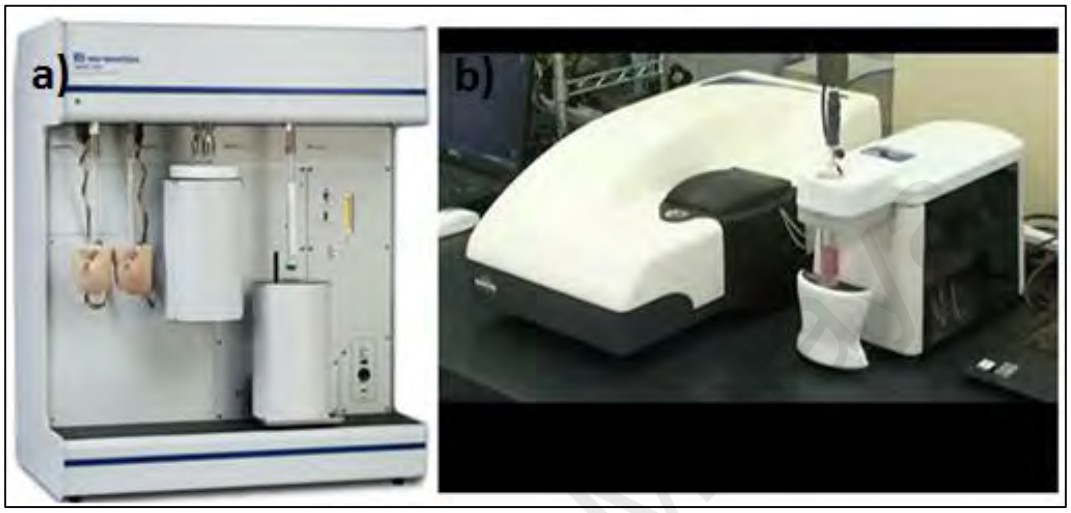

Figure 3.6: Brunauer-Emmett-Teller (a), and Zeta-potential analyzer (b).

1 ml sample solution was used in cuvette and surface charge and zeta-potential values of all synthesized ENMs and adsorbent material was determined. Each sample measurement was performed at least in a triplicate analysis and mean values were recorded.

3.4 Instruments Used for NMs Transport and Mobilization

3.4.1 Ultracentrifugation

The centrifugation of all samples was carried out using Thermo/Multifuge X3 FR ultracentrifugation (Figure 3.7a). The centrifugation of all the NMs samples used in transport investigation was performed at least at 4000 rpm for 20-30 min depending upon the centrifugation requirement. All centrifugation was performed in 10 ml centrifuge tube.

3.4.2 Conductivity Measurement

The conductivity of solution or the mobility of ions in sample was measured by Thermo Scientific Orion Star A112 conductivity meter (Figure 3.7b).

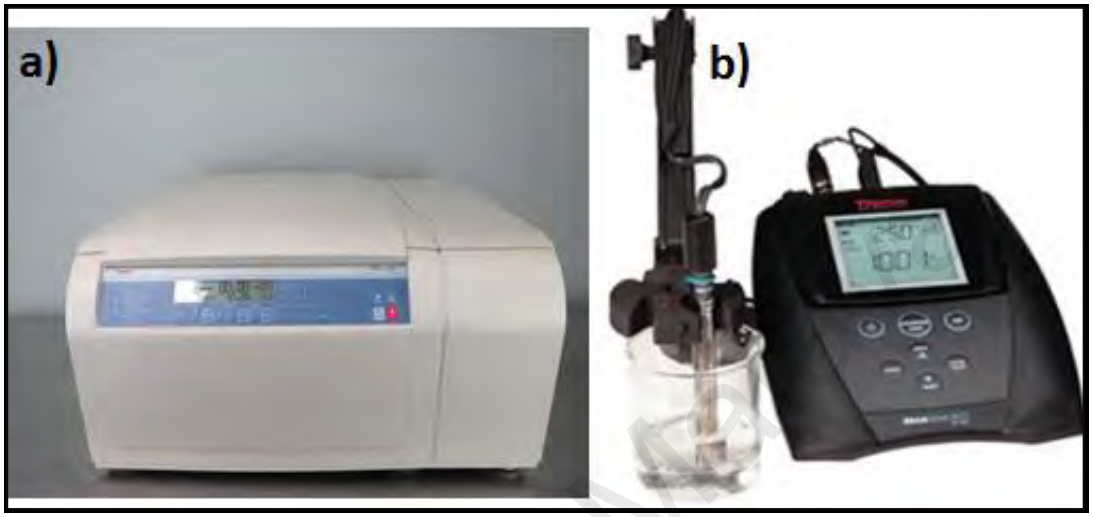

Figure 3.7: Ultracentrifuge (a), and conductivity meter (b).

Conductivity measurements were used in this research to measure the ionic content in a sample solution. Conductivity was measured in mS/cm which was directly linked to the total dissolved ions.

3.4.3 Inductively Coupled Plasma Mass Spectrometry (ICP-MS)

For the determination of metal ion concentrations in sample solutions for transport and mobilization investigations, ICP-MS, Agilent 7500-series (Figure 3.8a) was used with limit of detection (LOD) of 0.05 ppb. Typically, 10 ml volume of each sample was acidified using analytical grade HNO_3 (0.5 %) total volume and metal concentration was determined using standard reference solution. The natural RW dissolved metal ions concentration was investigated by diluting each sample 50 times,

acidified with HNO_3 (0.5 %) and total metal ions concentrations were investigated by ICP-MS analysis in ppm.

3.4.4 Ion Chromatography (IC)

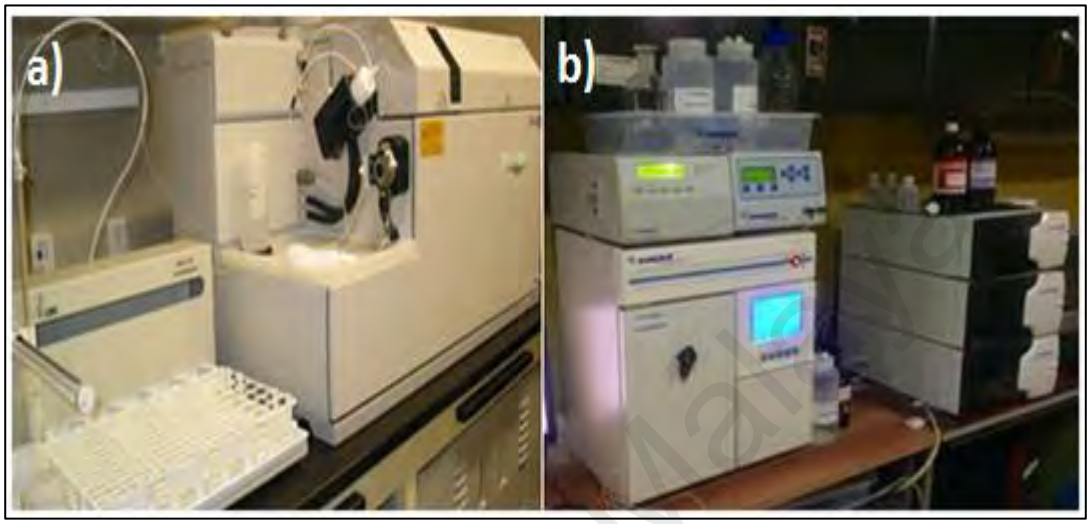

Figure 3.8: ICP-MS (a) and IC spectrometer (b).

For the determination of various anions present in river water, ion chromatography (86 Advance compact, IC) was used (Figure 3.8b). All the samples were filtered through 0.2 mm pore size filter paper, diluted 50 times and pass through the ion chromatographic column for the determination of respective anions.

3.5 Natural River Water Sampling and Processing

3.5.1 Pre-sampling Preparation

For the storage of water samples, 2L plastic bottles were first soaked in 10 % nitric acid solution for at least 24 h. Then the bottles were washed thoroughly with distilled water and dried at room temperature. All portable meters, pH meter (Orion Star A211), dissolved oxygen meter (HANNA-SN 08257498, Europe), Van Dorn horizontal (KC-Denmark) water sampler were calibrated before going to sampling location. Other

sampling necessities GPS apparatus for the measurement of longitudes and latitudes of sampling stations, distilled water, note book, gloves, face mask, lab coat, safety belts, tagging taps for labeling, and tissue box were kept ready.

3.5.2 River Water Sampling and Preservation

River water (RW) samples were collected at seven different locations (n = 3) between September and January 2015-2016 along Klang River (Figure 3.9). The RW sampling was performed from the seven different locations in order to cover the maximum change in water chemistry. Each sampling were performed in triplicate by using Van Dorn horizontal (KC-Denmark) water sampler and stored in pre-cleaned 2L plastic bottles. Each sample bottle were labeled and kept in an ice box.

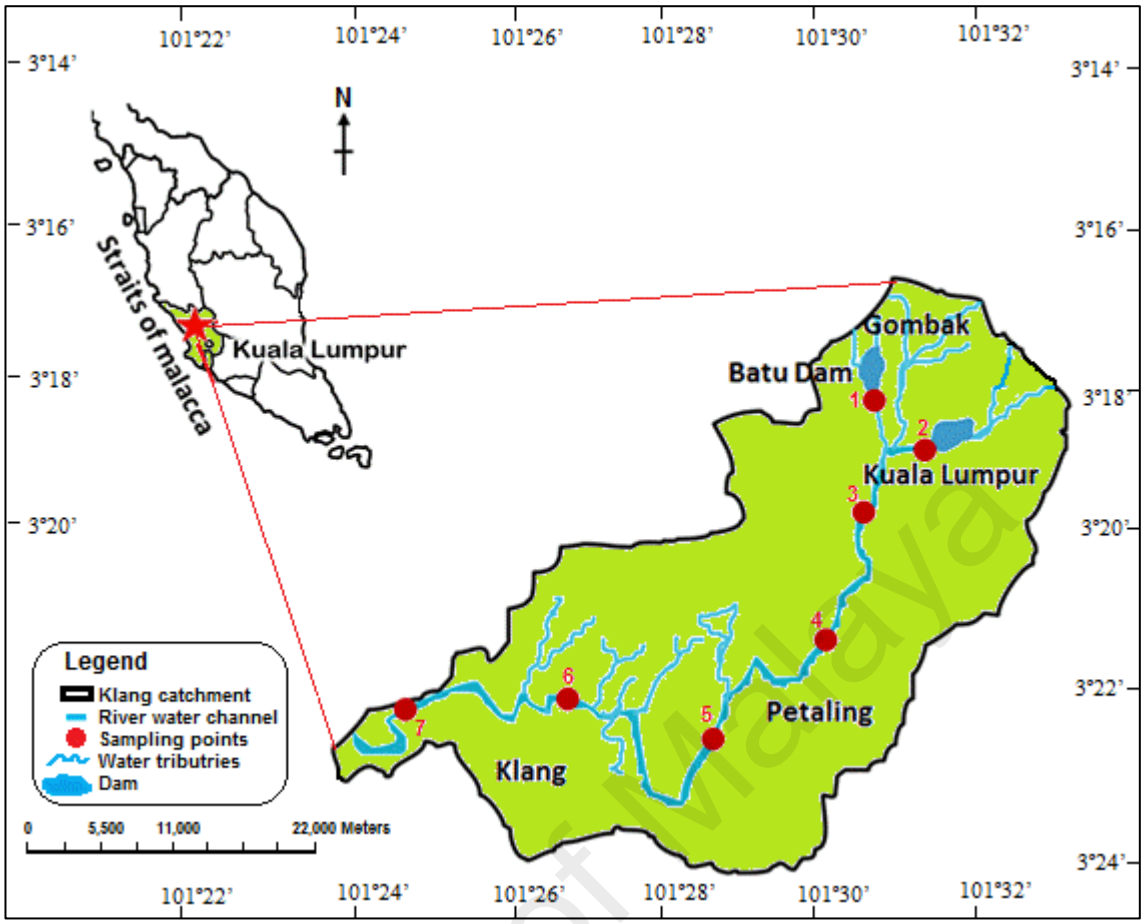

Figure 3.9: Study area and geographical locations of seven sampling stations in Klang River

After collection of water samples, initial parameters such as pH, turbidity, conductivity, temperature and total dissolved oxygen were measured using portable meters which were already calibrated using calibration standard solutions.

As soon as the field work was completed, samples were stored in the hydrogeology laboratory and preserved at 4 °C for future analysis. The samples were filtered through Whatman No.1 filter paper into pre-cleaned volumetric flasks. The supernatants of each fraction were analyzed for cations and anions determination using inductively coupled plasma mass spectrometry (ICP-MS) and ion chromatography (IC).

3.6 Water Analysis

3.6.1 Determination of Anions

Water samples collected from seven different locations of Klang River filtered through Whatman No.1 filter paper and was sent for ion chromatography-IC (861Advanced Compact-Metrohm, Switzerland) for determination of anions. The anions present in water samples such as chlorides (Cl^-), fluorides (F^-), sulfates (SO_4^{2-}), phosphate (PO_4^{3-}), bromides (Br^-) and nitrates (NO_3^-) were analyzed. Typically total 2 mL volume of each sample was run for 15 min in IC instrument and concentration of anions was obtained in the form of spectra. Multielement IC-standard solution (Sigma Aldrich) was used from 5 mg/L to 30 mg/L for the detection of all listed anions.

3.6.2 Determination of Cations

For determination of cations in water samples, 10 mL of samples were first acidified with nitric acid (5 % total volume), diluted up to 50 mL and analyzed using ICP-MS (Agilent 7500ce-USA). The important cations present in water samples such as sodium (Na^+), potassium (K^+), calcium (Ca^{2+}) and magnesium (Mg^{2+}) were analyzed. The Multielement standard solution for all cations were prepared and diluted as described above for water samples. For calibration plot, five standard solutions of Multielement standard solution (10, 30, 50, 70 and 100) ppm were prepared carefully. In the calibration plot for each element the correlation coefficient was 0.995 to 0.999 depending on the element. To verify the method, the efficiency of ICP-MS was detected by spiking different concentrations of Ag, and found to be in good agreement between certified and recovered values (Table 3.1).

Table 3.1: Recovery of spiked Ag by ICP-MS

Spiked value (ppb)	Analyzed value (ppb)	Recovery (%)
10 ± 0.76	9.7 ± 1.0	97
50 ± 0.02	49.4 ± 0.06	98.8
100 ± 0.23	98.9 ± 0.86	98.9

3.7 Transport Behavior of NMs

As discussed in chapter 2, porous column transport experiments were widely utilized to investigate the behavior of NMs. In this research the transport behavior of all synthesized metal and carbon based NMs was determined in natural river water. A glass column with an inner diameter and length of 3 cm and 15 cm respectively was wet-packed with Amberlite XAD4, 20-60 mesh size, with an average diameter of 560-710 μM corresponding to a total pore volume of ~0.55 ml/g. Amberlite was used as packing material because it is non-ionic cross-linked copolymer, with a large surface area and with a homogeneous pore distribution. It is the much use type of packing material in most of the studies because of its good physical, chemical and thermal stability even in wide range of acidic and basic media (Ozdemir et al., 2004). After a wet packing, the column was pre-equilibrated with at least 10 pore volumes of each RW sample, or NMs-free salt solutions of desired ionic strength and pH to equilibrate the chemical condition and to establish steady saturate flow.

Figure 3.10, representing the schematic diagram of the column experimental setup used in this research. The horizontal column with laminar flow (flow rate = 1 ml/min) was selected as it mimic the natural river water flow rate as also reported by

Subari, Osman, & Saim (2017). Since the RW water samples were taken from the middle of river, therefore, in order to mimic the realistic water flow rate 1 mL/min velocity was selected. The dispersed NMs were injected from the inlet, the column effluent was collected after every 10 min and the results were recorded.

For column transport experiments, RW samples from three locations (sampling station 1, station 4 and station 7) were selected because of obvious variations in terms of pH variation, dissolved oxygen and concentration of anions and cations. The choice of these sampling points was focused on the determination of the effect of solution chemistry on the mobility and transport of NMs as also considered by Gao et al., (2009) in prvious report. In this report Gao et al., (2009) found that water sample from different locations of same river displayed distinct solution chemistry which in turn greatly affect the transport or mobility of NMs. Therefore, in this research river water sample from three locations i.e., station 1, station 4 and station 7) were selected.

The same set of column experiment was also conducted using synthetic or deionized water (DW) and the effect of pH and ionic strength was examined. For all the column experiments, the ionic metal released and NMs retention into the column have been investigated in triplicate to permit the experimental variability to be assessed.

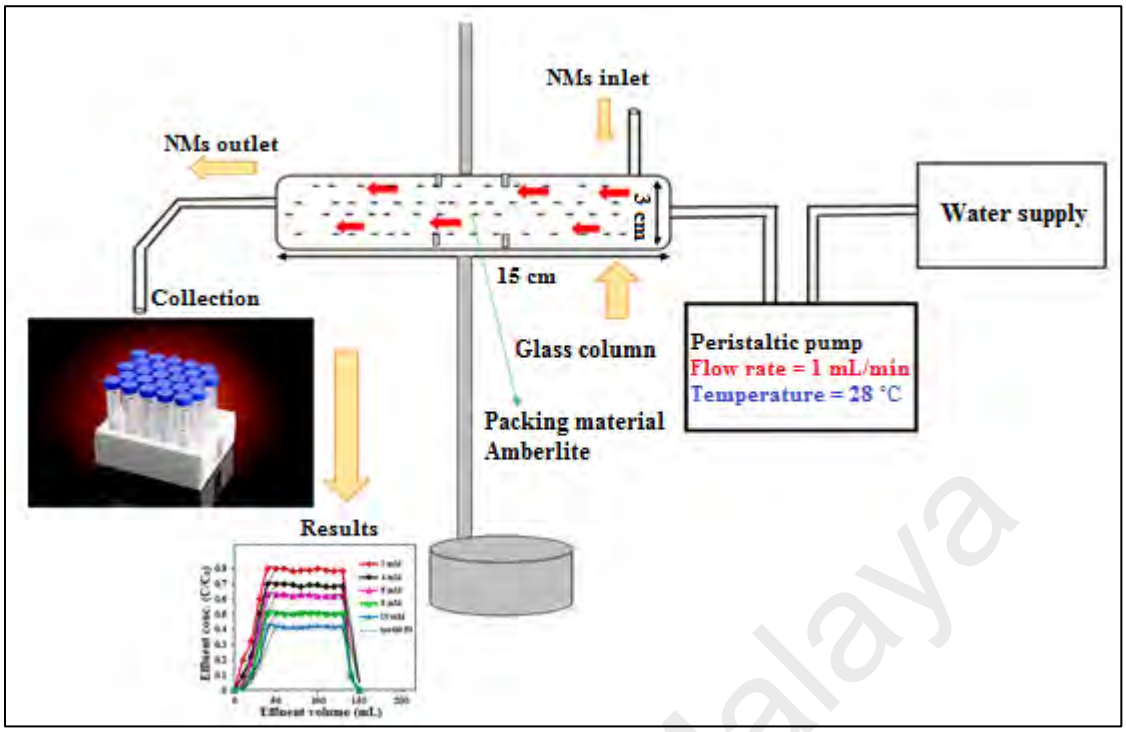

Figure 3.10: Schematic diagram of the column experiment.

3.7.1 Transport Behavior of Metal based NMs

The column transport behavior of metal based NMs particularly the ionic dissolution was quantified by ICP-MS analysis. The use of ICP-MS to measure metal ions offers a highly sensitive method and has been established as the most reliable technique for quantification of metal ions (Figueroa et al., 2016). Typically, 30 mg/L concentration of metal based NMs was used in this study as also reported previously (Phenrat et al., 2009) in the transport experiment of iron nanoparticles. The NMs dispersed in RW samples and ultrasonicated (POWERSONIC 405) for 20 min. The undissolved fraction of NMs was removed by centrifugation at 4000 rpm for 20 min. The concentration of dissolved NMs in suspensions was immediately determined by ICP-MS analysis. The NMs suspension was introduced into the column through the inlet, at 28 ºC (1 ml/min flow rate). To make sure the behavior of NMs is according to natural phenomenon and interrelated with actual sampling site other parameters like water flow,

pH and temperature was maintained. After every 10 min, 5 mL column effluent was collected in 10 mL sterile centrifuge tubes and centrifuged at 10,000 rpm for 40 minutes to remove any suspended particle or precipitates.

The clear supernatant was filtered through cellulose membranes with a particle size limit of 1-2 nm and UV-Vis absorption spectra were taken to ensure no detectable plasmon resonance optical absorption peak for metal nanoparticles (Liu et al., 2010a). This verified the metal based NMs existed as free ionic metal rather than bound nanoparticulate form. Then 1 mL of suspension was acid digested by 2 mL of trace-metal grade HNO_3 (70%, w/w, Fisher Scientific) and heated on a hot plate at 100 °C for 30 min (Zhang et al., 2011). The digested solutions were diluted and the concentrations of ionic metal, originated from metal based NMs ionic dissolution were measured using ICP-MS analysis. The kinetic of ionic metal release in deionized water was also evaluated by replacing the RW to deionized water for a similar time period. All column experiments were performed in a triplicate and the mean values were recorded.

To describe the experimental results with the kinetic model, the dissolution rate of metal based NMs was tentatively described by a modified first-order kinetic rate equation as described by Kittler et al., 2010.

$$y(t) = y\,(final)\,(1-\exp(-kt)) \quad \text{.....(Equation 3.1)}$$

Here y(t) is the $[M^+]_{released}$ (in the form of % of the original value), y(final) is the $[M]_{initial}$ i.e., at $t \rightarrow \infty$ (in the form of % of the original value), k is a rate coefficient, and *t* is the time (min). The values for y(final) and k were extracted from the data by suitable least-squares fitting. Mathematically, this corresponds to the product formation of a first-order reaction, which may be smaller than one. Using above equation the

experimental results were compared with the kinetic model equation, to derived the released ionic metal concentration ($[M^{+}]_{released}$) as a function of time (t).

3.7.2 Effect of Surface Coating

Surface coating effect on the mobility of metal based NMs was determined by two polymer coated (PEI@AgNPs & PEG@ZnONRs) and one uncoated metal nanoparticle (TiO_2NPs). All three NMs were dispersed in RW as described in section 3.7.1, transported from column and the concentration of ionic metals i.e., Ag(I), Zn(II) and Ti(IV) from PEI@AgNPs, PEG@ZnONRs and TiO_2NPs was determined by ICP-MS analysis. The results obtained from column transport experiment were also compared with kinetic model equation (Equation 3.1).

3.7.3 Effect of Size and Morphology

For the size and morphology investigation on the behavior of metal based NMs, three zinc xide structures (PEG@ZnONRs, ZnONNs and ZnOMFs) were selected and effect on the particle dissolution and ionic metal release was investigated. The results obtained were also compared by kinetic model equation (Equation 3.1).

3.7.4 Effect of pH

To determine the effect of change in the solution pH on the stability and ionic metal release, the influence of pH on synthesized NMs was investigated. A series of solutions complementary to RW pH (Station-1, Station-4 and Station-7) were prepared in DW. The solution pH was maintained by adding sodium hydroxide solution (1 mM). The effect of pH variation on the stability of metal based NMs was investigated by UV-Vis spectroscopy. Typically NMs were dispersed in DW, solution pH was adjusted and the effect of pH was monitored by change in the surface plasmon resonance (SPR) of added

metal based NMs. In order to investigate the variation in the surface charge under different pH values in both RW and DW, zeta potential analysis (Malvern Nanosizer zn3600 in low volume disposable cuvettes) was performed and the mean value of at least three measurements was recorded.

3.7.5 Effect of Ionic Strength and Natural Organic Matter

To compare the effects of RW ionic compositions on NMs transport, the kinetic sedimentation or aggregation study was also conducted in deionized water. The NMs were dispersed in a solution of desired monovalent or divalent salts concentrations in deionized water and column transport experiments were carried out in the same way as explained above. The effect of ionic salts concentrations (2-10 mM) on NMs ionic metal transport was elaborated and quantified by ICP-MS by using standard reference solutions for each salt concentration. The stability of newly synthesized PEI@AgNPs in RW for a longer incubation period of one month was also investigated, during this period the sedimentation or the aggregation behavior was determined by the changes occurred in surface plasmon resonance (SPR) through UV-visible absorption spectroscopy.

To evaluate the effect of dissolved natural organic matters (NOM) on the transport behavior of NMs, two sets of column experiment were designed. In the first column experiment dispersed NMs was injected and RW sample (Station-7) was flow through the column. In the second experiment, the synthetic solution of RW (Station-7), of similar ionic composition and pH in deionized water was synthesized and column transport was carried out and NMs % elution was determined both in presence and absence of NOM.

3.7.6 Transport Behavior of Carbon Based NMs

The transport, mobility and retention behavior of CNPs and GOQDs through porous medium was evaluated by introducing the dispersed carbon based NMs (30 mg/L) into the column with different ionic composition of flow medium. The column effluents were collected and concentrations of carbon based NMs passed through the column were determined by using UV absorbance at 330 nm and 280 nm for CNPs and GOQDs respectively. The breakthrough curve was constructed between the effluent volumes (mL) and normalized effluent concentration C/C_0.

To explain the experimental results with the model equation, the column transport of carbon based NMs was tentatively described by an advection dispersion equation as exploited in previous reports (Lanphere et al., 2014; Zhou et al., 2016) and stated below in Equation. 3.2.

$$\partial C_T/\partial t = v.\ \partial\ C_T/\partial x + D.\ \partial^2\ C_T/\partial x^2 \quad \text{(Equation 3.2)}$$

Where *C* is the carbon based NMs reduced concentration in effluent water, *t* is time (min), *x* is pore volume, *v* is pore velocity (cm/min) and *D* is dispersion coefficient (cm^2/min). The model equation is fit with experimental column break through curves (BTCs) and deposition rates (R_d) were estimated using mass balance or column mass recovery of added CNPs and GOQDs.

3.7.6.1 Effect of pH

The effect of solution pH on the transport and the deposition behavior of CNPs and GOQDs were also determined, both NMs were dispersed in DW (10 mg/L) and pH (comparable to RW pH) was adjusted. The solution pH was adjusted by adding sodium hydroxide solution (1 mM). The effect of pH variation on the stability of CNPs and

GOQDs was investigated by UV-Vis spectroscopy. Typically NMs were dispersed in DW, solution pH was adjusted and the effect of pH was monitored by change in the surface plasmon resonance (SPR) of added CNPs and GOQDs. The aggregation behavior was determined by variations observed at their corresponding absorption maxima.

3.7.6.2 Effect of Ionic Strength and Natural Organic Matter

The effect of ionic strength and natural organic matter on the column transport behavior was performed by the same methodology as discussed for metal based NMs (Section 3.7.1.4). For determination of effect of ionic strength on carbon based NMs, column transport experiment were conducted and BTCs were developed between effluent concentrations C/C_0 and effluent volume, and the total deposition rate (R_d) calculated from the mass recovery of added NMs into the column was investigated.

3.7.6.3 Column Attachment or Retention Profile

In order to determine the column retention ability of NMs, the column packing material (Amberlite) was carefully removed into 5 cm increments. The material was dissolved in 50 ml DW, centrifuged and the supernatant was collected to determine the concentration of retained NMs into the column using UV absorption spectroscopy.

Beside natural water electrolytes effects on transport of NMs, effect of naturally existing dissolved organic species also dictates the transport behavior of NMs. Therefore, in determination of NMs behavior, the effect of dissolved natural organic matter was also elucidated.

3.8 NMs Mobilization into the Plant

To investigate the ability of NMs to be absorbed and transported into the living systems, living model was needed to explore the mobilization and accumulation of NMs into the living tissues. For this purpose hydroponic growth of red bean (*Vigna angularis*) model plant was monitored under the exposure of NMs. Since low concentration of carbon based NMs to natural water was reported (Gottschalk et al., 2013) which limit its chances to expose to real plant growth system compared to metal based NMs. Therefore, because of this reason two metal based NMs i.e., PEG@ZnONRs and TiO_2NPs were used for the evaluation of NMs impact on plant growth.

3.8.1 Synthesis of NMs Suspensions

The homogenized suspensions of PEG@ZnONRs and TiO_2NPs nanomaterials (0-200 µg/mL) in deionized water were prepared by ultrasonication (POWERSONIC 405) for 20 min. The dissolved fraction of Zn(II) and Ti(IV) ions in suspensions were determined by ICP-MS analysis. The particle size and zeta potential of both nano-oxide were investigated by particle size analyzer (Malvern Nanosizer zn3600) in low volume disposable cuvettes and the mean value of triplicate analysis were recorded.

3.8.2 Transport of Metal Based NMs to Plant Seeds

Red bean seeds were soaked in formaldehyde 3% v/v for 15 min to remove fungal contaminants (Peralta-Videa et al., 2002), washed thrice with deionized water, and placed in a 150 mm × 30 glass Petri dish (12 seeds each) with 10 ml of each metal based NMs suspension. Filter paper was used as a membrane support in all test plates. The Petri plates were wrapped in aluminum foil and kept under incubator at 30º C for 5 days for germination. All samples were replicated three times and mean ± SE (n = 3) were

recorded. Seeds were considered germinated when 65% of root controls were at least 5 mm long (Figure 3.11, Step 1) according to US-environmental protection agency guidelines (USEPA, 2012). Germination data for both blank and test plates were collected and their % germination was calculated using reported method (Lopez-Moreno et al., 2010) by Equation 3.3.

% Germination = Seeds germinated/ Total seeds × 100..... (Equation 3.3)

3.8.3 Plant growth under NMs exposure

After germination, 4-5 seedlings (for each NP concentration) were selected randomly and placed on a plastic plate (having holes) such that the head of each seedling are up and roots were facing the medium solution downwards (Figure 3.11, Step 2). The plates were placed onto the 100 mm × 15 mm glass Petri dish (1-inch space from dish bottom was maintained for the roots to grow) and 250 ml of nutrient solution were added as described previously (Ebbs et al., 2016) except for adding Zn salt in the formulation.

The Petri plates were kept in sunlight for at least 5 hours daily at a light intensity around 3600 foot candles with temperatures of 30 °C/day, 7 hours in the shade at 28 ºC/day and for 12 hours in the dark at 26 °C/night. The day/night relative humidity was 50-55%.

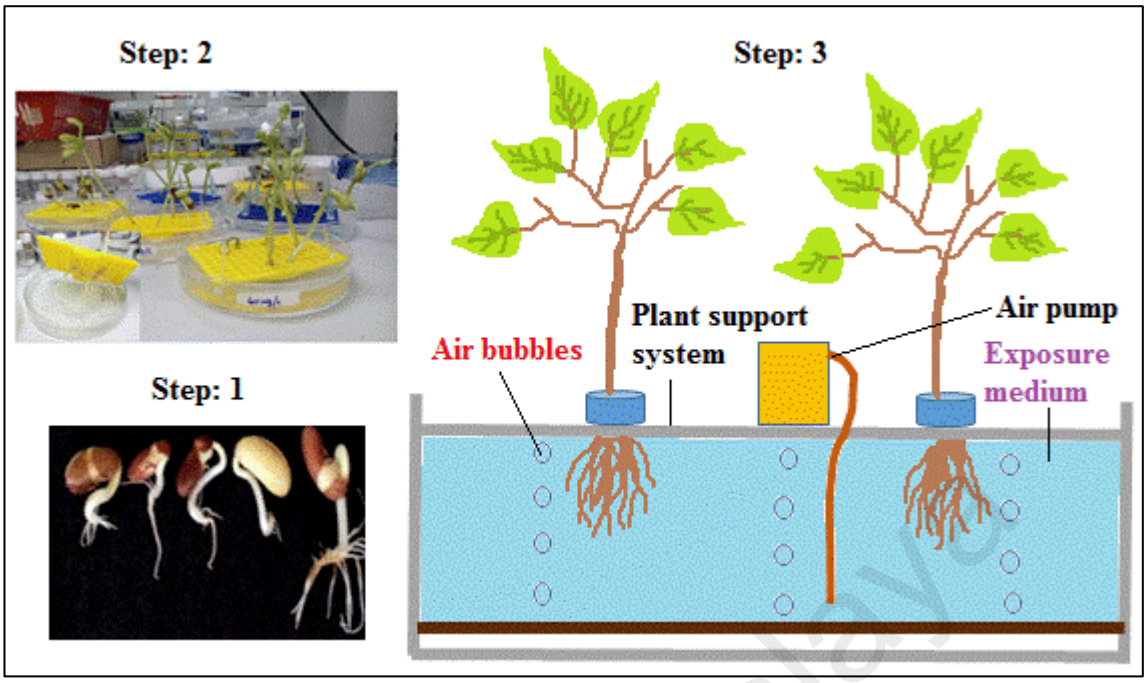

Figure 3.11: The corresponding steps for hydroponic cultivation of red bean plants

After one week, the seedlings were transferred to the glass tank (Figure 3.11, step 3) with approximately 500 ml medium capacity and exposed to PEG@ZnONRs and TiO_2NPs suspensions (0-200 µg/mL) either in single or co-exposure (1:1 ratio) treatment for one week.

These wide ranges of PEG@ZnONRs and TiO_2NPs concentrations were examined to determine the sub lethal dose to plant physiological and biochemical characteristics. For both metal-oxide treatments, the concentration 200 µg/mL was further exposed to two weeks and three week treatments in order to investigate the kinetic uptake and tissue distribution of metal ions. For all the experiments the medium solution was bubbled with air pump for frequent O_2 supply, sufficient aeration and to prevent PEG@ZnONRs and TiO_2NPs from aggregation (Rao and Shekhawat, 2014).

3.8.4 Effects on Plant Physiology

The effect of PEG@ZnONRs and TiO2NPs on plant physiological activity was investigated by measuring the growth rate in terms of roots length and shoots length. All

the data compared with the control plant grown under normal condition without NMs exposure treatment.

3.8.5 Effect on Plant Biochemistry

The effect of PEG@ZnONRs and TiO_2NPs exposure on plant biochemistry i.e., certain growth proteins and enzymes was also determined to investigate the plant response to PEG@ZnONRs and TiO_2NPs exposure. For this purpose analytical methods and anti-oxidant assays were performed.

3.8.6 Analytical Methods

After completion of exposure treatments (one week, two weeks & three week), the plant parts (roots & shoots) were separated, rinsed thoroughly with 1 mM HNO_3 followed by deionized water to remove the physically adsorbed PEG@ZnONRs and TiO_2NPs. To determine the uptake concentration of Zn(II) and Ti(IV), the plant tissues were microwave digested as reported previously by Rodushkin et al., 1999. The digested samples were diluted 50 times and the concentration of Zn(II) and Ti(IV) was quantified through inductively coupled plasma mass spectrometry (ICP-MS, Agilent 7500-series) using plant standard referring material (Apple leaves 1515a).

In addition, the standard was used after every 10 samples to monitor the matrix effect on the analyte. The total chlorophyll content, lipid peroxidation, and carotenoids were determined by following reported methods by Das et al., (2015), Heath et al., (1968), Lichtenthaler, (1987) and May et al., (1993) respectively. The total chlorophyll content in plants leaves was extracted using 80% acetone (pH 7.4) while lipid peroxidation was expressed as thiobarbituric reactive species (TBARS) at extinction coefficient of 155 mM^{-1} cm^{-1} (Heath et al., 1968).

3.8.7 Standard Reference Material (Apple leaves 1515a)

In order to determine the accuracy and performance of ICP-MS instrument a standard plant referring material was used. Typically 0.5 g of reference material were weighted, acid digested and diluted as mentioned for plant parts (section 3.8.6) and analyzed by ICP-MS.

Table 3.2: Recovery for standard reference materials (Apple leaves- 1515a).

Elements	Certified value (ppb)	Analyzed value (ppb)	Recovery (%)
Zn(II)	208.32 ± 0.76	204.10 ± 1.0	97.98
Mg(II)	4.5 ± 0.02	4.27 ± 0.06	94.8
Na(I)	406.4 ± 0.23	389.4 ± 0.86	95.8

The analyzed value of elements Zn(II), Mg(II) and Na(I) was compared with the certified value provided by the manufacturer (NIST) of referring material. Table 3.2 shows the results of plant reference material which was in good agreement between certified and recovered value.

3.8.8 Antioxidant Assays

The investigation of biochemical changes occurred in plant due to NMs exposure treatments were determined by the antioxidant enzyme assays. For all the enzyme studies, roots and shoots were separated, homogenized, centrifuged at 10,000 rpm for 20 min. The extract was analyzed for enzymes catalase, superoxide dismutase, ascorbate peroxidase, and glutathione reductase by following previous reports by Cho and Seo., (2005), Xu and Chen., (2011) and enzyme assay was performed by following the method described previously by Gallego et al., (1996), Beyer and Fridovich., (1987),

Nakano and Asada., (1981) and Foyer and Halliwell., (1976) respectively. The catalase activity was assayed by monitoring the H_2O_2 degradation extinction coefficient 39.4 mM^{-1} cm^{-1} (Wahlefeld and Bergmeyer, 1974). One unit of catalase is the amount necessary to decompose 1µmol of H_2O_2 per minute. In case of superoxide dismutase and glutathione reductase, one unit enzyme activity is the amount of enzyme which causes 50% inhibition of nitroblue tetrazolium reduction and 1 µmol of nicotinamide adenine dinucleotide phosphate (NADPH) oxidation per minute, respectively. Ascorbate peroxidase activity was measured by monitoring decrease in ascorbate at extinction coefficient of 2.8 mM^{-1} cm^{-1} (Nakano and Asada, 1981).

3.8.9 Statistical Analysis

All the data of seed germination, roots & shoots growth and enzymes assays were statistically analyzed by one-way ANOVA statistics using General Linear Model followed by Tukey test using IBM SPSS statistics V22 software (US). The statistical significance was based on the probabilities of $p < 0.05$.

3.9 Remediation of NMs

After investigations of the NMs aqueous transport and mobilization behavior, research on the second part of this project that is remediation of NMs under natural aqueous medium was elaborated. For the remediation of NMs, spiked in natural aqueous medium mesoporous silica based adsorbent material was synthesized. The complete detailed synthesis of adsorbent is described below.

3.9.1 Synthesis of Adsorbent For NMs Remediation

Polymer modified mesoporous silica iron microcubes (P@MSIMC) were synthesized by facile one-pot hydrothermal method. Briefly, 0.2 g of column silica gel was mixed with 100 µl of polymer PEI (diluted 1 ml to 5ml of DW) in 20 ml of DW.

The mixture was allowed to react at 75 ºC/1100 rpm on a magnetic stirrer for 10 min, then 0.025 g of $FeCl_2$ was added with continued stirring. The resulting brown mixture was heated and stirred for a further 1 hour for maximum synthesis of PEI-modified porous silica iron microcubes (Scheme 3.6).

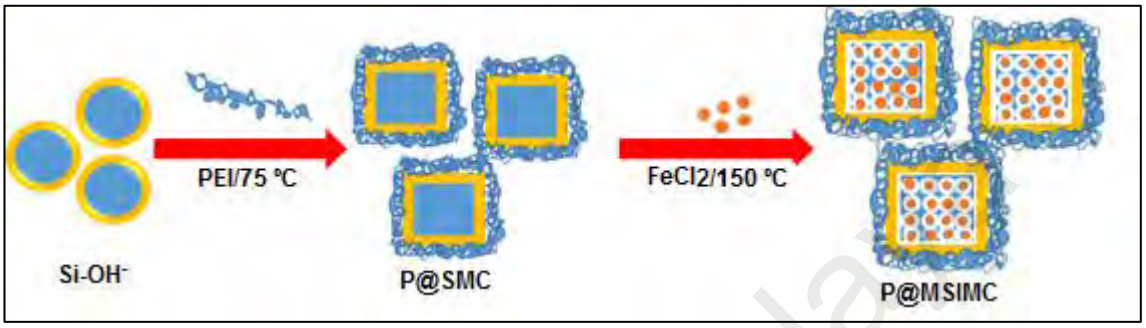

Scheme 3.6: Schematic representation for the synthesis of P@MSIMC.

To determine the effect of reaction temperature on the porosity of P@MSIMC, the similar reaction was also employed at 100 ºC, 150 ºC and 200 ºC. The synthesized silica microcubes were washed several times with 2-propanol and DW in order to remove the unreacted precursors. The P@MSIMC was dried in oven at 80 ºC for 1h and characterized.

3.9.2 Preparation of NMs dispersion

All synthesized NMs were dispersed in natural RW and sonicated at 20 ºC for 20 min. The insoluble fraction of NMs was removed by centrifugation at 10,000 rpm for 15 min and the concentration of NMs in the supernatant was determined by inductively coupled plasma mass spectrometry (ICP-MS, Agilent 7500-series) analysis. The NMs suspensions were stored at 28 ºC for adsorption analysis.

3.9.3 Adsorption of NMs

For NMs adsorption studies (10-1000 mg/L), batch experiments were performed on an orbital shaker (Model: OS-200, ORBIT 20 mm) with a shaking speed of 120 rpm at 25 ºC and pH values ranging from 4-9. For kinetic study, 10 ml solution of RW dispersed NMs (1000 mg/L) was mixed with P@MSIMC (10 mg) at optimum pH values. After a predetermined adsorption period, the fraction of metal based NMs solution (2 mL) was removed, acidified and the concentration of NMs was determined by ICP-MS using standard solution of Ag(I), Ti(IV) and Zn(II) of same initial concentration. The concentration of CNPs and GOQDs was determined by Shimadzu 3600-UV visible spectrophotometer at corresponding wavelength of 330 nm and 280 nm respectively. The NMs % removal efficiency was calculated by the Equation 3.4 (Zinchenko et al., 2013).

$$\% \text{ Removal efficiency} = (1-C/C^{o}) \times 100 \quad \text{(Equation 3.4)}$$

Where C^{o} and C are the initial and final concentrations of the NMs before and after the adsorption process respectively. The NMs maximum adsorption capacity (q) of P@MSIMC was calculated by the Equation 3.5 (Ma et al., 2015b).

$$q\ (mg/g) = (Co - Ce) \times V/W \quad \text{(Equation 3.5)}$$

Where, C_o and C_e are the initial and equilibrium concentration of NMs in solution (mg/L), V is the total volume of testing solution and W is the weight of adsorbent (P@MSIMC). For the kinetic adsorption study, following linear model equations of pseudo-first order (Equation 3.6) and pseudo-second order (Equation 3.7) was employed.

$$\log (qe - qt) = \log qe - k1/2.303 \times t \quad \text{(Equation 3.6)}$$

$t/qt = 1/k_2q2e + t/qe$…….…….. (Equation 3.7)

Here *qt* (mg/g), and qe (mg/g) represents the adsorption capacity at time *t*, and at equilibrium and k_1/ min and k_2 (g/mg min) are the pseudo first and second order rate constants respectively.

For adsorption isotherm study, the equilibrium data was described by using two well-known linear forms of Langmuir and Freundlich isotherm models (Liu et al., 2015c). For Langmuir and Freundlich isotherm following equations will be used respectively.

Ce/qe = 1/bqm + Ce/qm…….…….. (Equation 3.8)

Ce/qe = ln KF + 1/n ln Ce…… (Equation 3.9)

Where, q_e and C_e are the maximum removal efficiency (mg/g) of P@MSIMC and the equilibrium concentration of adsorbate (mg/L), the q_m and *b* are the Langmuir constant, for maximum absorption and binding energy respectively; *KF* and *n* are the Freundlich empirical constant (L/mg) and heterogeneity factor respectively.

3.9.4 Desorption and Recycling of Adsorbent

The desorption process of P@MSIMC was carried out by washing several times with ethanol followed by deionized water and dispersed in 10 mL of 1 mol/L HCl for 30 mins. This will remove the adsorbed NMs at the surface of P@MSIMC. The adsorbent was separated from the solution by centrifugation at 3000 rpm/min, washed several times with deionized water and used to check the recycling property. The particles were separated, washed thrice with deionized water, and used for recycling. The adsorption/desorption cycles were repeated five times and the NMs removal efficiency of P@MSIMC was determined.

3.10 Quality Control and Quality Assurance

Quality control (QC) and quality assurance (QA) are fundamental aspects of any laboratory measurement. In general both ensure that the results generated one day are consistent to next days with same accuracy and precision. During this project, in order to maintain good QC and QC following steps were undertaken. To preclude uncertain contaminations, all laboratory equipments and glasswares were washed with phosphate-free soap, double rinsed with distilled water and left in 10% HNO_3 for 24 h. All glassware were then rinsed twice with doubly distilled water and dried at room temperature.

In the synthesis of all NMs and adsorbent material, adequate ultrasonication and centrifugation were employed for the entire chemical dissolution during all the preparation and washing steps. All NMs behavior studies were performed in triplicate to minimize the chances of error. In all ICP-MS metal quantification, proper sample preparation steps was taken and external standard reference material was used after every 10 samples to monitor the matrix effect on analyte. In seed germination, NMs plant uptake and mobilization studies each experiment was performed in triplicates and mean values were recorded. For metal uptake investigations, proper tissue digestion was carried out in microwave digester using extra pure nitric acid (HNO_3) and hydrogen peroxide (H_2O_2). All the data were analyzed by one-way ANOVA statistics using General Linear Model followed by Tukey test using IBM SPSS statistics V22 software (US) with statistical significance based on the probabilities of $p < 0.05$ (APPENDIX A). All the NMs remediation experiments were also performed in triplicates in natural river water and the mean value of each experiment was recorded.

3.11 Process Safety Measures and Material Safety Data Sheet

Since, used solvents, metal salts and certain polymers and inorganic acids were belonging to the hazardous class of materials, therefore, safety measure were taken into account at all steps of the research carried out. The purchased chemicals were properly stored as described by chemical companies under controlled temperature conditions (below 30 ºC). During and after the experimental procedures, the used materials were disposed of appropriately and exhaust ventilation were used to avoid the airborne contaminations. In addition, lab coat, safety goggles, fume hood vapor respirator was used as personal protective equipment (PPE).

CHAPTER 4: RESULTS AND DISCUSSIONS

4.1 Characterization of NMs

4.1.1 Characterization of Metal Based NMs

To understand the surface potential and morphological features of synthesized metal based NMs, various material characterization techniques were employed. These techniques includes, UV-visible absorption spectroscopy, fourier transform infrared spectroscopy (FTIR), field emission scanning electron microscopy (FESEM), zeta-potential analysis and XRD analysis. The UV-visible spectroscopy is the most important technique and the simplest way to confirm the formation of NMs through specific surface plasmon resonance peak (Anandalakshmi et al., 2016; Bindhu et al., 2013). Figure 4.1, represented the UV-visible spectrum of all synthesized metal based NMs.

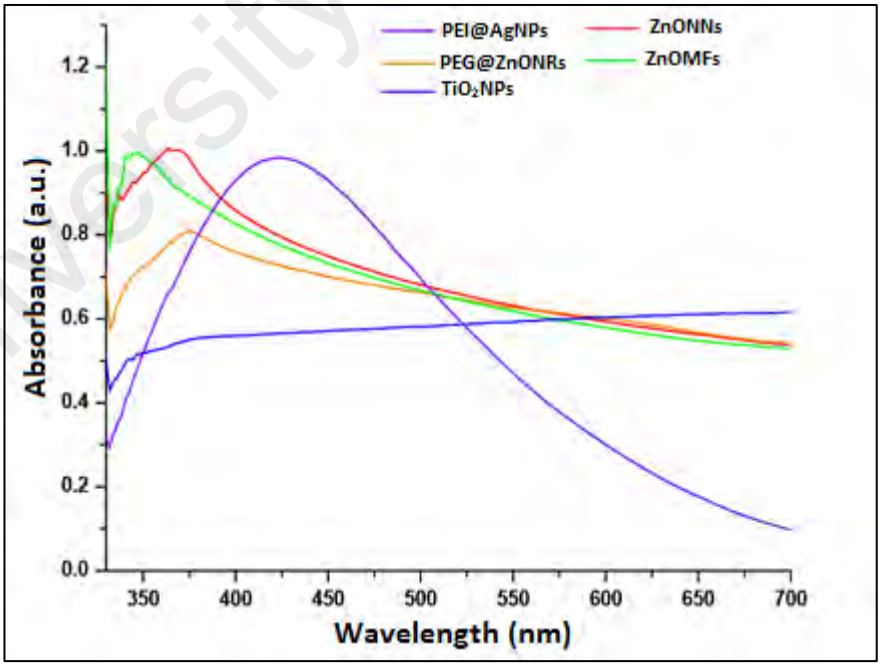

Figure 4.1: UV-visible absorption spectra of PEI@AgNPs, PEG@ZnONRs, TiO_2NPs, ZnONNs and ZnOMFs respectively.

The UV-visible spectrum of PEI@AgNPs, PEG@ZnONRs, TiO_2NPs, ZnONNs and ZnOMFs illustrates the surface plasmon absorption maxima at 427 nm, 376 nm and 375 nm, 370 nm, and 350 nm respectively, which are the corresponding absorption peaks for silver, zinc and titanium dioxide structures and are in accordance with the previous reports Han et al., (2012); Prasad et al., (2006); Reddy et al., (2003); Sun et al., (2003); and Wahab et al., (2007b). FTIR analysis was performed to determine the possible functional groups at the surface of all synthesized metal based NMs. Figure 4.2, presented the FTIR spectra of all synthesized metal based NMs. The FTIR spectra of PEI@AgNPs displayed three absorption bands at 600 cm^{-1} and 1570 cm^{-1}, 3400 cm^{-1} which are attributed to the -CO_2 group of ligand L-cystine and N-H bands of –NH_2 group of attached polymer PEI respectively (Liu et al., 2012a).

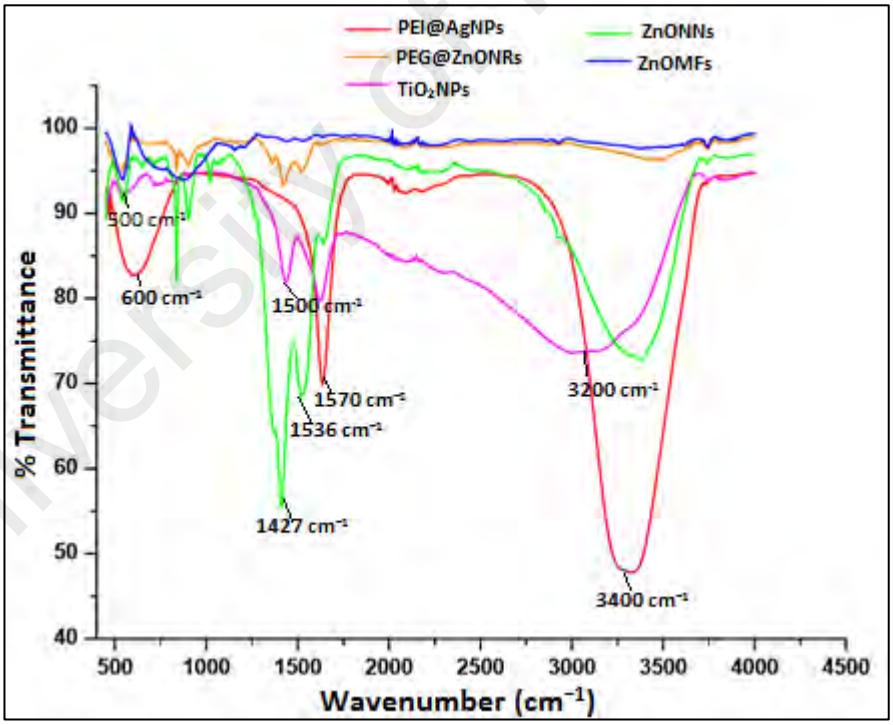

Figure 4.2: FTIR spectra of PEI@AgNPs, PEG@ZnONRs, TiO_2NPs, ZnONNs and ZnOMFs respectively. All the spectra were taken at ATR mode within the spectral range of 450-4500 cm^{-1}.

All synthesized ZnO structures displayed sharp vibrations around 500 cm^{-1} which are attributed to the Zn-O stretching modes, respectively (Wahab et al., 2007a). In PEG@ZnONRs, and ZnOMFs the broad vibrations at 3400 cm^{-1} was due to the hydroxyl group of attached polymer PEG (Liufu et al., 2004). Whereas in ZnONNs, the bands around 3400 cm^{-1} correspond to O–H mode of vibration. In all ZnO structures the stretching modes of C-O and C=O are observed at 1427 cm^{-1} and 1536 cm^{-1} respectively (Wahab et al., 2011). The spectra of TiO_2NPs shows an absorption maxima at 550-795 cm^{-1} which correspond to the Ti-O stretching mode whereas, the vibration centered at 1500 cm^{-1} and broad band at 3200 cm^{-1} correspond to carboxylate and O-H stretching mode of physisorbed water molecules (Brauer et al., 2014).

After UV-visible and FTIR characterizations, the morphological features of all synthesized metal based NMs were studied through FESEM analysis. The FESEM analysis (Figure 4.3a-e) revealed that the synthesized metal based NMs are of different size and surface structures. Typically the morphology of PEI@AgNPs are of uniform spherical shape with an average diameter of 50 ± 10 nm. PEG@ZnONRs displayed rod-shaped morphology with an average length and width of each rod was 1.0 ± 0.2 µm and 64 ± 10 nm respectively. The structure of TiO_2NPs represented roughly spherical morphology with an average diameter of 89 ± 20 nm. ZnONNs displayed needles shaped morphology with an average length and width of each needle was 151 ± 15 µm and 43 ± 10 nm, respectively. The surface structure of ZnOMFs represents very interesting flower shaped morphology. The average diameter of each flower was 1.09 ± 0.2 µm. The ZnOMFs were synthesized by following same methodology as PEG@ZnONRs, except the reaction temperature and time i.e., ZnOMFs were synthesized at 150 °C for 24 h compared to PEG@ZnONRs which were synthesized at 100 °C for 5 h. This flower behavior was also reported previously (Polsongkram et al., 2008) when zinc oxide nano-rods combine together to reduce the interfacial free energy

(Ostwald ripening). This combination was also reflected by the size increment of ZnOMFs from PEG@ZnONRs. It was a spontaneous process that occurs because larger zinc oxide structures are more energetically favored than smaller ones as reported in earlier work (Polsongkram et al., 2008).

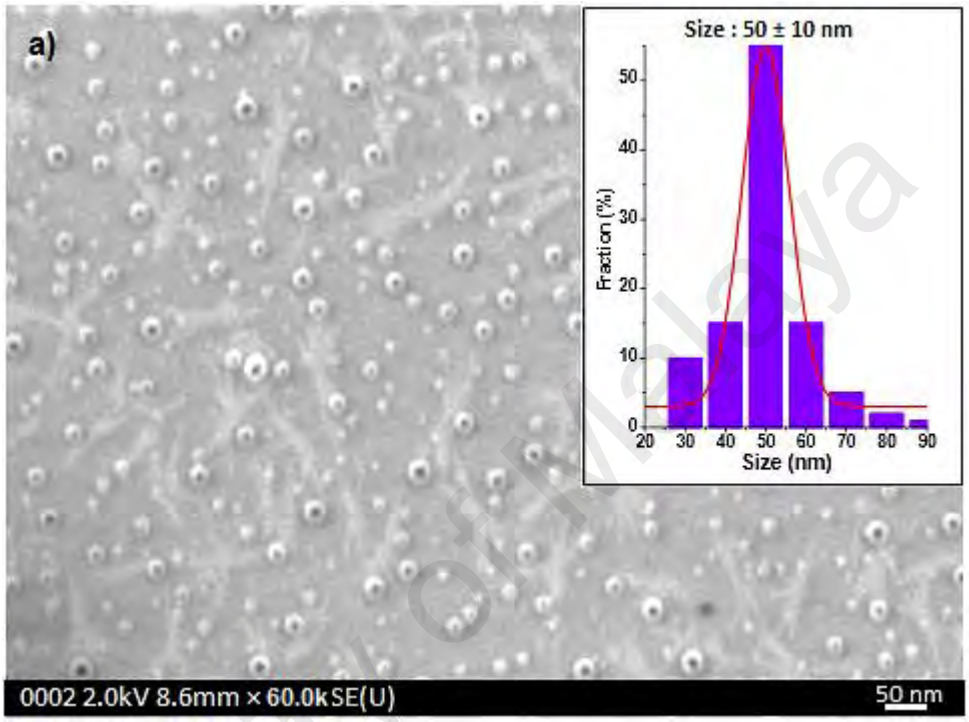

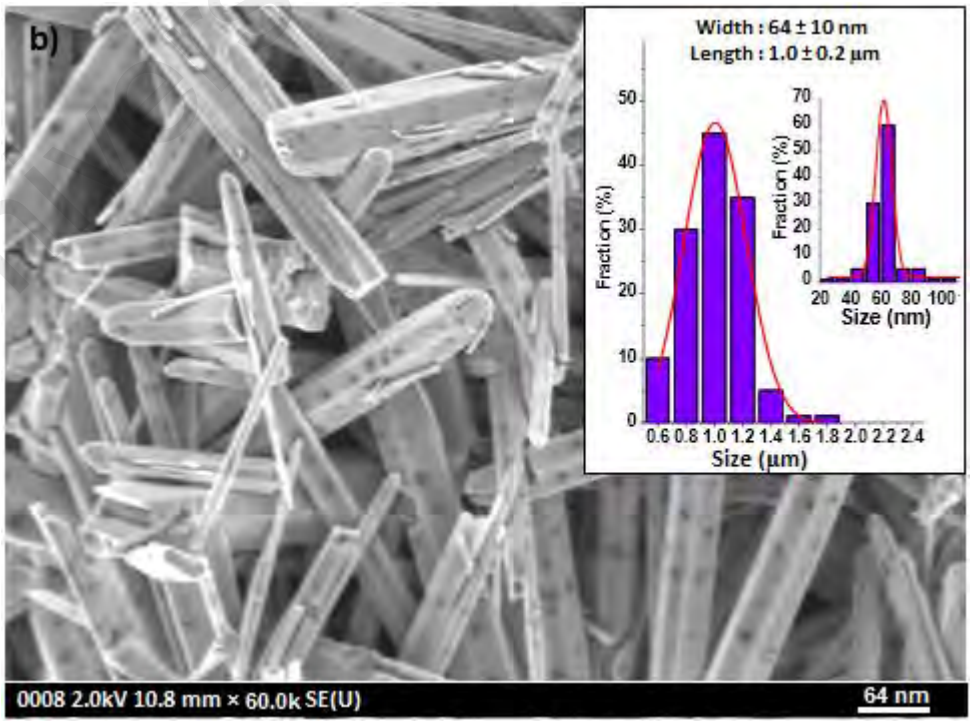

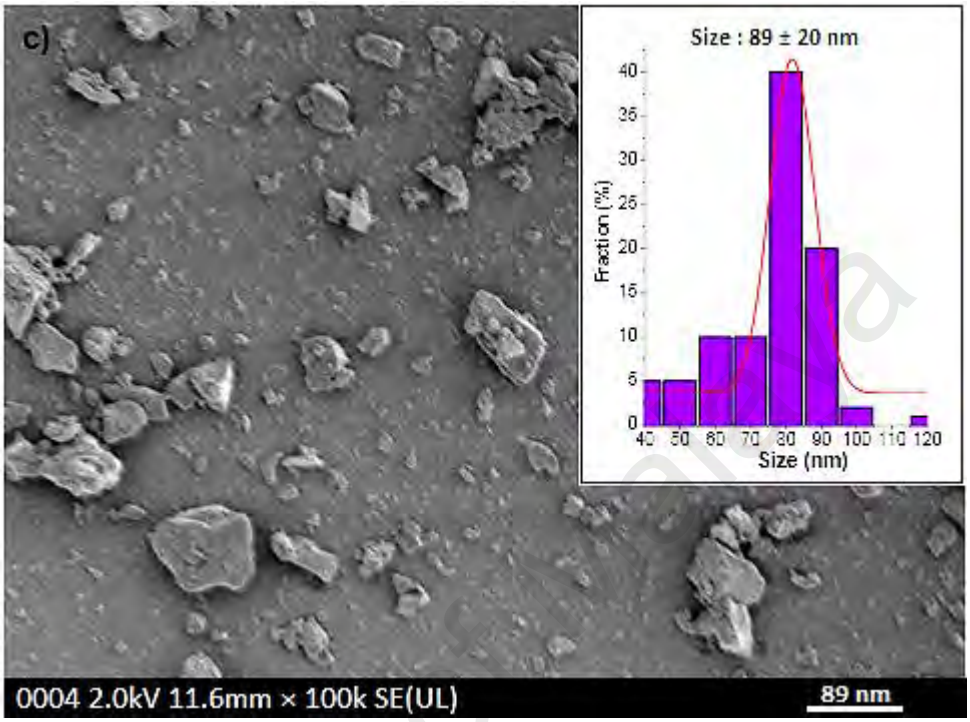

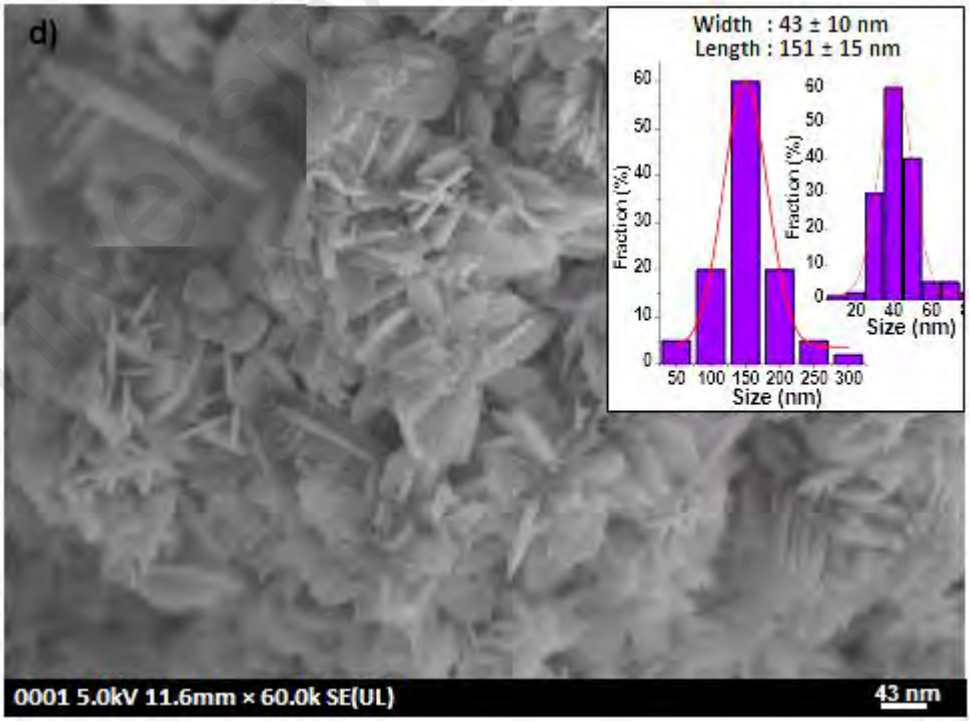

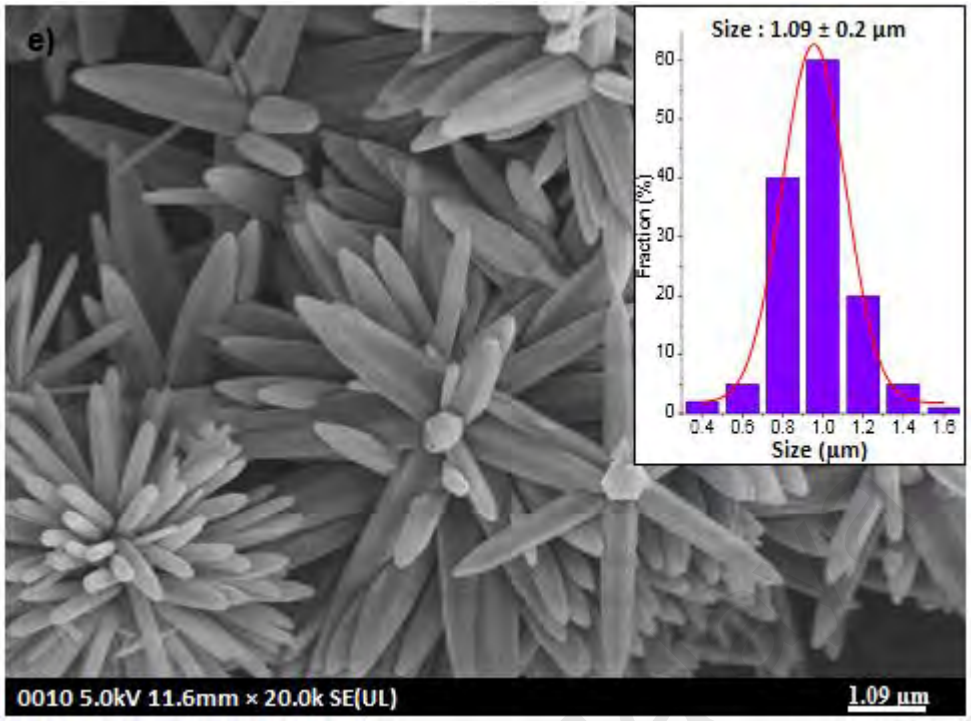

Figure 4.3: The FESEM analysis of synthesized PEI@AgNPs (a), PEG@ZnONRs (b), TiO_2NPs (c), ZnONNs (d), and ZnOMFs (e). Each sample was firstly drop-casted on ITO thin film, dried and then FESEM images were taken using bright field mode.

To determine the surface charge or surface potential of synthesized metal based NMs, zeta-potential analysis was performed. As it is well known that every solid surface is characterized by its own electrostatic charge which originates from the surface functional groups. Whereas, the composition of the interior of the material does not contribute to the charge (Gannon et al., 1991; Jastrzebska et al., 2016). Therefore, the zeta-potential observed in all synthesized metal based NMs was solely due to the surface functional groups present on the surface of metal based NMs. The zeta-potential analysis revealed that all synthesized zinc oxide structures i.e., PEG@ZnONRs, ZnONNs, ZnOMFs and TiO_2NPs possesses negative (–ve) surface charge due to the presence of hydroxyl and carboxylate groups at the surface, as also confirmed by FTIR analysis (Figure 4.2). Whereas, the surface charge of PEI@AgNPs was positive because of the attachment of cationic polymer layer at the surface (Sharonova et al.,

2016). The zeta-potential detail and other physicochemical properties of all synthesized metal based NMs are summarized in Table 4.1.

Table 4.1: Physicochemical properties of metal based NMs.

Properties	PEG@ZnONRs	TiO_2NPs	PEI@AgNPs	ZnONNs	ZnOMFs
Surface coating	PEG-coated	-	PEI-coated	-	PEG-coated
Morphology	Rod	Roughly spherical	Spherical	Needles	Flowers
FESEM Size	W: 64±10 nm L: 1±0.2µm	89±20 nm	50±10 nm	W: 43±10 nm L:151±15 nm	1.09 µm
ξ-potential	-20 mV	-16 mV	+17 mV	-18 mV	-19 mV

*W=width, L= length

4.1.1.1 XRD Characterization of Metal Based NMs

XRD is an important technique used to analyze the characteristics and structural details of nanomaterials. Powder XRD was used to determine the phase composition of metal based NMs. Figure 4.4, representing the XRD spectra of metal based NMs. The XRD spectra of PEI@AgNPs (a) showed peaks around 38˚, 46˚, 66˚ and 74˚ which are corresponding to the (111), (200), (220) and (322) Bragg reflections and confirming the presence of crystalline silver nanoparticles in the sample as also observed previously in the green synthesis of nano-crystalline silver particles (Sathishkumar et al., 2009). The spectrum of PEG@ZnONRs (b) was mainly on hexagonal wurtzite structure as reported in earlier research by Pimentel et al., (2014). The peak at 34.42° is assigned to the (001) crystal plane and two other peaks at 31º and 36.26º are assigned to the (100), and (101) crystal planes, respectively (Vayssieres, 2003).Whereas, in TiO_2NPs (c), the appearance of well-defined Bragg peaks corresponding to anatase phase (Brauer et al., 2014) with well-crystalized

structure as indicated by the sharp diffraction from anatase (101) planes (Li et al., 2009).

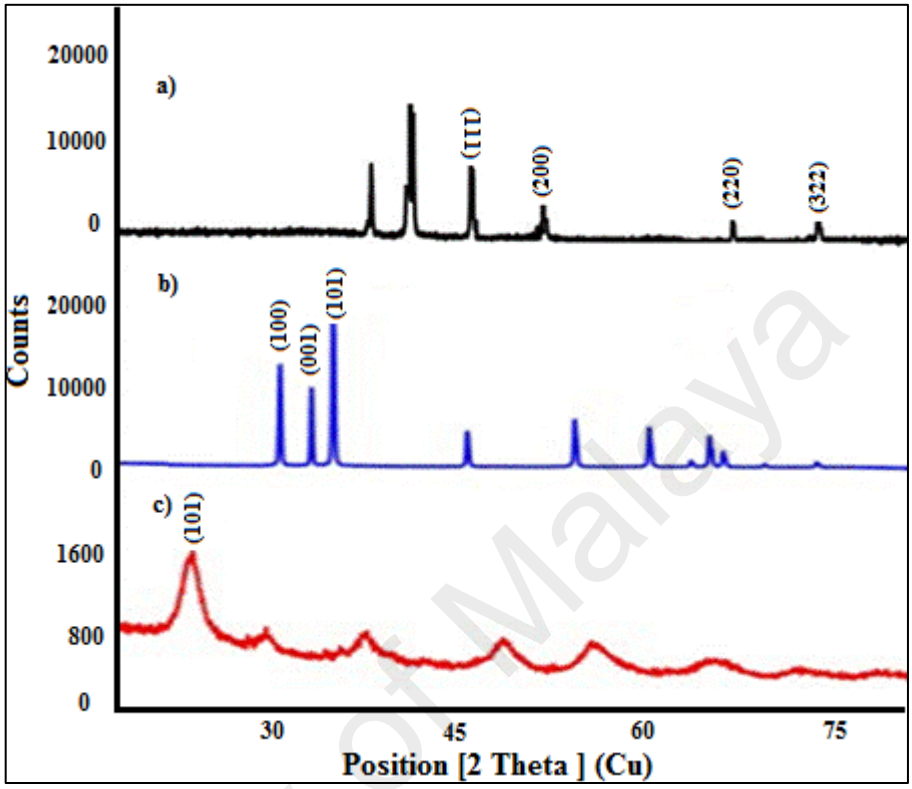

Figure 4.4: X-ray diffraction spectra of PEI@AgNPs (a), PEG@ZnONRs (b) and TiO_2NPs (c). The powder XRD was performed at the range between 20-80º at temperature 28 º C.

4.1.2 Characterization of Carbon Based NMs

Both carbon based NMs **(**CNPs and GOQDs) were also characterized by UV-visible, FTIR, FESEM, XRD and zeta-potential techniques as described for metal based NMs. Figure 4.5, represented the UV-visible absorption spectra of synthesized CNPs (a) and GOQDs (b) respectively. The typical absorption spectra show surface peak maxima at 330 nm and 280 nm which are the corresponding peak of CNPs and GOQDs respectively (Liu et al., 2016; Tang et al., 2012).

Analogous to metal based NMs, the details of the surface functional groups of both carbon-based materials were determined by FTIR study.

Figure 4.6, represents the FTIR spectra of CNPs and GOQDs. The FTIR spectra of CNPs represent the vibration around 3293 cm^{-1} which corresponding to the surface O-H group (Jahan et al., 2013). Whereas, the vibration centered at 1677 cm^{-1} and 1404 cm^{-1}, ascribed to C=O and C-OH groups of COOH (Jahan et al., 2013). The FTIR spectra of the GOQDs displayed an obvious absorption peak around 1670 cm^{-1} which was due to the C=C stretching mode. The vibration at 779 cm^{-1} and broad absorption band at 3375 cm^{-1} were attributed to CH_2 rocking and O-H group respectively. The absorption bands at 1017 and 2930 cm^{-1} indicated the presence of C-O and C-H groups respectively (Tang et al., 2012).

The morphological features of synthesized carbon based NMs was characterized by FESEM analysis and presented in Figure 4.7. As figure illustrates, the synthesized CNPs and GOQDs materials were of spherical morphology with an average diameter of approximately 20 ± 10 nm and 50 ± 20 nm respectively.

Just like metal based NMs, the surface charge or surface potential of synthesized carbon based materials was determined by zeta-potential analysis. The zeta-potential analysis displayed that both CNPs and GOQDs exhibited negative (–ve) surface potential due to the presence of hydroxyl group at the surface, which was also evident from the FTIR observation (Figure 4.6).

The zeta-potential values for CNPs and GOQDs and other physicochemical properties are summarized in Table 4.2.

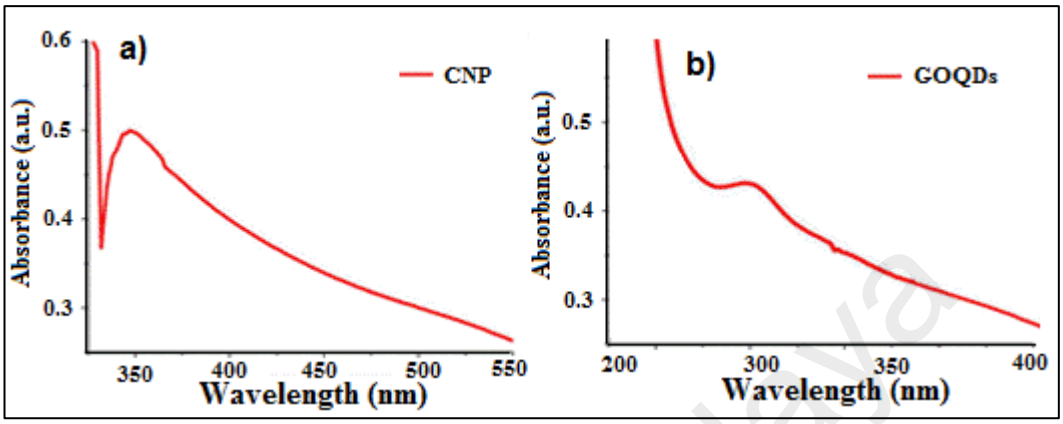

Figure 4.5: The UV-visible absorption spectra of CNPs (a) and GOQDs (b).

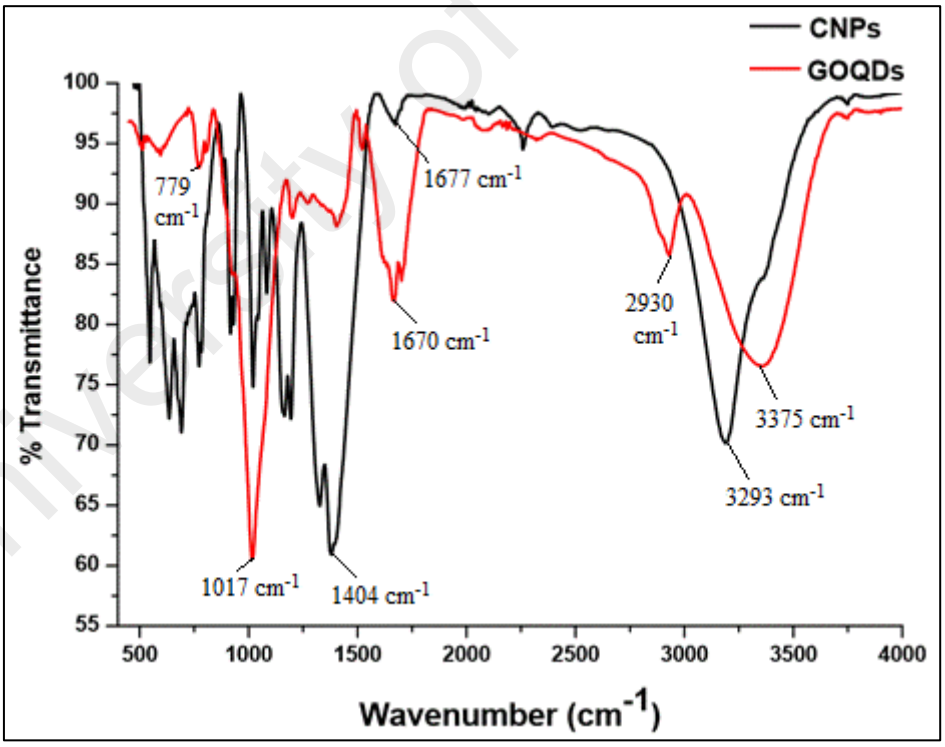

Figure 4.6: FTIR spectra of CNPs and GOQDs taken at ATR mode within the spectral range of 450-4000 cm^{-1}.

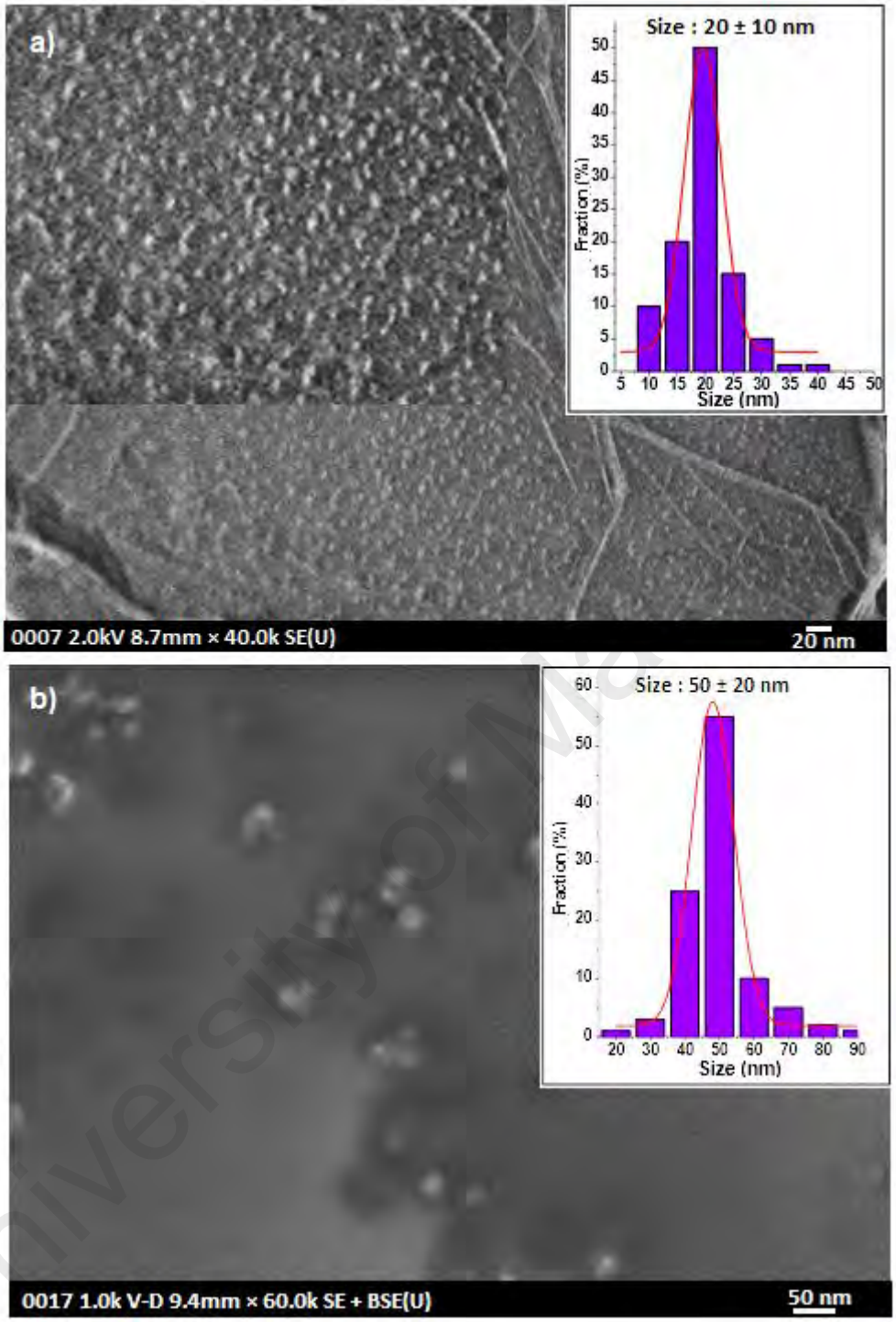

Figure 4.7: The FESEM images of CNPs (a) and GOQDs (b) respectively. The sample was firstly drop-casted on ITO thin film, dried and then FESEM images were taken using bright field mode.

Table 4.2: Physicochemical properties of CNPs and GOQDs.

Physicochemical properties	CNPs	GOQDs
Morphology	Spherical	Spherical
FESEM Size	20 ± 10 nm	50 ± 20 nm
ξ-potential value	-40 mV	-24 mV

4.1.2.1 XRD Characterization of CNPs and GOQDs

The X-ray powder diffraction analysis was performed to determine the phase composition of synthesized carbon based NMs.

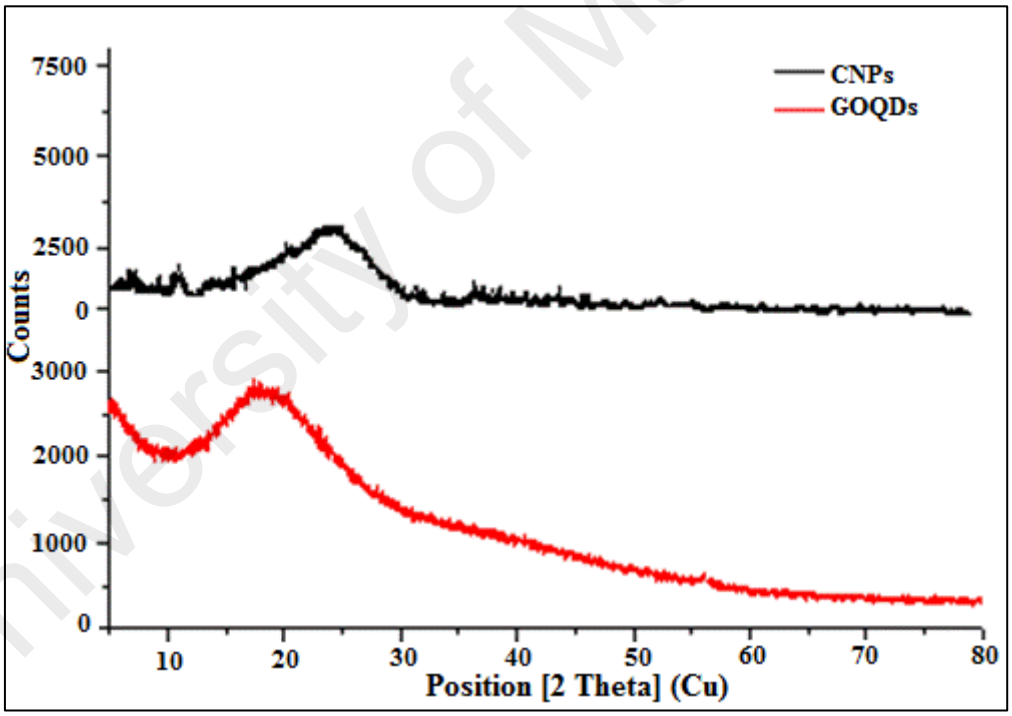

Figure 4.8: X-ray diffraction patterns recorded for CNPs and GOQDs and CNPs at 20 °C temperature within the spectral range 5°- 80°.

Figure 4.8, represented the XRD spectra of synthesized CNPs and GOQDs. As illustrated by the figure, the XRD profile of the CNPs reflect wide peak centered at 26° which was the corresponding peaks of CNPs (Hsu et al., 2012). Whereas, the spectrum

of the GOQDs displayed an obvious peak and 18° which represent the graphitic structure of GOQDs as reported in earlier report (Tang et al., 2012).

4.2 Properties of Natural River Water

To explore the behavior and remediation of NMs in natural aqueous medium, firstly the properties of natural river water was investigated. In order to develop a clear understanding, results of water quality were divided into two sections.

Table 4.3: Physical water quality parameters of RW samples.

Sampling stations	pH	Temperature (ºC)	Dissolved oxygen (mg/L)	Total suspended solids (mg/L)	Electro conductivity (mS/cm)
Station 1	5.66 ± 0.01	27.5 ± 0.10	7.1 ± 0.01	120 ± 0.60	3.01 ± 0.01
Station 2	6.21 ± 0.03	28.2 ± 0.61	11.0 ± 0.05	90 ± 2.16	3.57 ± 0.02
Station 3	6.33 ± 0.02	28.6 ± 0.43	8.1 ± 0.03	115 ± 0.65	3.54 ± 0.02
Station 4	6.09 ± 0.01	28.7 ± 0.42	8.5 ± 0.02	101 ± 1.25	3.36 ± 0.01
Station 5	6.38 ± 0.06	28.4 ± 0.63	7.8 ± 0.04	110 ± 2.03	3.39 ± 0.02
Station 6	6.61 ± 0.04	28.9 ± 0.64	8.6 ± 0.03	100 ± 2.11	4.08 ± 0.04
Station 7	6.86 ± 0.04	28.6 ± 0.65	11.5 ± 0.02	75 ± 0.53	4.29 ± 0.05

First section includes physical water quality parameters like pH, temperature, concentration of dissolved oxygen, total suspended solids, and electroconductivity (Table 4.3). Second section includes concentrations (mg/L) of anions and cations

present in RW (Figure 4.9). As shown in Table 4.3, each sampling station represents variation in terms of temperature, pH, dissolved oxygen, total suspended solids which was also reflected in the variable electroconductivity of each water sample.

Figure 4.9, revealed that the maximum concentrations of anions such as chloride, fluoride, bromide, carbonate, nitrate, phosphate, sulfate and concentration of some important cations such as sodium, potassium, calcium (except for magnesium) was observed in RW station 7, which also represents the complexity of this water sample.

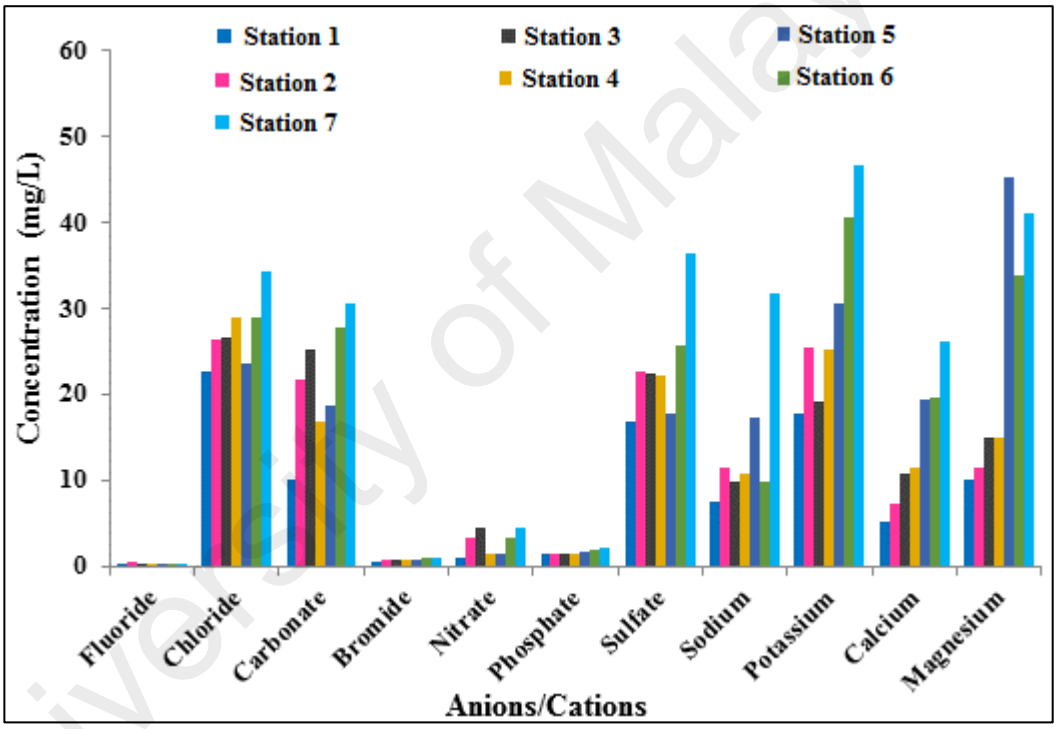

Figure 4.9: The total concentration (mg/L) of anions and cations present in each RW sample. For cations measurement the RW sample was first acidified with 0.5% HNO3 and their respective ICP-MS analysis was performed.

4.3 Behavior of Metal and Carbon Based NMs

4.3.1 Behavior of Metal Based NMs

In determination of the behavior of metal based NMs, the effect of surface coatings, particle size and morphology, influence of solution pH, effect of ionic strength and

dissolved natural organic matter was elaborated. Typically, the effect of all above mentioned factors on the particle dissolution and kinetics of ionic metal release profiles i.e., Ag(I), Zn(II) and Ti(IV) from PEI@AgNPs, PEG@ZnONRs and TiO_2NPs were explored.

4.3.1.1 Kinetics of Ionic Metal release

The kinetics of ionic metal release i.e., Ag(I), Zn(II) and Ti(IV) from polymer-coated (PEI@AgNPs and PEG@ZnONRs) and uncoated TiO_2NPs was investigated into RW of three sampling stations i.e., station 1, station 4 & station 7. These RW samples was selected because of the notable differences in terms of solution pH, dissolved oxygen (DO), total suspended solid (TSS) and concentration of dissolved anions and cations (Table 4.3 and Figure 4.9) therefore, the effect of different solution chemistry on the behavior of metal based NMs can easily be monitored. The choice of three distinct RW samples on the transport behavior of NMs based on the clear effect of solution chemistry as reported previously in many reports such as Gao et al., (2009), Keller et al., (2010) and Praetorius et al., (2012). According to these reports the reactivity of NMs dispersed in natural waters varies significantly with variation in water chemistry. Typically, RW solution pH, concentration of dissolved oxygen and concentration of anions and cations dictated the mobility and reactivity of NMs. Therefore, in this research RW samples from three different locations i.e., RW station-1, RW station-4 and RW station-7 were selected because of their sharp differences in terms of pH, dissolved oxygen and concentration of anions and cations to determine the transport or mobility of synthesized NMs.

Effect of surface coating

The ICP-MS results (Figure 4.10a, b & c) suggested that the maximum kinetic ionic metal release was occurred during the first 10-20 min in case of PEI@AgNPs, and 100

min in case of both PEG@ZnONRs and TiO_2NPs. After that, the concentration of ionic metal was decreased. As can be seen from the figure, in RW Station-7 the efflux of ionic metal from coated and uncoated NMs were significant, comparing to Station-1 and Station-4 of lower ionic composition. Typically the ionic metal loss was 1.6%, 8.3% and 13.6% in Station-1, 2.0%, 10.1% and 15.3% in Station-4, and 3.3%, 12.6% and 19.0% in the case of Station-7 for PEI@AgNPs, TiO_2NPs and PEG@ZnONRs, respectively, suggesting that maximum column retention occurred in order of PEI@AgNPs > TiO_2NPs > PEG@ZnONRs.

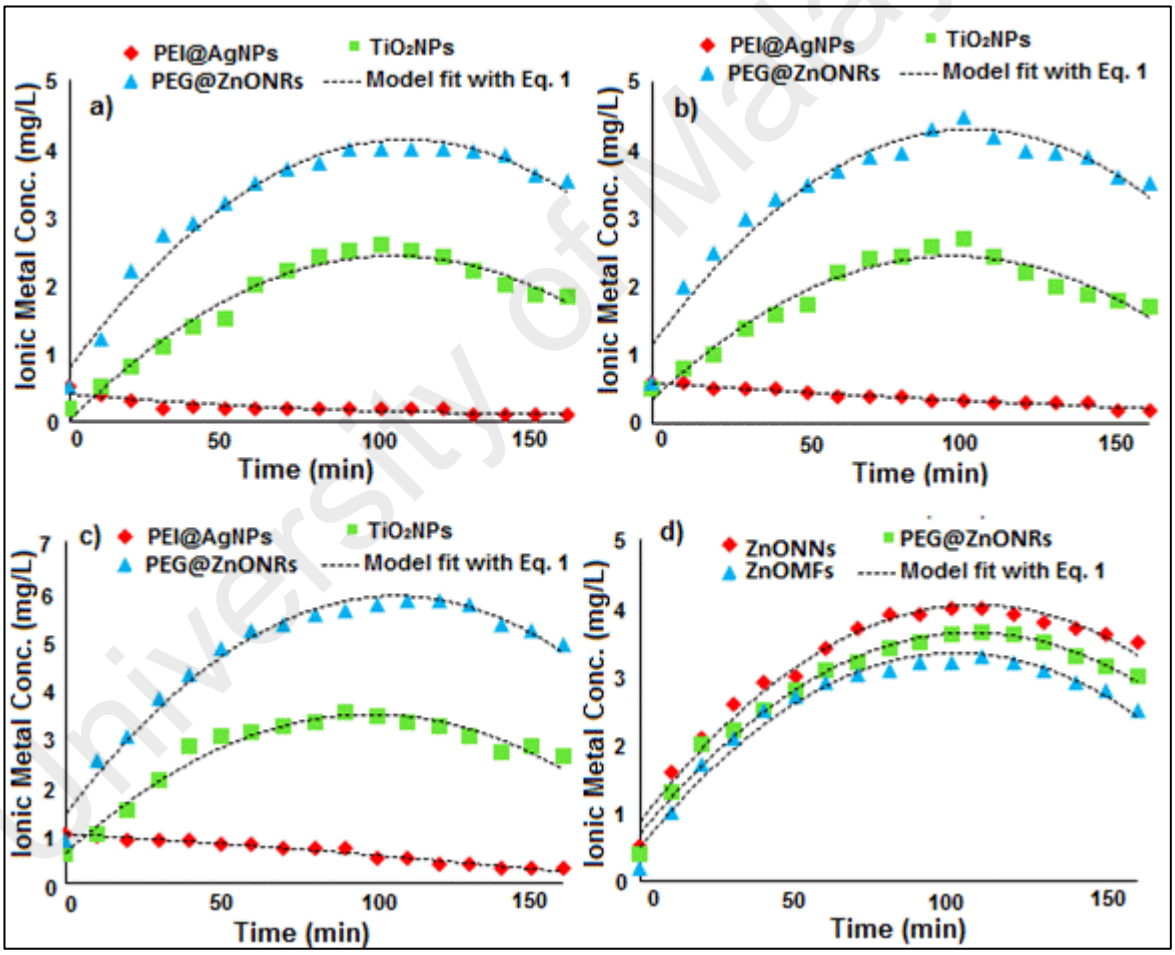

Figure 4.10: Ionic metal release breakthrough curve for experiments conducted in the column at flow rate 1 ml/min and at 28 ºC temperature using RW Station-1(a), Station-4(b) and Station-7(c). Typically 30 mg/L metal based NMs were added to the column and RW was flowing (0-160 min). The ionic metal release breakthrough curve obtained from ZnONNs, PEG@ZnONRs and ZnOMFs of different morphology (d). The kinetic rate equation calculated fits are shown by the dotted lines.

The smaller ionic metal loss from PEI@AgNPs indicated that, cationic polymer PEI coating at the surface of AgNPs encompasses great stability and inhibits the ionic dissolution and the ionic metal release as compared to anionic PEG coated ZnONRs and uncoated TiO_2NPs.

In Station-7, the ionic dissolution was higher in all metal based NMs and more ionic metal release was observed. This was because of the higher DO concentration in Station-7, which significantly favor the oxidative dissolution and ionic metal release. This behavior was also observed previously (Liu et al., 2010a) when the time dependent dissolution of ionic silver was observed in the presence and absence of dissolved oxygen. The study found that the ionic silver dissolution from silver nanoparticles was facilitated in presence of dissolved oxygen.

Whereas, the dissolution was completely inhibited in deoxygenated water. This indicated the essential role of dissolved oxygen in the oxidative dissolution and release of ionic metals. Interestingly, the phenomenon of kinetic ionic metal release was very low (0.5-2 %) when 30 mg/L metal based NMs was dispersed in deionized water (pH-6) and passed through the column. This suggested that the ionic metal loss by dissolution was largely dependent upon the chemical composition of aqueous medium.

Effect of Particle Size and Morphology

The kinetic ionic metal release from all synthesized ZnO structures was investigated in RW (Station-1) and presented in Figure 4.10(d). If the size and morphological features of ZnO structures were compared on the dissolution profiles it is found that, in ZnONNs the high ionic metal release was observed compared to PEG@ZnONRs and ZnOMFs.

The difference in dissolution profiles was due to the differences in particle shape and size that affects transport in terms of attachment or retention of ZnO structures to the column surface. ZnONNs owing to its smaller size (length and width) compared to other two mentioned ZnO structures, exhibited high transport and ionic dissolution rate. This behavior may be explained well by "size-selective retention", i.e., preferential retention of larger particles and elution of smaller particles during the porous media transport (Wang et al., 2015a). In case of PEG@ZnONRs and ZnOMFs, since both constructed with similar materials, the less ionic metal dissolution and less column transport was observed in ZnOMFs which was because of their angular-shaped morphology that resist the transport in saturated porous media (Knappenberger et al., 2015). The ionic metal dissolution of ZnONNs, PEG@ZnONRs and ZnOMFs was 13.6%, 12.3% and 11.3% respectively. All experimental kinetic ionic metal release data were fit using Equation 3.1 and the details of the kinetic parameters and experimental conditions are mentioned in Table 4.4.

Table 4.4: Experimental conditions and kinetic parameters.

Station 1	**Concentration**	**Temperature**	**pH**	**Y(final)**	**k (min)**
Ag(I)	30 mg/L	28 °C	5.92	1.6%	0.0049
Ti(IV)			5.95	8.3%	0.0460
Zn(II)			5.97	13.6%	0.0560
Station 4	**Concentration**	**Temperature**	**pH**	**Y(final)**	**k (min)**
Ag(I)	30 mg/L	28 °C	6.09	2.0%	0.0018
Ti(IV)			6.11	10.1%	0.0417
Zn(II)			6.12	15.3%	0.0501
Station 7	**Concentration**	**Temperature**	**pH**	**Y(final)**	**k (min)**
Ag(I)	30 mg/L	28 °C	6.84	3.3%	0.0073
Ti(IV)			6.87	12.6%	0.0620
Zn(II)			6.89	19.0%	0.0770
Morphology	**Concentration**	**Temperature**	**pH**	**Y(final)**	**k (min)**
ZnONNs	30 mg/L	28 °C	6.02	13.6%	0.0560
ZnONRs			5.97	12.3%	0.0577
ZnOMFs			5.98	11.3%	0.0578

4.3.1.2 Influence of pH variations

Figure 4.11, illustrates the effect of pH variation on stability of PEI@AgNPs. Interestingly, as the pH of the solution in dissolved oxygen increases, the absorption maxima were slightly red shifted along with peak broadening (Figure 4.11a). This effect was due to the reduction in particle-particle repulsive interactions among the cationic PEI@AgNPs by the addition of –OH ions. The reduction in repulsive forces results in the cross-linking among the particles through hydrogen bonding of axial amine groups of the polymer (Lin et al., 2008a). The red-shifted absorbance due to cross-linking also decreased the zeta-potential values (Figure 4.11b) due to the involvement of surface amine groups by increasing medium pH (Akaighe et al., 2012).

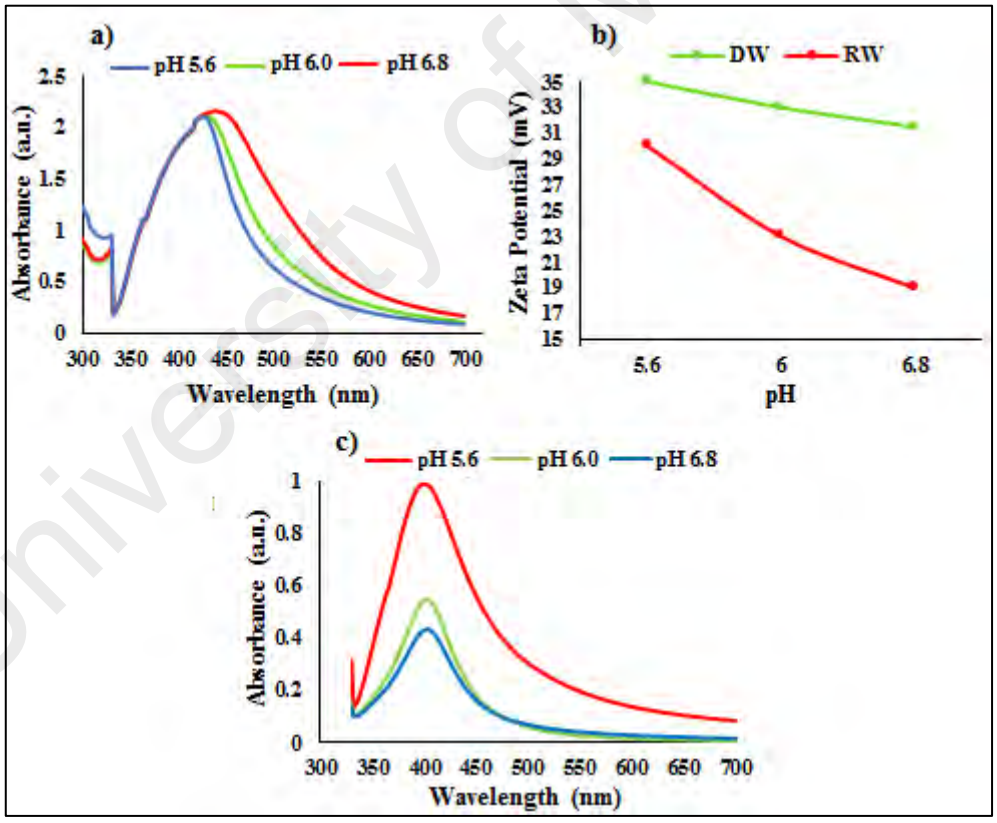

Figure 4.11: The effect of pH on PEI@AgNPs in DW (a) and RW (c) and the corresponding zeta potential values of PEI@AgNPs under different solution pH of DW and RW (b).

To check the effect of pH variation in three RW samples i.e., pH-5.6, 6.0, and 6.8, these particles were subjected to introduce in Station-1, Station-4 and Station-7, respectively. The changes occurred in the surface plasmon resonance (SPR) feature at 427 nm were recorded at 28 ºC after 2 hours. The result revealed that these particles rapidly undergo dissolution by releasing ionic metal from the outer polymer layer (Figure 4.11c). As shown by the figure, the peak intensity of PEI@AgNPs lowered as the RW pH increases, however, no peak broadening and shifting to higher frequency was observed. These results suggested that in the case of DW the broadening and shifting in absorption peak was due to more compact structure and cross-linking among the particles (Sato et al., 2003). This cross-linking of PEI@AgNPs might play a role in the wrapping of NPs and therefore prohibiting the rapid release of ionic metal (Soliman et al., 2015).

Also, as can be seen from the zeta potential analysis (Figure 4.11b), the cationic charge on the PEI@AgNPs surface greatly decreases when exposed to RW. This decrease in surface charge values confirmed the disintegration of the outer polymer layer by medium constituents. In DW, the slight decrease in cationic charge was may be due to the involvement of surface amine groups in cross-linking among the particles.

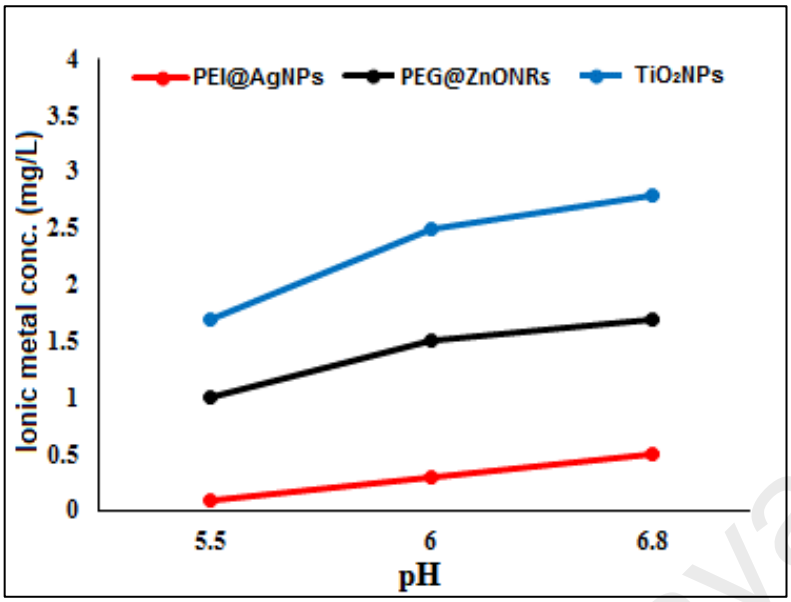

Figure 4.12: Ionic metal release profile from PEI@AgNPs, PEG@ZnONRs and TiO_2NPs under solution pH (5.6, 6.0, and 6.8).

In contrast, no such phenomenon of cross linking was observed when either PEG@ZnONRs or TiO_2NPs was exposed to deionized water of similar RW pH (pH 5.6, 6.0 and 6.8). More specifically, the absorption spectra of both PEG@ZnONRs and TiO_2NPs were slightly decreased due to electrostatic repulsion between negatively charged surface group and added OH- ions. The ionic metal release profile from metal based NMs in all three solution pH is presented in Figure 4.12.

As figure represents, ionic metal release from metal based NMs increases as the solution pH increases from 5.6-6.8. However, the minimum ionic release (0.5%) was observed in case of PEI@AgNPs compared to PEG@ZnONRs and TiO_2NPs which was 3% to 2% respectively. Previous study has shown that the particle dissolution and ionic metal release was decreased approximately 3 fold as the pH values increases from 5.68 to 8 (Liu et al., 2010a).

However, this study attribute to the different outcome of result and ionic metal release was predominant with increasing pH values from 5.6 to 6.8, which may be

due to the specific solution chemistry of river water used in this study. In addition to this, another research report (Miao et al., 2010), concluded that the dissolution of ionic metal from metal nanoparticles was found to be pH dependent and quick dissolution occurred with substantial change of solution pH.

4.3.1.3 Effect of Ionic Strength (IS)

The surface water bodies typically consist of dissolved concentration of monovalent and divalent salts, which determine its reactivity and eventually dictates the fate and transport of nanomaterials (Lanphere et al., 2014). The complexity of RW depends on the presence of several anions, cations and certain dissolved organic and inorganic molecules at water interface (Pensini et al., 2012). In order to characterize the effect of ionic strength of both monovalent (KCl, NaCl) and divalent ($CaCl_2$, $MgCl_2$) salts, the coated and uncoated metal based NMs were dispersed in DW with salt concentrations ranging from 2-10 mM. This range of ionic strength was selected because it is more relevant to the natural aqueous environments. The aqueous solution of metal based NMs with variable ionic strength were then pass through the column and the dissolved ionic metal concentration was investigated through ICP-MS analysis.

Figure 4.13, illustrates the concentration of ionic metal release from coated and uncoated NMs under the influence of monovalent Figure 4.13(a, b) and divalent salts Figure 4.13(c, d). In monovalent salt the ionic metal release was (2.6% - 3.3%) from PEI@AgNPs, 7.0% - 14.3% from TiO_2NPs and 8.3% - 26% from PEG@ZnONRs. Whereas, in divalent salts 2.6% - 3.6% from PEI@AgNPs, 8.3% - 10% from TiO_2NPs and 14.3% - 16.6% ionic metal release was observed from PEG@ZnONRs respectively. The minimum ionic metal release from PEI@AgNPs in turn, revealed the stability of PEI@AgNPs after exposure to both monovalent and divalent salts.

It was assumed that due to the PEI surface shielding, the Cl^- ions from monovalent and divalent salts accumulate at the surface by forming ionic double layer. However, only little oxidative complexation and ionic metal release occurred which was consistent with previous report (Kent et al., 2012). These results revealed that, the PEI coating predominantly resists the oxidative dissolution resulting in less ionic metal release from PEI@AgNPs. Whereas, in the case of PEG@ZnONRs and TiO_2NPs, the maximum ionic metal release were observed at 2 mM NaCl salt concentration. As the concentration of salts increases from 2 mM to 10 mM, the addition of more Cl^- ions resulted in particle-particle interaction which leads to the aggregation and particle settling (Badawy et al., 2010). The result indicated that, in KCl solution the dissolution rate increases from 2-6 mM in case of all metal based NMs.

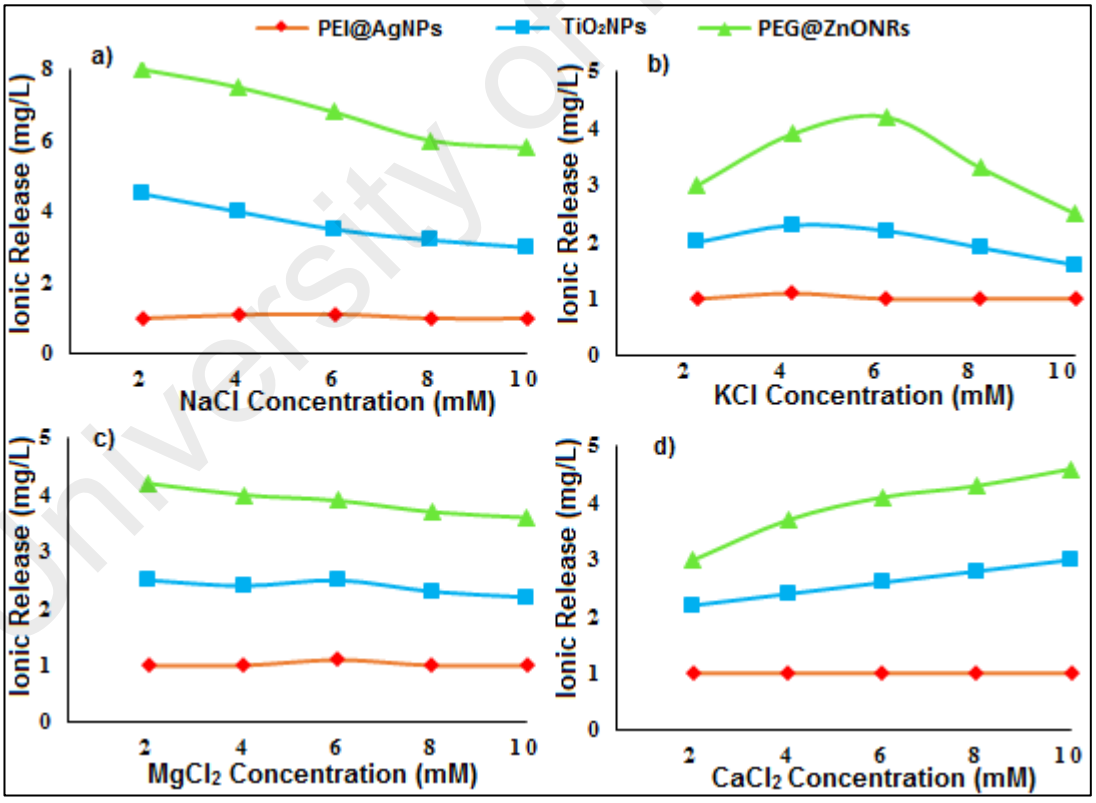

Figure 4.13: Effect of monovalent (a, b) and divalent salt (c, d) concentrations (2-10 mM) on the ionic metal release from coated PEI@AgNPs (red lines), PEG@ZnONRs (green lines) and uncoated TiO_2NPs (blue lines).

However, further increase in KCl concentration leads to the decrease in ionic metal release, particularly in case of PEG@ZnONRs due to increased column retention or aggregation state. Interestingly, in case of divalent salt ($MgCl_2$) both coated and uncoated NMs were less susceptible to both ionic metal release and retention. Similarly, the minimum retention was observed at all tested concentration of $CaCl_2$. This effect may be due to the smaller diffusion coefficient of $CaCl_2$ salts (Yang et al., 2014).

Consequently, these result suggested that, metal based NMs in the presence of divalent salts will be more resistant to aggregation and will be more mobile in the natural water bodies compared to monovalent salts. Since PEI@AgNPs was most stable towards ionic metal release and aggregation, the kinetic sedimentation rate PEI@AgNPs (in both types of salts) was investigated for one month. The aggregation or sedimentation rate was investigated through a change in absorption maxima at 427 nm. For this purpose, we employed UV-visible measurements because of the fact that surface plasmon resonance (SPR) clearly reveals the colloidal stability of PEI@AgNPs (Akaighe et al., 2012). As can be seen from Figure 4.14(a, b), the incubation with KCl resulted in the greater decrease of SPR at 427 nm after 4 weeks of incubation than with $MgCl_2$.

This support our earlier result that in divalent salt NMs was less coagulated and less aggregated and therefore can travel a longer distance when exposed to natural water of higher divalent salt formulation. In a previous study by Huynh et al., (2011), it was reported that polymer surface coating increases the particles stability towards aggregation and hence more ionic metal dissolution was possible. A similar finding was observed in this study when metal based NMs were exposed to $CaCl_2$ (10 mM), maximum dissolution with no aggregation was observed. Therefore, it is reasonable to conclude that aggregation may quench the NMs dissolution in monovalent salts (Huynh

et al., 2011) through electrostatic destabilization of outer polymer layer (Chen et al., 2006).

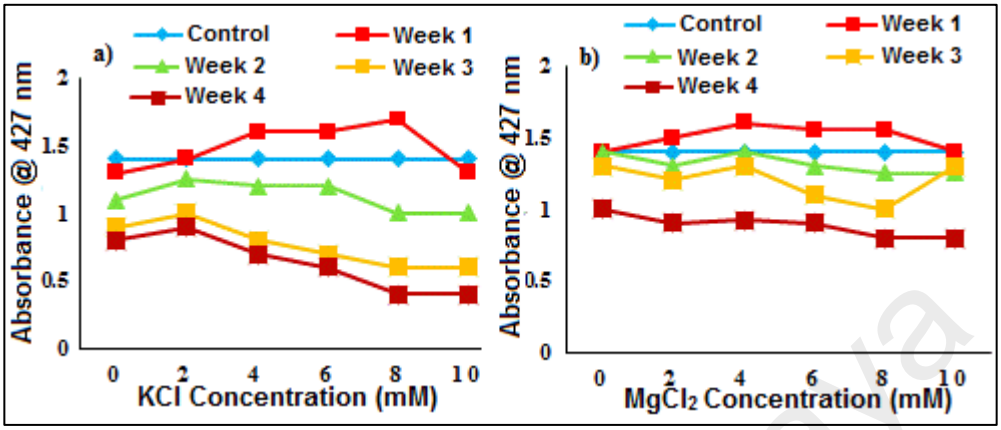

Figure 4.14: The aggregation rate of PEI@AgNPs in presence of KCl (a) and $MgCl_2$ (b) for 1-4 weeks, respectively. The PEI@AgNPs was incubated with 1-10 mM salt concentration in DW and absorbance was recorded at 427 nm at 28 ºC.

Basically, the aggregation behavior was due the increased coagulation of metal based NMs in monovalent salts. As the degree of coagulation increases, the electrostatic repulsion decrease at the surface of NMs. Therefore, in the case of monovalent salts, the aggregation rate was higher due to coagulation of the system which was in accordance with a previous report (Li et al., 2011b). This indicates that, the dissolution or aggregation of metal based NMs was highly dependent upon the type and concentration of ionic salts.

Altogether, the oxidative dissolution or aggregation is a significant factor that controlling the extent of ionic metal release from metal based NMs. Furthermore, it is also obvious that like previous study (Li et al., 2010) the dissolution of metal based NMs is highly dependent upon the type of ionic salts and its concentration. Furthermore, based on the above results, it is suggested that the surface coating plays an important role to resist the dissolution and release of ionic metal. However, the type and

concentration of electrolyte play an important role in aggregation, dissolution, and ionic metal release behavior and determine the mobility of NMs in natural aquatic systems.

4.3.1.4 Effect of Natural organic matter (NOM)

To determine the behavior of metal based NMs in natural aqueous medium, the effect of NOM was also investigated through column transport study. Figure 4.15, representing the effect of NOM on the transport and retention of metal based NMs. The % elution or column transport of PEI@AgNPs, PEG@ZnONRs and TiO_2NPs was increased in natural RW (Station-7) in the presence of NOM as compared to the synthetic water in the absence of NOM.

This behavior was due to the adsorption of NOM at the surface of NMs which resulted in increased negative surface potential of NMs (Findlay et al., 1996). As reported in earlier report by Leenheer, (2007), NOM are negatively charged substances due to the presence of hydroxyl, carboxyl and amino functional groups. The presence of these functional groups at the surface of NOM imparts negative surface potential to the NMs after being adsorbed at the surface. The increase in negative surface potential at the surface of NMs was also observed previously when metal nanoparticles were coated with NOM (Zhang et al., 2009). This increased surface potential resulted in electrostatic repulsion among particles and there by decreases the propensity of NMs to aggregate (Zhang et al., 2009).

This repulsion resulted in the reduced column attachment for all three metal based NMs and consequently more column elution was observed. In the case of PEG@ZnONRs, more % elution was observed as compare to TiO_2NPs because of high zeta-potential value (Table 4.1) which confers higher electrostatic repulsion and comparatively more % elution was observed. However, in case of PEI@AgNPs, the

presence of NOM in solution change the surface charge from positive to slight negative and increase the extent of column transport or % elution capability of PEI@AgNPs.

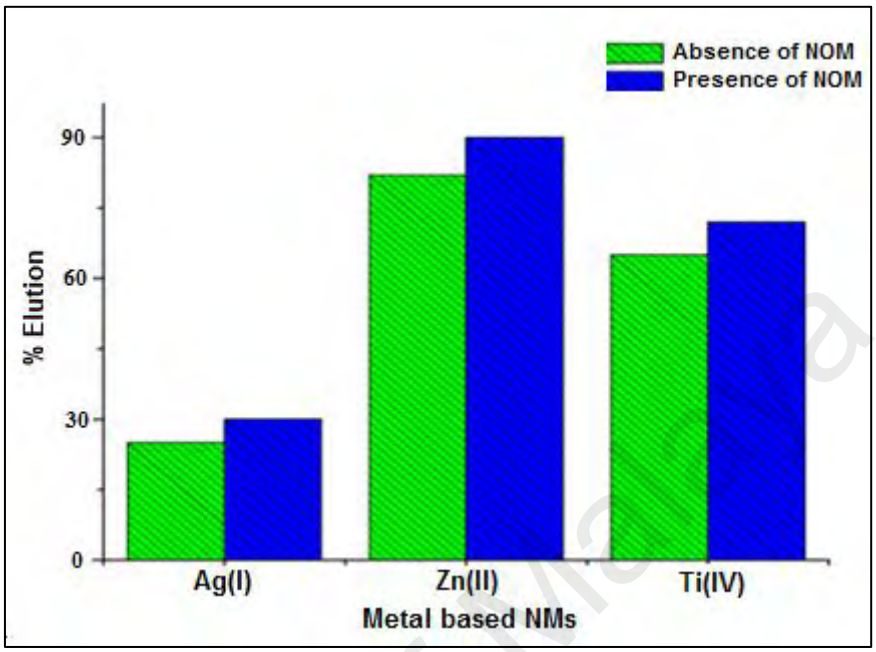

Figure 4.15: The % elution of PEI@AgNPs, PEG@ZnONRs and TiO_2NPs in the presence and absence of NOM.

To confirm the adsorption of NOM at the surface of NMs, the zeta-potential analysis of all three metal based NMs was carried out. As shown in Figure 4.16, in the presence of NOM, the zeta-potential values of all metal based NMs was negative regardless of their original zeta-potential values. After NOM adsorption at the surface, the zeta-potential value for PEI@AgNPs changed from +17 mV to -10 mV, for PEG@ZnONRs from -21 mV to -32 mV and in case of TiO_2NPs zeta-potential value changed from -17 mV to -25 mV respectively. It indicates that NOM imparted negative charge to NMs surfaces and increased their absolute surface potentials as reported previously (Zhang et al., 2009).

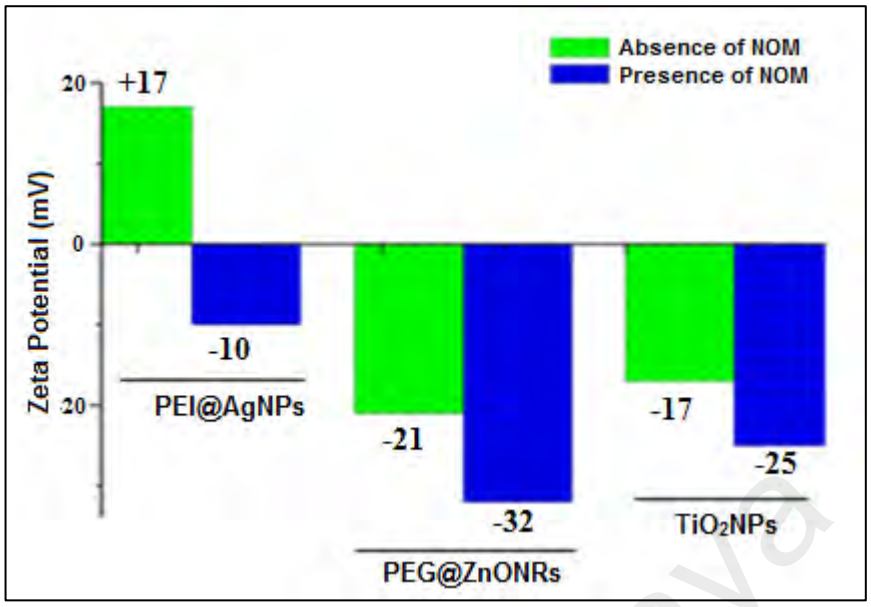

Figure 4.16: The Zeta-potential values of PEI@AgNPs, PEG@ZnONRs and TiO_2NPs NMs in presence and absence of NOM.

It was also evident that, in the presence of NOM the surface coating of NMs (both negative and positive) had a less impact on the transport potential of NMs and was mainly determined by the adsorption of NOM at the surface. This effect was also observed previously when gold nanoparticles stabilized with different capping agents were reacted with NOM (Stankus et al., 2010). The mechanism of NOM adsorption at the surface of PEI@AgNPs was electrostatic attraction between positively charged particles and negatively charged NOM, which was confirmed by negative surface of PEI@AgNPs in zeta-potential analysis (Figure 4.16). Whereas in PEG@ZnONRs and TiO_2NPs, the adsorption affinity of NOM may be due to the ligand exchange between the carboxyl/hydroxyl groups of NOM and the hydroxyl groups on the PEG@ZnONRs and TiO_2NPs surface as discussed in detail in earlier report (Wang et al., 2016b). Thus, the presence of NOM influences the behavior of NMs by adsorption or surface coating, resulting in NMs surface transformation which provides stability to the NMs towards aggregation in natural water as reported by Findlay et al., (1996).

4.3.2 Behavior of Carbon Based NMs

Figure 4.17, represented the observed breakthrough curve (BTCs) for the transport of CNPs and GOQDs in RW samples of different ionic compositions. The experimental breakthrough curves described well with model advection dispersion equation (Equation 3.2) with all the R^2 values higher than 0.90. As shown by the BTCs, the transport of CNPs was greater in all experiments as compared to GOQDs and more CNPs were eluted from the column. If the size and zeta potential values of both NMs were compared (Table 4.2) it was notable that the particle size of CNPs is smaller whereas, the zeta potential value is higher than the GOQDs.

As it was reported earlier (Zhou et al., 2016) that the less negative zeta potential value bound to induce weaker electrostatic repulsion forces between the particles and therefore more column retention was observed in GOQDs. This suggested that the transport behavior of both NMs is largely dependent upon the particle size and zeta potential value and more transport occurred with smaller particle size and higher zeta potential value.

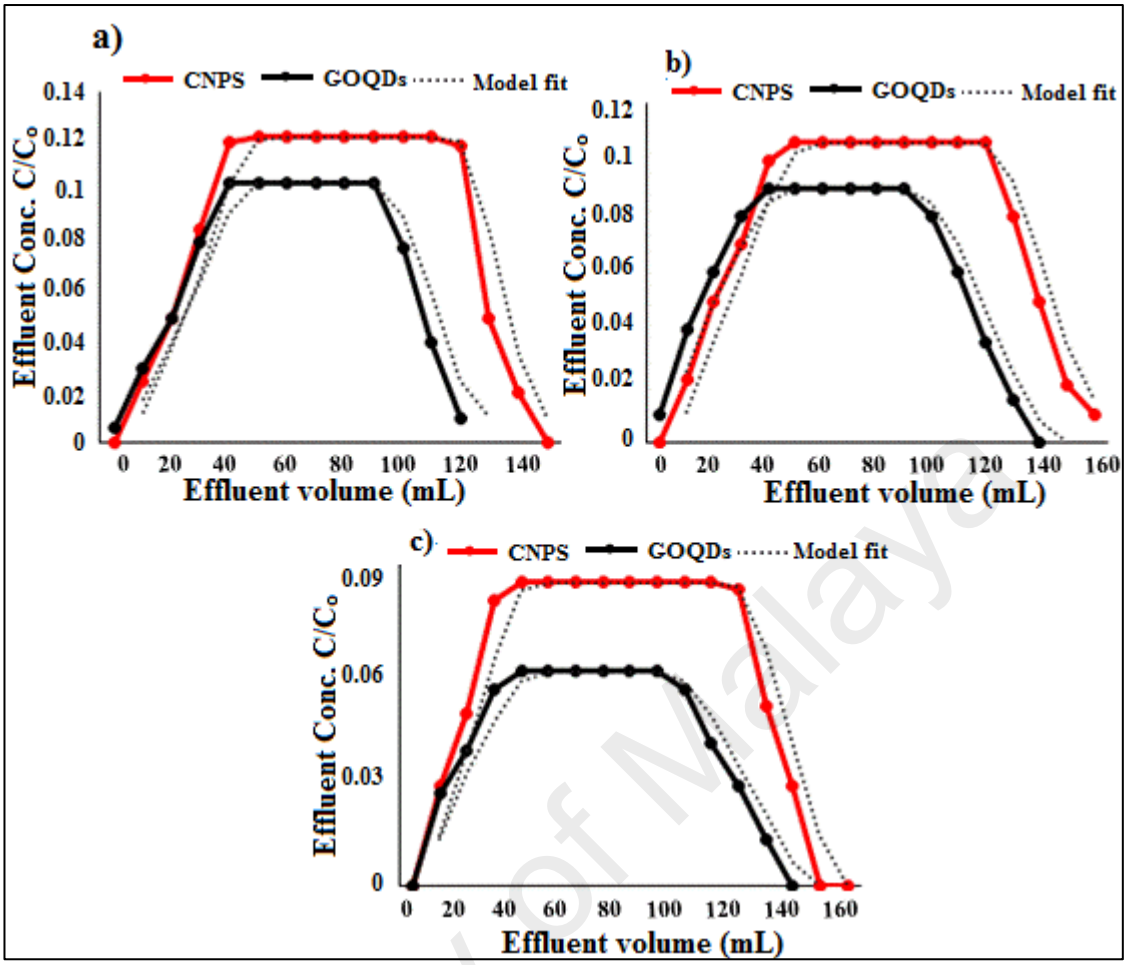

Figure 4.17: Breakthrough curves (BTCs) for the transport experiments of CNPs and GOQDs in RW Station-1 (a), Station-4 (b) and Station-7 (c) samples. The model calculated transport fits are shown by the black dotted lines.

From all these three transport experiments, it was also observed that the elution concentration of both NMs decreases as the ionic composition of dissolved substances increases from RW Station-1, Station-4 & Station-7 samples. This result is consistent with previous report (Zhou et al., 2016) when graphene oxide transported through column at low ionic strength (1 and10 mM) whereas, greater column retention occurred at higher ionic strength value i.e., 100 mM. Typically in the BTCs, the peak effluent concentrations (C/C_o) max at Station-1 was 1.5 times higher in the case of CNPs and 1.9 times higher in case of GOQDs as that of Station-7. The peak effluent concentration (C/C_o) max was decreased from 0.12-0.09 and 0.1-0.06 for CNPs and GOQDs respectively, from Station-1 to Station-7. It means that the concentration of

eluted NMs or the transport of NMs is largely controlled by the ionic composition of RW. This effect of decreased BTC plateaus due to increased ionic strength was also observed previously (Jiang et al., 2012). Basically, the increased ionic strength of solution resulted in the column flocculation (Lin et al., 2010) and therefore less transport and more column retention of NMs were observed.

Figure 4.18, represents the spatial distribution of retained CNPs and GOQDs in the column right after the transport experiments. As figure shows, the retention of GOQDs was higher than the CNPs which also reflect the result of a transport study (Figure 4.17). The retention of both NMs decreases as the distance from the column inlet increases.

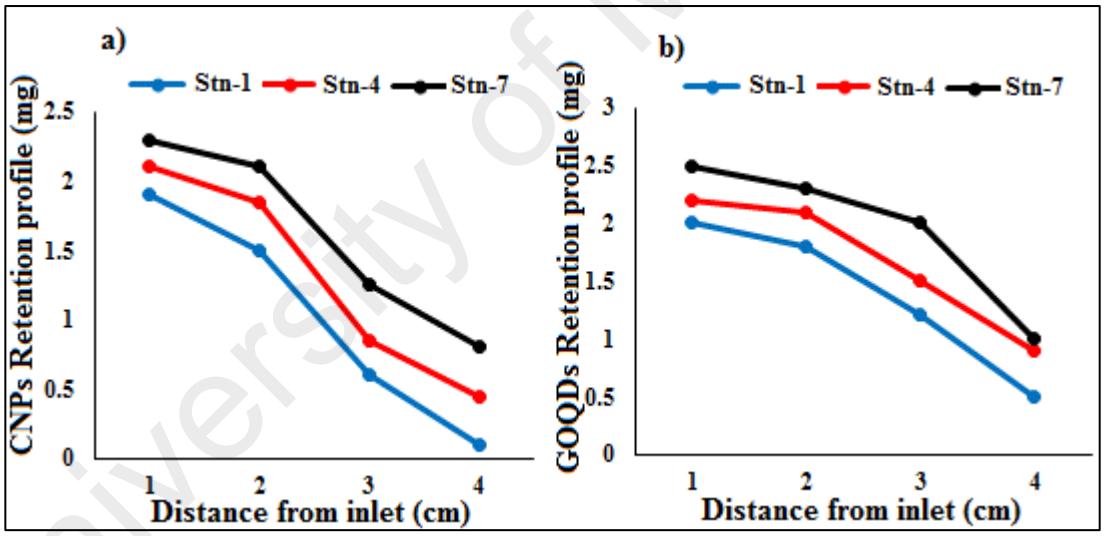

Figure 4.18: The column retention profile of CNP (a) and GOQDs (b) in RW samples from Station-1, Station-4 and Station-7.

Similar to column transport, the retention of NMs into the column was strongly dependent on the ionic strength of the solution and more retention was observed in the high ionic strength solution i.e., Station-7. These retention profiles are consistent with the previous work (Fan et al., 2015) which showed that the retention of graphene oxide in sand column was strongly dependent on ionic strength resulting serious

deposition rates (R_d) at the higher ionic strength values. Therefore, it is anticipated that the retention profiles or column attachment of both NMs increases as the ionic strength of the solution increased.

4.3.2.1 Effect of Solution pH

Figure 4.19, revealed the effect of pH on the behavior of CNPs and GOQDs. Sharp BTCs were observed at 10 pore volume for all three solution pH i.e., pH=5.6 (a), pH=6.0 (b) and pH=6.8 (c). Similarly, during the rinse phase of column transport experiment, the normalized effluent concentration (C/C_0) decreased sharply to almost zero when particle free solution was fed to the column. The mathematical model fit (Equation 3.2) closely matched the experimental BTCs for CNPs and GOQDs at all pH values with R^2 higher than 0.92. As depicted by the figure, sharp BTCs was observed for CNPs at all tasted solution pH with little to no column retention. On the contrary, small BTCs was observed for the transport of GOQDs particularly at lowest pH (pH-5.6), realizing the fact that, the transport of GOQDs was more susceptible to solution pH. Typically, the peak effluent concentration (C/C_0) max for CNPs was 0.5 ± 0.02, 0.5 ± 0.01 and 0.45 ± 0.02 for pH values 5.6, 6.0 and 6.8 respectively. While, C/C_0 values for GOQDs were in the order of 0.2 ± 0.01, 0.4 ± 0.03 and 0.3 ± 0.03 for pH values 5.6, 6.0 and 6.8 respectively.

The model results also demonstrated that solution pH had influence on the retention and transport of GOQDs. The pH dependent transport phenomenon was also observed previously when CeO_2 nanoparticles were transported through porous column transport (Li et al., 2011d). According to this study, the transport of CeO_2 nanoparticles was inhibited which was evident from little to no BTCs, when solution pH was decreased from pH-9 to pH-3 indicating the stronger attachment of CeO_2 to the column surface.

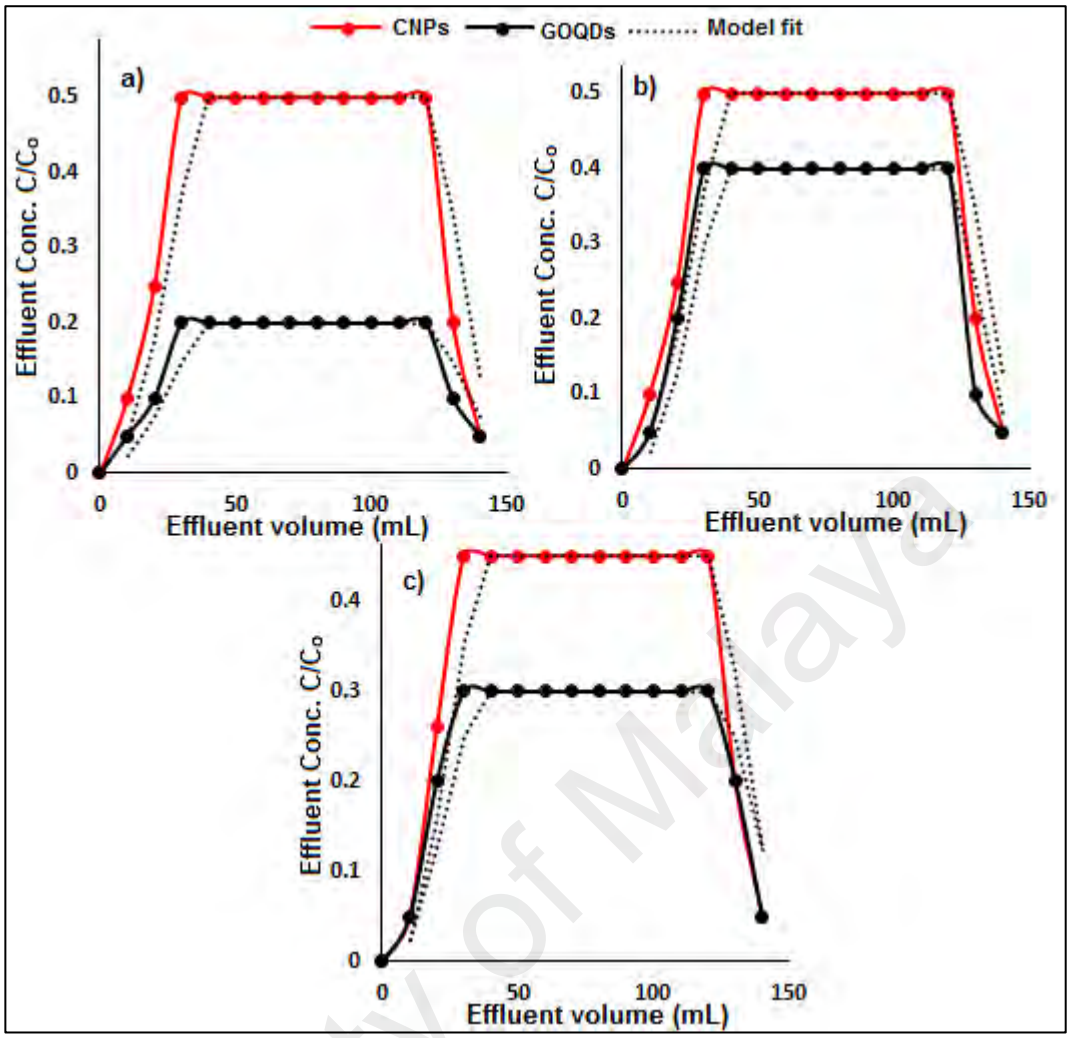

Figure 4.19: Breakthrough curves (BTCs) for the transport experiments of CNPs and GOQDs at pH 5.6 (a), 6.0 (b) and 6.8 (c). The model calculated transport fits are shown by the black dotted lines.

Similar trend was observed in this study when GOQDs was transported at pH values from pH-5.6 to pH-6.8. In addition to this, another recent report concluded that pH has a significant influence on the transport of graphene oxide nanoparticles which was decreased from 51.7% to 40.3% when solution pH decreased from 9.5 to 4.5 (Dong et al., 2017). The reason of low transport behavior of GOQDs compared to CNPs may be explained well by surface potential values. As presented in Table 4.2, the zeta-potential value for GOQDs was lower than CNPs which were -24 mV and -40 mV respectively.

The low transport of GOQDs at pH-5.6 is attributed to the fact that, GOQDs contains small amounts of surface hydroxyl (OH^-) functional groups in contrast to CNPs, which can dissociate at relatively low pH values (pH 5.6) resulting in less negative surface charge, less electrostatic repulsion and more column deposition (Dong et al., 2017). This suggested that surface potential has a strong influence on the transport behavior of carbon based colloids. Therefore, CNPs with high surface charge was more stable towards all three solution pH with little to no column deposition. On the other hand GOQDs transport was retarded at lower pH value (pH-5.6).

4.3.2.2 Effect of Ionic Strength

For the transport behavior study of both carbon based materials, the effect of monovalent salt (NaCl) and divalent salts ($CaCl_2$) was also taken into consideration. For this purpose these two salts were selected because Na^+ and Ca^{2+} are the dominant cations present in most natural aqueous medium (Lanphere et al., 2014). Figure 4.20, represented the breakthrough curves for the transport and retention behavior of CNPs and GOQDs in presence of NaCl (a, c) and $CaCl_2$ (b, d).

The transport of CNPs and GOQDs just like metal based NMs (Figure 4.13), were more susceptible to column retention towards monovalent salt/NaCl (Figure 4.20a, c). Whereas, the transport of both NMs was less susceptible towards divalent salt/$CaCl_2$ (Figure 4.20b, d) with little column retention. Results revealed that the presence of NaCl with varying aqueous concentrations, resulted in the maximum retention of both NMs which was evident from the concomitant decrease in breakthrough curves at NaCl concentrations 2-10mM.

The peak effluent concentration (C/C_0) max at maximum NaCl concentration (10 mM) was decreased from 0.8 ± 0.02 to 0.3 ± 0.01 in case of CNPs (Figure 4.20a) and from 0.60 ± 0.02 to 0.25 ± 0.03 in case of GOQDs (Figure 4.20c) respectively. However, this significant decrease in peak effluent concentration (C/C_0) max was not such prevalent in case of $CaCl_2$ even at maximum concentration of 10 mM. The peak effluent concentration (C/C_0) max was decreased from 0.8 ± 0.02 to 0.6 ± 0.01 in case of CNPs (Figure 4.20b), and from 0.65 ± 0.03 to 0.45 ± 0.01 in case of GOQDs (Figure 4.20d) respectively in presence of 10 mM $CaCl_2$.

The total deposition rate (R_d) calculated from the mass recovery of added NMs in presence of NaCl (10 mM) at pH value 6.8, was 63% in case of CNPs, and 45% in case of GOQDs. Whereas, the R_d were 25% for CNPs and 23% for GOQDs in presence of $CaCl_2$ (10 mM), respectively. This suggested that the transport behavior of both carbon based NMs was strongly influenced by the concentration of monovalent salt/NaCl. While in the presence of divalent salt/$CaCl_2$ the transport of CNPs and GOQDs was less affected. These results were consistent with previous report when gold nanoparticles were transported in saturated porous media in presence of NaCl (Afrooz et al., 2016). According to this study the transport behavior of gold nanoparticles was significantly decreased as the concentration of NaCl electrolyte increases from 1 mM to 100 mM and lowest break through profile was observed at 100 mM NaCl concentration.

The mechanism of CNPs and GOQDs decreased transport behavior in presence of NaCl can be described well with previous report (Chowdhury et al., 2013) that this behavior was because of the cation bridging effect with increasing NaCl concentration. This cation bridging between surface hydroxyl (OH^-) of carbon based colloids and added NaCl, resulting in the progressive deposition of electronegative CNPs and

GOQDs as the concentration of NaCl increased. Analogous finding of cation bridging was also observed in earlier reports for the transport of several other carbon-based materials (Bouchard et al., 2009; Saleh et al., 2008).

In presence of $CaCl_2$ (2-10 mM), the BTCs for CNPs and GOQDs were also decreased to some extent. However, the retention of both NMs was about 38% to 22% lower as that of retention observed in presence of NaCl (2-10 mM). The minimum column retention observed in presence of $CaCl_2$ may be due to the smaller diffusion coefficient of $CaCl_2$ salts as observed before (Yang et al., 2014).

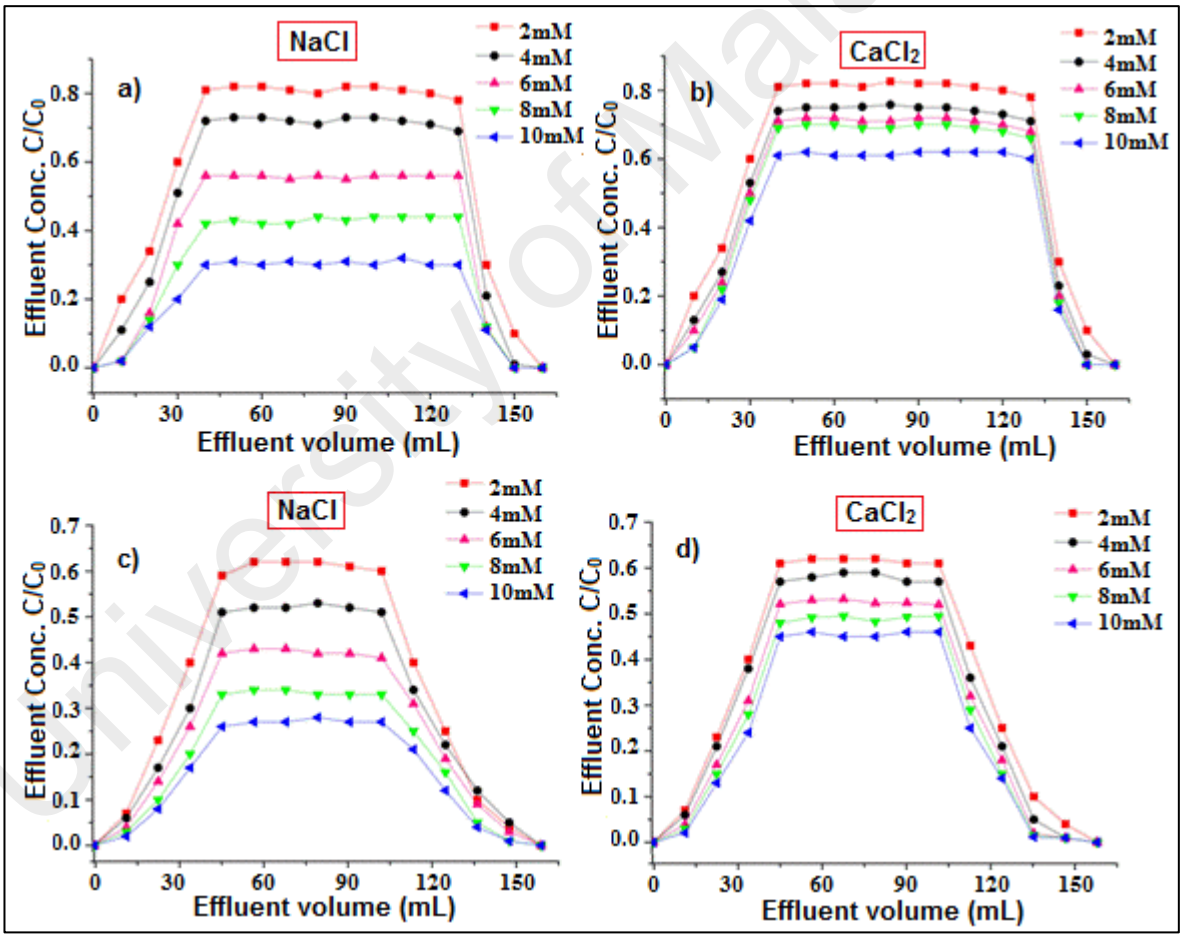

Figure 4.20: Breakthrough curves (BTCs) for the transport of CNPs (a, b) and GOQDs (c, d) in presence of monovalent (NaCl) and divalent ($CaCl_2$) salts with concentration range varied from 2-10 mM respectively at pH value 6.8.

4.3.2.3 Effect of Natural Organic Matter (NOM)

Figure 4.21, illustrates the effect of NOM on the transport behavior of CNPs and GOQDs. As figure represents, the percent elution of both NMs slightly enhanced in the presence of dissolved NOM in RW (Station-7) compared to the synthetic water in the absence of NOM. Likewise metal based NMs, this effect may be due to the adsorption of NOM at the surface of carbon based NMs which increases the particle-particle repulsion between the negatively charged NMs and dissolved NOM. This repulsion was also confirmed by less column attachment and more elution as was also observed in previous report (Afrooz et al., 2016). The increased % elution or mass recovery values obtained in this study correlate well with the stability characterization results obtained from the literature for the transport of NMs in the presence of NOM (Godinez et al., 2013; Wang et al., 2013a).

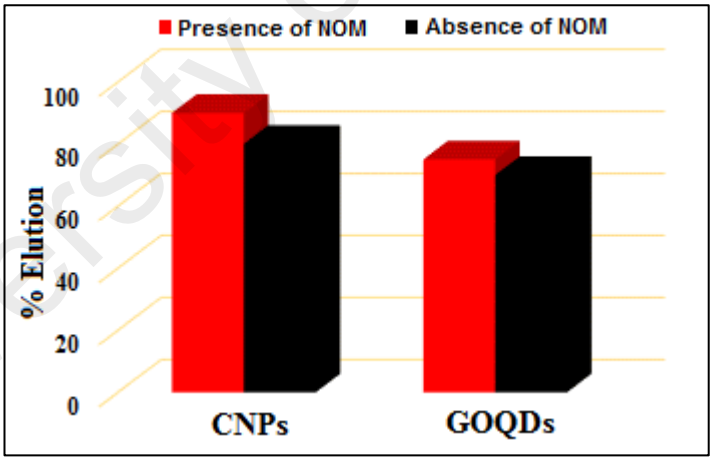

Figure 4.21: The % elution of CNPs and GOQDs with or without NOM.

According to these reports, as the NOM adsorbed at the surface of nanoparticles, a decrease in column attachment and an increase in relative mass recovery of nanoparticles were observed, suggesting that the presence of NOM enhances steric hindrance among the particles and subsequently particle stability during transport. This

observation is in agreement with what was observed in this study, when CNPs and GOQDs transport were investigated in presence of NOM. The interaction of graphene oxide nanoparticle with NOM was also observed in earlier study showing that graphene oxide exhibited specific interaction with NOM via functional group association under electrostatically unfavorable condition (Chowdhury et al., 2014). Hence, it is anticipated that, presence of NOM in natural water play vital role on the transport of carbon based colloids as reported before (Franchi et al., 2003; Qi et al., 2014b). To confirm the adsorption of NOM at the surface of carbon based NMs, zeta potential analysis was performed. Figure 4.22 displaying the effect of NOM attachment at the surface of carbon based NMs.

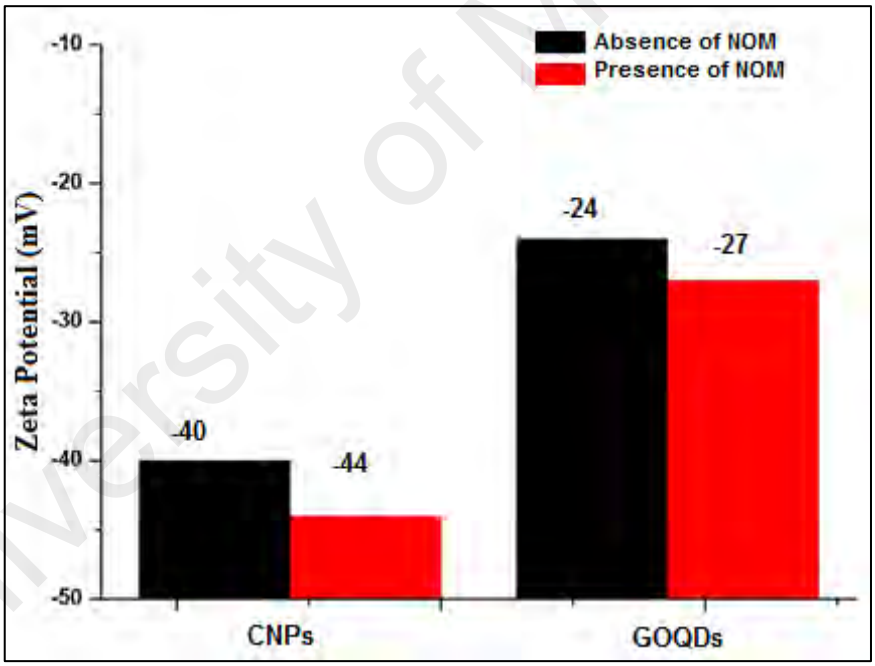

Figure 4.22: The Zeta-potential values of CNPs and GOQDs in the presence and absence of NOM.

As shown by figure the zeta-potential values of both NMs increased in the presence of NOM. Typically in case of CNPs, the surface potential change from -40 mV to -44 mV whereas, in case of GOQDs the zeta-potential value modified from -24 mV to -27 mV. It

means that the NOM adsorbed at the surface of carbon based NMs and provide stability via electrostatic repulsion among particles (Wang et al., 2015b). This enhanced stability resulted in improved transport potential of both CNPs and GOQDs. Consequently, these results depicted that the transport behavior of carbon based NMs selected in this study, was mainly controlled by factors such as, ionic composition of solution, solution pH and surface potential of CNPs and GOQDs.

4.4 Mobilization of Metal Based NMs into the Plant

This study evaluated the physiological impact, uptake and distribution of negatively charged PEG@ZnONRs and TiO_2NPs of different shape and sizes, on the growth of red bean (*Vigna angularis)* model plant. Since the dissolution rate of PEI@AgNPs was lower than PEG@ZnONRs and TiO_2NPs (Figure 4.10) therefore, for plant mobilization behavior PEG@ZnONRs and TiO_2NPs were studied. For this study, the red bean model plant was selected to evaluate the toxicity of PEG@ZnONRs and TiO_2NPs because these types of beans are widely consumed in a variety of recipes around most of the Asian countries and can easily be grows even in the lab under mild environmental conditions.

The objectives of this study are, to determine the comparative physiological and biochemical impact of PEG@ZnONRs and TiO_2NPs on red-bean plant growth (1), to investigate the effect of exposure period on the kinetic uptake and tissue distribution of both PEG@ZnONRs and TiO_2NPs (2), and to evaluate the competitive uptake and translocation of PEG@ZnONRs and TiO_2NPs in mixture of both materials (3) respectively.

4.4.1 Physicochemical Properties of PEG@ZnONRs and TiO_2NPs

The physicochemical properties of PEG@ZnONRs and TiO_2NPs in suspension are presented in the Table 4.5. As can be seen from the table, the sizes of both materials in suspensions was increased compared to its dry solid state (Figure 4.3) which largely depend upon the pH of the solution. The reason of increased size may be explained well when PEG@ZnONRs and TiO_2NPs immersed in the water, the surface of the particles was hydrolyzed because of the physically and chemically adsorbed polar water molecules (Adams, 1988).

For instance, the average diameter of PEG@ZnONRs was increased from 64 nm to 493 ± 3.01 nm whereas, in case of TiO_2NPs the maximum particles diameter in suspension was observed to increase from 89 nm to 440 ± 0.87 nm. Furthermore, as the pH of the solution decreases from 7.8-7.5 in PEG@ZnONRs and 7.5-6.9 in TiO_2NPs the zeta potential values were also varied considerably. This behavior was also observed previously (Jiang et al., 2009) that the surface charge (zeta potential) and consequently the hydrodynamic diameter can be altered by changing the solution pH.

However, in the case of the mixture of both NMs, as the pH value decreases, the corresponding particle size decreases whereas zeta potential values increases. The reason of this variation is unknown, but it was assumed that in each suspension the changes in the sizes metal nanoparticles were largely depend on the aggregation state and pH of the solution.

Table 4.5: Physicochemical properties of PEG@ZnONRs and TiO_2NPs in DI water suspension. Each data value is an average of three successive trials.

Concentration (µg/mL)	PEG@ZnONRs			TiO_2NPs			TiO_2NPs + PEG@ZnONRs		
	Size (nm)	ζ-potential (mV)	pH	Size (nm)	ζ-potential (mV)	pH	Size (nm)	ζ-potential (mV)	pH
20	474 ± 1.15	-22	7.5	105 ± 0.03	-9	7.2	415 ± 4.12	-17	7.0
40	396 ± 3.21	-21	7.6	231 ± 1.03	-12	7.3	521± 3.53	-20	7.0
60	370 ± 1.41	-25	7.6	264 ± 0.54	-22	6.9	233 ± 1.27	-34	6.8
80	468 ± 2.01	-28	7.8	295 ± 0.72	-24	7.0	335 ± 2.67	-20	6.7
100	482 ± 2.54	-40	7.6	438 ± 0.34	-27	7.5	367± 3.12	-16	7.0
200	493 ± 3.01	-44	7.5	440 ± 0.87	-29	7.3	337 ± 2.87	-13	7.0

4.4.2 Physiological impacts on plant growth

4.4.2.1 Effect of PEG@ZnONRs and TiO_2NPs on Seed Germination

As shown in Figure 4.23, the % germination was significantly enhanced particularly at concentrations 20 µg/mL to 100 µg/mL under exposure of both NMs. The mean values of the % germination for PEG@ZnONRs and TiO_2NPs were compared using one-way ANOVA statistics and found to be significant ($p < 0.05$) as compared to control test (0 µg/mL). Basically, metal-oxide suspensions increases the water uptake capacity in a concentration dependent manner (Figure 4.24) and enhance the % germination as was also observed previously (Khodakovskaya et al., 2009). The overall change in % germination was 32% and 34% in suspensions of both PEG@ZnONRs and TiO_2NPs, respectively.

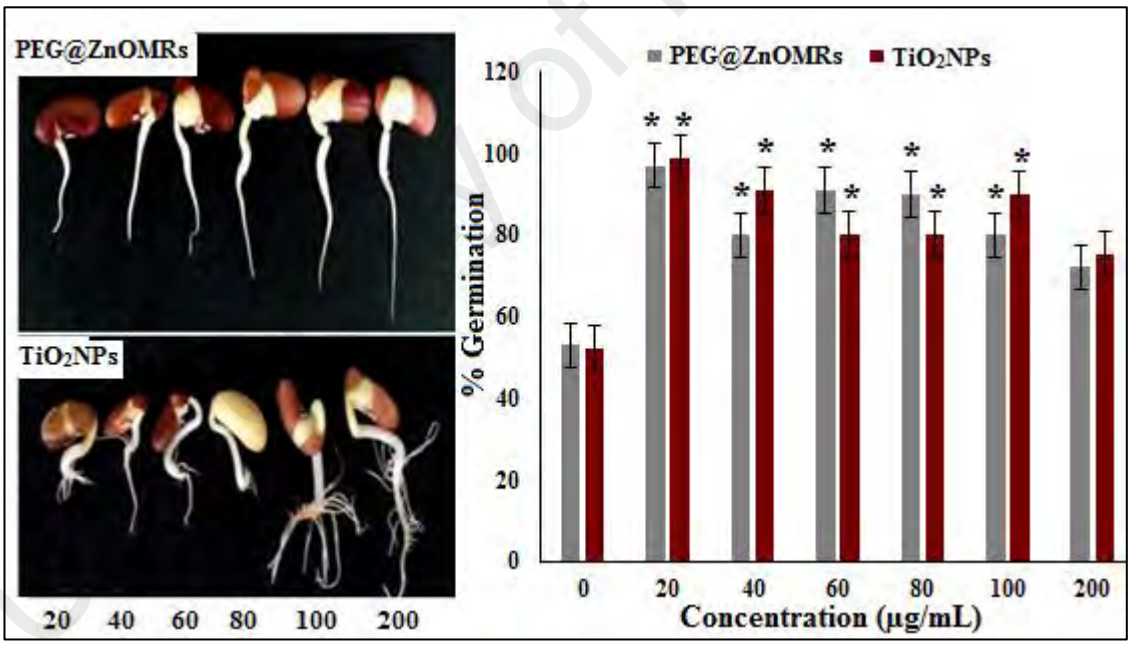

Figure 4.23: Effect of PEG@ZnONRs and TiO_2NPs suspensions (20-200 µg/mL) on % G. The % G data of both NMs were compared using one-way ANOVA statistics and found to be significant ($p < 0.05$) when comparing to control (0 µg/mL).

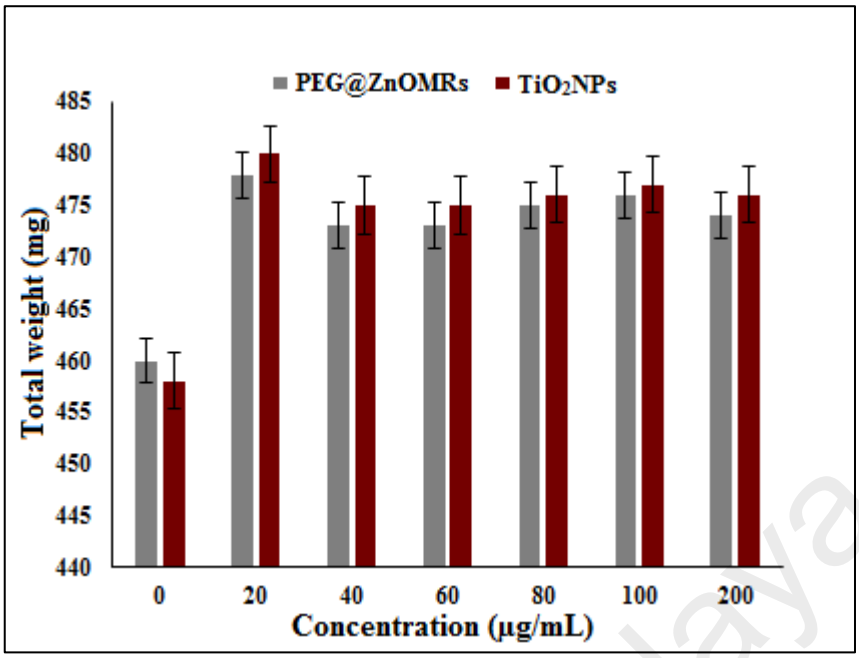

Figure 4.24: The total weight of the red-bean seeds after germination without (0) or with PEG@ZnONRs and TiO_2NPs concentration (20-200 µg/L). Total weight of seeds increases due to increase in water uptake capacity under PEG@ZnONRs and TiO_2NPs exposure.

The effect of both NMs mixture on the % germination was also examined and found that mixture of both NMs decreases the % germination by 30% compared to control (0 µg/mL) which may be due to the counter ion effect and competition among the particles which resulted in less water uptake and reduced % germination. To investigate the penetration of PEG@ZnONRs and TiO_2NPs into the seed coat, the FESEM analysis with EDS and FTIR studies of grounded cotyledon powder was carried out. The FESEM images of a cotyledon cross section with EDS spectra (Figure 4.25), revealed that both NMs successfully penetrated into the cotyledon and significantly increases the % germination. To investigate the penetration of PEG@ZnONRs and TiO_2NPs into the seed coat, the grounded cotyledon powder was investigated through the FTIR observation.

As depicted by Figure 4.26, the concentration dependent increase in vibrations around 500 cm^{-1} and 550 cm^{-1} were observed which provide direct evidence for the

internalization of PEG@ZnONRs and TiO_2NPs into the cotyledon resulting in noticeable variation in seed germination.

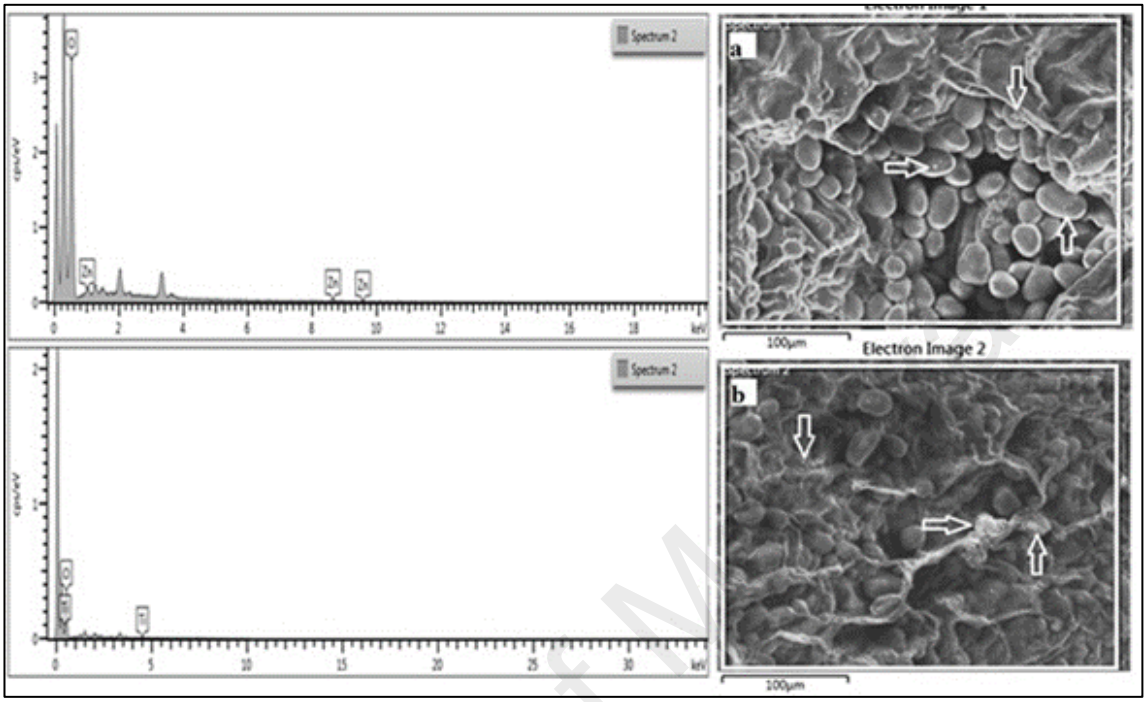

Figure 4.25: FESEM images with EDS elemental spectra of cotyledon cross section exposed to 20 µg/mL PEG@ZnONRs (a) and TiO_2NPs (b). The arrow heads representing the seeds covered by NMs.

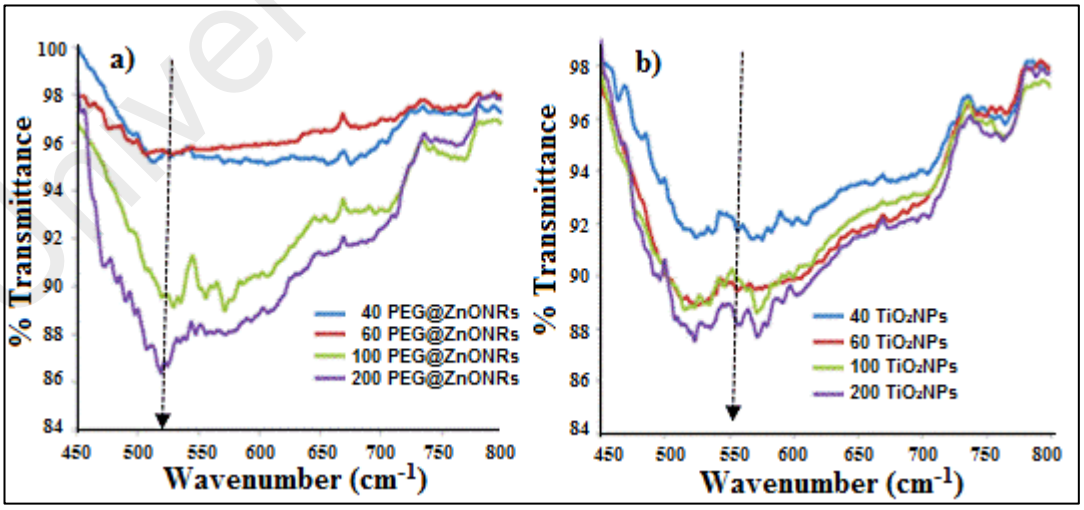

Figure 4.26: FTIR spectra of red bean cotyledon after exposure to PEG@ZnONRs (a) and TiO_2NPs (b) at concentration 40, 60, 100, 200 µg/mL. Each cotyledon was dried at 80 ºC for 5 hours, grounded into a fine powder and their respective FTIR spectra were taken at the ATR mode.

4.4.2.2 Effects on root /shoot length

Figure 4.27(a, b), disclose the effect of PEG@ZnONRs and TiO_2NPs suspensions on roots and shoots elongation. Results revealed that unlike previous study (Mukherjee et al., 2014), PEG@ZnONRs significantly inhibit ($p < 0.05$) the roots growth particularly at concentrations 40 µg/mL and 60 µg/mL when comparing to the control (0 µg/mL). Whereas, the shoot length were predominantly increased at concentrations 100 µg/mL and 200 µg/mL that was approximately ~3.5 times higher than the control. Table 4.6 revealed that the particle sizes of PEG@ZnONRs at concentrations 80 µg/mL and 100 µg/mL were quite bigger than 40 µg/mL and 60 µg/mL which limit their mobility across the roots tissues and therefore, no significant growth inhibition was observed.

Since the root tissues have smaller pores, through which only limited particles size less than several nm may freely pass. Thus, particles with diameters larger than the pores would be restricted in their ability to penetrate (Carpita et al., 1979). Therefore, fewer particles were internalized from suspensions of 80 µg/mL to 200 µg/mL and comparatively less root inhibition was observed. It was also noted that the internalization of PEG@ZnONRs in the root tissues was independent of corresponding zeta potential values (Table 4.6) and largely depends on the particle size and their concentration of dissolved ions.

Conversely, all exposed concentrations of TiO_2NPs stimulate both roots and shoots growth with significant ($p < 0.05$) root and shoot growth at 20 µg/mL and 60 µg/mL to 200 µg/mL, respectively. The root elongation depended upon the particle size in suspensions. For example, the more root elongation was observed with less particle size of TiO_2NPs. In addition, it was interesting to note that the shoots length were higher when the zeta potential values of PEG@ZnONRs and TiO_2NPs were higher.

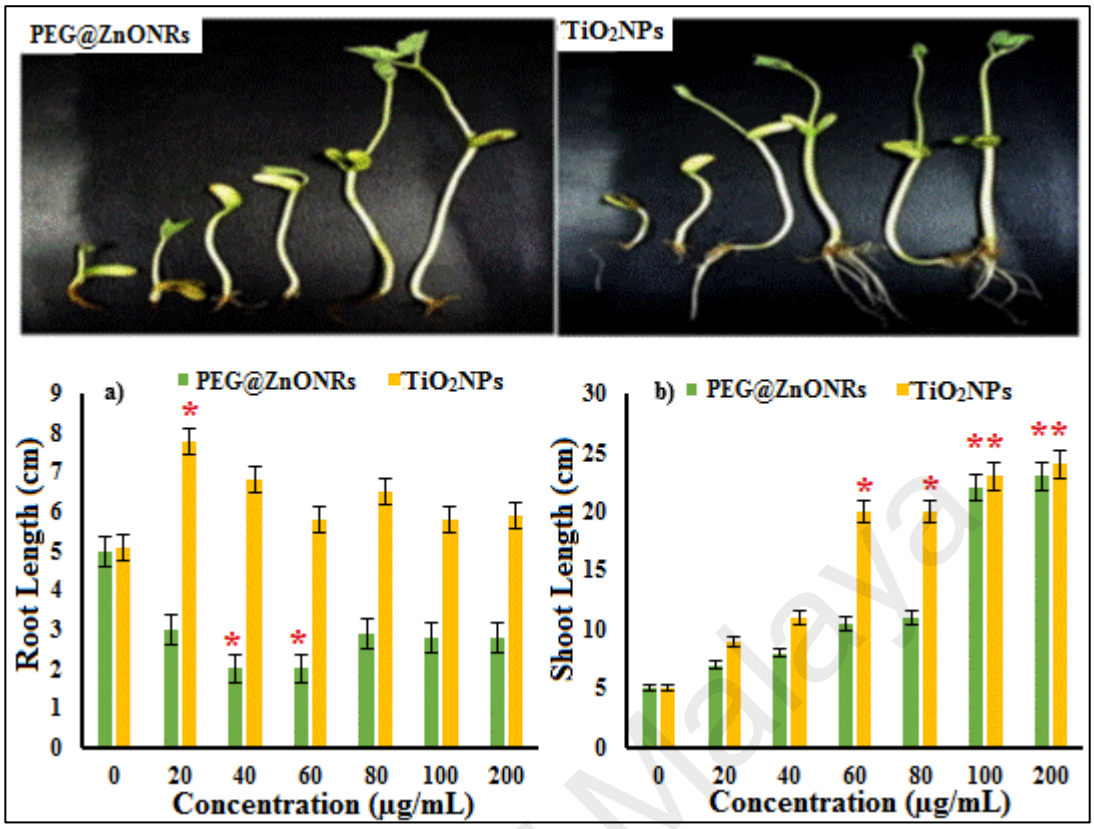

Figure 4.27: The corresponding effect of PEG@ZnONRs and TiO_2NPs concentration (0-200 µg/mL) on roots (a) and shoots (b) length of the red bean plant after one week of exposure. The bars with asterisks represents significant values ($p < 0.05$) compared to control (0).

This effect was due to the fact that particles with the less negative charge binds to the root tissues more effectively as the root surfaces are also negatively due to the presence of abundant polysaccharides and glucuronic acid units (Meychik and Yermakov, 2001). Therefore, particles with higher negative charge produce counter effect and were efficiently translocate into the plant shoots rather than accumulation into the roots tissues. Furthermore, it was also reported previously (Zhu et al., 2012) that the negatively charged particles accumulated into the root tissue to a lesser extent and move across the root epidermis into plant shoot.

The plants grown under co-exposure treatment of both PEG@ZnONRs and TiO_2NPs, revealed that the roots and shoots length was quite similar to the control

values i.e., at 0 µg/mL and no significant change was observed. Overall, the effect of PEG@ZnONRs on roots growth was negative whereas, TiO_2NPs promoted the growth of both roots and shoots. The positive growth impact of TiO_2NPs was also reported in previous reports (Hong et al., 2005; Yang et al., 2006) when spinach plant was grown in presence of TiO_2NPs.

4.4.3 Biochemical impacts on plant growth

4.4.3.1 Total chlorophyll content, Carotenoids and Lipid peroxidation

Figure 4.28, represented the significant reduction in the total chlorophyll content, and carotenoids particularly in case of PEG@ZnONRs exposed leaves. As shown by the figure, both total chlorophyll content and carotenoids like earlier reports (Nair and Chung, 2014; Rao and Shekhawat, 2014) was decreased at all PEG@ZnONRs treated leaves. This reduction negatively affects the plant ability to quench oxidative stress as also observed previously (Sharma and Hall, 1991).

Typically at 40-80 µg/mL of PEG@ZnONRs suspensions, the total chlorophyll content and carotenoids was significantly decreased ($p < 0.05$) after one week exposure respectively. This significant reduction in the total chlorophyll content and carotenoids was due to increased lipid peroxidation level significantly at 40, 60 and 80 µg/mL of chloroplast membrane generated by reactive oxygen species (ROS) as described in previous report (Mukherjee et al., 2014).

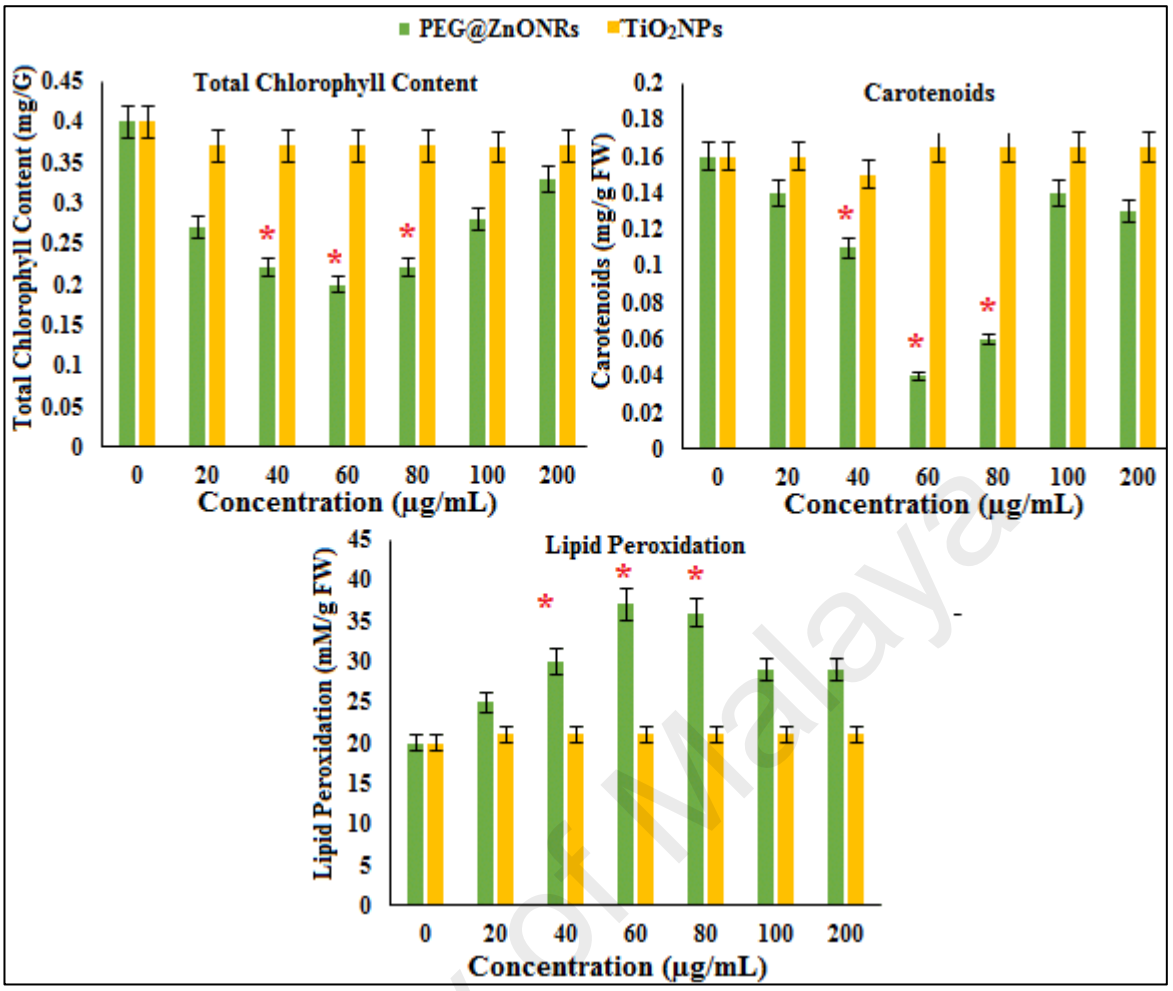

Figure 4.28: Comparison of the total chlorophyll content, carotenoid and lipid peroxidation in plant leaves grown in PEG@ZnONRs and TiO_2NPs suspensions for one week treatment. Error bars representing the mean ± SE (n = 3). Bars with an asterisk symbol show statistical significant values.

At 100 µg/mL and 200 µg/mL PEG@ZnONRs concentrations, the reduction of the total chlorophyll content and carotenoids and production of lipid peroxidation was low due to the more particle aggregation state at these concentrations. This consequently resulted in less uptake and less oxidative damage to plant leaves. In contrast to PEG@ZnONRs, the total chlorophyll content production was promoted (10%) and no decreased carotenoids and increased lipid peroxidation was observed at any concentration of TiO_2NPs.

It was believed that, TiO_2NPs stimulated the nitrogen adsorption by plant tissues, significantly promote the photosynthesis and greatly improve the growth (Hong et al.,

2005; Yang et al., 2006). The effect of PEG@ZnONRs in plant leaves exposed to two weeks and three weeks was also investigated and found that, the observed decreased in the total chlorophyll content and carotenoids, and the increase in lipid peroxidation level was nearly constant and no significant change was observed (Appendix B).

This observation contradicts the earlier report (Mukherjee et al., 2014) and revealed that the decrease in the total chlorophyll content was prominent during the one week of plant growth by inhibiting the photosynthetic process. However, the difference observed was may be due to changes in experimental conditions and the properties of PEG@ZnONRs used. The results obtained from PEG@ZnONRs and TiO_2NPs co-exposure manifested that, co-exposure of PEG@ZnONRs and TiO_2NPs mixture failed to produce any significant change in terms of the total chlorophyll content, carotenoids and lipid peroxidation level compared to control value (0 µg/mL).

4.4.3.2 Oxidative Stress and Antioxidant Enzyme Activity

Antioxidant enzymes defense system, such as catalase, glutathione reductase, superoxide dismutase and ascorbate peroxidase protects the plants against oxidative stress (Foyer and Shigeoka, 2011). To investigate the effects of PEG@ZnONRs and TiO_2NPs on plant antioxidant defense system, the activities of all above mentioned enzyme were investigated. Figure 4.29 & 4.30, displays the catalase, glutathione reductase, superoxide dismutase and lipid peroxidation activities in plant roots and shoots exposed to PEG@ZnONRs (Figure 4.29) and TiO_2NPs (Figure 4.30) for one week treatments. Results showed that, there was a significant ($p < 0.05$) decrease in the catalase and glutathione reductase activity at concentrations 40 µg/mL and 60 µg/mL in plant roots exposed to PEG@ZnONRs compared with that of control (0 µg/mL). On the other hand, no significant change was observed in shoots tissues at all PEG@ZnONRs concentrations may be due to less translocation of PEG@ZnONRs in shoot tissues.

Contradictory, the catalase, and glutathione reductase activity was unaltered in both roots and shoots at all tasted TiO_2NPs concentrations (Figure 4.30).

This recommended that, PEG@ZnONRs predominantly produced oxidative stress, particularly in the plant roots which also reflected in retarded root growth (Figure 4.27). Reduction in root length was in good agreement with previous report (Priester et al., 2012) when soybean plant grown in presence of ZnO nanoparticles. At concentrations 40 µg/mL, 60 µg/mL, and 80 µg/mL the superoxide dismutase, and at concentrations 60 µg/mL and 80 µg/mL the ascorbate peroxidase activities, significantly ($p < 0.05$) increased which indicate an increased ROS generation in roots tissues as observed previously (Xu and Chen, 2011).

The stimulated activities of both enzymes in response to metal toxicity was also observed previously and believed to reduce the oxidative damage produced in plants (Sharma et al., 2012). Nevertheless, no significant change in activity of superoxide dismutase and ascorbate peroxidase was observed at any concentration of TiO_2NPs suggesting no stress development due to overproduction of ROS. Additionally, the plant grown in the mixture of PEG@ZnONRs and TiO_2NPs, showed no evidence of significant oxidative stress via inhibiting catalase and glutathione reductase and no enhanced activities of superoxide dismutase and ascorbate peroxidase was observed compared to control treatments.

These altered toxicity compared to individual metal-oxide exposure was also observed previously (Tong et al., 2015) when toxicity of ZnO and TiO_2 was evaluated in bacterial cells in a single and co-exposure approach. Key findings obtained from this study revealed that PEG@ZnONRs and TiO_2NPs interactions and surface complexation reactions alter the original toxicity of PEG@ZnONRs and TiO_2NPs and therefore comprehensive assessments of potential ENM toxicity in the environment require

careful integration of complex physicochemical interactions between NMs and various biological responses.

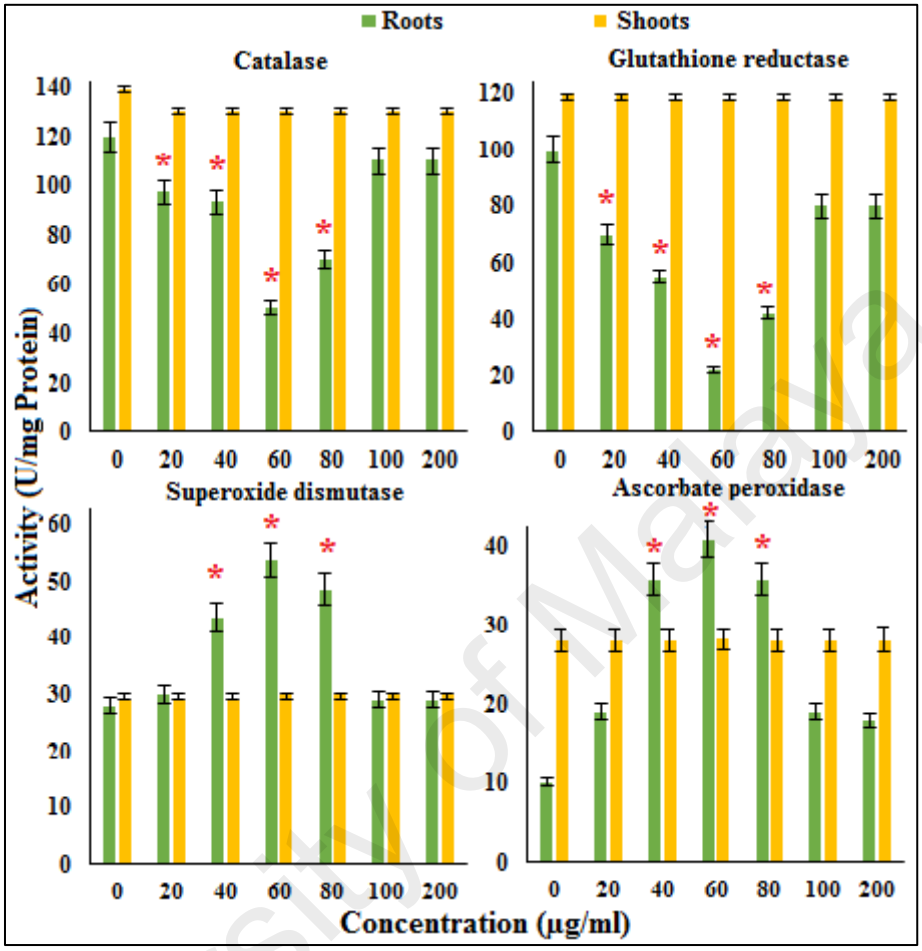

Figure 4.29: Antioxidant enzyme activities in the roots and shoots of plant grown in PEG@ZnONRs suspension for one week. Error bars representing the mean ± SE (n = 3). The bars with the asterisk symbol are significant values ($p < 0.05$).

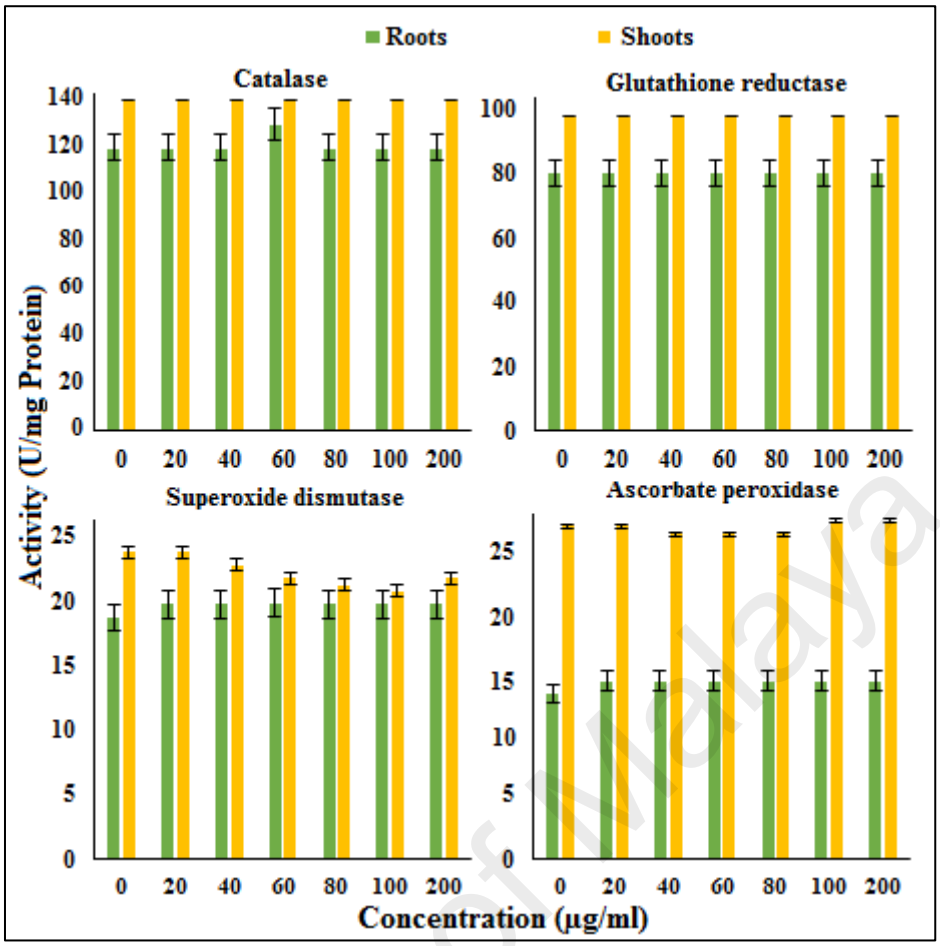

Figure 4.30: Antioxidant enzyme activities in the roots and shoots of plant grown in TiO_2NPs suspension for week 1. Error bars representing the mean ± SE (n = 3). As graph shows in all TiO_2NPs exposed plant, no significant reduction in enzyme activity was observed.

4.4.4 Uptake and Translocation

4.4.4.1 Single ENM approach

As seen in the Figure 4.31(a, b), the accumulated concentration of Zn(II) from PEG@ZnONRs in plant tissues was approximately 4 times higher than that of Ti(IV) from TiO_2NPs. It was due to the higher dissolution pattern of PEG@ZnONRs than TiO_2NPs (Figure 4.32) which showed comparatively low dissolution in aqueous solution as also reported in earlier research (Schmidt and Vogelsberger, 2009).

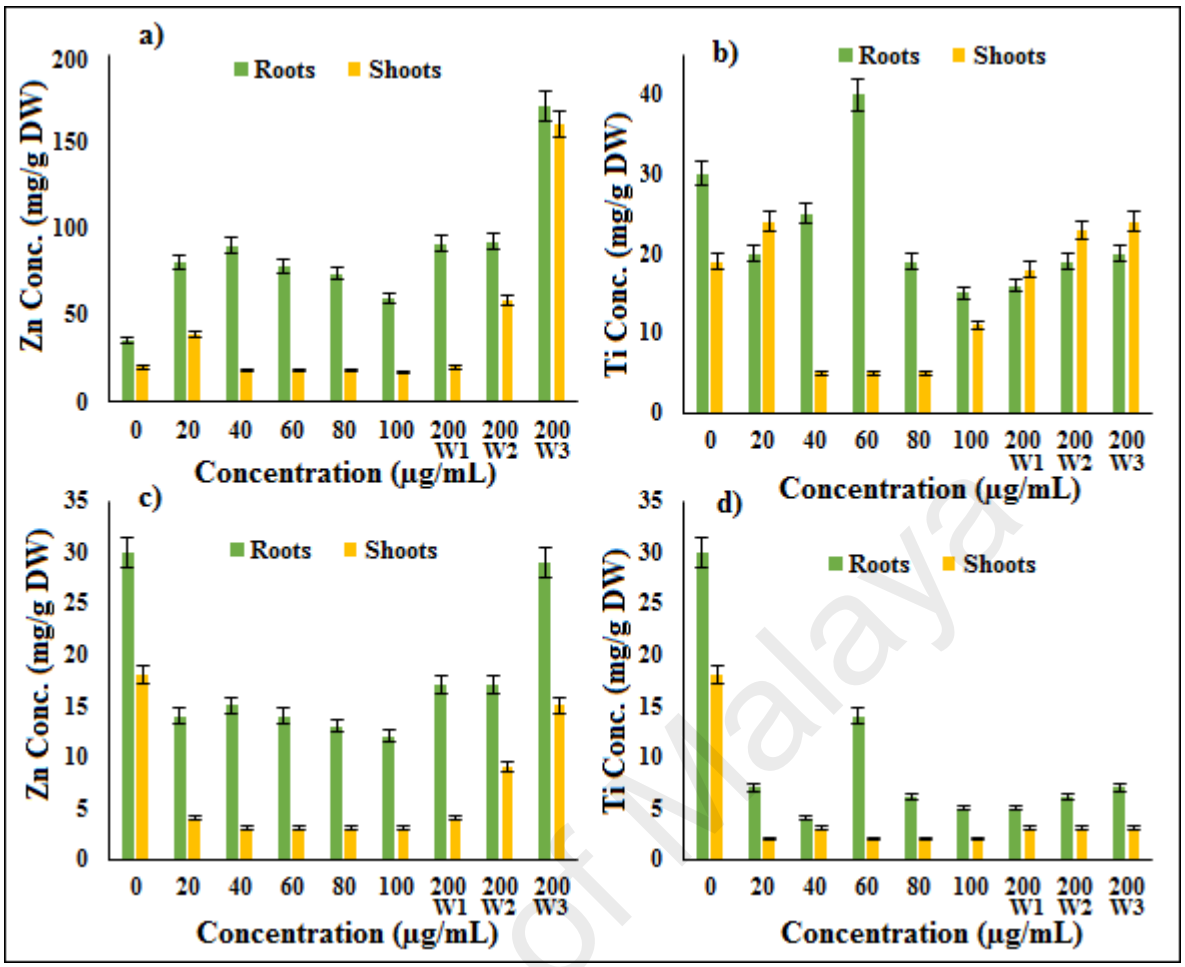

Figure 4.31: Uptake and translocation of Zn(II) and Ti(IV) from PEG@ZnONRs and TiO_2NPs into plant tissues after one week (W1) exposures under single (a, b), and NMs mixture approach (c, d). For both sets of reaction, the concentrations 200 µg/mL were also exposed to two weeks (W2) and three weeks (W3) respectively.

At the highest concentration (200 µg/mL), the accumulation of Zn(II) in roots was approximately 5 times higher than Ti(IV). However, the translocation ability to shoot tissues was limited in case of Zn(II) and less translocation to aerial parts was observed. In roots tissues, the maximum accumulation was observed at 40 µg/mL in the case of PEG@ZnONRs and at 60 µg/mL in the case of TiO_2NPs. In shoots tissues, Zn(II) accumulation was highest at concentration 20 µg/mL whereas, the accumulation of Ti(IV) correlated well with the corresponding concentration and increased linearly for one week hydroponic treatment. Overall Zn(II) from PEG@ZnONRs was largely taken

up by root cells with low translocation to shoot tissues as also observed previously when corn plants were grown in the presence of ZnONPs (Zhao et al., 2012).

Interestingly, for the kinetic uptake study (two weeks and three weeks) at concentration 200 µg/mL, we found that the accumulation of Zn(II) negligibly increased in root tissues in two weeks exposure. However, the translocation of Zn(II) to shoot tissues was approximately 3.5 times increased than one week. In three weeks, the accumulation was approximately 2 times and 10 times increases in roots and shoots respectively when compared to one week exposure.

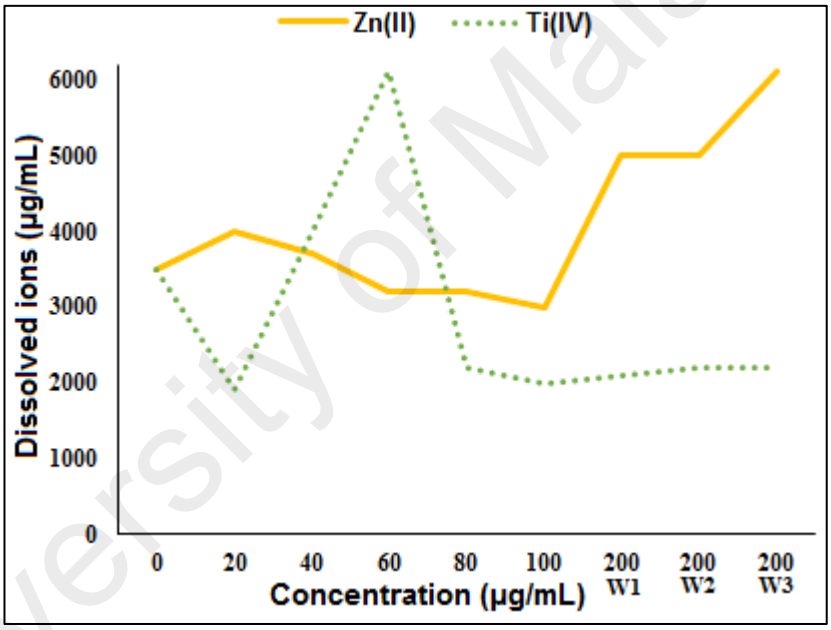

Figure 4.32: The dissolved ions concentrations of Zn(II) and Ti(IV) in PEG@ZnONRs and TiO_2NPs suspension analyzed by ICP-MS. The dissolution pattern mainly depends on the solution pH and aggregation state.

Whereas, in TiO_2NPs, the accumulations of Ti(IV) was approximately 1.3 times increased in both roots and shoot tissues. The overall kinetic increase in accumulation (two weeks and three weeks) revealed that PEG@ZnONRs and TiO_2NPs were capable of a high accumulation in plant tissues with increasing respective time. This effect may be due to the increased permeability of root cell wall at two weeks exposure period

which facilitates the extended accumulation at three weeks as indicated previously (Kurepa et al., 2010).

4.4.4.2 NMs Mixture Approach

Figure 4.31(c, d), represented the accumulation of PEG@ZnONRs and TiO_2NPs mixture (1: 1 ratios) into roots and shoot tissues. Interestingly, the uptake of Zn(II) and Ti(IV) at the highest concentration (200 µg/mL) was approximately 6 times to 3 times in root and 10 times to 12 times in shoot tissues decreases respectively compared to a single ENM approach for one week. Additionally, the similar trends were observed when the same concentration (200 µg/mL), further exposure to two weeks and three weeks. In NMs mixture approach, the overall reduction in the roots accumulation and translocation might be due to the surface complexation (Tong et al., 2015) and competition among PEG@ZnONRs and TiO_2NPs which greatly alters its comprehensive uptake and translocation.

In both single and co-exposure of PEG@ZnONRs and TiO_2NPs, some interesting uptake and translocation trends were observed at the roots physiology. The result suggested that Zn(II) binds more effectively to root tissues and was less translocated to shoot. This behavior might be due to the larger particle sizes of PEG@ZnONRs which prone to restrict their high accumulation and less translocation to shoot tissues. However, in the case of TiO_2NPs, the accumulation in the root was more prevalent in co-exposure of NMs mixture. PEG@ZnONRs and TiO_2NPs mixture owing to its reduced uptake and translocation capacity, resulted in less physiological effects on plant growth and no significant inhibition of the total chlorophyll content and carotenoids and no representative variation in oxidative enzymes activity was observed. Therefore, in this study, although the combination of PEG@ZnONRs and TiO_2NPs pose attenuated uptake and translocation behavior, however, did not influence oxidative stress as

observed previously (Tong et al., 2015) because of surface complexation and competition among the PEG@ZnONRs and TiO_2NPs in mixture.

4.4.5 Translocation Factor (TF)

Figure 4.33, displays the TF of both NMs. As shown in the figure (4.33a), in a single ENM approach, the overall TF of Ti(IV) (at concentrations 40 µg/mL and 80-200 µg/mL) was higher than Zn(II) with significant translocation ($p < 0.05$) at concentrations 100 and 200 µg/mL.

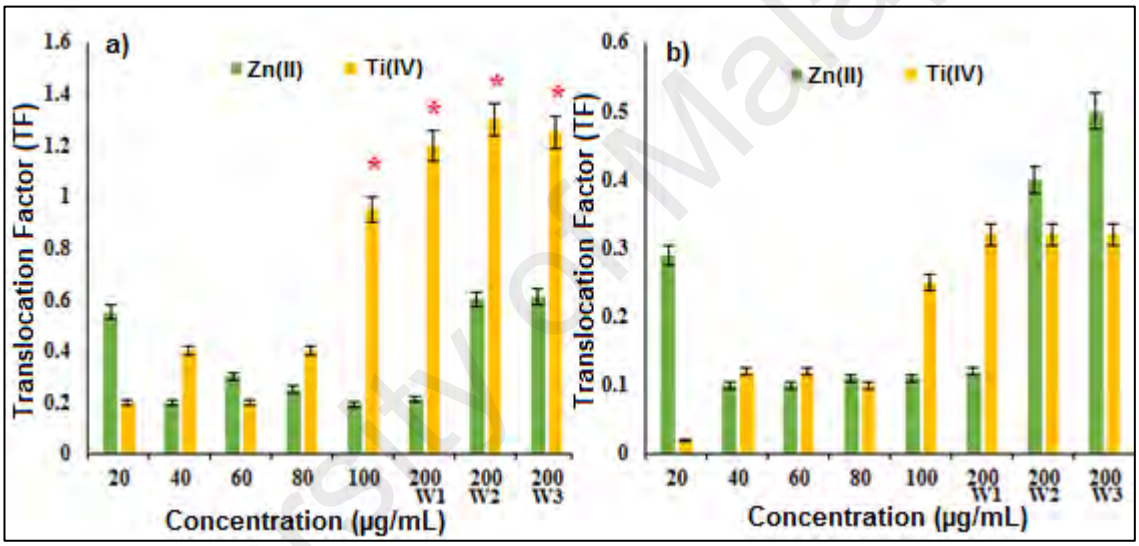

Figure 4.33: TF of Zn(II) and Ti(IV) in a single (a) and NMs mixture (b) approach.

However, at concentrations 20 µg/mL and 60 µg/mL, the TF of Zn(II) to shoot tissues was slightly higher. The reason lies in the fact that, the TF of metal nanoparticles mainly depends on the surface charge (Zhu et al., 2012) more negative surface charge facilitates more translocation (Table 4.6*)*. In the case of PEG@ZnONRs, at concentrations 80, 100 and 200 µg/mL although the surface charge was more negative, but exhibit low TF of Zn(II) this was probably due to a higher aggregation state of PEG@ZnONRs at these concentrations which resulted in a high roots accumulation and low translocation. Interestingly, in a NMs mixture approach (Figure

4.33b) the TF was about ~1.8 times and 4 times decreases in both PEG@ZnONRs and TiO_2NPs respectively. It means that the in a PEG@ZnONRs and TiO_2NPs co-exposure approach, the TF for Zn(II) were ~2.2 times higher compared to Ti(IV) and more Zn(II) were translocated from roots to shoot tissues. It indicates that in NMs co-exposure treatment, the translocation of Ti(IV) was inhibited or suppressed by Zn(II) ions which was not observed in a single NMs approach where more translocation of Ti(IV) to shoot tissues was notable. All these contrast findings up to the comparative and competitive level suggested that the PEG@ZnONRs and TiO_2NPs displayed distinct physiological and biochemical effects on plant growth.

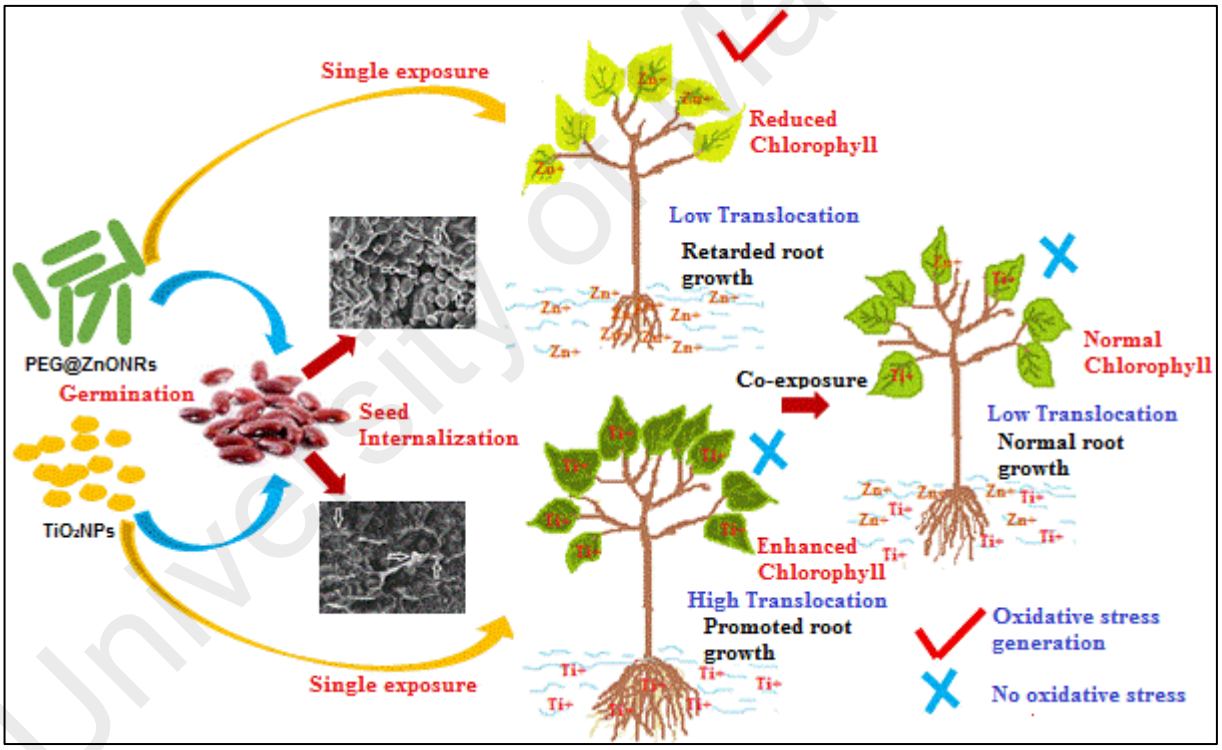

Scheme 4.1: Graphical representation of the effects of PEG@ZnONRs and TiO_2NPs on plant growth.

The overall transport effects of PEG@ZnONRs and TiO_2NPs on plant growth are graphically presented in scheme 4.1.

In relation to the findings obtained from this study, it is suggested that NMs transport under natural environmental route such as from contaminated water will greatly effect the physiological and biochemical activity of plants growing on site under natural exposure. However, NMs interaction and surface complexation modify the original effect of individual metal-oxide. Therefore comprehensive assessments of ENM toxicity in the environment require careful assimilation of complex physicochemical interactions between NMs and various biological responses.

4.5 Remediation of NMs

4.5.1 Characterization of Adsorbent (P@MSIMC)

As discussed in chapter 3 (section 3.9.1), that the typical synthesis of P@MSIMC was started by the colloidal interaction between negatively charged Si-OH^- and cationic polymer polyethylene imine (PEI). This interaction resulted in the formation of self templated silica microcubes (Figure 4.34a). The addition of $FeCl_2$ into the reaction mixture resulted in the etching of the silica surface; creating pores in the microcubes structure and the Fe were embedded inside the pores. The process of etching and Fe embedding was facilitated by temperature. As the temperature increased from 75 ºC to 150 ºC the porosity of microcubes was also increased (Figure 4.34a-c) and consequently more atomic percentage of Fe embedded into the porous structure (Table 4.7). However, as the reaction temperature increased beyond 150 ºC, i.e., at temperature value (200 ºC), the outer polymer layer was disintegrated resulting in altered cubic morphology with irregular porous structure (Figure 4.34d).

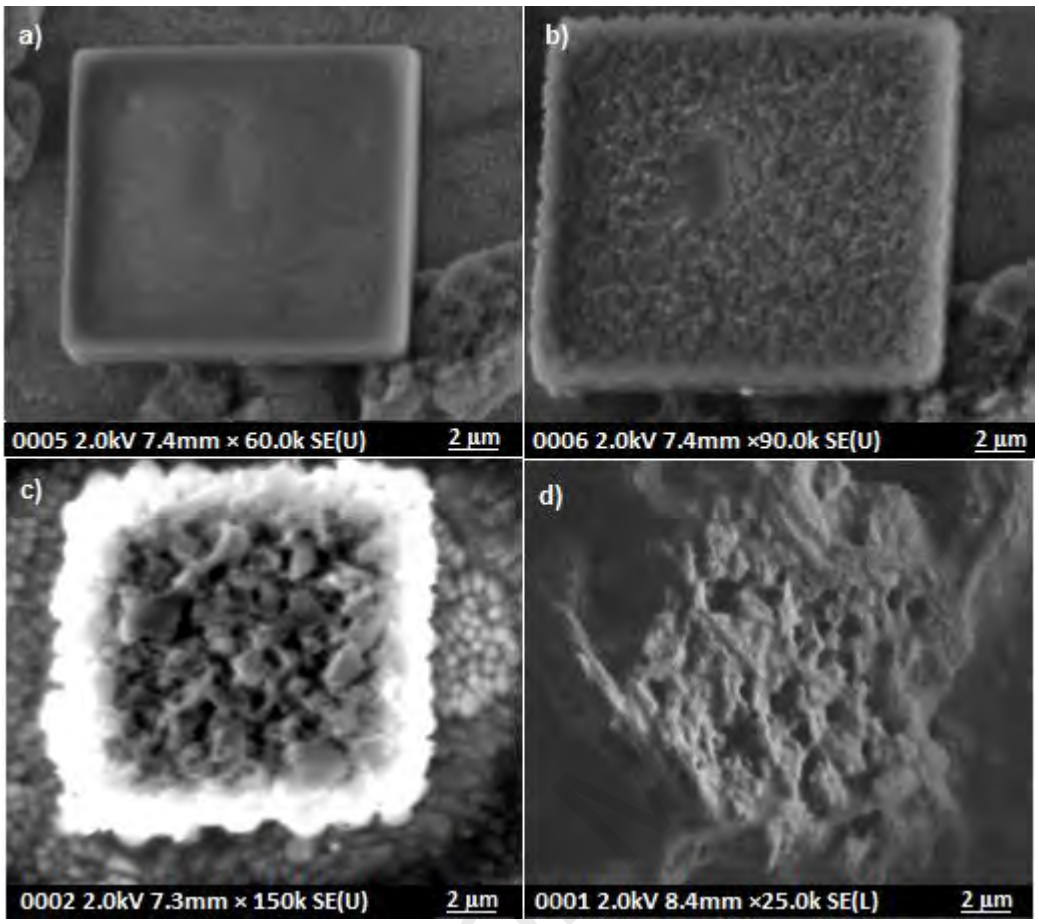

Figure 4.34: FESEM images of P@MSIMC synthesized at 75 ºC (a), 100 ºC (b), 150 ºC (c) and 200 ºC (d) respectively. All images were taken after drop-casting at ITO thin film, dried and images were taken at bright field mode.

Figure 4.35 represented the EDS analysis of adsorbent (P@MSIMC) synthesized at 150 ºC. As shown in the EDS spectra, the P@MSIMC was mainly composed of major peaks for iron, chlorine, oxygen and silica which also represented the purity of synthesized material. In order to investigate the effect of temperature on the elemental distribution and atomic % values, the EDS analysis was performed and data is summarized in Table 4.6. The elemental atomic % values demonstrate that, as temperature increases from 75 ºC to 150 ºC the atomic % of silica decreases while the atomic % of Fe and Cl increases. This observation further confirmed the etching and embedding phenomenon of Si and Fe respectively. Furthermore, the % of O from Si-OH^- decreases well with an increase in the % of N due to incorporation of the polymer

layer at the surface. However, at temperature 200 ºC, the % of O increases due to the disintegration of PEI layer at the surface.

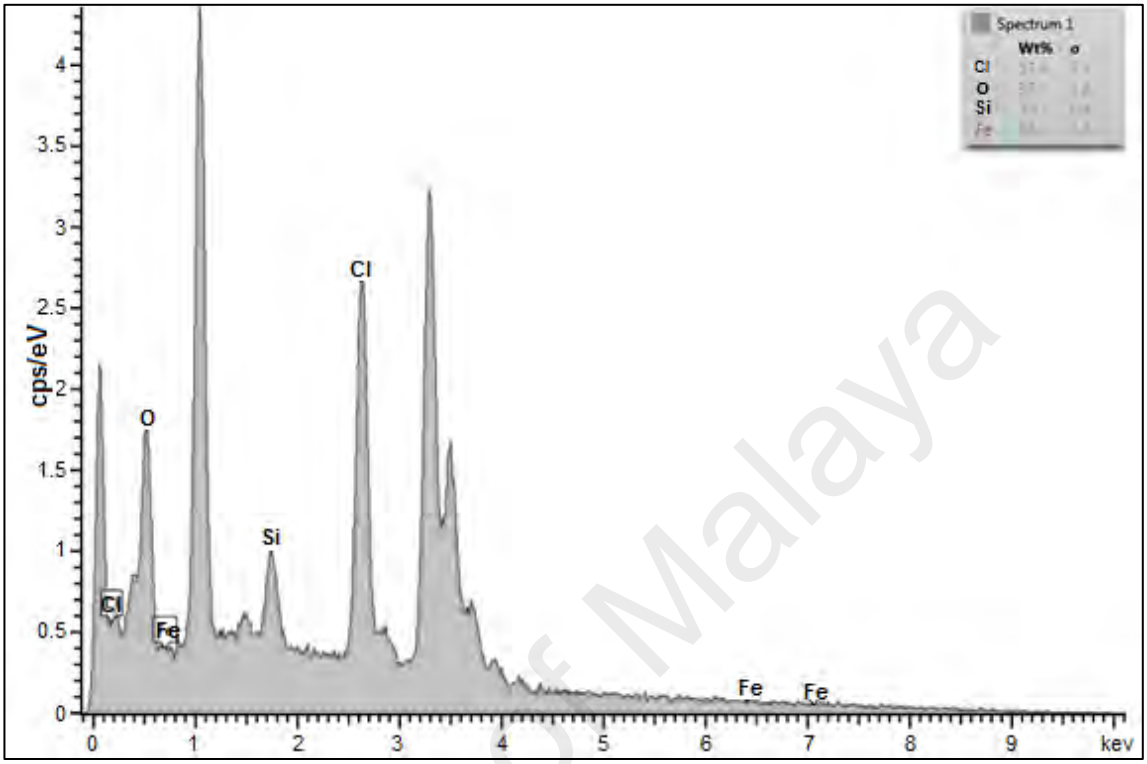

Figure 4.35: The EDS elemental analysis of P@MSIMC synthesized at 150 ºC.

Table 4.6: Atomic composition of synthesized P@MSIMC at different reaction temperature determined from EDS analysis.

Adsorbents	Temperature (ºC)	Atomic composition (%)				
		N	O	Si	Cl	Fe
P@MSIMC a	75	8.1	35.1	19.3	37.0	0.5
P@MSIMC b	100	15.5	29.3	14.5	38.5	2.2
P@MSIMC c	150	20.9	21.1	12.5	40.7	4.8
P@MSIMC d	200	15.7	32.5	10.3	38.6	2.86

In order to investigate the functional groups at the surface of synthesized adsorbent, FTIR analysis was performed. Figure 4.36, shows the FTIR spectra of P@MSIMC, synthesized under three temperature values (100 ºC, 150 ºC & 200 ºC). Typically, the vibrations observed around 784 cm^{-1}, 1052 cm^{-1} and 972 cm^{-1} correspond to the asymmetric stretching mode of Si-O-Si and Si-O stretching vibrations (Amutha et al., 2010; Witoon et al., 2008). The vibration around 1605 cm^{-1} associated with the $–NH_2$ groups of polymer PEI coated at the surface of adsorbent (Jahan et al., 2013).

Whereas, the broad peak centered at 3311 cm^{-1} indicated the existence of residual hydroxyl group of $Si\text{-}OH^-$. As the temperature increased from 100 ºC to 200 ºC, both Si-O-Si band and the surface OH^- decreases due to silica etching and PEI incorporation which further confirmed the result of FESEM and EDS analysis. The streching vibration around 477 cm^{-1} assigned to the Fe-O bond as reported in previous report (Gupta et al., 2011).

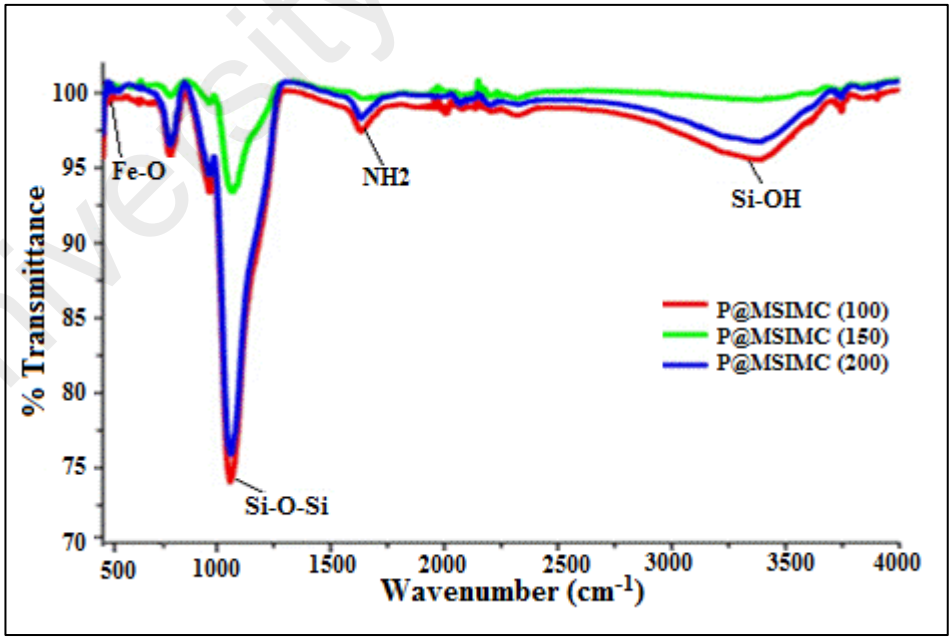

Figure 4.36: FTIR spectra (at ATR mode) of P@MSIMC at temperature range of (100-200 ºC) with spectral range from 500-4000 cm^{-1}.

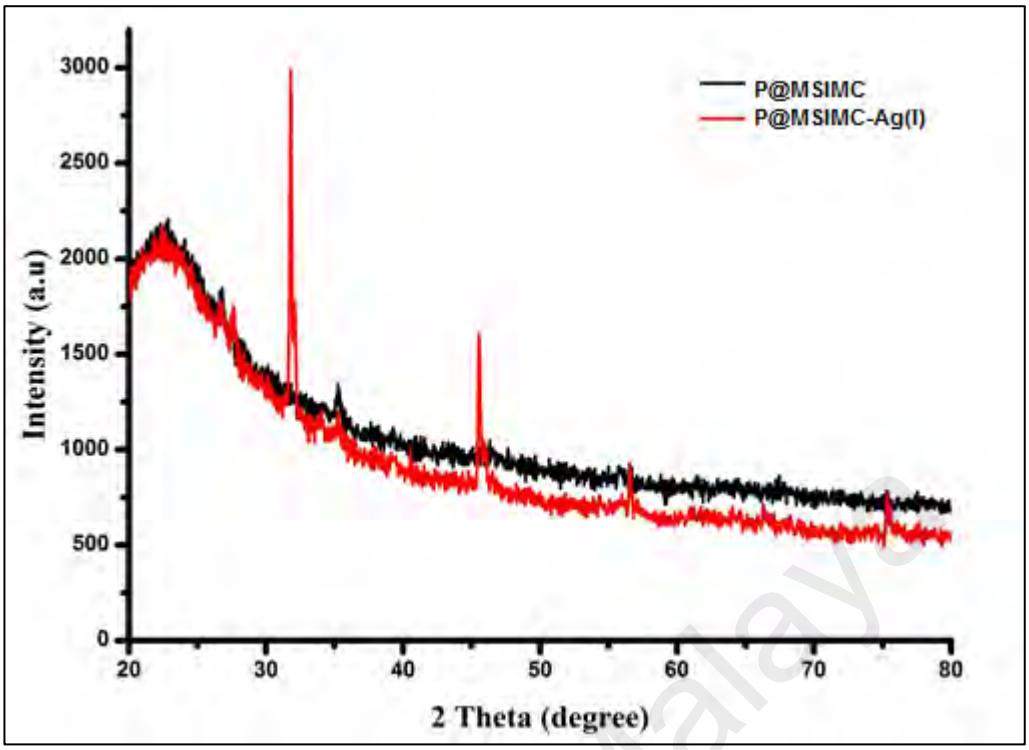

Figure 4.37: The powder XRD pattern of as-produced P@MSIMC in the 2θ range of 20-80º with Cu Kα radiation (1.5418 Å)before (black peak pattern) and after Ag(I) removal (red peak pattern).

The phase purity of the as-prepared P@MSIMC was identified by XRD analysis in the 2θ range of 20-80º with Cu Kα radiation (1.5418 Å). The powder XRD pattern of P@MSIMC (black pattern in **Figure 4.37**) showed the peak at 22º, which indicate that the material mainly consist of amorphous silica (Rida et al., 2014).

The low intensity peaks at 2θ = 25.2º, 35.25º, 45.1º, 56º, and 68º are well indexed with the diffraction pattern of Fe (Venkateswarlu et al., 2016). Moreover, no other respective peak in the pattern indicating the high purity of synthesized materials. The surface area, pore volume, and pore diameter were measured by nitrogen adsorption-desorption isotherm (Figure 4.38) and data summarized in Table 4.7. The synthesized material P@MSIMC fitted well with Langmuir isotherm plot for BET surface area. Langmuir linear plot and t-plot are presented in Appendix C.

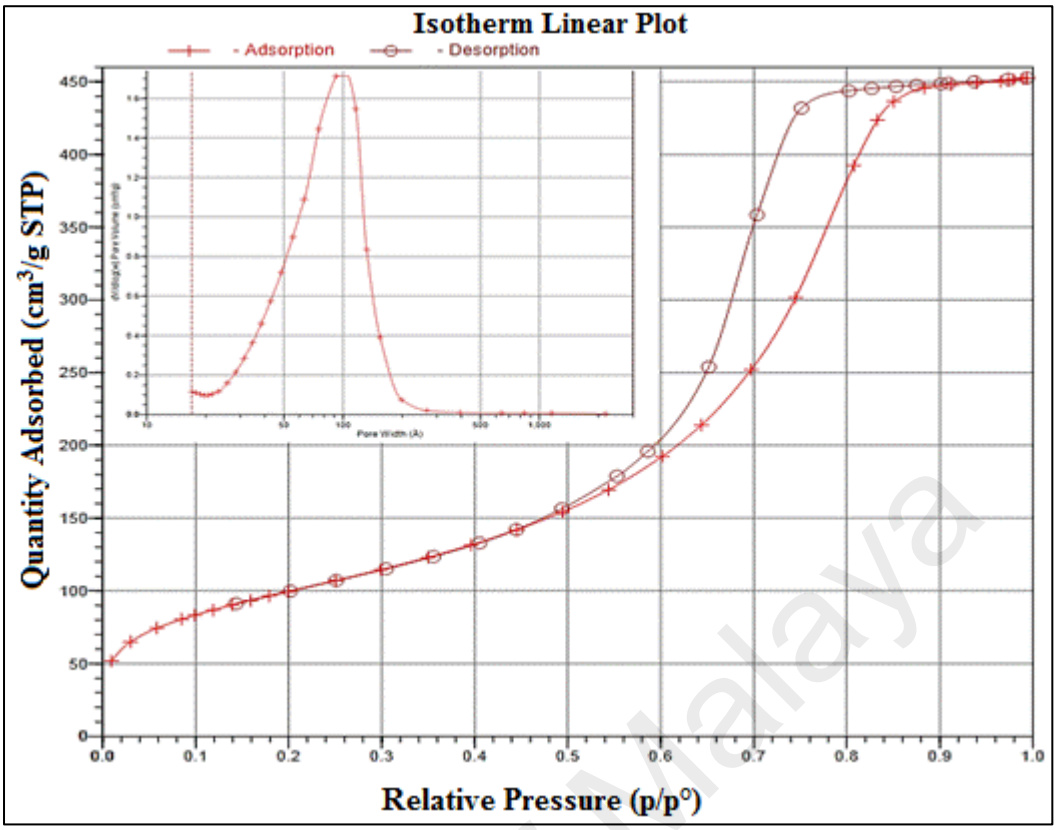

Figure 4.38: Nitrogen adsorption-desorption isotherm of P@MSIMC. The inset graph represents the pore diameter which is 100 A°= 10nm

Table 4.7: Brunauer-Emmett-Teller (BET) analysis of P@MSIMC.

	Surface area (m^2/g)	**Pore volume (cm^3/g)**	**Pore diameter (nm)**
Sample: P@MSIMC	Single point surface area at p/p° = 346.7830	Single point adsorption total pore volume = 0.699990	Adsorption average pore diameter = 7.68938
	BET surface area =364.1332	Single point desorption total pore volume = 0.699990	Desorption average pore diameter = 7.67946
	Langmuir surface area = 506.6064	t-Plot micropore volume = -0.006097	Adsorption average pore width = 6.3985
	t-Plot External surface area = 366.8323	-	Desorption average pore width = 6.0235

The surface area measured by multipoint BET method from the adsorption branch and observed as high as 364.1332 m^2 g^{-1} with an average pore volume and pore diameter of 0.699 cm^3 g^{-1} and 7.68 nm respectively. This high BET surface area, high value of pore volume and an ideal pore size distribution allow the P@MSIMC to be promising candidate for remediation application. The stability and ionic mobility of synthesized P@MSIMC was investigated through conductivity measurement under pH range from 3-9. Figure 4.39, representing the ionic mobility of P@MSIMC between pH values 3 to 9. As shown in the figure, the synthesized P@MSIMC is quite stable between pH 3 to 8; thus the maximum adsorption capacity can be observed in this broad range of solution pH. Since P@MSIMC synthesized at 150 ºC was more stable under pH range 3-8, therefore, it was selected for remediation of metal and carbon based NMs.

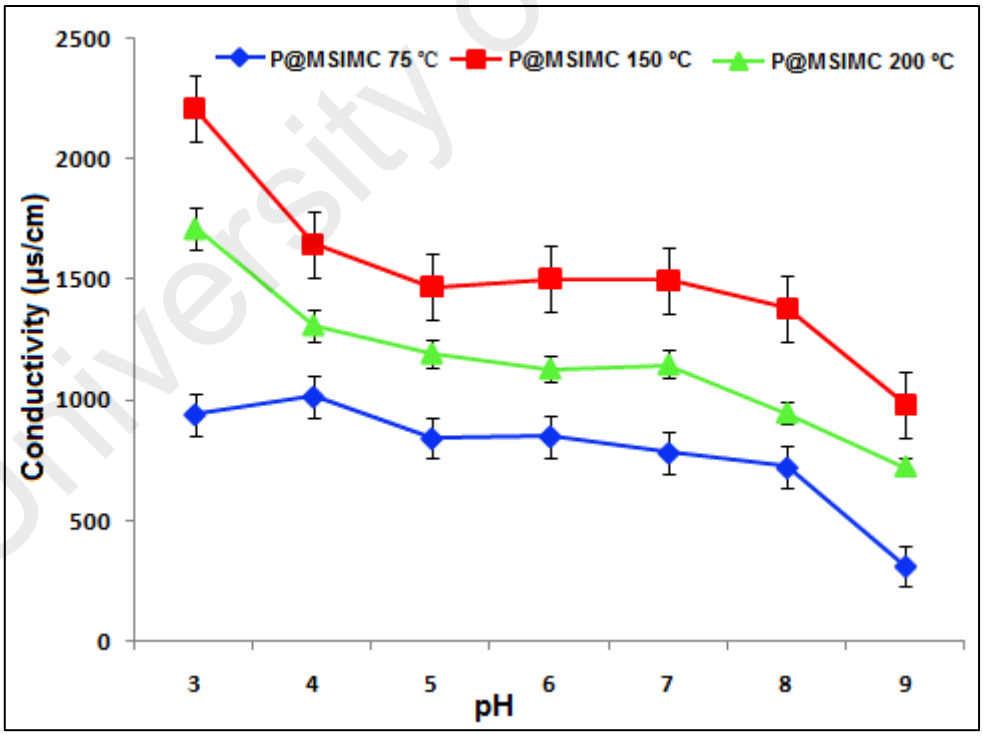

Figure 4.39: The stability of P@MSIMC (synthesized at 75 ºC, 150 ºC & 200 ºC) at different solution pH. The error bars representing the standard error of three replicate analysis.

4.5.2 Remediation of Metal Based NMs

The remediation of metal based NMs dispersed in natural RW (station 7) was investigated by using PEI-modified mesoporous silica iron microcubes (P@MSIMC) as adsorbent. NMs dispersed in natural water, interact with P@MSIMC and form an aggregated complex. This complex was easily removed either by centrifugation, filtration or simply by decantation. During this process the removal efficiency was determined for each metal based NMs under different solution pH. The kinetics of adsorption process and adsorption isotherm was also investigated.

4.5.2.1 Effect of solution pH

The pH of the solution is the most important factor that affects the adsorption process (Wang et al., 2010). The effect of pH values (ranging from 4 to 9) on the adsorption performance of P@MSIMC was investigated with an initial NMs concentration of 40 mg/L. From the Figure 4.40, it was found that the removal performance of P@MSIMC was significantly higher in pH value 6, in case of PEG@ZnONRs and TiO_2NPs NMs except PEI@AgNPs, which shows the maximum absorption at pH value 5. This variation in adsorption capacity can be explained well by the electrostatic action.

At higher pH values, the electrostatic repulsion occurs between the negatively charged NMs and the added -OH ions, which restrict the interaction between NMs and P@MSIMC, so the adsorption capacity is less at pH values higher than 6. Whereas, at lower pH values, the protonation of surface amino group of polymer polyethylene imine (PEI) increases increased, which restrict the interaction between NMs and the P@MSIMC. Therefore, pH 6 for PEG@ZnONRs and TiO_2NPs, and pH 5 for PEI@AgNPs were selected for subsequent adsorption study.

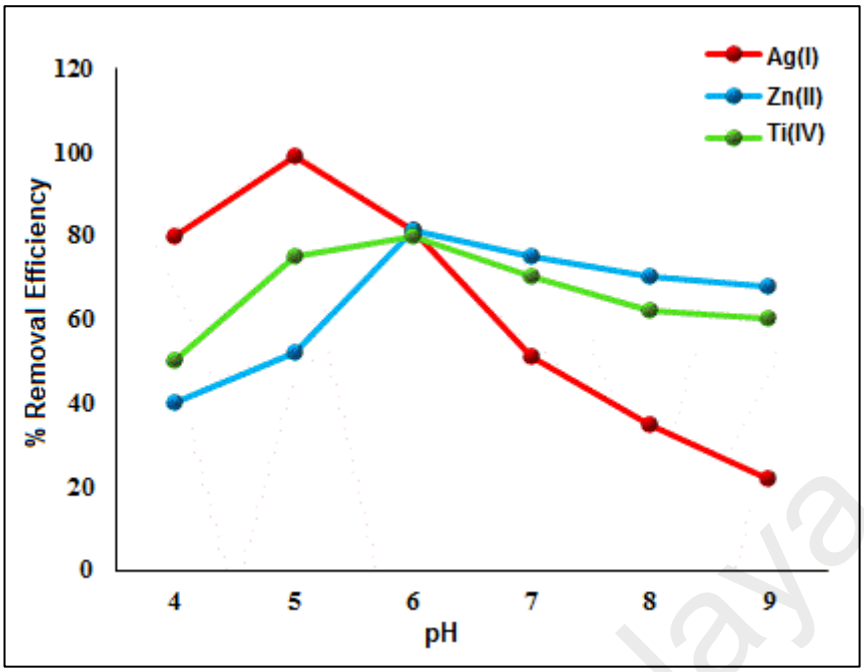

Figure 4.40: The comparison of NMs % removal efficiency for Ag(I), Zn(II) and Ti(IV) at 4 to 9 solution pH values (at 28 ± 2 ºC) within a treatment duration of 10 min (with NMs initial concentration of 40 mg/L).

4.5.2.2 Adsorption Kinetics

The rate of adsorption process is very important parameter to design a batch adsorption experiment, because of its accurate prediction of the rate at which pollutant removed from aqueous solution. Figure 4.41, represents the adsorption kinetics of all metal NMs. It can be seen that during the first 30 min, all NMs exhibited fast adsorption process and reached equilibrium within 60-90 min. It means that within 90 min all active adsorption sites of P@MSIMC were saturated. The adsorption capacity of P@MSIMC for Zn(II) was highest (850 mg/g) compared to Ag(I) and Ti(IV) which was 550 and 720 mg/g respectively. However, Zn(II) takes more time to reach equilibrium which may be due to the large sizes of PEG@ZnONRs (1 µm in length). To investigate the controlling mechanism of adsorption kinetics, the linear forms of

pseudo first (Nandi et al., 2009) and second order (Liu et al., 2015b) model was employed.

The linear plots of log (*qe-qt*) for first order kinetics are presented in Figure 4.42 and t/qt versus t for pseudo-second-order model is shown in Figure 4.41 (inset). The obtained correlation coefficient (R^2) values for the second-order kinetic model are higher than pseudo-first-order kinetic model (Table 4.8).

More specifically, the calculated normalized root-mean-square error for second-order was smaller than first- order model. Furthermore, the calculated qe values of the pseudo-second-order model were in good agreement with the experimental qe values. This confirmed that an empirical pseudo-second-order kinetic model fitted well for the description of NMs adsorption on P@MSIMC.

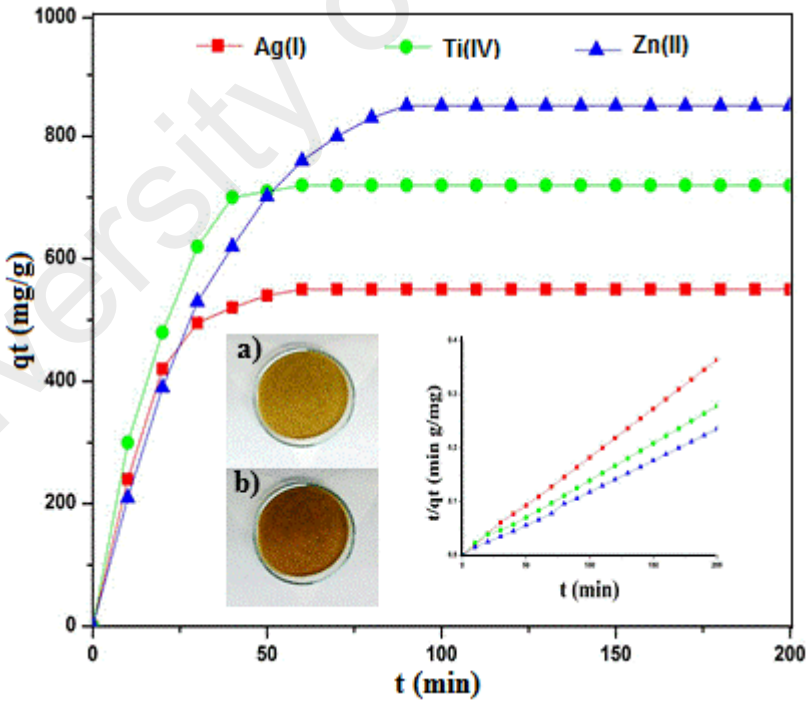

Figure 4.41: Adsorption amount variation with time at 28 ºC/ pH values 5, 6, and 6 for Ag(I), Ti(IV) and Zn(II) (initial conc. 1000 mg/L) respectively. The representative color change of P@MSMC before (a) and after adsorption process (b). The inset plot represents Pseudo-second-order kinetics (R^2 value = 0.999 for Ag(I), Ti(IV) and 0.998 for Zn(II) respectively).

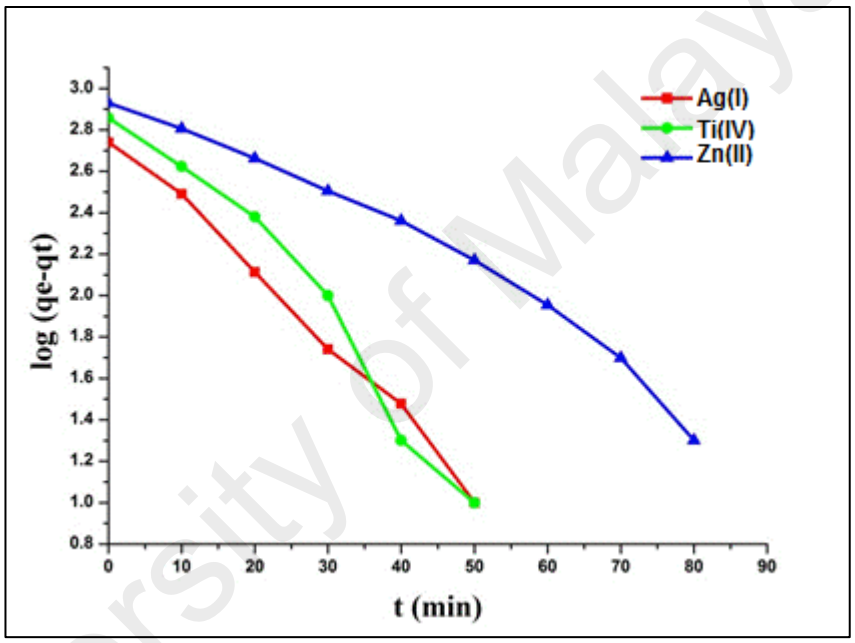

Figure 4.42: The Pseudo-first-order kinetics plots for NMs adsorption on P@MSIMC (R2 value = 0.993, 0.964 and 0.966 for Ag(I), Ti(IV) and Zn(II) respectively.

Table 4.8: Pseudo-first-order and pseudo-second-order kinetic model constants of as-prepared P@MSIMC.

Metal based NMs	qe.exp (mg/g)	Pseudo-first-order model				Pseudo-second-order model			
		qe.cal (mg/g)	k_1 (x 10^{-2}/min)	R^2	RMSE %	qe.cal (mg/g)	k_2 (x 10^{-3} g/mg min)	R^2	RMSE %
Ag(I)	550	436	0.15	0.993	21.3	519	1.1	0.999	0.23
Ti(IV)	720	648	0.11	0.964	53.2	722	7.6	0.999	4.5
Zn(II)	850	763	0.12	0.966	8.2	852	4.2	0.998	1.9

4.5.2.3 Adsorption Isotherm

The results of the two isotherm model are listed in Table 4.9. The higher correlation coefficient (R^2) of Langmuir model suggested that the adsorption data of all three metal NMs on P@MSIMC better fit with the Langmuir isotherm model, indicating that the adsorption process is relatively homogenous with a monolayer adsorption (Baba et al., 2006).

Table 4.9: Summary of the Langmuir and Freundlich isotherm parameter for metal ions adsorption on P@MSIMC.

Langmuir isotherm				**Freundlich isotherm**		
Metal ions	q max (mg/g)	b (L/mg)	R^2	K_F	n	R^2
Ag(1)	550	3.6×10^{-3}	0.995	13.3	1.78	0.893
Ti(IV)	720	3.0×10^{-3}	0.987	17.2	1.76	0.882
Zn(II)	850	2.6×10^{-3}	0.980	17.4	1.75	0.880

4.5.2.4 NMs Adsorption Mechanism

To understand the metal adsorption mechanism on P@MSIMC, FTIR spectroscopy was used. Figure 4.43, represents the FTIR spectra of adsorbent before and after metal adsorption. Compared with the FTIR spectrum of P@MSIMC, the FTIR spectra of P@MSIMC-Ti, P@MSIMC-Zn and P@MSIMC-Ag shows the slight red shifting of the peak at 1605 cm^{-1} which may be attributed to the vibration of surface nitrogen atoms of PEI forming coordination bonds with metal ions. The shifting of peak to higher vibrations were likely due to the adsorption of Ag(I), Zn(II) and Ti(IV) ions onto the imine (-NH) groups on the adsorbent surfaces (Bao et al., 2017). Furthermore, the streching vibration of Fe-O at 477 cm^{-1} was disappeared after adsorption of metals

owing to the reduction of embedded iron oxides into the porous structure of P@MSIMC.

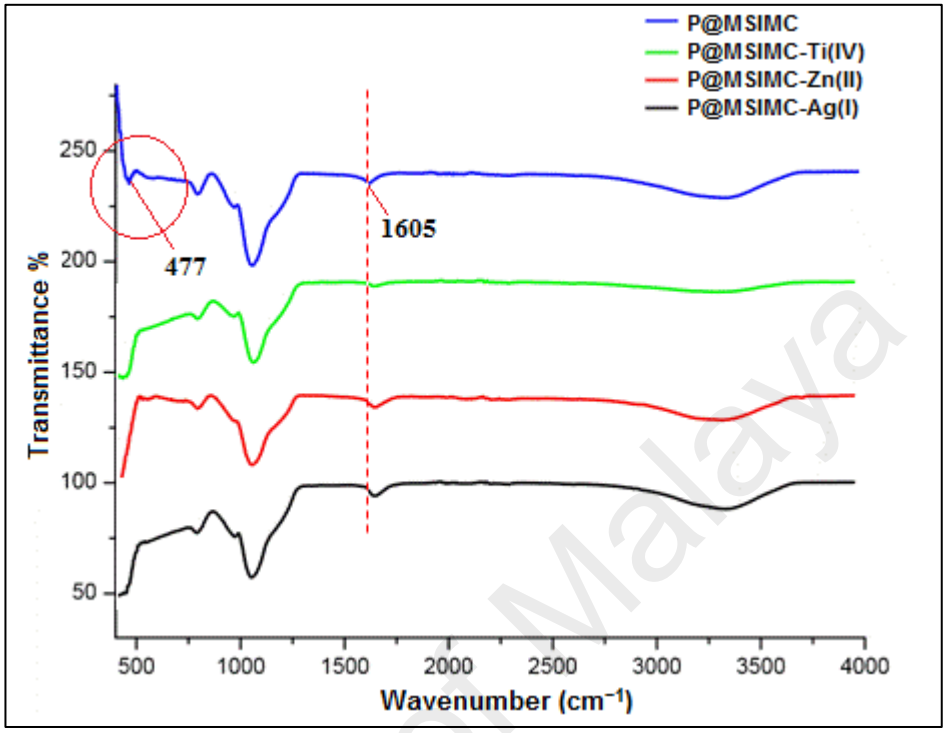

Figure 4.43: FTIR spectra of P@MSIMC before and after adsorption of Ti(IV), Zn(II) and Ag(I).

To further verify the adsorption mechanism of metals removal, EDS elemental mapping analysis was performed. After the adsorption of metal Ag(I), the P@MSIMC were removed from solution by centrifugation, dried and EDS analysis was carried out. As can be seen from the Figure 4.44a, the Ag peak is incorporated into the EDS spectra of P@MSIMC which is also confirmed by the elemental mapping (Figure 4.44b). Furthermore, the XRD analysis (Figure 4.37) revealed that the embedded iron in the P@MSIMC, after the removal of the Ag(I) from the solution becomes reduced, which is confirmed by the stronger peak intensity (red-peak pattern) of diffraction pattern of Fe (Yao et al., 2016). Typically, the metal ions interact with the electronegative oxygen of embedded iron through oxidation-reduction reaction and the Fe-O was converted into

reduced form. This suggested that, NMs interact with the surface amide group of polymer PEI and with embedded Fe-O through oxidation-reduction reaction and adsorbed inside the porous structure of P@MSIMC. The overall reaction mechanism is presented in Scheme 4.2.

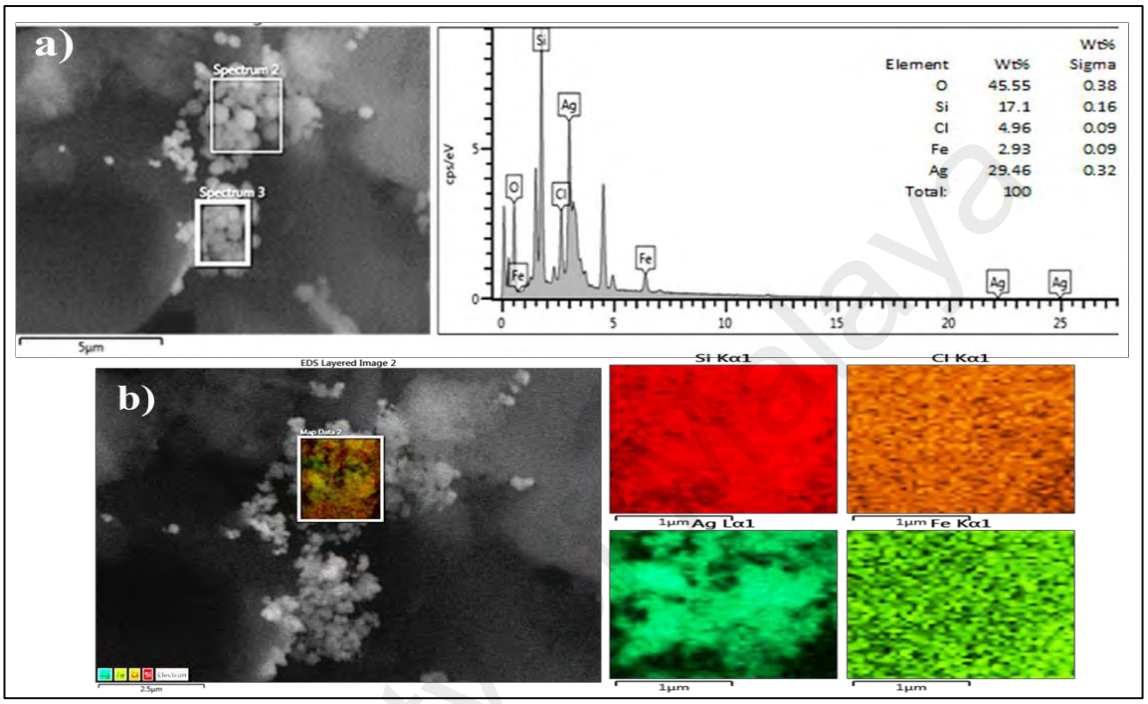

Figure 4.44: The representative EDS spectra with the atomic composition of P@MSIMC after the removal of an AgNPs form RW sample (a) with its elemental mapping showing the incorporation of Ag(I) in the aggregates of P@MSIMC after the removal process (b).

To evaluate the effect of co-existing ions of natural RW on the removal efficiency, the adsorption process was also carried out in deionized water. Figure 4.45, demonstrated the small decrease in removal efficiency of P@MSIMC. As shown by the figure, the removal efficiency was only 10-12 % inhibited in the presence of co-existing ions realizing the fact that the adsorption of metal based NMs was not predominantly affected in the presence of natural existing ions. This suggested that, the synthesized P@MSIMC can be effective for the remediation of NMs under complex natural aqueous medium.

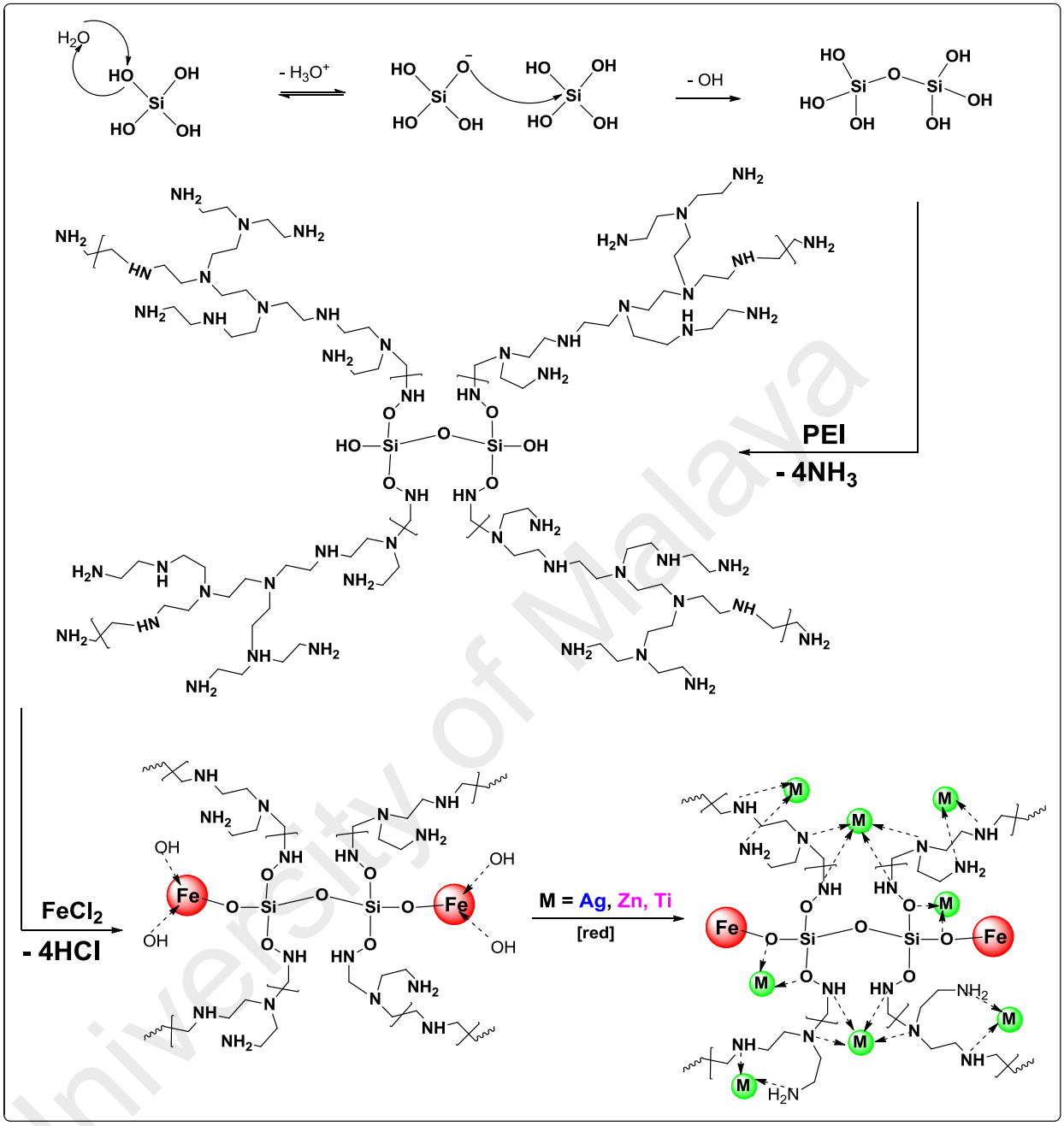

Scheme 4.2: Mechanistic scheme for the preparation and metal adsorption process of P@MSIMC.

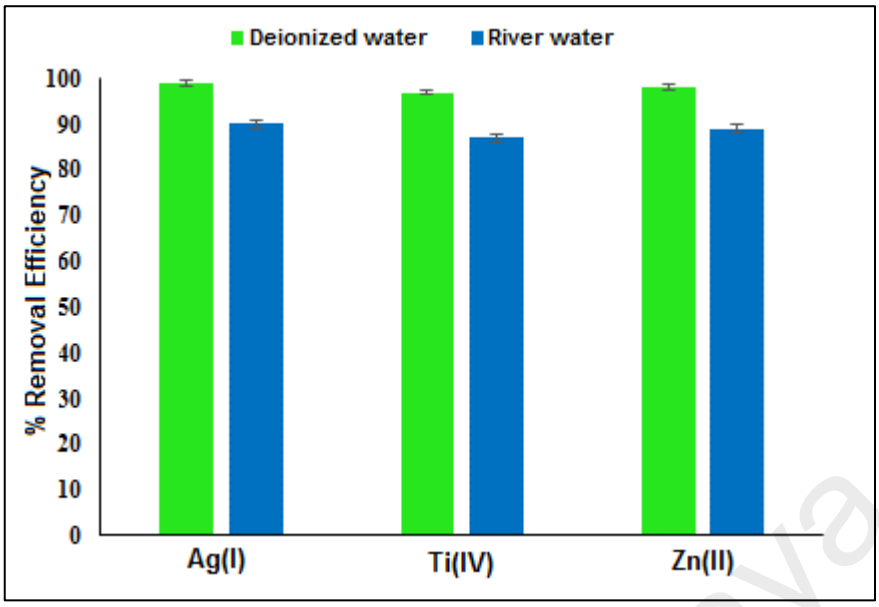

Figure 4.45: The comparison of P@MSIMC removal efficiency in deionized water and river water. Adsorption conditions: NMs = 10 ml (40 mg/L), P@MSIMC (10 mg) at 28 ºC. The error bar representing the standard error of three replicate analysis.

4.5.2.5 P@MSIMC Desorption & Recycling

The adsorption and desorption are the two key parameters to evaluate the adsorbent efficiency. An ideal adsorbent should possess both adsorption properties as well as disruption capabilities in order to recycle them and to significantly reduce the adsorbent cost for practical applications. After the removal process, the recycling property of P@MSIMC was investigated. The desorption of P@MSIMC was carried out by washing several times with ethanol followed by deionized water and dispersed in 10 mL of 1 mol/L HCl for 30 mins. The particles were separated, washed with deionized water, and used for recycling. The adsorption/desorption cycles were repeated five times and the metal removal efficiency of P@MSIMC was determined. Figure 4.46, gives the percent recycling ability of P@MSIMC which was around 94 %, even after 5 successive recycling attempts.

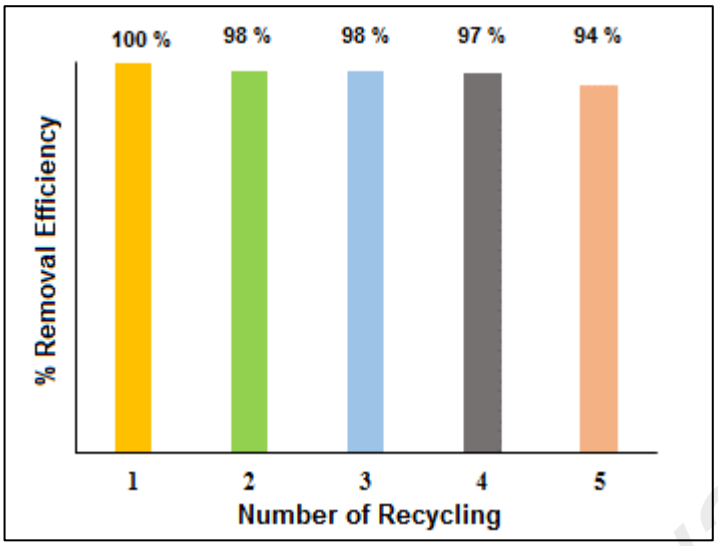

Figure 4.46: Recycling property of synthesized P@MSIMC.

4.5.2.6 Comparison With Other Silica Based Adsorbent

Table 4.10 representing the number of reported silica-based adsorbent used for the removal of metals ions from the aqueous solution. The synthesized adsorbent P@MSIMC has relatively higher uptake capacities for the metal ions compared to the other reported adsorbents. This attributed to the high surface area and higher numbers of available active sites in P@MSIMC for strong adsorption/reduction properties. Though with all these properties the synthesized adsorbent proved to be a promising candidate for the removal of NMs from natural aqueous samples.

Table 4.10: Comparison of maximum removal efficiency between P@MSIMC and other silica based adsorbents.

S. No	Adsorbent Type	Synthetic Method	Adsorbate	Removal Efficiency (mg/g, mg/L)	Time Taken (min)	Ref.
1	Thiol functionalized magnetic mesoporous silica	Stober method	Hg(II) and Pb(II)	260 and 91.5 mg/g	20	(Li et al., 2011a)
2	Fe/SiO_2-NH_2 hollow sphere	Stober method	Cr(IV)	8 mg/L	5	(Yao et al., 2016)
3	Mercaptoamine-functionalised silica-coated magnetic nano-adsorbents	Co-precipitation methods	Hg(II) and Pb(II)	355 and 292 mg/g respectively	120	(Bao et al., 2017)
4	Amino-functionalized Fe_3O_4@SiO_2 magnetic nano-adsorbent	solvothermal method	Zn(II)	169.5 mg/g	120	(Bao et al., 2016)
5	Chitosan-g-poly(butylacrylate)/ silica gel nanocomposite	sol–gel method	Cr(IV)	55.71 (mg/g)	120	(Nithya et al., 2016)
6	Silica nanocomposites	Hydrothermal method	Cr(III)	37.44 mg/g	120	(Egoda watte et al., 2015)
7	Multi-carboxyl-functionalized silica gel	Surface grafting method	Cu(II), Cd(II), Ni(II) and Zn(II)	47.07, 41.48, 30.80 and 39.96 mg/g	-	(Li et al., 2014)
8	PEI-modified mesoporous silica iron microcubes	Hydrothermal method	Zn(II), Ti(II) and Ag(I)	850, 720 and 550 mg/g	90	Present study

4.5.3 Remediation of Carbon Based NMs

4.5.3.1 Effect of Solution pH

The effect of solution pH on the removal efficiency of P@MSIMC was studied. As shown by Figure 4.47, the maximum removal of both CNPs and GOQDs in solution (40 mg/L) was occurred at pH value 6 whereas, at pH values higher or lower than 6 the removal efficiency decreases. This subsequent decrease in removal efficiency at pH

higher or lower than 6 was due the electrostatic repulsion (Zinchenko et al., 2013) between the negatively charged CNPs or GOQDs and added –OH ions and between positively charged P@MSIMC and added H^+ ions from acid. Therefore, pH 6 was selected as a suitable pH for maximum removal of both NMs from natural RW.

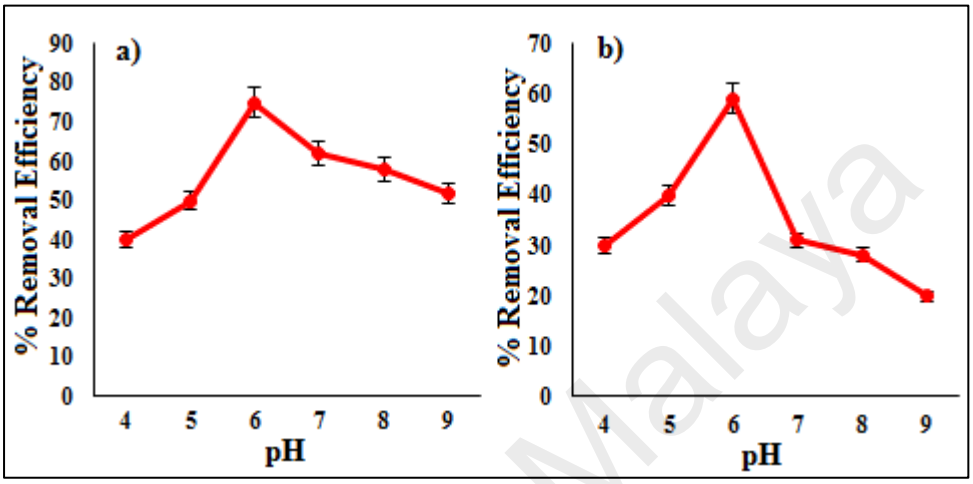

Figure 4.47: Effect of pH on the removal efficiency of CNP (a) and GOQDs (b) at initial concentration of 40 mg/L, P@MSIMC dose 10 mg/10 ml of GOQDs solution, temperature 28 ± 2 ˚C and contact time 80 and 50 min respectively.

4.5.3.2 Adsorption Kinetics

Figure 4.48, represents the adsorption kinetics of CNPs (a) and GOQDs (b) in RW. The results shows that, during the first 60 and 50 min, CNPs and GOQDs exhibit fast adsorption process and reached equilibrium within 60 min. It means that within 60 min, all active adsorptive sites of P@MSIMC were filled and saturated with CNPs and GOQDs respectively. The maximum adsorption capacity of CNPs and GOQDs was found to be 600 mg/g for CNPs and 504 mg/g for GOQDs. The kinetics of adsorption mechanism was also investigated by the linear forms of pseudo-first-order (Nandi et al., 2009) and pseudo-second order (Liu et al., 2015b) models.

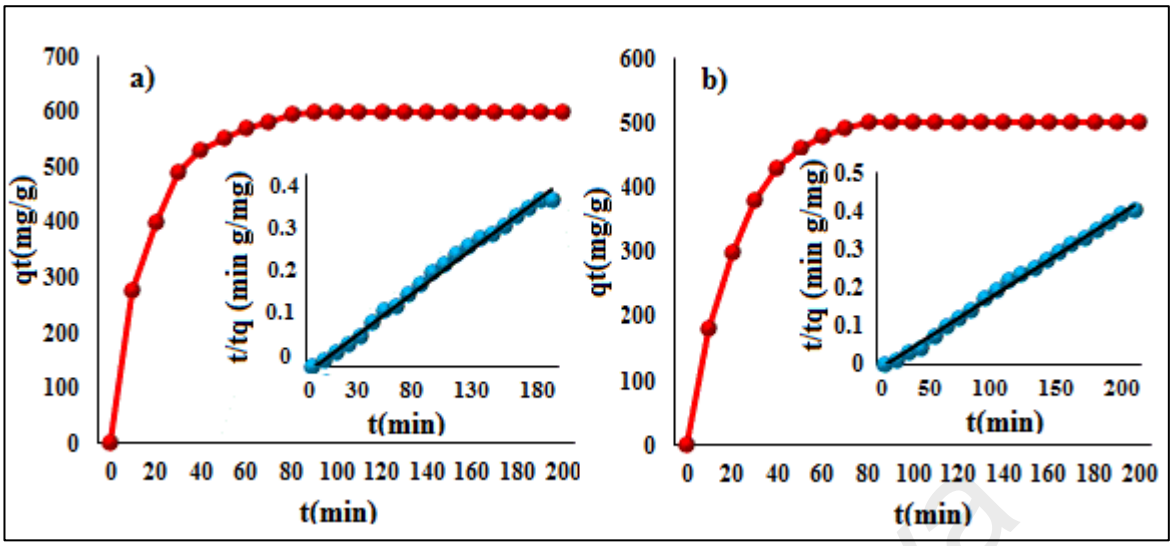

Figure 4.48: Variation of adsorption amount with time (min), for CNPs (a) and GOQDs (b) with initial concentration of 700 mg/L, P@MSIMC dose 10 mg/10 ml. The linear graph in the inset represents modeled pseudo-second-order kinetics.

The linear plots of log (*qe-qt*) and *t/qt* versus *t* are summarized in Table 4.11. The data obtained from the two empirical models suggested the adsorption mechanism of both NMs fitted well with the pseudo-second-order model (Figure 4.48a, b (inset)). As can be seen from Table 4.11, the obtained correlation coefficient (R^2) value in the second-order kinetic model was higher than pseudo-first-order kinetic model (Figure 4.49). Furthermore, the calculated *qe* value from the pseudo-second-order model was in good agreement with the experimental *qe* value. This confirmed that an empirical pseudo- second-order kinetic model fitted well for the description of both NMs adsorption on P@MSIMC.

Table 4.11: Pseudo-first-order and pseudo-second-order kinetic model constants.

NMs	Pseudo-first-order model				Pseudo-second-order model		
	qe exp (mg/g)	qe cal (mg/g)	K_1 ($\times 10^{-2}$/min)	R^2	qe cal (mg/g)	K_2 ($\times 10^{-3}$g/mg min	R^2
CNP	600	578	0.79	0.989	602	0.23	0.999
GOQDs	504	574	0.73	0.964	500	0.21	0.998

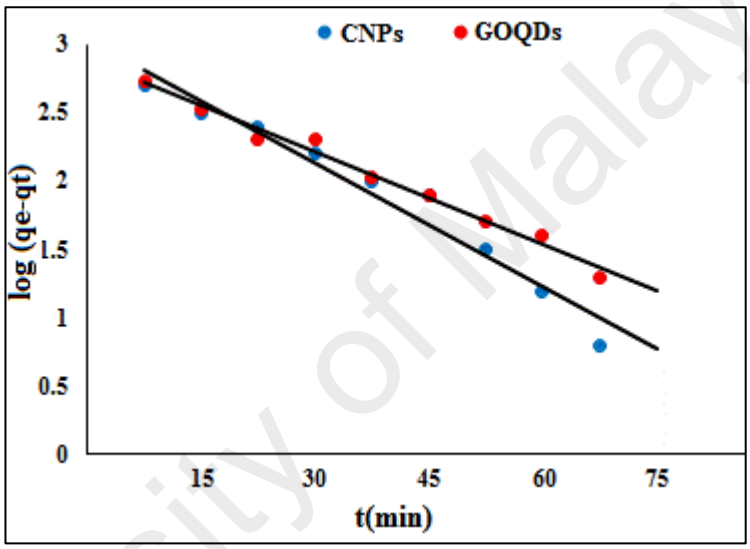

Figure 4.49: First-order kinetic model of CNP and GOQDs.

4.5.3.3 Adsorption Isotherm

The results of the two isotherm model are presented in Table 4.12. The data obtained revealed that the analogous to metal based NMs, the adsorption of CNPs and GOQDs follow Langmuir isotherm model with higher correlation coefficient (R^2) values compared to correlation coefficient of Freundlich isotherm model.

Table 4.12: Summary of the Langmuir and Freundlich Isotherm Parameter for CNPs and GOQDs adsorption on P@MSIMC.

Langmuir isotherm				Freundlich isotherm		
NMs	q max (mg/g)	b (L/mg)	R^2	K_F	N	R^2
CNPs	600	3.4×10^{-3}	0.996	12.6	1.72	0.885
GOQDs	504	3.7×10^{-3}	0.990	12.2	1.75	0.872

4.5.3.4 P@MSIMC Desorption & Recycling

After adsorption investigation of both CNPs and GOQDs in natural RW, the recycling ability of synthesized P@MSIMC was investigated by following same way as described for metal based NMs. Typically, the desorption of P@MSIMC was carried out by washing the adsorbent several times with ethanol followed by deionized water and then dispersed in 10 mL of 1 mol/L HCl for 30 mins. This will remove the adsorbed NMs at the surface of P@MSIMC. The adsorbent was separated from the solution by centrifugation at 3000 rpm/min, washed several times with deionized water and used to check the recycling property. The adsorption/desorption cycles were repeated five times and the CNPs and GOQDs removal efficiency of P@MSMC was determined. Figure 4.50, representing the recycling ability of P@MSIMC. As can see from the figure, the adsorption capacity of P@MSIMC was almost the same even after five successive recycling steps. Therefore, these results suggested that P@MSIMC owing to its novel cubic mesoporous structure with special surface properties is potentially applicable for the removal of carbon-based NMs from natural water.

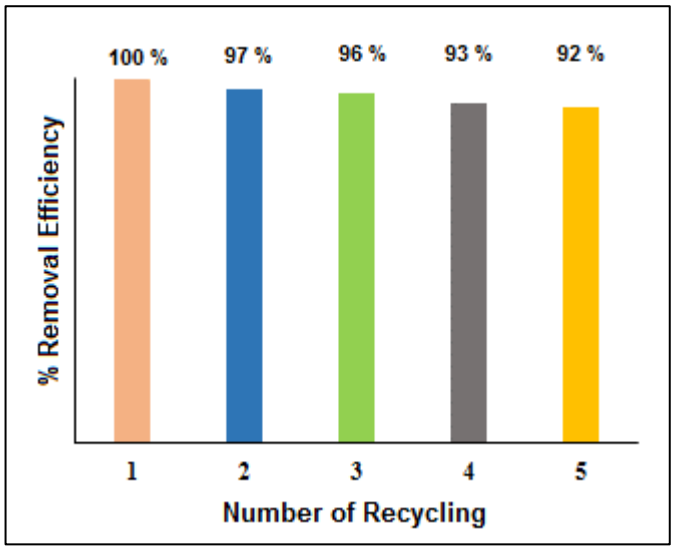

Figure 4.50: The removal efficiency of P@MSIMC after 5 successive recycling.

CHAPTER 5: CONCLUSIONS

In conclusion, three metal based nanomaterials (NMs) including one newly synthesized polyethylene imine coated silver nanoparticles, PEI@AgNPs (50 ± 10nm) and two already reported polyethylene glycol coated zinc oxide nano-rods, PEG@ZnONRs (64 ± 10 nm) and titanium dioxide nanoparticles, TiO_2NPs (89 ± 20 nm) were synthesized. Carbon based NMs comprising of carbon nanoparticles, CNPs (20 ± 10 nm) and graphene oxide quantum dots, GOQDs (50 ± 20 nm) were also synthesized by following earlier reports. For morphological investigation, two more zinc oxide structures i.e., zinc oxide nano-needles, ZnONNs (43 ± 10 nm) and zinc oxide microflowers, ZnOMFs (1.09 ± 0.2 μm) were synthesized by following modified previous methods. The physiochemical properties of all synthesized NMs were well characterized using various material characterization techniques.

The key findings obtained from the aqueous transport or mobility of all synthesized materials revealed that, the surface coating, particle size, morphology and ionic composition of natural river water (RW) dictates the dissolution, ionic release and transport behavior of NMs. For example, surface coating of silver nanoparticles with cationic polymer polyethylene imine (PEI@AgNPs) significantly inhibit the particle dissolution and ionic silver Ag(I) release, as compared to anionic polymer coated zinc oxide nano-rods (PEG@ZnONRs) and uncoated titanium dioxide nanoparticles (TiO_2NPs). In addition, the ionic metal release profiles were also dependent upon the physicochemical properties of RW such as pH, dissolved oxygen and concentration of dissolved ions. Typically the robust positive ionic metal release was observed in RW (Station-7) due to its high chemical composition and dissolved oxygen concentration. By comparing the results obtained from the RW of different chemical composition (station-1, station-4 and station-7), the ionic metal release were 1.6%, 8.3% and 13.6%

in Station-1, 2.0%, 10.1% and 15.3% in Station-4, and 3.3%, 12.6% and 19.0% in Station-7 for PEI@AgNPs, TiO_2NPs and PEG@ZnONRs respectively. The size and morphology investigation of PEG@ZnONRs, ZnONNs and ZnOMFs suggested that, ZnONNs with smaller average diameter of needles (43 ± 10 nm) displayed the high ionic metal release profiles compared to PEG@ZnONRs with an average rods diameter of 64 ± 10 nm, and ZnOMFs with an average diameter of 1.09 ± 0.2 µm. In case of PEG@ZnONRs and ZnOMFs, since both constructed with the similar materials, the less ionic metal dissolution in ZnOMFs was because of the angular-shaped structure that retained during transport in porous media. This implies that the transport behavior is limited for NMs with large particle size and angular morphology. Whereas, the small size and simple straight morphology facilites the transport of NMs. Analogous to metal based NMs, the behavior of CNPs and GOQDs was also controlled by the particle size, surface charge and ionic composition of RW.

The results obtained from the impact of solution chemistry on the behavior of NMs disclosed that, the solution pH effect the aqueous behavior of metal and carbon based NMs. The particle dissolution and ionic metal release increased with substantial increase in solution pH (5.6-6.8). On the other hand, the transport of GOQDs as compared to CNPs was more suseptible towards solution pH and minimum trasport was observed at lowest solution pH (pH-5.6). It was because of the less surface charge of GOQDs (-24 mV) and compared to CNPs (-40 mV). As reported earlier that particles with more surface charge are more stable towards pH variation. Similarly, the transport behavior of both metal and carbon based NMs were remarkably inhibited in presence of monovalent salt (NaCl, 2-10 mM). More specifically, the increasing concentration of NaCl in the aqueous suspension (2-10 mM), resulted in the maximum column retention with a small breakthrough curves. For instance, the particle dissolution and ionic metal release from PEI@AgNPs, TiO_2NPs and PEG@ZnONRs were 2.6-3.3%, 7.0-14.3%

and 8.3-10% respectively. Whereas, the total column deposition rate (R_d) was 63% in case of CNPs and 45% in case of GOQDs in presence of NaCl (2-10 mM). However, the transport behavior of both metal and carbon based NMs were not significantly altered in presence of divalent salt ($CaCl_2$). In addition, the presence of dissolved natural organic matter (NOM) also affects the transport of metal and carbon based NMs. The NOM absorbed at the particle surface and increased the negative surface potential of NMs which resulted in increased electrostatic repulsion among particles and thereby increased the transport.

The findings from the aqueous mobilization of PEG@ZnONRs and TiO_2NPs into the hydroponic growth of red bean plant concluded that, PEG@ZnONRs due to its higher dissolution rate and strong binding capacity, largely taken up and significantly inhibit the plant physiological and biochemical activity. Whereas, no adverse effect on plant physiological and biochemical activity was observed in TiO_2NPs. The kinetic uptake study revealed that the uptake capacity of both PEG@ZnONRs and TiO_2NPs increased with increasing the exposure period from one week to three weeks. However, the findings from competitive uptake in a co-exposure of both metal based NMs suggested that, NMs mobilization was largely suppressed in a mixture of PEG@ZnONRs and TiO_2NPs because of the complexation and aggregation among the particles. These results indicated that, both NMs displayed distinctive transport pattern and physiological and biochemical effect on plant growth and may behave differently when exposed to plant.

In remediation part, polymer modified mesoporous silica iron microcubes (P@MSIMC) adsorbent was successfully synthesized via hydrothermal method. The synthesized adsorbent exhibited excellent removal efficiency for PEI@AgNPs, TiO_2NPs and PEG@ZnONRs as well as for CNPs and GOQDs respectively. The

maximum removal efficiency was 850 mg/g, 720 mg/g and 550 mg/g for PEG@ZnONRs, TiO_2NPs and PEI@AgNPs, whereas 600 mg/g and 504 mg/g was recorded for CNPs and GOQDs respectively. The kinetic results revealed that the adsorption process is rather fast and follow the pseudo-second-order kinetics model. The adsorption isotherm of all NMs fitted-well with the Langmuir isotherm model with higher correlation coefficient ($R^2 = 0.99$). Recycling results revealed that even after five adsorption/desorption cycles, the P@MSIMC maintained high adsorption performance. Most importantly, the removal efficiency of P@MSIMC was not inhibited in the presence of natural water coexisting ions. These experimental results imply that P@MSIMC owing to its novel cubic mesoporous structure with special surface properties is potentially applicable for water remediation.

5.1 Recommendations for Future Work

This work has enabled the development of the understanding of the behavior of NMs under a range of natural RW solution chemistry. The findings of this research contributed significant knowledge and added useful information to the available literature. More specifically, these findings will help to understand the impact of aqueous composition as well as NMs intrinsic physicochemical properties in demonstrating their transport behavior and mobilization. In addition, it is anticipated that remediation study will provide an exciting opportunity to advance the researchers knowledge about the novel mesoporous silica-based adsorbent for the fast and efficient removal of environmental pollutants and will likely cause to open new research avenues in related fields. In the future, the behavior of other metal and carbon NMs, hybrid metal-composites, and other surface functionalized NMs including their remediation against silica-based adsorbent can be evaluated in natural river water. Furthermore, another class of pollutants like persistent organic pollutants (POPs) can be investigated for remediation from environmental surfaces. Most importantly, the major

recommendation of this work is to design a natural environmental model to simulate and scale up the behavior of different NMs under variable or similar environmental conditions for the sustainable utilization of NMs.

REFERENCES

Adams, E. (1988). Introduction to the principles of ceramic processing: *John Wiley & Sons*. 2nd Edition. *Pg.486.*

Adeleye, A. S., Conway, J. R., Garner, K., Huang, Y., Su, Y., & Keller, A. A. (2016). Engineered nanomaterials for water treatment and remediation: costs, benefits, and applicability. *Chemical Engineering Journal, 286*, 640-662.

Afrooz, A. N., Das, D., Murphy, C. J., Vikesland, P., & Saleh, N. B. (2016). Co-transport of gold nanospheres with single-walled carbon nanotubes in saturated porous media. *Water Research, 99*, 7-15.

Ahn, J. Y., Moon, K. J., Kim, J. H., Lee, S. H., Kang, J. W., Lee, H. W., & Kim, S. H. (2014). Designed synthesis and stacking architecture of solid and mesoporous TiO_2 nanoparticles for enhancing the light-harvesting efficiency of dye-sensitized solar cells. *ACS Applied Materials & Interfaces, 6*, 903-909.

Aiken, G. R., Hsu-Kim, H., & Ryan, J. N. (2011). Influence of dissolved organic matter on the environmental fate of metals, nanoparticles, and colloids. *Environmental Science & Technology, 45*, 3196-3201.

Akaighe, N., Depner, S. W., Banerjee, S., Sharma, V. K., & Sohn, M. (2012). The effects of monovalent and divalent cations on the stability of silver nanoparticles formed from direct reduction of silver ions by suwannee river humic acid/natural organic matter. *Science of the Total Environment, 441*, 277-289.

Alatalo, S.M., Qiu, K., Preuss, K., Marinovic, A., Sevilla, M., Sillanpää, M., Guo, X., & Titirici, M.-M. (2016). Soy protein directed hydrothermal synthesis of porous carbon aerogels for electrocatalytic oxygen reduction. *Carbon, 96*, 622-630.

Ali, R. M., Hamad, H. A., Hussein, M. M., & Malash, G. F. (2016). Potential of using green adsorbent of heavy metal removal from aqueous solutions: adsorption kinetics, isotherm, thermodynamic, mechanism and economic analysis. *Ecological Engineering, 91*, 317-332.

Amutha, K., Ravibaskar, R., & Sivakumar, G. (2010). Extraction, synthesis and characterization of nanosilica from rice husk ash. *International Journal of Nanotechnology and Applications, 4*, 61-66.

Anandalakshmi, K., Venugobal, J., & Ramasamy, V. (2016). Characterization of silver nanoparticles by green synthesis method using Pedalium murex leaf extract and their antibacterial activity. *Applied Nanoscience, 6*, 399-408.

Angiola, M., Rutherglen, C., Galatsis, K., & Martucci, A. (2016). Transparent carbon nanotube film as sensitive material for surface plasmon resonance based optical sensors. *Sensors and Actuators B: Chemical, 236*, 1098-1103.

Anjum, N. A., Singh, N., Singh, M. K., Sayeed, I., Duarte, A. C., Pereira, E., & Ahmad, I. (2014). Single-bilayer graphene oxide sheet impacts and underlying potential

mechanism assessment in germinating faba bean (Vicia faba L.). *Science of the Total Environment, 472*, 834-841.

Aschberger, K., Micheletti, C., Sokull-Klüttgen, B., & Christensen, F. M. (2011). Analysis of currently available data for characterising the risk of engineered nanomaterials to the environment and human health-lessons learned from four case studies. *Environment International, 37*, 1143-1156.

Atchudan, R., Edison, T. N. J. I., Perumal, S., Karthikeyan, D., & Lee, Y. R. (2016). Facile synthesis of zinc oxide nanoparticles decorated graphene oxide composite via simple solvothermal route and their photocatalytic activity on methylene blue degradation. *Journal of Photochemistry and Photobiology B: Biology, 162*, 500-510.

Azam, A., Ahmed, A. S., Oves, M., Khan, M., & Memic, A. (2012). Size-dependent antimicrobial properties of CuO nanoparticles against Gram-positive and-negative bacterial strains. *International Journal of Nanomedicine, 7*, 3527-3535.

Baba, Y., Ohe, K., Kawasaki, Y., & Kolev, S. D. (2006). Adsorption of mercury (II) from hydrochloric acid solutions on glycidylmethacrylate–divinylbenzene microspheres containing amino groups. *Reactive and Functional Polymers, 66*, 1158-1164.

Badawy, A. M. E., Luxton, T. P., Silva, R. G., Scheckel, K. G., Suidan, M. T., & Tolaymat, T. M. (2010). Impact of environmental conditions (pH, ionic strength, and electrolyte type) on the surface charge and aggregation of silver nanoparticles suspensions. *Environmental Science & Technology, 44*, 1260-1266.

Badruddoza, A. Z. M., Shawon, Z. B. Z., Tay, W. J. D., Hidajat, K., & Uddin, M. S. (2013). Fe_3O_4/cyclodextrin polymer nanocomposites for selective heavy metals removal from industrial wastewater. *Carbohydrate Polymers, 91*, 322-332.

Bag, S., Roy, K., Gopinath, C. S., & Raj, C. R. (2014). Facile single-step synthesis of nitrogen-doped reduced graphene oxide-Mn_3O_4 hybrid functional material for the electrocatalytic reduction of oxygen. *ACS Applied Materials & Interfaces, 6*, 2692-2699.

Bagbi, Y., Sarswat, A., Tiwari, S., Mohan, D., Pandey, A., & Solanki, P. R. (2017). Synthesis of l-cysteine stabilized zero-valent iron (nZVI) nanoparticles for lead remediation from water. *Environmental Nanotechnology, Monitoring & Management, 7*, 34-45.

Bai, H., Jiang, W., Kotchey, G. P., Saidi, W. A., Bythell, B. J., Jarvis, J. M., Marshall, A. G., Robinson, R. A., & Star, A. (2014). Insight into the mechanism of graphene oxide degradation via the photo-Fenton reaction. *The Journal of Physical Chemistry C, 118*, 10519-10529.

Bao, S., Li, K., Ning, P., Peng, J., Jin, X., & Tang, L. (2017). Highly effective removal of mercury and lead ions from wastewater by mercaptoamine-functionalised

silica-coated magnetic nano-adsorbents: Behaviours and mechanisms. *Applied Surface Science, 393*, 457-466.

Bao, S., Tang, L., Li, K., Ning, P., Peng, J., Guo, H., Liu, Y. (2016). Highly selective removal of Zn(II) ion from hot-dip galvanizing pickling waste with amino-functionalized Fe_3O_4@SiO_2 magnetic nano-adsorbent. *Journal of Colloid and Interface Science, 462*, 235-242.

Barhoum, A., Melcher, J., Van Assche, G., Rahier, H., Bechelany, M., Fleisch, M., & Bahnemann, D. (2017). Synthesis, growth mechanism, and photocatalytic activity of Zinc oxide nanostructures: porous microparticles versus nonporous nanoparticles. *Journal of Materials Science, 52*, 2746-2762.

Bayram, S., Zahr, O. K., & Blum, A. S. (2015). Short ligands offer long-term water stability and plasmon tunability for silver nanoparticles. *RSC Advances, 5*, 6553-6559.

Beyer, W. F., & Fridovich, I. (1987). Assaying for superoxide dismutase activity: some large consequences of minor changes in conditions. *Analytical Biochemistry, 161*, 559-566.

Bhuyan, B., Paul, B., Purkayastha, D. D., Dhar, S. S., & Behera, S. (2016). Facile synthesis and characterization of zinc oxide nanoparticles and studies of their catalytic activity towards ultrasound-assisted degradation of metronidazole. *Materials Letters, 168*, 158-162.

Bindhu, M., & Umadevi, M. (2013). Synthesis of monodispersed silver nanoparticles using Hibiscus cannabinus leaf extract and its antimicrobial activity. *Spectrochimica acta part A: Molecular and Biomolecular Spectroscopy, 101*, 184-190.

Boonyanitipong, P., Kositsup, B., Kumar, P., Baruah, S., & Dutta, J. (2011). Toxicity of ZnO and TiO_2 nanoparticles on germinating rice seed Oryza sativa L. *International Journal of Bioscience, Biochemistry and Bioinformatics, 1*, 282.

Bouchard, D., Ma, X., & Isaacson, C. (2009). Colloidal properties of aqueous fullerenes: isoelectric points and aggregation kinetics of C60 and C60 derivatives. *Environmental Science & Technology, 43*, 6597-6603.

Bouchard, D., Zhang, W., Powell, T., & Rattanaudompol, U.s. (2012). Aggregation kinetics and transport of single-walled carbon nanotubes at low surfactant concentrations. *Environmental Science & Technology, 46*, 4458-4465.

Boverhof, D. R., Bramante, C. M., Butala, J. H., Clancy, S. F., Lafranconi, M., West, J., & Gordon, S. C. (2015). Comparative assessment of nanomaterial definitions and safety evaluation considerations. *Regulatory Toxicology and Pharmacology, 73*, 137-150.

Boxall, A. B., Chaudhry, Q., Sinclair, C., Jones, A., Aitken, R., Jefferson, B., & Watts, C. (2007a). Current and future predicted environmental exposure to engineered nanoparticles. *Central Science Laboratory, Department of the Environment and Rural Affairs, London, UK, 89*.

Boxall, A. B., Tiede, K., & Chaudhry, Q. (2007b). Engineered nanomaterials in soils and water: how do they behave and could they pose a risk to human health?. *Nanomedicine, 2*, 919-927.

Brauer, J. I., & Szulczewski, G. (2014). Important role of surface fluoride in nitrogen-doped TiO_2 nanoparticles with visible light photocatalytic activity. *The Journal of Physical Chemistry B, 118*, 14188-14195.

Caballero Díaz, E., Pfeiffer, C., Kastl, L., Rivera- Gil, P., Simonet, B., Valcárcel, M., Jiménez Lamana, J., Laborda, F., & Parak, W. J. (2013). The toxicity of silver nanoparticles depends on their uptake by cells and thus on their surface chemistry. *Particle & Particle Systems Characterization, 30*, 1079-1085.

Canas, J. E., Long, M., Nations, S., Vadan, R., Dai, L., Luo, M., Ambikapathi, R., Lee, E. H., & Olszyk, D. (2008). Effects of functionalized and nonfunctionalized single-walled carbon nanotubes on root elongation of select crop species. *Environmental Toxicology and Chemistry, 27*, 1922-1931.

Carpita, N., Sabularse, D., Montezinos, D., & Delmer, D. P. (1979). Determination of the pore size of cell walls of living plant cells. *Science, 205*, 1144-1147.

Castiglione, M. R., Giorgetti, L., Cremonini, R., Bottega, S., & Spanò, C. (2014). Impact of TiO_2 nanoparticles on Vicia narbonensis L.: potential toxicity effects. *Protoplasma, 251*, 1471-1479.

Catauro, M., Bollino, F., Papale, F., Ferrara, C., & Mustarelli, P. (2015). Silica–polyethylene glycol hybrids synthesized by sol–gel: biocompatibility improvement of titanium implants by coating. *Materials Science and Engineering: C, 55*, 118-125.

Chen, J., Yang, H. B., Miao, J., Wang, H.-Y., & Liu, B. (2014). Thermodynamically Driven One-Dimensional Evolution of Anatase TiO_2 Nanorods: One-Step Hydrothermal Synthesis for Emerging Intrinsic Superiority of Dimensionality. *Journal of the American Chemical Society, 136*, 15310-15318.

Chen, K. L., Mylon, S. E., & Elimelech, M. (2006). Aggregation kinetics of alginate-coated hematite nanoparticles in monovalent and divalent electrolytes. *Environmental Science & Technology, 40*, 1516-1523.

Chen, L., Sabatini, D. A., & Kibbey, T. C. (2010). Retention and release of TiO_2 nanoparticles in unsaturated porous media during dynamic saturation change. *Journal of contaminant hydrology, 118*, 199-207.

Chen, W., Duan, L., & Zhu, D. (2007). Adsorption of polar and nonpolar organic chemicals to carbon nanotubes. *Environmental Science & Technology, 41*, 8295-8300.

Cho, U.-H., & Seo, N.-H. (2005). Oxidative stress in Arabidopsis thaliana exposed to cadmium is due to hydrogen peroxide accumulation. *Plant Science, 168*, 113-120.

Chowdhury, I., Duch, M. C., Mansukhani, N. D., Hersam, M. C., & Bouchard, D. (2013). Colloidal properties and stability of graphene oxide nanomaterials in the aquatic environment. *Environmental Science & Technology, 47*, 6288-6296.

Chowdhury, I., Duch, M. C., Mansukhani, N. D., Hersam, M. C., & Bouchard, D. (2014). Interactions of graphene oxide nanomaterials with natural organic matter and metal oxide surfaces. *Environmental Science & Technology, 48*, 9382-9390.

Combarros, R., Collado, S., & Diaz, M. (2016). Toxicity of graphene oxide on growth and metabolism of Pseudomonas putida. *Journal of Hazardous Materials, 310*, 246-252.

Costa-Fernández, J. M., Menéndez-Miranda, M., Bouzas-Ramos, D., Encinar, J. R., & Sanz-Medel, A. (2016). Mass spectrometry for the characterization and quantification of engineered inorganic nanoparticles. *TrAC Trends in Analytical Chemistry, 84*, 139-148.

Cupi, D., Hartmann, N. B., & Baun, A. (2015). The influence of natural organic matter and aging on suspension stability in guideline toxicity testing of silver, zinc oxide, and titanium dioxide nanoparticles with Daphnia magna. *Environmental Toxicology and Chemistry, 34*, 497-506.

Dan, Y., Ma, X., Zhang, W., Liu, K., Stephan, C., & Shi, H. (2016). Single particle ICP-MS method development for the determination of plant uptake and accumulation of CeO2 nanoparticles. *Analytical and Bioanalytical Chemistry, 408*, 5157-5167.

Das, S., Wolfson, B. P., Tetard, L., Tharkur, J., Bazata, J., & Santra, S. (2015). Effect of N-acetyl cysteine coated CdS: Mn/ZnS quantum dots on seed germination and seedling growth of snow pea (Pisum sativum L.): imaging and spectroscopic studies. *Environmental Science: Nano, 2*, 203-212.

De Matteis, L., Germani, R., Mancini, M. V., Di Renzo, F., & Spreti, N. (2015). Encapsulation of chloroperoxidase in novel hybrid polysaccharide-silica biocomposites: Catalytic efficiency, re-use and thermal stability. *Applied Catalysis A: General, 492*, 23-30.

Dobias, J., & Bernier-Latmani, R. (2013). Silver Release from Silver Nanoparticles in Natural Waters. *Environmental Science & Technology, 47*, 4140-4146.

Dong, S., Sun, Y., Gao, B., Shi, X., Xu, H., Wu, J., & Wu, J. (2017). Retention and transport of graphene oxide in water-saturated limestone media. *Chemosphere, 180*, 506-512.

Duncan, T. V. (2014). Release of engineered nanomaterials from polymer nanocomposites: the effect of matrix degradation. *ACS Applied Materials & Interfaces, 7*, 20-39.

Durán, N., Duran, M., de Jesus, M. B., Seabra, A. B., Fávaro, W. J., & Nakazato, G. (2016). Silver nanoparticles: A new view on mechanistic aspects on antimicrobial activity. *Nanomedicine: Nanotechnology, Biology and Medicine, 12*, 789-799.

Dutta, A. K., Maji, S. K., & Adhikary, B. (2014). γ-Fe_2O_3 nanoparticles: an easily recoverable effective photo-catalyst for the degradation of rose bengal and methylene blue dyes in the waste-water treatment plant. *Materials Research Bulletin, 49*, 28-34.

Duvall, M., & Wyatt, A. (2011). Regulation of nanotechnology and nanomaterials at EPA and around the world: Recent developments and context. *Washington, DC: Beveridge & Diamond, PC*.

Ebbs, S. D., Bradfield, S. J., Kumar, P., White, J. C., Musante, C., & Ma, X. (2016). Accumulation of zinc, copper, or cerium in carrot (Daucus carota) exposed to metal oxide nanoparticles and metal ions. *Environmental Science: Nano, 3*, 114-126.

Eckelman, M. J., Mauter, M. S., Isaacs, J. A., & Elimelech, M. (2012). New perspectives on nanomaterial aquatic ecotoxicity: production impacts exceed direct exposure impacts for carbon nanotoubes. *Environmental Science & Technology, 46*, 2902-2910.

Egodawatte, S., Datt, A., Burns, E. A., & Larsen, S. C. (2015). Chemical insight into the adsorption of chromium (III) on iron oxide/mesoporous silica nanocomposites. *Langmuir, 31*, 7553-7562.

El-Temsah, Y. S., & Joner, E. J. (2012). Impact of Fe and Ag nanoparticles on seed germination and differences in bioavailability during exposure in aqueous suspension and soil. *Environmental Toxicology, 27*, 42-49.

Ellis, L.J. A., Valsami-Jones, E., Lead, J. R., & Baalousha, M. (2016). Impact of surface coating and environmental conditions on the fate and transport of silver nanoparticles in the aquatic environment. *Science of The Total Environment, 568*, 95-106.

Elsaesser, A., & Howard, C. V. (2012). Toxicology of nanoparticles. *Advanced Drug Delivery Reviews, 64*, 129-137.

European commission., (2011). Commission Recommendation of 18 October 2011 on the definition of nanomaterial. *Official Journal of European Union, 38*, 275.

Fabrega, J., Luoma, S. N., Tyler, C. R., Galloway, T. S., & Lead, J. R. (2011). Silver nanoparticles: Behaviour and effects in the aquatic environment. *Environment International, 37*, 517-531.

Fadeel, B., Pietroiusti, A., & Shvedova, A. A. (2012). Adverse effects of engineered nanomaterials: exposure, toxicology, and impact on human health: *Elsevier Academic Press*. pp , 1-463.

Fan, W., Jiang, X., Yang, W., Geng, Z., Huo, M., Liu, Z., & Zhou, H. (2015). Transport of graphene oxide in saturated porous media: effect of cation composition in mixed Na-Ca electrolyte systems. *Science of The Total Environment, 511*, 509-515.

Fang, B., Bonakdarpour, A., Reilly, K., Xing, Y., Taghipour, F., & Wilkinson, D. P. (2014). Large-scale synthesis of TiO_2 microspheres with hierarchical nanostructure for highly efficient photodriven reduction of CO_2 to CH_4. *ACS Applied Materials & Interfaces, 6*, 15488-15498.

Farre, M., Gajda-Schrantz, K., Kantiani, L., & Barcelo, D. (2009). Ecotoxicity and analysis of nanomaterials in the aquatic environment. *Analytical and Bioanalytical Chemistry, 393*, 81-95.

Feng, L., Wu, L., & Qu, X. (2013). New horizons for diagnostics and therapeutic applications of graphene and graphene oxide. *Advanced Materials, 25*, 168-186.

Feng, X., Yan, Y., Wan, B., Li, W., Jaisi, D. P., Zheng, L., Zhang, J., & Liu, F. (2016). Enhanced Dissolution and Transformation of ZnO Nanoparticles: The Role of Inositol Hexakisphosphate. *Environmental Science & Technology, 50*, 5651-5660.

Figueroa, J. A. L., Stiner, C. A., Radzyukevich, T. L., & Heiny, J. A. (2016). Metal ion transport quantified by ICP-MS in intact cells. *Scientific Reports, 6*. 20551.

Findlay, A. D., Thompson, D., & Tipping, E. (1996). The aggregation of silica and haematite particles dispersed in natural water samples. *Colloids and Surfaces A: Physicochemical and Engineering Aspects, 118*, 97-105.

Foyer, C. H., & Halliwell, B. (1976). The presence of glutathione and glutathione reductase in chloroplasts: a proposed role in ascorbic acid metabolism. *Planta, 133*, 21-25.

Foyer, C. H., & Shigeoka, S. (2011). Understanding oxidative stress and antioxidant functions to enhance photosynthesis. *Plant Physiology, 155*, 93-100.

Franchi, A., & O'Melia, C. R. (2003). Effects of natural organic matter and solution chemistry on the deposition and reentrainment of colloids in porous media. *Environmental Science & Technology, 37*, 1122-1129.

Frazier, T. P., Burklew, C. E., & Zhang, B. (2014). Titanium dioxide nanoparticles affect the growth and microRNA expression of tobacco (Nicotiana tabacum). *Functional & Integrative Genomics, 14*, 75-83.

Fu, H., Qu, X., Chen, W., & Zhu, D. (2014). Transformation and destabilization of graphene oxide in reducing aqueous solutions containing sulfide. *Environmental Toxicology and Chemistry, 33*, 2647-2653.

Fu, R., Zhang, X., Xu, Z., Guo, X., Bi, D., & Zhang, W. (2017). Fast and highly efficient removal of chromium (VI) using humus-supported nanoscale zero-valent iron: Influencing factors, kinetics and mechanism. *Separation and Purification Technology, 174*, 362-371.

Furman, O., Usenko, S., & Lau, B. L. (2013). Relative importance of the humic and fulvic fractions of natural organic matter in the aggregation and deposition of silver nanoparticles. *Environmental Science & Technology, 47*, 1349-1356.

Gallego, S. M., Benavídes, M. P., & Tomaro, M. L. (1996). Effect of heavy metal ion excess on sunflower leaves: evidence for involvement of oxidative stress. *Plant Science, 121*, 151-159.

Gannon, J., Tan, Y., Baveye, P., & Alexander, M. (1991). Effect of sodium chloride on transport of bacteria in a saturated aquifer material. *Applied and Environmental Microbiology, 57*, 2497-2501.

Gao, J., Youn, S., Hovsepyan, A., Llaneza, V. L., Wang, Y., Bitton, G., & Bonzongo, J.-C. J. (2009). Dispersion and toxicity of selected manufactured nanomaterials in natural river water samples: effects of water chemical composition. *Environmental science & technology, 43*, 3322-3328.

Gardea-Torresdey, J. L., Rico, C. M., & White, J. C. (2014). Trophic transfer, transformation, and impact of engineered nanomaterials in terrestrial environments. *Environmental Science & Technology, 48*, 2526-2540.

Garner, K. L., & Keller, A. A. (2014). Emerging patterns for engineered nanomaterials in the environment: a review of fate and toxicity studies. *Journal of Nanoparticle Research, 16*, 2503.

Gatabi, M. P., Moghaddam, H. M., & Ghorbani, M. (2016). Point of zero charge of maghemite decorated multiwalled carbon nanotubes fabricated by chemical precipitation method. *Journal of Molecular Liquids, 216*, 117-125.

Ge, Y., Priester, J. H., Van De Werfhorst, L. C., Schimel, J. P., & Holden, P. A. (2013). Potential mechanisms and environmental controls of TiO_2 nanoparticle effects on soil bacterial communities. *Environmental Science & Technology, 47*, 14411-14417.

George, S., Pokhrel, S., Xia, T., Gilbert, B., Ji, Z., Schowalter, M., Rosenauer, A., Damoiseaux, R., Bradley, K. A., & Mädler, L. (2009). Use of a rapid cytotoxicity screening approach to engineer a safer zinc oxide nanoparticle through iron doping. *ACS Nano, 4*, 15-29.

Godinez, I. G., Darnault, C. J., Khodadoust, A. P., & Bogdan, D. (2013). Deposition and release kinetics of nano-TiO_2 in saturated porous media: effects of solution ionic strength and surfactants. *Environmental Pollution, 174*, 106-113.

Goldberg, E., McNew, C., Scheringer, M., Bucheli, T. D., Nelson, P., & Hungerbühl r, K. (2017). What factors determine the retention behavior of engineered nanomaterials in saturated porous media? *Environmental Science & Technology, 51*, 2729-2737.

Gondikas, A. P., Morris, A., Reinsch, B. C., Marinakos, S. M., Lowry, G. V., & Hsu-Kim, H. (2012). Cysteine-induced modifications of zero-valent silver nanomaterials: implications for particle surface chemistry, aggregation, dissolution, and silver speciation. *Environmental Science & Technology, 46*, 7037-7045.

Gottschalk, F., & Nowack, B. (2011). The release of engineered nanomaterials to the environment. *Journal of Environmental Monitoring, 13*, 1145-1155.

Gottschalk, F., Sun, T., & Nowack, B. (2013). Environmental concentrations of engineered nanomaterials: review of modeling and analytical studies. *Environmental Pollution, 181*, 287-300.

Gupta, V., Agarwal, S., & Saleh, T. A. (2011). Chromium removal by combining the magnetic properties of iron oxide with adsorption properties of carbon nanotubes. *Water Research, 45*, 2207-2212.

Han, Y., Kim, D., Hwang, G., Lee, B., Eom, I., Kim, P. J., Tong, M., & Kim, H. (2014). Aggregation and dissolution of ZnO nanoparticles synthesized by different methods: Influence of ionic strength and humic acid. *Colloids and Surfaces A: Physicochemical and Engineering Aspects, 451*, 7-15.

Han, Z., Liao, L., Wu, Y., Pan, H., Shen, S., & Chen, J. (2012). Synthesis and photocatalytic application of oriented hierarchical ZnO flower-rod architectures. *Journal of Hazardous Materials, 217*, 100-106.

Happo, M. S., Uski, O., Jalava, P. I., Kelz, J., Brunner, T., Hakulinen, P., Maki-Paakkanen, J., Kosma, V.-M., Jokiniemi, J., & Obernberger, I. (2013). Pulmonary inflammation and tissue damage in the mouse lung after exposure to PM samples from biomass heating appliances of old and modern technologies. *Science of the Total Environment, 443*, 256-266.

He, X., Aker, W. G., Fu, P. P., & Hwang, H.-M. (2015). Toxicity of engineered metal oxide nanomaterials mediated by nano–bio–eco–interactions: a review and perspective. *Environmental Science: Nano, 2*, 564-582.

Heath, R. L., & Packer, L. (1968). Photoperoxidation in isolated chloroplasts: I. Kinetics and stoichiometry of fatty acid peroxidation. *Archives of Biochemistry and Biophysics, 125*, 189-198.

Hedberg, Y. S., Pradhan, S., Cappellini, F., Karlsson, M.-E., Blomberg, E., Karlsson, H., Wallinder, I. O., & Hedberg, J. F. (2016). Electrochemical surface oxide characteristics of metal nanoparticles (Mn, Cu and Al) and the relation to toxicity. *Electrochimica Acta, 212*, 360-371.

Hegde, K., Brar, S. K., Verma, M., & Surampalli, R. Y. (2016). Current understandings of toxicity, risks and regulations of engineered nanoparticles with respect to environmental microorganisms. *Nanotechnology for Environmental Engineering, 1*, 5.

Hendren, C. O., Mesnard, X., Dröge, J., & Wiesner, M. R. (2011). Estimating production data for five engineered nanomaterials as a basis for exposure assessment: *Environmental Science and Technology, 45*, 2562-2569

Hoffmann, M. R., Martin, S. T., Choi, W., & Bahnemann, D. W. (1995). Environmental applications of semiconductor photocatalysis. *Chemical Reviews, 95*, 69-96.

Hong, F., Zhou, J., Liu, C., Yang, F., Wu, C., Zheng, L., & Yang, P. (2005). Effect of nano-TiO2 on photochemical reaction of chloroplasts of spinach. *Biological Trace Element Research, 105*, 269-279.

Hsu, P.-C., Shih, Z.-Y., Lee, C.-H., & Chang, H. T. (2012). Synthesis and analytical applications of photoluminescent carbon nanodots. *Green Chemistry, 14*, 917-920.

Hu, Y., He, L., Ding, J., Sun, D., Chen, L., & Chen, X. (2016). One-pot synthesis of dextran decorated reduced graphene oxide nanoparticles for targeted photo-chemotherapy. *Carbohydrate Polymers, 144*, 223-229.

Huang, H., Lv, J. J., Zhou, D. L., Bao, N., Xu, Y., Wang, A. J., & Feng, J. J. (2013). One-pot green synthesis of nitrogen-doped carbon nanoparticles as fluorescent probes for mercury ions. *RSC Advances, 3*, 21691-21696.

Huynh, K. A., & Chen, K. L. (2011). Aggregation kinetics of citrate and polyvinylpyrrolidone coated silver nanoparticles in monovalent and divalent electrolyte solutions. *Environmental Science & Technology, 45*, 5564-5571.

Ide, M., De Canck, E., Van Driessche, I., Lynen, F., & Van Der Voort, P. (2015). Developing a new and versatile ordered mesoporous organosilica as a pH and temperature stable chromatographic packing material. *Rsc Advances, 5*, 5546-5552.

Jahan, S., Mansoor, F., Naz, S., Lei, J., & Kanwal, S. (2013). Oxidative synthesis of highly fluorescent boron/nitrogen co-doped carbon nanodots enabling detection of photosensitizer and carcinogenic dye. *Analytical Chemistry, 85*, 10232-10239.

Jaisi, D. P., Saleh, N. B., Blake, R. E., & Elimelech, M. (2008). Transport of single-walled carbon nanotubes in porous media: filtration mechanisms and reversibility. *Environmental Science & Technology, 42*, 8317-8323.

Jastrzebska, A., Karcz, J., Letmanowski, R., Zabost, D., Ciecierska, E., Zdunek, J., Karwowska, E., Siekierski, M., Olszyna, A., & Kunicki, A. (2016). Synthesis of the RGO/Al_2O_3 core-shell nanocomposite flakes and characterization of their unique electrostatic properties using zeta potential measurements. *Applied Surface Science, 362*, 577-594.

Ji, Z., Wang, Y., Shen, X., Ma, H., Yang, J., Yuan, A., & Zhou, H. (2017). Facile synthesis and enhanced catalytic performance of reduced graphene oxide decorated with hexagonal structure Ni nanoparticles. *Journal of Colloid and Interface Science, 487*, 223-230.

Jiang, J., Oberdörster, G., & Biswas, P. (2009). Characterization of size, surface charge, and agglomeration state of nanoparticle dispersions for toxicological studies. *Journal of Nanoparticle Research, 11*, 77-89.

Jiang, X., Tong, M., Lu, R., & Kim, H. (2012). Transport and deposition of ZnO nanoparticles in saturated porous media. *Colloids and Surfaces A: Physicochemical and Engineering Aspects, 401*, 29-37.

Kalbassi, M. R., Salari-joo, H., & Johari, A. (2011). Toxicity of silver nanoparticles in aquatic ecosystems: salinity as the main cause in reducing toxicity. *Iranian Journal of Toxicology, 5*, 436-443.

Karami, H. (2013). Heavy metal removal from water by magnetite nanorods. *Chemical Engineering Journal, 219*, 209-216.

Kasel, D., Bradford, S. A., Simunek, J., Heggen, M., Vereecken, H., & Klumpp, E. (2013). Transport and retention of multi-walled carbon nanotubes in saturated porous media: Effects of input concentration and grain size. W*ater Research, 47*, 933-944.

Keller, A. A., Wang, H., Zhou, D., Lenihan, H. S., Cherr, G., Cardinale, B. J., Ji, Z. (2010). Stability and aggregation of metal oxide nanoparticles in natural aqueous matrices. *Environmental science & technology, 44*, 1962-1967.

Keller, A. A., & Lazareva, A. (2013). Predicted releases of engineered nanomaterials: from global to regional to local. *Environmental Science & Technology Letters, 1*, 65-70.

Kent, R. D., & Vikesland, P. J. (2012). Controlled evaluation of silver nanoparticle dissolution using atomic force microscopy. *Environmental Science & Technology, 46*, 6977-6984.

Khin, M. M., Nair, A. S., Babu, V. J., Murugan, R., & Ramakrishna, S. (2012). A review on nanomaterials for environmental remediation. *Energy & Environmental Science, 5*, 8075-8109.

Khodakovskaya, M., Dervishi, E., Mahmood, M., Xu, Y., Li, Z., Watanabe, F., & Biris, A. S. (2009). Carbon nanotubes are able to penetrate plant seed coat and dramatically affect seed germination and plant growth. *ACS Nano, 3*, 3221-3227.

Kittler, S., Greulich, C., Diendorf, J., Koller, M., & Epple, M. (2010). Toxicity of silver nanoparticles increases during storage because of slow dissolution under release of silver ions. *Chemistry of Materials, 22*, 4548-4554.

Knappenberger, T., Aramrak, S., & Flury, M. (2015). Transport of barrel and spherical shaped colloids in unsaturated porous media. *Journal of Contaminant Hydrology, 180*, 69-79.

Konkena, B., & Vasudevan, S. (2012). Understanding aqueous dispersibility of graphene oxide and reduced graphene oxide through pKa measurements. *The Journal of Physical Chemistry Letters, 3*, 867-872.

Krishnan, K. A., Sreejalekshmi, K., Vimexen, V., & Dev, V. V. (2016). Evaluation of adsorption properties of sulphurised activated carbon for the effective and economically viable removal of Zn (II) from aqueous solutions. *Ecotoxicology and Environmental Safety, 124*, 418-425.

Kumar, S., Nair, R. R., Pillai, P. B., Gupta, S. N., Iyengar, M., & Sood, A. K. (2014). Graphene Oxide-$MnFe_2O_4$ Magnetic Nanohybrids for Efficient Removal of Lead and Arsenic from Water. *ACS Applied Materials & Interfaces, 6*, 17426-17436.

Kurepa, J., Paunesku, T., Vogt, S., Arora, H., Rabatic, B. M., Lu, J., Wanzer, M. B., Woloschak, G. E., & Smalle, J. A. (2010). Uptake and distribution of ultrasmall

anatase TiO_2 Alizarin red S nanoconjugates in Arabidopsis thaliana. *Nano Letters, 10*, 2296-2302.

Kurian, M., & Nair, D. S. (2015). Heterogeneous Fenton behavior of nano nickel zinc ferrite catalysts in the degradation of 4-chlorophenol from water under neutral conditions. *Journal of Water Process Engineering, 8*, 37-49.

Lannone, M. F., Groppa, M. D., de Sousa, M. E., Fernández van Raap, M. B., & Benavides, M. P. (2016). Impact of magnetite iron oxide nanoparticles on wheat (Triticum aestivum L.) development: Evaluation of oxidative damage. *Environmental and Experimental Botany, 131*, 77-88.

Lanphere, J. D., Rogers, B., Luth, C., Bolster, C. H., & Walker, S. L. (2014). Stability and transport of graphene oxide nanoparticles in groundwater and surface water. *Environmental Engineering Science, 31*, 350-359.

Larue, C., Castillo-Michel, H., Sobanska, S., Cecillon, L., Bureau, S., Barthes, V., Ouerdane, L., Carriere, M., & Sarret, G. (2014). Foliar exposure of the crop Lactuca sativa to silver nanoparticles: evidence for internalization and changes in Ag speciation. *Journal of Hazardous Materials, 264*, 98-106.

Lee, E.-J., An, A. K., He, T., Woo, Y. C., & Shon, H. K. (2016). Electrospun nanofiber membranes incorporating fluorosilane-coated TiO_2 nanocomposite for direct contact membrane distillation. *Journal of Membrane Science, 520*, 145-154.

Leenheer, J. A. (2007). Progression from model structures to molecular structures of natural orgabic matter components. *Annals of Environmental Science*. 1,15.

Lei, C., Zhang, L., Yang, K., Zhu, L., & Lin, D. (2016). Toxicity of iron-based nanoparticles to green algae: Effects of particle size, crystal phase, oxidation state and environmental aging. *Environmental Pollution, 218*, 505-512.

Lei, C., Zhu, X., Zhu, B., Jiang, C., Le, Y., & Yu, J. (2017). Superb adsorption capacity of hierarchical calcined Ni/Mg/Al layered double hydroxides for Congo red and Cr (VI) ions. *Journal of Hazardous Materials, 321*, 801-811.

Lem, K., Choudhury, A., A Lakhani, A., Kuyate, P., R Haw, J., S Lee, D., Iqbal, Z., & J Brumlik, C. (2012). Use of nanosilver in consumer products. *Recent Patents on Nanotechnology, 6*, 60-72.

Levard, C., Hotze, E. M., Lowry, G. V., & Brown Jr, G. E. (2012). Environmental transformations of silver nanoparticles: impact on stability and toxicity. *Environmental Science & Technology, 46*, 6900-6914.

Lewicka, Z. A., Benedetto, A. F., Benoit, D. N., William, W. Y., Fortner, J. D., & Colvin, V. L. (2011). The structure, composition, and dimensions of TiO_2 and ZnO nanomaterials in commercial sunscreens. *Journal of Nanoparticle Research, 13*, 3607.

Li, G., Richter, C. P., Milot, R. L., Cai, L., Schmuttenmaer, C. A., Crabtree, R. H., Brudvig, G. W., & Batista, V. S. (2009). Synergistic effect between anatase and

rutile TiO_2 nanoparticles in dye-sensitized solar cells. *Dalton Transactions*(45), 10078-10085.

Li, G., Zhao, Z., Liu, J., & Jiang, G. (2011a). Effective heavy metal removal from aqueous systems by thiol functionalized magnetic mesoporous silica. *Journal of Hazardous Materials, 192*, 277-283.

Li, J., Liu, J., Tan, G., Jiang, J., Peng, S., Deng, M., Qian, D., Feng, Y., & Liu, Y. (2014). High-sensitivity paracetamol sensor based on Pd/graphene oxide nanocomposite as an enhanced electrochemical sensing platform. *Biosensors and Bioelectronics, 54*, 468-475.

Li, K., Zhang, W., Huang, Y., & Chen, Y. (2011b). Aggregation kinetics of CeO_2 nanoparticles in KCl and $CaCl_2$ solutions: measurements and modeling. *Journal of Nanoparticle Research, 13*, 6483-6491.

Li, K., Zhao, X., K. Hammer, B., Du, S., & Chen, Y. (2013). Nanoparticles inhibit DNA replication by binding to DNA: modeling and experimental validation. *ACS Nano, 7*, 9664-9674.

Li, M., Li, M. y., Feng, C. g., & Zeng, Q. x. (2014). Preparation and characterization of multi-carboxyl-functionalized silica gel for removal of Cu(II), Cd(II), Ni(II) and Zn(II) from aqueous solution. *Applied Surface Science, 314*, 1063-1069.

Li, X., Lenhart, J. J., & Walker, H. W. (2011c). Aggregation kinetics and dissolution of coated silver nanoparticles. *Langmuir, 28*, 1095-1104.

Li, X., Lenhart, J. J., & Walker, H. W. (2010). Dissolution-accompanied aggregation kinetics of silver nanoparticles. *Langmuir, 26*, 16690-16698.

Li, Y., Zhang, P., Ouyang, Z., Zhang, M., Lin, Z., Li, J., Su, Z., & Wei, G. (2016). Nanoscale graphene doped with highly dispersed silver nanoparticles: quick synthesis, facile fabrication of 3D membrane-modified electrode, and super performance for electrochemical sensing. *Advanced Functional Materials*. *26*, 2122-2134.

Li, Z., Sahle-Demessie, E., Hassan, A. A., & Sorial, G. A. (2011d). Transport and deposition of CeO_2 nanoparticles in water-saturated porous media. *Water Research, 45*, 4409-4418.

Liang, Y., Bradford, S. A., Simunek, J., Heggen, M., Vereecken, H., & Klumpp, E. (2013). Retention and remobilization of stabilized silver nanoparticles in an undisturbed loamy sand soil. *Environmental Science & Technology, 47*, 12229-12237.

Lichtenthaler, H. K. (1987). Chlorophylls and carotenoids: pigments of photosynthetic biomembranes. *Methods in Enzymology, 148*, 350-382.

Lin, C. A. J., Sperling, R. A., Li, J. K., Yang, T. Y., Li, P. Y., Zanella, M., Chang, W. H., & Parak, W. J. (2008a). Design of an amphiphilic polymer for nanoparticle coating and functionalization. *Small, 4*, 334-341.

Lin, D., Tian, X., Wu, F., & Xing, B. (2010). Fate and transport of engineered nanomaterials in the environment. *Journal of Environmental Quality, 39*, 1896-1908.

Lin, D., & Xing, B. (2008b). Root uptake and phytotoxicity of ZnO nanoparticles. *Environmental Science & Technology, 42*, 5580-5585.

Lingamdinne, L. P., Chang, Y.-Y., Yang, J.-K., Singh, J., Choi, E.-H., Shiratani, M., Koduru, J. R., & Attri, P. (2017). Biogenic reductive preparation of magnetic inverse spinel iron oxide nanoparticles for the adsorption removal of heavy metals. *Chemical Engineering Journal, 307*, 74-84.

Liu, C., Zhang, P., Zhai, X., Tian, F., Li, W., Yang, J., Liu, W. (2012a). Nano-carrier for gene delivery and bioimaging based on carbon dots with PEI-passivation enhanced fluorescence. *Biomaterials, 33*, 3604-3613.

Liu, J., Chen, Y., Wang, W., Feng, J., Peng, S., Ma, S., Chen, H., & Chen, X. (2016). Effective synthesis of highly fluorescent nitrogen doped carbon nanoparticles for selective sensing of Hg^{2+} in food and cosmetics samples. *RSC Advances, 6*, 89916-89924.

Liu, J., & Hurt, R. H. (2010a). Ion release kinetics and particle persistence in aqueous nano-silver colloids. *Environmental Science & Technology, 44*, 2169-2175.

Liu, J., Legros, S., Ma, G., Veinot, J. G., Von der Kammer, F., & Hofmann, T. (2012b). Influence of surface functionalization and particle size on the aggregation kinetics of engineered nanoparticles. *Chemosphere, 87*, 918-924.

Liu, J., Sonshine, D. A., Shervani, S., & Hurt, R. H. (2010b). Controlled release of biologically active silver from nanosilver surfaces. *ACS Nano, 4*, 6903-6913.

Liu, L., Gao, B., Wu, L., Morales, V. L., Yang, L., Zhou, Z., & Wang, H. (2013). Deposition and transport of graphene oxide in saturated and unsaturated porous media. *Chemical Engineering Journal, 229*, 444-449.

Liu, L., Gao, B., Wu, L., Sun, Y., & Zhou, Z. (2015a). Effects of surfactant type and concentration on graphene retention and transport in saturated porous media. *Chemical Engineering Journal, 262*, 1187-1191.

Liu, L., Yang, P., Li, J., Zhang, Z., Yu, X., & Lu, L. (2017). Temperature-controlled cross-linking of silver nanoparticles with diels-alder reaction and its application on antibacterial property. *Applied Surface Science*. *403*, 435-440.

Liu, M., Xu, J., Cheng, B., Ho, W., & Yu, J. (2015b). Synthesis and adsorption performance of $Mg(OH)_2$ hexagonal nanosheet–graphene oxide composites. *Applied Surface Science, 332*, 121-129.

Liu, Q., Lazouskaya, V., He, Q., & Jin, Y. (2010c). Effect of particle shape on colloid retention and release in saturated porous media. *Journal of Environmental Quality, 39*, 500-508.

Liu, Q., Zhong, L.-B., Zhao, Q.-B., Frear, C., & Zheng, Y.-M. (2015c). Synthesis of Fe_3O_4/polyacrylonitrile composite electrospun nanofiber mat for effective adsorption of tetracycline. *ACS Applied Materials & Interfaces, 7*, 14573-14583.

Liufu, S., Xiao, H., & Li, Y. (2004). Investigation of PEG adsorption on the surface of zinc oxide nanoparticles. *Powder Technology, 145*, 20-24.

Lopez-Moreno, M. L., de la Rosa, G., Cruz-Jiménez, G., Castellano, L., Peralta-Videa, J. R., & Gardea-Torresdey, J. L. (2017). Effect of ZnO nanoparticles on corn seedlings at different temperatures; X-ray absorption spectroscopy and ICP/OES studies. *Microchemical Journal, 134*, 54-61.

Lopez-Moreno, M. L., de la Rosa, G., Hernández-Viezcas, J. A., Peralta-Videa, J. R., & Gardea-Torresdey, J. L. (2010). X-ray absorption spectroscopy (XAS) corroboration of the uptake and storage of CeO_2 nanoparticles and assessment of their differential toxicity in four edible plant species. *Journal of Agricultural and Food Chemistry, 58*, 3689-3693.

Lowry, G. V., Gregory, K. B., Apte, S. C., & Lead, J. R. (2012). Transformations of nanomaterials in the environment: *Environmental Science & Technolology.*, *46*, 6893-6899.

Lu, A. H., Salabas, E. e. L., & Schüth, F. (2007). Magnetic nanoparticles: synthesis, protection, functionalization, and application. *Angewandte Chemie International Edition, 46*, 1222-1244.

Luo, P., Roca, A., Tiede, K., Privett, K., Jiang, J., Pinkstone, J., Ma, G., Veinot, J., & Boxall, A. (2017). Application of nanoparticle tracking analysis for characterising the fate of engineered nanoparticles in sediment-water systems. *Journal of Environmental Sciences*. *19*, 1-10.

Lv, O., Tao, Y., Qin, Y., Chen, C., Pan, Y., Deng, L., Liu, L., & Kong, Y. (2016). Highly fluorescent and morphology-controllable graphene quantum dots-chitosan hybrid xerogels for in vivo imaging and pH-sensitive drug carrier. *Materials Science and Engineering: C, 67*, 478-485.

Ma, H., Wang, H., & Na, C. (2015a). Microwave-assisted optimization of platinum-nickel nanoalloys for catalytic water treatment. *Applied Catalysis B: Environmental, 163*, 198-204.

Ma, J., Wang, X., Fu, Q., Si, Y., Yu, J., & Ding, B. (2015b). Highly carbonylated cellulose nanofibrous membranes utilizing maleic anhydride grafting for efficient lysozyme adsorption. *ACS Applied Materials & Interfaces, 7*, 15658-15666.

Ma, X., Geiser-Lee, J., Deng, Y., & Kolmakov, A. (2010). Interactions between engineered nanoparticles (ENPs) and plants: phytotoxicity, uptake and accumulation. *Science of the Total Environment, 408*, 3053-3061.

Ma, Y., He, X., Zhang, P., Zhang, Z., Ding, Y., Zhang, J., Wang, G., Xie, C., Luo, W., Zhang, J., Zheng, L., Chai, Z., & Yang, K. (2017). Xylem and phloem based

transport of CeO2 nanoparticles in hydroponic cucumber plants. *Environmental Science & Technology, 51*, 5215-5221.

Madadrang, C. J., Kim, H. Y., Gao, G., Wang, N., Zhu, J., Feng, H., Gorring, M., Kasner, M. L., & Hou, S. (2012). Adsorption behavior of EDTA-graphene oxide for Pb (II) removal. *ACS Applied Materials & Interfaces, 4*, 1186-1193.

Madrakian, T., Afkhami, A., Zolfigol, M. A., & Solgi, M. (2006). Separation, preconcentration and determination of silver ion from water samples using silica gel modified with 2, 4, 6-trimorpholino-1, 3, 5-triazin. *Journal of Hazardous Materials, 128*, 67-72.

Majedi, S. M., Kelly, B. C., & Lee, H. K. (2014). Combined effects of water temperature and chemistry on the environmental fate and behavior of nanosized zinc oxide. *Science of The Total Environment, 496*, 585-593.

Marchesan, S., Kostarelos, K., Bianco, A., & Prato, M. (2015). The winding road for carbon nanotubes in nanomedicine. *Materials Today, 18*, 12-19.

Maurer-Jones, M. A., Gunsolus, I. L., Murphy, C. J., & Haynes, C. L. (2013). Toxicity of engineered nanoparticles in the environment. *Analytical Chemistry, 85*, 3036-3049.

May, M. J., & Leaver, C. J. (1993). Oxidative stimulation of glutathione synthesis in Arabidopsis thaliana suspension cultures. *Plant Physiology, 103*, 621-627.

Mehta, S., Kumar, S., Chaudhary, S., & Bhasin, K. (2009). Effect of cationic surfactant head groups on synthesis, growth and agglomeration behavior of ZnS nanoparticles. *Nanoscale Research Letters, 4*, 1197.

Meychik, N., & Yermakov, I. (2001). Ion exchange properties of plant root cell walls. *Plant and Soil, 234*, 181-193.

Mhamane, D., Aravindan, V., Kim, M.-S., Kim, H.-K., Roh, K. C., Ruan, D., Lee, S. H., Srinivasan, M., & Kim, K. B. (2016). Silica-assisted bottom-up synthesis of graphene-like high surface area carbon for highly efficient ultracapacitor and Li-ion hybrid capacitor applications. *Journal of Materials Chemistry A, 4*, 5578-5591.

Miao, A. J., Zhang, X. Y., Luo, Z., Chen, C. S., Chin, W. C., Santschi, P. H., & Quigg, A. (2010). Zinc oxide–engineered nanoparticles: Dissolution and toxicity to marine phytoplankton. *Environmental Toxicology and Chemistry, 29*, 2814-2822.

Mou, Z., Wu, Y., Sun, J., Yang, P., Du, Y., & Lu, C. (2014). TiO_2 Nanoparticles-Functionalized N-Doped Graphene with Superior Interfacial Contact and Enhanced Charge Separation for Photocatalytic Hydrogen Generation. *ACS Applied Materials & Interfaces, 6*, 13798-13806.

Moussa, H., Merlin, C., Dezanet, C., Balan, L., Medjahdi, G., Ben-Attia, M., & Schneider, R. (2016). Trace amounts of Cu^{2+} ions influence ROS production and

cytotoxicity of ZnO quantum dots. *Journal of Hazardous Materials, 304*, 532-542.

Mueller, N. C., & Nowack, B. (2008). Exposure modeling of engineered nanoparticles in the environment. *Environmental Science & Technology, 42*, 4447-4453.

Mukherjee, A., Peralta-Videa, J. R., Bandyopadhyay, S., Rico, C. M., Zhao, L., & Gardea-Torresdey, J. L. (2014). Physiological effects of nanoparticulate ZnO in green peas (Pisum sativum L.) cultivated in soil. *Metallomics, 6*, 132-138.

Mulvaney, P., Liz-Marzan, L., Giersig, M., & Ung, T. (2000). Silica encapsulation of quantum dots and metal clusters. *Journal of Materials Chemistry, 10*, 1259-1270.

Naftaly, A., Dror, I., & Berkowitz, B. (2016). Measurement and modeling of engineered nanoparticle transport and aging dynamics in a reactive porous medium. *Water Resources Research, 52*, 5473-5491.

Nair, P. M. G., & Chung, I. M. (2014). Physiological and molecular level effects of silver nanoparticles exposure in rice (Oryza sativa L.) seedlings. *Chemosphere, 112*, 105-113.

Naji, A., Ismail, A., & Ismail, A. R. (2010). Chemical speciation and contamination assessment of Zn and Cd by sequential extraction in surface sediment of Klang River, Malaysia. *Microchemical Journal, 95*, 285-292.

Nakano, Y., & Asada, K. (1981). Hydrogen peroxide is scavenged by ascorbate-specific peroxidase in spinach chloroplasts. *Plant and Cell Physiology, 22*, 867-880.

Nam, D.-H., Lee, B.-c., Eom, I.-c., Kim, P., & Yeo, M.-K. (2014). Uptake and bioaccumulation of titanium-and silver-nanoparticles in aquatic ecosystems. *Molecular & Cellular Toxicology, 10*, 9-17.

Nandi, B., Goswami, A., & Purkait, M. (2009). Removal of cationic dyes from aqueous solutions by kaolin: kinetic and equilibrium studies. *Applied Clay Science, 42*, 583-590.

Nandi, S., Majji, S. N., & Misra, A. (2016). Effects of optical and magnetic fields on the electrical characteristics of colloidal graphene quantum dots. *RSC Advances, 6*, 40577-40584.

Nathalie Adam , C. S., Josep Galceran , Encarna Companys , Alexander Vakurov , Rachel Wallace , Dries Knapen , Ronny Blust. (2014). The chronic toxicity of ZnO nanoparticles and $ZnCl_2$ to Daphnia magna and the use of different methods to assess nanoparticle aggregation and dissolution. *Nanotoxicology, 8*, 709-717.

Nel, A., Xia, T., Madler, L., & Li, N. (2006). Toxic potential of materials at the nanolevel. *Science, 311*, 622-627.

Nithya, R., Gomathi, T., Sudha, P., Venkatesan, J., Anil, S., & Kim, S. K. (2016). Removal of Cr(VI) from aqueous solution using chitosan-g-poly (butyl

acrylate)/silica gel nanocomposite. *International Journal of Biological Macromolecules, 87*, 545-554.

Nordmann, J., Buczka, S., Voss, B., Haase, M., & Mummenhoff, K. (2015). In vivo analysis of the size-and time-dependent uptake of NaYF 4: Yb, Er upconversion nanocrystals by pumpkin seedlings. *Journal of Materials Chemistry B, 3*, 144-150.

Ocsoy, I., Temiz, M., Celik, C., Altinsoy, B., Yilmaz, V., & Duman, F. (2017). A green approach for formation of silver nanoparticles on magnetic graphene oxide and highly effective antimicrobial activity and reusability. *Journal of Molecular Liquids, 227*, 147-152.

Oleszczuk, P., Josko, I., & Xing, B. (2011). The toxicity to plants of the sewage sludges containing multiwalled carbon nanotubes. *Journal of Hazardous Materials, 186*, 436-442.

Ong, W. J., Yeong, J. J., Tan, L. L., Goh, B. T., Yong, S. T., & Chai, S.-P. (2014). Synergistic effect of graphene as a co-catalyst for enhanced daylight-induced photocatalytic activity of Zn 0.5 Cd 0.5 S synthesized via an improved one-pot co-precipitation-hydrothermal strategy. *RSC Advances, 4*, 59676-59685.

Ozdemir, N., Soylak, M., Elci, L., & Dogan, M. (2004). Speciation analysis of inorganic Sb (III) and Sb (V) ions by using mini column filled with Amberlite XAD-8 resin. *Analytica Chimica Acta, 505*, 37-41.

Pang, Y., Zeng, G., Tang, L., Zhang, Y., Liu, Y., Lei, X., Li, Z., Zhang, J., & Xie, G. (2011). PEI-grafted magnetic porous powder for highly effective adsorption of heavy metal ions. *Desalination, 281*, 278-284.

Pattanayak, J., Mondal, K., Mathew, S., & Lalvani, S. (2000). A parametric evaluation of the removal of As (V) and As (III) by carbon-based adsorbents. *Carbon, 38*, 589-596.

Peijnenburg, W. J. G. M., Baalousha, M., Chen, J., Chaudry, Q., Von der kammer, F., Kuhlbusch, T. A. J., Lead, J., Nickel, C., Quik, J. T. K., Renker, M., Wang, Z., & Koelmans, A. A. (2015). A Review of the Properties and Processes Determining the Fate of Engineered Nanomaterials in the Aquatic Environment. *Critical Reviews in Environmental Science and Technology, 45*, 2084-2134.

Peng, J., Gao, W., Gupta, B. K., Liu, Z., Romero-Aburto, R., Ge, L., Song, L., Alemany, L. B., Zhan, X., & Gao, G. (2012). Graphene quantum dots derived from carbon fibers. *Nano Letters, 12*, 844-849.

Peng, S., Wu, D., Ge, Z., Tong, M., & Kim, H. (2017). Influence of graphene oxide on the transport and deposition behaviors of colloids in saturated porous media. *Environmental Pollution, 225*, 141-149

Pensini, E., Yip, C. M., O'Carroll, D. M., & Sleep, B. E. (2012). Effect of water chemistry and aging on iron mica interaction forces: implications for iron particle transport. *Langmuir, 28*, 10453-10463.

Peralta-Videa, J., Gardea-Torresdey, J., Gomez, E., Tiemann, K., Parsons, J., & Carrillo, G. (2002). Effect of mixed cadmium, copper, nickel and zinc at different pHs upon alfalfa growth and heavy metal uptake. *Environmental Pollution, 119*, 291-301.

Peretyazhko, T. S., Zhang, Q., & Colvin, V. L. (2014). Size-controlled dissolution of silver nanoparticles at neutral and acidic pH conditions: kinetics and size changes. *Environmental Science & Technology, 48*, 11954-11961.

Pereira, A., Castro, A. M., Costa, J. T., & Baptista, J. S. (2017). *Health effects on workers exposed to engineered nanomaterials: Short review.* Paper presented at the Occupational Safety and Hygiene V: Proceedings of the International Symposium on Occupational Safety and Hygiene (SHO 2017), April 10-11, 2017, Guimarães, Portugal.

Perni, S., Hakala, V., & Prokopovich, P. (2014). Biogenic synthesis of antimicrobial silver nanoparticles capped with l-cysteine. *Colloids and Surfaces A: Physicochemical and Engineering Aspects, 460*, 219-224.

Petala, E., Baikousi, M., Karakassides, M. A., Zoppellaro, G., Filip, J., Tuček, J., Vasilopoulos, K. C., Pechoušek, J., & Zbořil, R. (2016). Synthesis, physical properties and application of the zero-valent iron/titanium dioxide heterocomposite having high activity for the sustainable photocatalytic removal of hexavalent chromium in water. *Physical Chemistry Chemical Physics, 18*, 10637-10646.

Phenrat, T., Kim, H.-J., Fagerlund, F., Illangasekare, T., Tilton, R. D., & Lowry, G. V. (2009). Particle size distribution, concentration, and magnetic attraction affect transport of polymer-modified Fe nanoparticles in sand columns. *Environmental Science & Technology, 43*, 5079-5085.

Philippe, A., & Schaumann, G. E. (2014). Interactions of dissolved organic matter with natural and engineered inorganic colloids: a review. *Environmental Science & Technology, 48*, 8946-8962.

Piccapietra, F., Sigg, L., & Behra, R. (2011). Colloidal stability of carbonate-coated silver nanoparticles in synthetic and natural freshwater. *Environmental Science & Technology, 46*, 818-825.

Piccinno, F., Gottschalk, F., Seeger, S., & Nowack, B. (2012). Industrial production quantities and uses of ten engineered nanomaterials in Europe and the world. *Journal of Nanoparticle Research, 14*, 1109.

Pimentel, A., Nunes, D., Duarte, P., Rodrigues, J., Costa, F. M., Monteiro, T., Martins, R., & Fortunato, E. (2014). Synthesis of long ZnO nanorods under microwave irradiation or conventional heating. *The Journal of Physical Chemistry C, 118*, 14629-14639.

Ping, G., Huimin, L., Xiaoxiao, H., Kemin, W., Jianbing, H., Weihong, T., Shouchun, Z., & Xiaohai, Y. (2007). Preparation and antibacterial activity of Fe_3O_4@Ag nanoparticles. *Nanotechnology, 18*, 285604.

Polsongkram, D., Chamninok, P., Pukird, S., Chow, L., Lupan, O., Chai, G., Khallaf, H., Park, S., & Schulte, A. (2008). Effect of synthesis conditions on the growth of ZnO nanorods via hydrothermal method. *Physica B: Condensed Matter, 403*, 3713-3717.

Ponder, S. M., Darab, J. G., Bucher, J., Caulder, D., Craig, I., Davis, L., Edelstein, N., Lukens, W., Nitsche, H., & Rao, L. (2001). Surface chemistry and electrochemistry of supported zerovalent iron nanoparticles in the remediation of aqueous metal contaminants. *Chemistry of Materials, 13*, 479-486.

Praetorius, A., Scheringer, M., & Hungerbühler, K. (2012). Development of environmental fate models for engineered nanoparticles: A case study of TiO_2 nanoparticles in the Rhine River. *Environmental science & technology, 46*, 6705-6713.

Prasad, V., D'Souza, C., Yadav, D., Shaikh, A., & Vigneshwaran, N. (2006). Spectroscopic characterization of zinc oxide nanorods synthesized by solid-state reaction. *Spectrochimica Acta Part A: Molecular and Biomolecular Spectroscopy, 65*, 173-178.

Priester, J. H., Ge, Y., Mielke, R. E., Horst, A. M., Moritz, S. C., Espinosa, K., An, Y.-J. (2012). Soybean susceptibility to manufactured nanomaterials with evidence for food quality and soil fertility interruption. *Proceedings of the National Academy of Sciences, 109*, 451-456.

Qi, Z., Hou, L., Zhu, D., Ji, R., & Chen, W. (2014a). Enhanced transport of phenanthrene and 1-naphthol by colloidal graphene oxide nanoparticles in saturated soil. *Environmental Science & Technology, 48*, 10136-10144.

Qi, Z., Zhang, L., Wang, F., Hou, L., & Chen, W. (2014b). Factors controlling transport of graphene oxide nanoparticles in saturated sand columns. *Environmental Toxicology and Chemistry, 33*, 998-1004.

Quik, J., Velzeboer, I., Wouterse, M., Koelmans, A., & Van de Meent, D. (2014). Heteroaggregation and sedimentation rates for nanomaterials in natural waters. *Water Research, 48*, 269-279.

Rajput, S., Singh, L. P., Pittman, C. U., & Mohan, D. (2017). Lead (Pb^{2+}) and copper (Cu^{2+}) remediation from water using superparamagnetic maghemite (γ-Fe_2O_3) nanoparticles synthesized by Flame Spray Pyrolysis (FSP). *Journal of Colloid and Interface Science, 492*, 176-190.

Ranjan, S., Dasgupta, N., Rajendran, B., Avadhani, G. S., Ramalingam, C., & Kumar, A. (2016). Microwave-irradiation-assisted hybrid chemical approach for titanium dioxide nanoparticle synthesis: microbial and cytotoxicological evaluation. *Environmental Science and Pollution Research, 23*, 12287-12302.

Rao, S., & Shekhawat, G. (2014). Toxicity of ZnO engineered nanoparticles and evaluation of their effect on growth, metabolism and tissue specific accumulation in Brassica juncea. *Journal of Environmental Chemical Engineering, 2*, 105-114.

Raychoudhury, T., Tufenkji, N., & Ghoshal, S. (2012). Aggregation and deposition kinetics of carboxymethyl cellulose-modified zero-valent iron nanoparticles in porous media. *Water Research, 46*, 1735-1744.

Razzaz, A., Ghorban, S., Hosayni, L., Irani, M., & Aliabadi, M. (2016). Chitosan nanofibers functionalized by TiO_2 nanoparticles for the removal of heavy metal ions. *Journal of the Taiwan Institute of Chemical Engineers, 58*, 333-343.

Reddy, K. M., Manorama, S. V., & Reddy, A. R. (2003). Bandgap studies on anatase titanium dioxide nanoparticles. *Materials Chemistry and Physics, 78*, 239-245.

Ren, X., Li, J., Tan, X., Shi, W., Chen, C., Shao, D., Wen, T., Wang, L., Zhao, G., & Sheng, G. (2014). Impact of Al_2O_3 on the aggregation and deposition of graphene oxide. *Environmental Science & Technology, 48*, 5493-5500.

Rida, M. A., & Harb, F. (2014). Synthesis and characterization of amorphous silica nanoparitcles from aqueous silicates uisng cationic surfactants. *Journal of Metals, Materials and Minerals, 24*, 37-42.

Rodrigues, A., Brito, A., Janknecht, P., Proença, M. F., & Nogueira, R. (2009). Quantification of humic acids in surface water: effects of divalent cations, pH, and filtration. *Journal of Environmental Monitoring, 11*, 377-382.

Rodriguez, A. R. C., Saiz-Poseu, J., García-Pardo, J., García, B., Lorenzo, J., Ojea-Jiménez, I., Komilis, D., Sedó, J., Busqué, F., & Sánchez, A. (2016). Biocompatible polydopamine-like particles for the removal of heavy metals at extremely low concentrations. *RSC Advances, 6*, 40058-40066.

Rodushkin, I., Ruth, T., & Huhtasaari, Å. (1999). Comparison of two digestion methods for elemental determinations in plant material by ICP techniques. *Analytica Chimica Acta, 378*, 191-200.

Ruparelia, J., Duttagupta, S., Chatterjee, A., & Mukherji, S. (2008). Potential of carbon nanomaterials for removal of heavy metals from water. *Desalination, 232*, 145-156.

Sabba, D., Agarwala, S., Pramana, S. S., & Mhaisalkar, S. (2014). A maskless synthesis of TiO_2-nanofiber-based hierarchical structures for solid-state dye-sensitized solar cells with improved performance. *Nanoscale Research Letters, 9*, 1-9.

Saetia, K., Schnorr, J. M., Mannarino, M. M., Kim, S. Y., Rutledge, G. C., Swager, T. M., & Hammond, P. T. (2014). spray-layer-by-layer carbon nanotube/electrospun fiber electrodes for flexible chemiresistive sensor applications. *Advanced Functional Materials, 24*, 492-502.

Salam, O. E. A., Reiad, N. A., & ElShafei, M. M. (2011). A study of the removal characteristics of heavy metals from wastewater by low-cost adsorbents. *Journal of Advanced Research, 2*, 297-303.

Saleh, N. B., Pfefferle, L. D., & Elimelech, M. (2008). Aggregation kinetics of multiwalled carbon nanotubes in aquatic systems: measurements and

environmental implications. *Environmental Science & Technology, 42*, 7963-7969.

Salerno, M. B., Flamm, M., Logan, B. E., & Velegol, D. (2006). Transport of rodlike colloids through packed beds. *Environmental Science & Technology, 40*, 6336-6340.

Sarkka, H., Bhatnagar, A., & Sillanpaa, M. (2015). Recent developments of electro-oxidation in water treatment-a review. *Journal of Electroanalytical Chemistry, 754*, 46-56.

Sasidharan, S., Torkzaban, S., Bradford, S. A., Dillon, P. J., & Cook, P. G. (2014). Coupled effects of hydrodynamic and solution chemistry on long-term nanoparticle transport and deposition in saturated porous media. *Colloids and Surfaces A: Physicochemical and Engineering Aspects, 457*, 169-179.

Satheesh, R., Vignesh, K., Rajarajan, M., Suganthi, A., Sreekantan, S., Kang, M., & Kwak, B. S. (2016). Removal of Congo red from water using quercetin modified α-Fe 2 O 3 nanoparticles as effective nanoadsorbent. *Materials Chemistry and Physics, 180*, 53-65.

Sathishkumar, M., Sneha, K., Won, S., Cho, C.-W., Kim, S., & Yun, Y.-S. (2009). Cinnamon zeylanicum bark extract and powder mediated green synthesis of nano-crystalline silver particles and its bactericidal activity. *Colloids and Surfaces B: Biointerfaces, 73*, 332-338.

Sato, K., Hosokawa, K., & Maeda, M. (2003). Rapid aggregation of gold nanoparticles induced by non-cross-linking DNA hybridization. *Journal of the American Chemical Society, 125*, 8102-8103.

Schmidt, J., & Vogelsberger, W. (2009). Aqueous long-term solubility of titania nanoparticles and titanium (IV) hydrolysis in a sodium chloride system studied by adsorptive stripping voltammetry. *Journal of Solution Chemistry, 38*, 1267-1282.

Sharma, P., Bao, D., & Fagerlund, F. (2014). Deposition and mobilization of functionalized multiwall carbon nanotubes in saturated porous media: effect of grain size, flow velocity and solution chemistry. *Environmental Earth Sciences, 72*, 3025-3035.

Sharma, P., Jha, A. B., Dubey, R. S., & Pessarakli, M. (2012). Reactive oxygen species, oxidative damage, and antioxidative defense mechanism in plants under stressful conditions. *Journal of Botany, 2012,* 1-26

Sharma, P. K., & Hall, D. O. (1991). Interaction of salt stress and photoinhibition on photosynthesis in barley and sorghum. *Journal of Plant Physiology, 138*, 614-619.

Sharonova, A., Loza, K., Surmeneva, M., Surmenev, R., Prymak, O., & Epple, M. (2016). Synthesis of positively and negatively charged silver nanoparticles and their deposition on the surface of titanium. Paper presented at the IOP Conference Series: *Materials Science and Engineering, 116, 1-9.*

Shi, Y., & Seliskar, C. J. (1997). Optically transparent polyelectrolyte-silica composite materials: preparation, characterization, and application in optical chemical sensing. *Chemistry of Materials, 9*, 821-829.

Shih, Y. C., Ke, C. Y., Yu, C. J., Lu, C. Y., & Tseng, W. L. (2014). Combined Tween 20-Stabilized Gold Nanoparticles and Reduced Graphite Oxide-Fe_3O_4 Nanoparticle Composites for Rapid and Efficient Removal of Mercury Species from a Complex Matrix. *ACS Applied Materials & Interfaces, 6*, 17437-17445.

Sigdel, S., Dubey, A., Elbohy, H., Aboagye, A., Galipeau, D., Zhang, L., Fong, H., & Qiao, Q. (2014). Dye-sensitized solar cells based on spray-coated carbon nanofiber/TiO_2 nanoparticle composite counter electrodes. *Journal of Materials Chemistry A, 2*, 11448-11453.

Silva, T., Pokhrel, L. R., Dubey, B., Tolaymat, T. M., Maier, K. J., & Liu, X. (2014). Particle size, surface charge and concentration dependent ecotoxicity of three organo-coated silver nanoparticles: comparison between general linear model-predicted and observed toxicity. *Science of the Total Environment, 468*, 968-976.

Sirelkhatim, A., Mahmud, S., Seeni, A., Kaus, N. H. M., Ann, L. C., Bakhori, S. K. M., Hasan, H., & Mohamad, D. (2015). Review on zinc oxide nanoparticles: antibacterial activity and toxicity mechanism. *Nano-Micro Letters, 7*, 219-242.

Sleiman, N., Deluchat, V., Wazne, M., Mallet, M., Courtin-Nomade, A., Kazpard, V., & Baudu, M. (2017). Phosphate removal from aqueous solutions using zero valent iron (ZVI): Influence of solution composition and ZVI aging. *Colloids and Surfaces A: Physicochemical and Engineering Aspects, 514*, 1-10.

Soliman, M. G., Pelaz, B., Parak, W. J., & del Pino, P. (2015). Phase transfer and polymer coating methods toward improving the stability of metallic nanoparticles for biological applications. *Chemistry of Materials, 27*, 990-997.

Som, C., Nowack, B., Krug, H. F., & Wick, P. (2012). Toward the development of decision supporting tools that can be used for safe production and use of nanomaterials. *Accounts of Chemical Research, 46*, 863-872.

Soni, D., Naoghare, P. K., Saravanadevi, S., & Pandey, R. A. (2015). Release, transport and toxicity of engineered nanoparticles, *Reviews of Environmental Contamination and Toxicology, 234,* Springer, Pg. 1-47

Stankus, D. P., Lohse, S. E., Hutchison, J. E., & Nason, J. A. (2010). Interactions between natural organic matter and gold nanoparticles stabilized with different organic capping agents. *Environmental Science & Technology, 45*, 3238-3244.

Strobel, C., Torrano, A. A., Herrmann, R., Malissek, M., Bräuchle, C., Reller, A., Treuel, L., & Hilger, I. (2014). Effects of the physicochemical properties of titanium dioxide nanoparticles, commonly used as sun protection agents, on microvascular endothelial cells. *Journal of Nanoparticle Research, 16*, 2130.

Subari, S. N. M., Osman, R., & Saim, N. (2017). Occurrence, source apportionment and environmental risk assessment of pharmaceuticals in Klang River, Malaysia. *Journal of Science & Technology, 25,* 119-128

Sun, T. Y., Bornhoft, N. A., Hungerbühl r, K., & Nowack, B. (2016a). Dynamic probabilistic modeling of environmental emissions of engineered nanomaterials. *Environmental Science & Technology, 50*, 4701-4711.

Sun, X., He, J., Meng, Y., Zhang, L., Zhang, S., Ma, X., Dey, S., Zhao, J., & Lei, Y. (2016b). Microwave-assisted ultrafast and facile synthesis of fluorescent carbon nanoparticles from a single precursor: preparation, characterization and their application for the highly selective detection of explosive picric acid. *Journal of Materials Chemistry A, 4*, 4161-4171.

Sun, Y., & Xia, Y. (2003). Gold and silver nanoparticles: a class of chromophores with colors tunable in the range from 400 to 750 nm. *Analyst, 128*, 686-691.

Surette, M., & Nason, J. (2016). Effects of surface coating character and interactions with natural organic matter on the colloidal stability of gold nanoparticles. *Environmental Science: Nano, 3*, 1144-1152.

Syberg, K., & Hansen, S. F. (2016). Environmental risk assessment of chemicals and nanomaterials, The best foundation for regulatory decision-making? *Science of the Total Environment, 541*, 784-794.

Tabrizi, M. A., & Varkani, J. N. (2014). Green synthesis of reduced graphene oxide decorated with gold nanoparticles and its glucose sensing application. *Sensors and Actuators B: Chemical, 202*, 475-482.

Tamez, C., Hernandez, R., & Parsons, J. (2016). Removal of Cu (II) and Pb (II) from aqueous solution using engineered iron oxide nanoparticles. *Microchemical Journal, 125*, 97-104.

Tang, L., Ji, R., Cao, X., Lin, J., Jiang, H., Li, X., Teng, K. S., Luk, C. M., Zeng, S., & Hao, J. (2012). Deep ultraviolet photoluminescence of water-soluble self-passivated graphene quantum dots. *ACS Nano, 6*, 5102-5110.

Thuesombat, P., Hannongbua, S., Akasit, S., & Chadchawan, S. (2014). Effect of silver nanoparticles on rice (Oryza sativa L. cv. KDML 105) seed germination and seedling growth. *Ecotoxicology and Environmental Safety, 104*, 302-309.

Tong, T., Wilke, C. M., Wu, J., Binh, C. T. T., Kelly, J. J., Gaillard, J.-F., & Gray, K. A. (2015). Combined toxicity of nano-ZnO and nano-TiO_2: from single-to multinanomaterial systems. *Environmental Science & Technology, 49*, 8113-8123.

Torkzaban, S., Bradford, S. A., van Genuchten, M. T., & Walker, S. L. (2008). Colloid transport in unsaturated porous media: The role of water content and ionic strength on particle straining. *Journal of Contaminant Hydrology, 96*, 113-127.

USEPA. (2012). Ecological Effects Test Guidelines OCSPP 850.4100: Seedling Emergence and Seedling Growth *Office of Chemical Safety and Pollution Prevention 7101*, 1-30.

Vannini, C., Domingo, G., Onelli, E., De Mattia, F., Bruni, I., Marsoni, M., & Bracale, M. (2014). Phytotoxic and genotoxic effects of silver nanoparticles exposure on germinating wheat seedlings. *Journal of Plant Physiology, 171*, 1142-1148.

Vayssieres, L. (2003). Growth of arrayed nanorods and nanowires of ZnO from aqueous solutions. *Advanced Materials, 15*, 464-466.

Venkateswarlu, S., Lee, D., & Yoon, M. (2016). Bioinspired 2D-Carbon Flakes and Fe_3O_4 Nanoparticles Composite for Arsenite Removal. *ACS Applied Materials & Interfaces, 8*, 23876-23885.

Verdugo, E. M., Krause, C., Genskow, K., Han, Y., Baltrusaitis, J., Mattes, T. E., Valentine, R. L., & Cwiertny, D. M. (2014). N-Functionalized Carbon Nanotubes As a Source and Precursor of N-Nitrosodimethylamine: Implications for Environmental Fate, Transport, and Toxicity. *Environmental Science & Technology, 48*, 9279-9287.

Vidmar, J., Milačič, R., & Ščančar, J. (2017). Sizing and simultaneous quantification of nanoscale titanium dioxide and a dissolved titanium form by single particle inductively coupled plasma mass spectrometry. *Microchemical Journal, 132*, 391-400.

Vinkovic, T., Novak, O., Strnad, M., Goessler, W., Jurašin, D. D., Parađikovic, N., & Vrcek, I. V. (2017). Cytokinin response in pepper plants (Capsicum annuum L.) exposed to silver nanoparticles. *Environmental Research, 156*, 10-18.

Vunain, E., Mishra, A., & Mamba, B. (2016). Dendrimers, mesoporous silicas and chitosan-based nanosorbents for the removal of heavy-metal ions: A review. *International Journal of Biological Macromolecules, 86*, 570-586.

Wahab, R., Ansari, S., Kim, Y. S., Seo, H.-K., & Shin, H.-S. (2007a). Room temperature synthesis of needle-shaped ZnO nanorods via sonochemical method. *Applied Surface Science, 253*, 7622-7626.

Wahab, R., Ansari, S., Kim, Y., Seo, H., Kim, G., Khang, G., & Shin, H.-S. (2007b). Low temperature solution synthesis and characterization of ZnO nano-flowers. *Materials Research Bulletin, 42*, 1640-1648.

Wahab, R., Hwang, I., Kim, Y. S., & Shin, H. S. (2011). Photocatalytic activity of zinc oxide micro-flowers synthesized via solution method. *Chemical Engineering Journal, 168*, 359-366.

Wahlefeld, A., & Bergmeyer, H. (1974). Methods of enzymatic analysis. 2nd Edition. *New York, NY, USA: Academic, Pg. 1064*.

Wang, D., Jin, Y., & Jaisi, D. P. (2015a). Effect of size-selective retention on the cotransport of hydroxyapatite and goethite nanoparticles in saturated porous media. *Environmental Science & Technology, 49*, 8461-8470.

Wang, D., Zhang, W., & Zhou, D. (2013a). Antagonistic effects of humic acid and iron oxyhydroxide grain-coating on biochar nanoparticle transport in saturated sand. *Environmental Science & Technology, 47*, 5154-5161.

Wang, H., Hsieh, B., Jiménez-Oses, G., Liu, P., Tassone, C. J., Diao, Y., Lei, T., Houk, K. N., & Bao, Z. (2015b). Solvent effects on polymer sorting of carbon nanotubes with applications in printed electronics. *Small, 11*, 126-133.

Wang, L., Zhang, J., Zhao, R., Li, Y., Li, C., & Zhang, C. (2010). Adsorption of Pb (II) on activated carbon prepared from Polygonum orientale Linn.: kinetics, isotherms, pH, and ionic strength studies. *Bioresource Technology, 101*, 5808-5814.

Wang, M., Gao, B., & Tang, D. (2016a). Review of key factors controlling engineered nanoparticle transport in porous media. *Journal of Hazardous Materials, 318*, 233-246.

Wang, M., Gao, B., Tang, D., Sun, H., Yin, X., & Yu, C. (2017). Effects of temperature on graphene oxide deposition and transport in saturated porous media. *Journal of Hazardous Materials, 331*, 28-35.

Wang, P., Menzies, N. W., Lombi, E., McKenna, B. A., Johannessen, B., Glover, C. J., Kappen, P., & Kopittke, P. M. (2013b). Fate of ZnO nanoparticles in soils and cowpea (Vigna unguiculata). *Environmental Science & Technology, 47*, 13822-13830.

Wang, Q., Zhao, S., Zhao, Y., Rui, Q., & Wang, D. (2014). Toxicity and translocation of graphene oxide in Arabidopsis plants under stress conditions. *RSC Advances, 4*, 60891-60901.

Wang, Y., Gao, B., Morales, V. L., Tian, Y., Wu, L., Gao, J., Yang, L. (2012). Transport of titanium dioxide nanoparticles in saturated porous media under various solution chemistry conditions. *Journal of Nanoparticle Research, 14*, 1095.

Wang, Z., Zhang, L., Zhao, J., & Xing, B. (2016b). Environmental processes and toxicity of metallic nanoparticles in aquatic systems as affected by natural organic matter. *Environmental Science: Nano, 3*, 240-255.

Wang, Z., Zhao, C., Han, T., Zhang, Y., Liu, S., Fei, T., Lu, G., & Zhang, T. (2017). High-performance reduced graphene oxide-based room-temperature NO_2 sensors: A combined surface modification of SnO_2 nanoparticles and nitrogen doping approach. *Sensors and Actuators B: Chemical, 242*, 269-279.

Weaver, C. L., LaRosa, J. M., Luo, X., & Cui, X. T. (2014). Electrically controlled drug delivery from graphene oxide nanocomposite films. *ACS Nano, 8*, 1834-1843.

Weir, A., Westerhoff, P., Fabricius, L., Hristovski, K., & Von Goetz, N. (2012). Titanium dioxide nanoparticles in food and personal care products. *Environmental Science & Technology, 46*, 2242-2250.

Witoon, T., Chareonpanich, M., & Limtrakul, J. (2008). Synthesis of bimodal porous silica from rice husk ash via sol–gel process using chitosan as template. *Materials Letters, 62*, 1476-1479.

Wu, L., Liu, L., Gao, B., Muño -Carpena, R., Zhang, M., Chen, H., Zhou, Z., & Wang, H. (2013). Aggregation kinetics of graphene oxides in aqueous solutions: experiments, mechanisms, and modeling. *Langmuir, 29*, 15174-15181.

Wu, S., Li, F., Xu, R., Wei, S., & Li, G. (2010). Synthesis of thiol-functionalized MCM-41 mesoporous silicas and its application in Cu (II), Pb (II), Ag (I), and Cr (III) removal. *Journal of Nanoparticle Research, 12*, 2111-2124.

Xia, T., Kovochich, M., Liong, M., Meng, H., Kabehie, S., George, S., Zink, J. I., & Nel, A. E. (2009). Polyethyleneimine coating enhances the cellular uptake of mesoporous silica nanoparticles and allows safe delivery of siRNA and DNA constructs. *ACS Nano, 3*, 3273-3286.

Xia, T., Qi, Y., Liu, J., Qi, Z., Chen, W., & Wiesner, M. R. (2017). Cation-Inhibited Transport of Graphene Oxide Nanomaterials in Saturated Porous Media: The Hofmeister Effects. *Environmental science & technology, 51*, 828-837.

Xiao, A., Wang, C., Chen, J., Guo, R., Yan, Z., & Chen, J. (2016). Carbon and metal quantum dots toxicity on the microalgae chlorella pyrenoidosa. *Ecotoxicology and Environmental Safety, 133*, 211-217.

Xiao, J., Pan, X., Guo, S., Ren, P., & Bao, X. (2014). Toward fundamentals of confined catalysis in carbon nanotubes. *Journal of the American Chemical Society, 137*, 477-482.

Xiao, S., Shen, M., Guo, R., Huang, Q., Wang, S., & Shi, X. (2010). Fabrication of multiwalled carbon nanotube-reinforced electrospun polymer nanofibers containing zero-valent iron nanoparticles for environmental applications. *Journal of Materials Chemistry, 20*, 5700-5708.

Xie, J., Ming, Z., Li, H., Yang, H., Yu, B., Wu, R., Liu, X., Bai, Y., & Yang, S. T. (2016). Toxicity of graphene oxide to white rot fungus Phanerochaete chrysosporium. *Chemosphere, 151*, 324-331.

Xu, Q. M., & Chen, H. (2011). Antioxidant responses of rice seedling to Ce^{4+} under hydroponic cultures. *Ecotoxicology and Environmental Safety, 74*, 1693-1699.

Xu, T., Zheng, H., Zhang, P., Lin, W., & Sekiguchi, Y. (2015). Hydrothermal preparation of nanoporous TiO_2 films with exposed {001} facets and superior photocatalytic activity. *Journal of Materials Chemistry A, 3*, 19115-19122.

Xue, K., Zhou, S., Shi, H., Feng, X., Xin, H., & Song, W. (2014). A novel amperometric glucose biosensor based on ternary gold nanoparticles/polypyrrole/reduced graphene oxide nanocomposite. *Sensors and Actuators B: Chemical, 203*, 412-416.

Yang, F., Hong, F., You, W., Liu, C., Gao, F., Wu, C., & Yang, P. (2006). Influence of nano-anatase TiO2 on the nitrogen metabolism of growing spinach. *Biological Trace Element Research, 110*, 179-190.

Yang, X., Lin, S., & Wiesner, M. R. (2014). Influence of natural organic matter on transport and retention of polymer coated silver nanoparticles in porous media. *Journal of Hazardous Materials, 264*, 161-168.

Yao, H., Ding, Q., Zhou, H., Zhao, Z., Liu, G., & Wang, G. (2016). An adsorption-reduction synergistic effect of mesoporous Fe/SiO_2–NH_2 hollow spheres for the removal of Cr (vi) ions. *RSC Advances, 6*, 27039-27046.

Yecheskel, Y., Dror, I., & Berkowitz, B. (2016). Transport of engineered nanoparticles in partially saturated sand columns. *Journal of Hazardous Materials, 311*, 254-262.

Yu, S.j., Yin, Y.-g., Chao, J.b., Shen, M.h., & Liu, J.-f. (2013). Highly dynamic PVP-coated silver nanoparticles in aquatic environments: chemical and morphology change induced by oxidation of Ag^0 and reduction of Ag^+. *Environmental Science & Technology, 48*, 403-411.

Yu, Y., Addai-Mensah, J., & Losic, D. (2012). Functionalized diatom silica microparticles for removal of mercury ions. *Science and Technology of Advanced Materials, 13*, 1-11.

Zeng, C., Shadman, F., & Sierra-Alvarez, R. (2017). Transport and abatement of fluorescent silica nanoparticle (SiO_2NP) in granular filtration: effect of porous media and ionic strength. *Journal of Nanoparticle Research, 19*, 105.

Zhang, H., Noonan, O., Huang, X., Yang, Y., Xu, C., Zhou, L., & Yu, C. (2016a). Surfactant-free assembly of mesoporous carbon hollow spheres with large tunable pore sizes. *ACS Nano*, *10*, 4579-4586.

Zhang, W., Yao, Y., Sullivan, N., & Chen, Y. (2011). Modeling the primary size effects of citrate-coated silver nanoparticles on their ion release kinetics. *Environmental Science & Technology, 45*, 4422-4428.

Zhang, Y., Chen, Y., Westerhoff, P., & Crittenden, J. (2009). Impact of natural organic matter and divalent cations on the stability of aqueous nanoparticles. *Water Research, 43*, 4249-4257.

Zhang, Y., Ye, Y., Zhou, X., Liu, Z., Zhu, G., Li, D., & Li, X. (2016b). Monodispersed hollow aluminosilica microsphere@ hierarchical γ-AlOOH deposited with or without Fe (OH) 3 nanoparticles for efficient adsorption of organic pollutants. *Journal of Materials Chemistry A, 4*, 838-846.

Zhang, Y., Yuan, S., Zhao, Y., Wang, H., & He, C. (2014). Synthesis of novel yttrium-doped graphene oxide nanocomposite for dye removal. *Journal of Materials Chemistry A, 2*, 7897-7903.

Zhang, Z., Gao, P., Qiu, Y., Liu, G., Feng, Y., & Wiesner, M. (2016c). Transport of cerium oxide nanoparticles in saturated silica media: influences of operational parameters and aqueous chemical conditions. *Scientific Reports, 6, 1-11*.

Zhang, Z., & Kong, J. (2011). Novel magnetic Fe_3O_4@C nanoparticles as adsorbents for removal of organic dyes from aqueous solution. *Journal of Hazardous Materials, 193*, 325-329.

Zhang, Z., Maji, S., da Fonseca Antunes, A. B., De Rycke, R., Hoogenboom, R., & De Geest, B. G. (2016d). Salt-driven deposition of thermoresponsive polymer-coated metal nanoparticles on solid substrates. *Angewandte Chemie International Edition, 55*, 7086-7090.

Zhao, C.Y., Tan, S.X., Xiao, X.Y., Qiu, X.S., Pan, J.Q., & Tang, Z.X. (2014). Effects of dietary zinc oxide nanoparticles on growth performance and antioxidative status in broilers. *Biological Trace Element Research, 160*, 361-367.

Zhao, L., Peralta-Videa, J. R., Ren, M., Varela-Ramirez, A., Li, C., Hernandez-Viezcas, J. A., Aguilera, R. J., & Gardea-Torresdey, J. L. (2012). Transport of Zn in a sandy loam soil treated with ZnONPs and uptake by corn plants: Electron microprobe and confocal microscopy studies. *Chemical Engineering Journal, 184*, 1-8.

Zhao, R., Wang, Y., Li, X., Sun, B., & Wang, C. (2015). Synthesis of β-cyclodextrin-based electrospun nanofiber membranes for highly efficient adsorption and separation of methylene blue. *ACS Applied Materials & Interfaces, 7*, 26649-26657.

Zhao, S., Wang, Q., Zhao, Y., Rui, Q., & Wang, D. (2015). Toxicity and translocation of graphene oxide in Arabidopsis thaliana. *Environmental Toxicology and Pharmacology, 39*, 145-156.

Zhou, D., Jiang, X., Lu, Y., Fan, W., Huo, M., & Crittenden, J. (2016). Cotransport of graphene oxide and Cu (II) through saturated porous media. *Science of The Total Environment, 550*, 717-726.

Zhou, N., He, B., Wang, X., & Hu, Z. (2014). Preparation and characterization of Au@ TiO_2 core–shell hollow nanoparticles with CO oxidation performance. *Journal of Nanoparticle Research, 16*, 1-11.

Zhu, J., Wei, S., Gu, H., Rapole, S. B., Wang, Q., Luo, Z., Haldolaarachchige, N., Young, D. P., & Guo, Z. (2011). One-pot synthesis of magnetic graphene nanocomposites decorated with core@ double-shell nanoparticles for fast chromium removal. *Environmental Science & Technology, 46*, 977-985.

Zhu, Z.J., Wang, H., Yan, B., Zheng, H., Jiang, Y., Miranda, O. R., Rotello, V. M., Xing, B., & Vachet, R. W. (2012). Effect of surface charge on the uptake and distribution of gold nanoparticles in four plant species. *Environmental Science & Technology, 46*, 12391-12398.

Zimoch, I., & Łobos, E. (2014). The optimization of chlorine dose in water treatment process in order to reduce the formation of disinfection by-products. *Desalination and Water Treatment, 52*, 3719-3724.

Zinchenko, A. A., Maeda, N., Pu, S., & Murata, S. (2013). Entrapping of fullerenes, nanotubes, and inorganic nanoparticles by a DNA–chitosan complex: a method for nanomaterials removal. *Environmental Science & Technology, 47*, 4489-4496.

Zuverza-Mena, N., Martinez-Fernandez, D., Du, W., Hernandez-Viezcas, J. A., Bonilla-Bird, N., Lopez-Moreno, M. L., Komarek, M., Peralta-Videa, J. R., & Gardea-Torresdey, J. L. (2017). Exposure of engineered nanomaterials to plants: Insights into the physiological and biochemical responses-A review. *Plant Physiology and Biochemistry, 110*, 236-264.

LIST OF PUBLICATIONS

1- Jahan, S., Yusoff, I. B., Alias, Y. B., & Bakar, A. F. B. A. (2017). Reviews of the toxicity behavior of five potential engineered Nanomaterials (NMs) into the aquatic ecosystem. *Toxicology Reports, 4,* 211-220.

2- Jahan, S., Alias, Y. B., Bakar, A. F. B. A., & Yusoff, I. B. (2017). Ionic release behavior of polymer-coated and uncoated metal nanoparticles (MNPs) in various conditions: effects of particle shape, size, and natural media reactivity. *Colloid and Polymer Science*, 1-11.

3- Jahan, S., Alias, Y. B., Bakar, A. F. B. A., & Yusoff, I. B. (2018). Toxicity evaluation of ZnO and TiO_2 nanomaterials in hydroponic red bean (Vigna angularis) plant: Physiology, biochemistry and kinetic transport. *Journal of Environmental Sciences*. doi.org/10.1016/j.jes.2017.12.022.

4- Jahan, S., Alias, Y. B., Bakar, A. F. B. A., & Yusoff, I. B. (2018). Transport and retention behavior of carbonaceous colloids in natural aqueous medium: Impact of water chemistry. (under revision, *Chemosphere*).

5- Jahan, S., Alias, Y. B., Bakar, A. F. B. A., & Yusoff, I. B. (2018). Synthesis of polymer-modified mesoporous silica microcubes (P@MSMC) for efficient removal of metal pollutants from river water (under review, Chemical Engineering Journal).

6- Jahan, S., Alias, Y. B., Bakar, A. F. B. A., & Yusoff, I. B. (2018). Use of Silica nanostructures for water treatment: State-of-the-art and future prospects. (under write-up).

LIST OF SEMINAR AND PAPER PRESENTED

1- Presented a course on UHR Field Emission Scanning Electron Microscope, STEM, EDS & Sample Preparations at Department of Chemistry, University of Malaya (July-2016).

2- Efficient Removal of Graphene Oxide Quantum Dots (GOQDs) from Natural water by PEI-Modified Silica Nanocomposites, Post graduate symposium on green engineering and technology (PSGET-2016) Malacca, Kuala Lumpur Malaysia.